POLITECNICO DI TORINO

Master's Degree in Civil Engineering

Infrastructures and Transportation Systems

Preliminary investigation toward a Mechanistic-Empirical Pavement Design Framework for Italy: a Sensitivity Analysis of Traffic, Climate, and Material Inputs

ADVISORS:

Prof. Davide Dalmazzo
Prof. Lucia Tsantilis
Dr. Michele Lanotte

CANDIDATE:

Elisa Bergamino

Academic Year 2025/2026

A colei che mi emoziona ogni giorno,
Alla persona più resiliente che conosco.
Questo lavoro è dedicato a te,
Aurora.

Aknowledgments

I would like to acknowledge the Italian Air Force for providing meteorological data from the Torino–Caselle weather station, which was essential to the climatic analyses conducted in this study.

I would also like to acknowledge the Autonomous Province of Trento and the Bisonte by iWIM company for granting access to the WIM traffic data used for research purposes. In this regard, I would like to thank Guido Farinacci and Paolo Armani for their support and collaboration, and for providing the data used in this work.

I am sincerely grateful to Michigan State University for hosting and supporting me during the six-month research period in which this thesis was developed.

I would like to personally express my gratitude to all my advisors for their support throughout this work and for the stimulating discussions that challenged me and ultimately contributed to my intellectual growth.

I would like to thank Prof. Dalmazzo for first suggesting this research topic and for providing the opportunity for this period abroad.

I would like to thank Prof. Tsantilis for introducing me to pavement design and for sparking my interest in this field.

Last but not least, I am grateful to Dr. Lanotte for his support and guidance throughout this research. His insight and trust have been essential to both the development of this thesis and my personal growth.

Finally, I am grateful to my family and friends from both sides of the Ocean for their constant support and for being an essential part of my journey. Each of them has contributed, in different ways, to shaping the person I am today.

Abstract

This thesis investigates the feasibility of introducing a mechanistic–empirical pavement design approach in the Italian context, where no unified national procedure currently exists. The work focuses on the preliminary implementation of the Mechanistic–Empirical Pavement Design Guide (MEPDG) framework, intended as an initial step toward a broader process that would ultimately include local calibration.

A set of structured case studies is developed, and a sensitivity analysis is carried out to investigate the influence of traffic characterization and material behavior on predicted pavement performance. Alternative traffic input descriptions and two hot-mix asphalt materials exhibiting different distress responses are considered in order to assess their impact on the distress and damage evolution. Climatic conditions are examined to provide an environmental context to the analysis. Since the transfer functions adopted in the simulations are not locally calibrated, the study does not aim to provide definitive design solutions, but rather to identify trends, quantify sensitivities, and discuss methodological implications.

The results emphasize the critical role of input characterization in mechanistic–empirical design, particularly with respect to traffic representation and material response in specific climate conditions. The observed variability in predicted distress evolution confirms the necessity of a consistent, performance-based framework capable of systematically accounting for differences in traffic demand, environmental conditions, and material behavior. Beyond the specific findings of the case studies, this work contributes to the broader discussion on the modernization of pavement design practices in Italy and represents an initial step toward future local calibration and the structured adoption of a mechanistic–empirical design methodology.

Sintesi

Il presente lavoro di tesi analizza la fattibilità dell'introduzione di un approccio di progettazione delle pavimentazioni di tipo empirico-razionale nel contesto italiano, caratterizzato attualmente dall'assenza di una procedura nazionale unificata. Il lavoro si focalizza sull'implementazione preliminare del framework MEPDG (Mechanistic-Empirical Pavement Design Guide), intesa come fase iniziale di un processo più ampio volto alla futura calibrazione locale dei modelli.

Lo studio si articola attraverso lo sviluppo di casi studio strutturati e la conduzione di un'analisi di sensibilità finalizzata a investigare l'influenza della caratterizzazione del traffico e del comportamento dei materiali sulle prestazioni attese della sovrastruttura. Al fine di valutare l'impatto sull'evoluzione del danno e dei dissesti, sono state considerate diverse modalità di descrizione degli input di traffico e due differenti miscele bituminose a caldo (hot-mix asphalt), aventi risposte diverse al degrado. L'analisi integra inoltre l'esame delle condizioni climatiche per fornire il necessario contesto ambientale alle simulazioni. Poiché le funzioni di trasferimento adottate non sono calibrate localmente, lo studio non mira a fornire soluzioni progettuali definitive, bensì a identificare trend, quantificare le sensibilità e discutere le implicazioni metodologiche.

I risultati evidenziano il ruolo critico della caratterizzazione degli input nella progettazione empirico-razionale, con particolare riferimento alla rappresentazione del traffico e alla risposta dei materiali in specifiche condizioni climatiche. La variabilità osservata nell'evoluzione dei dissesti conferma la necessità di un framework coerente e basato sulle prestazioni (performance-based), in grado di tenere conto sistematicamente delle differenze nella domanda di traffico, nelle variabili ambientali e nel comportamento dei materiali. Oltre alle risultanze specifiche dei casi studio, il presente lavoro contribuisce al dibattito sulla modernizzazione delle pratiche di progettazione stradale in Italia, ponendosi come passo iniziale verso la calibrazione locale e l'adozione strutturata di una metodologia di progetto empirico-razionale.

Contents

Acknowledgments ii

Abstract iii

Sintesi iv

Introduction 1

1 The current Italian practice for pavement design 3

2 The MEPDG and NCHRP 1-37A Project 8

2.1 Time and pavement structure discretizations 10

2.2 Transfer functions and calibration coefficients for damage calculation . 12

2.2.1 Transfer functions and damage accumulation: fatigue cracking . 12

2.2.2 Transfer functions and equivalent cycles approach: rutting . . . 17

2.2.3 Transfer functions and crack propagation: thermal cracking . . 21

2.3 Output and iterative process: the reliability analysis 23

3 Requirements and processing for the input data within the MEPDG framework 26

3.1 Climate input data 26

3.1.1 The heat transfer model for frost-action and temperature-related effects 27

3.2 Traffic input data 33

3.2.1 Traffic volume – base year information 36

3.2.2 Traffic volume adjustment factors 37

3.2.3 Axle load distribution factors 40

3.2.4 General traffic inputs 41

3.2.5 Traffic input data processing . . . 42
3.3 Materials input data . . . 43
3.3.1 HMA input data for the Master Curve . . . 43
3.3.1.1 The Global Aging System for aging simulation . . . 44
3.3.1.2 Input Level 1 . . . 46
3.3.1.3 Input Level 2 . . . 48
3.3.1.4 Input Level 3 . . . 50
3.3.2 HMA: other properties . . . 50
3.3.2.1 Poisson's ratio . . . 51
3.3.2.2 Additional materials inputs required for climatic modeling 52
3.3.2.3 Additional materials inputs required for distress and transfer functions . . . 52
3.3.3 Input data for unbound granular materials . . . 54
3.3.3.1 Pavement response model material inputs . . . 54
3.3.3.2 EICM material inputs . . . 55
3.3.3.3 Other material properties . . . 56
3.3.4 Input data for bedrock materials . . . 56

4 Full implementation: preliminary implementation vs. calibration 58
4.1 The MEPDG in the US . . . 59
4.2 The MEPDG outside the US . . . 59
4.3 The MEPDG State of the art in Italy . . . 61
4.4 Introduction of the MEPDG in the Italian context . . . 61

5 Framework for the local implementation of the MEPDG 62
5.1 Climate section . . . 62
5.1.1 Available climate data for the local implementation . . . 63
5.1.1.1 Field observations from weather stations . . . 63
5.1.1.2 Reanalysis models: ERA5 and MERRA-2 datasets . . . 64
5.1.2 Processing and statistical comparison of climatic data . . . 67
5.1.2.1 Temperature . . . 68
5.1.2.2 Wind speeed . . . 77
5.1.2.3 Sunshine . . . 81
5.1.2.4 Precipitation . . . 85
5.1.2.5 Relative humidity . . . 89
5.1.3 Final considerations . . . 93

5.2 Traffic section . . . 93
5.2.1 Traffic input levels: a new approach for the Italian implementation 93
5.2.2 Traffic data processing . . . 95
5.2.2.1 WIM data processing for the new Input Level 1 . . . 97
5.2.2.2 AVC or camera data analysis for the new Input Level 2 98
5.2.2.3 Manual traffic count for the new Input Level 3 . . . 98
5.3 Materials section . . . 98
5.3.1 Mixture-specific calibration for the damage models . . . 98
5.3.1.1 Fatigue cracking model . . . 99
5.3.1.2 Rutting model . . . 101
5.3.1.3 Thermal cracking model . . . 105
5.3.2 Italian Standards for the materials characterization . . . 105
5.3.2.1 Experimental procedures for the input variables determination . . . 106
5.3.2.2 Experimental procedures for the damage functions calibration . . . 107

6 Case studies **109**
6.1 The AASHTOWare Pavement ME Design software . . . 111
6.2 Data for the local implementation and sensitivity analysis . . . 111
6.2.1 Climate data . . . 111
6.2.2 Traffic data . . . 115
6.2.2.1 Input Level 1: the Salerno to Napoli A3 motorway . . 115
6.2.2.2 Input Level 1: the SS45bis highway in Trento . . . 122
6.2.2.3 Input Levels 2 & 3 . . . 128
6.2.3 Materials data . . . 134
6.3 The sensitivity analysis matrix . . . 137

7 Results and discussion **140**
7.1 Traffic sensitivity analysis . . . 140
7.1.1 Trento . . . 140
7.1.2 Napoli . . . 142
7.2 Materials sensitivity analysis . . . 143
7.3 Climate sensitivity analysis . . . 149

8 Conclusions **152**
8.1 Limitations and future work 152

A Climate and traffic data processing for the local implementation **158**
A.1 ERA5 reanalysis raw data processing 158
A.2 WIM data processing for the new Input Level 1 165
A.3 Development of the CNR-based axle load distributions 180

B Axle load distributions for the case studies **186**
B.1 Axle load distributions for the A3 motorway in Napoli 186
B.2 Axle load distributions for the SS45bis highway in Trento 197

C User guide to AASHTOWare Pavement ME Design **208**
C.1 Climate module 209
C.2 Materials module 211
C.3 Traffic module 214

List of Figures

1.1 Typical vehicle class distribution for each road category, [7] 3
1.2 Truck classes, number of axles, and load distribution on each axle, [7] . 4
1.3 Traffic volume on the most loaded lane, [7] 4
1.4 Prevailing climate conditions of central Italy, [7] 4
1.5 Physical and mechanical properties of materials, [7] 5
1.6 Catalog page for rural motorways, [7] 6

2.1 Temperature distribution for a given analysis period, [4] 11
2.2 Transverse positions for tensile strain calculation, [21] 13
2.3 Linear damage accumulation according to the Miner's law 15
2.4 In-field actual damage accumulation for bottom-up fatigue cracking . . 16
2.5 In-field actual damage accumulation for top-down fatigue cracking . . . 16
2.6 Equivalent cycles approach for the calculation of the plastic deformation in the HMA layer, [21] 20
2.7 Standard Normal PDF and z-score 25

3.1 Finite difference pavement section, [9] 28
3.2 Variation in solar intensity, [9] 31
3.3 Effect of the temperature on the heat capacity, [9] 33
3.4 FHWA vehicle classification scheme [17] 34

4.1 Aggregation of the Italian CNR-based vehicle classes into the FHWA classes, [6] 61

5.1 MERRA-2 inst1_2d_asm_Nx dataset 65
5.2 MERRA-2 tavg1_2d_rad_Nx dataset 65
5.3 MERRA-2 tavg1_2d_flx_Nx dataset 66
5.4 Comparison between measured and modeled temperature data 69

5.5 Comparison between measured and modeled temperature data for the 1st quintile . . . 70
5.6 Comparison between measured and modeled temperature data for the 2nd quintile . . . 71
5.7 Comparison between measured and modeled temperature data for the 3rd quintile . . . 72
5.8 Comparison between measured and modeled temperature data for the 4th quintile . . . 73
5.9 Comparison between measured and modeled temperature data for the 5th quintile . . . 74
5.10 Trend of the monthly mean bias for temperature . . . 75
5.11 Trend of the monthly mean RMSE for temperature . . . 76
5.12 Comparison between measured and modeled wind speed data . . . 78
5.13 Trend of the monthly mean bias for wind speed . . . 79
5.14 Trend of the monthly mean RMSE for wind speed . . . 80
5.15 Comparison between measured and modeled sunshine data . . . 82
5.16 Trend of the monthly mean bias for sunshine . . . 83
5.17 Trend of the monthly mean RMSE for sunshine . . . 84
5.18 Comparison between measured and modeled precipitation data . . . 86
5.19 Trend of the monthly mean bias for precipitation . . . 87
5.20 Trend of the monthly mean RMSE for precipitation . . . 88
5.21 Comparison between measured and modeled RH data . . . 90
5.22 Trend of the monthly mean bias for RH . . . 91
5.23 Trend of the monthly mean RMSE for RH . . . 92
5.24 Italian to FHWA class mapping . . . 97
5.25 Exponential trend of the C–S curve in the VECD model . . . 100
5.26 RLPD test configuration, [38] . . . 102
5.27 ϵ_p-N plot, [38] . . . 102
5.28 RLPD curve horisontal shifting, [35] . . . 104

6.1 The SS45bis highway (TN). Source: OpenStreetMap . . . 110
6.2 The A3 motorway (NA). Source: OpenStreetMap . . . 110
6.3 AASHTOWare PavME Design logo . . . 111
6.4 Monthly temperature summary – Trento . . . 112
6.5 Monthly wind speed summary – Trento . . . 112

6.6 Monthly sunshine summary – Trento . . . 113
6.7 Monthly precipitation summary – Trento . . . 113
6.8 Monthly RH summary – Trento . . . 113
6.9 Monthly temperature summary – Napoli . . . 114
6.10 Monthly wind speed summary – Napoli . . . 114
6.11 Monthly sunshine summary – Napoli . . . 114
6.12 Monthly precipitation summary – Napoli . . . 115
6.13 Monthly RH summary – Napoli . . . 115
6.14 Location of the WIM devices on the A3 motorway, [18] . . . 116
6.15 Single axle load distributions of vehicle classes 4 and 5 – August . . . 120
6.16 Single axle load distributions of vehicle classes 6 and 8 – August . . . 121
6.17 Single axle load distributions of vehicle classes 9 and 11 – August . . . 121
6.18 Tandem axle load distributions – August . . . 122
6.19 Tridem axle load distributions – August . . . 122
6.20 Single axle load distributions of vehicle classes 4 and 5 – October . . . 125
6.21 Single axle load distributions of vehicle classes 6 and 8 – October . . . 126
6.22 Single axle load distributions of vehicle classes 9, 10, and 11 – October 126
6.23 Tandem axle load distributions of vehicle classes 6 and 8 – October . . 127
6.24 Tandem axle load distributions of vehicle classes 9 and 10 – October . 127
6.25 Tridem axle load distributions – October . . . 128
6.26 Quad axle load distribution – October . . . 128
6.27 Single axle load distributions of vehicle classes 4 and 5 – Napoli . . . 129
6.28 Single axle load distributions of vehicle classes 6 and 8 – Napoli . . . 129
6.29 Single axle load distributions of vehicle classes 9 and 11 – Napoli . . . 130
6.30 Tandem axle load distributions – Napoli . . . 130
6.31 Tridem axle load distributions – Napoli . . . 131
6.32 Single axle load distributions of vehicle classes 4 and 5 – Trento . . . 131
6.33 Single axle load distributions of vehicle classes 6 and 8 – Trento . . . 132
6.34 Single axle load distributions of vehicle classes 9 and 11 – Trento . . . 132
6.35 Tandem axle load distributions – Trento . . . 133
6.36 Tridem axle load distributions – Trento . . . 133

7.1 Optimized pavement section for Trento base scenario #1 . . . 141
7.2 Damage and IRI evolution over time for scenario #1, 2, and 3 . . . 141
7.3 Optimized pavement section for Napoli base scenario #8 . . . 142

7.4 Damage and IRI evolution over time for scenarios #8, 9, and 10 143
7.5 Damage and IRI evolution over time for scenarios #1 and 4 144
7.6 Damage and IRI evolution over time for scenarios #5 and 6 145
7.7 Optimized pavement section for scenario #7 146
7.8 Optimized pavement section for scenario #11 147
7.9 Damage and IRI evolution over time for scenario #7 148
7.10 Damage and IRI evolution over time for scenario #11 149
7.11 Damage and IRI evolution over time for scenarios #1 and 13 150
7.12 Damage and IRI evolution over time for scenarios #8 and 12 151

A.1 Road type-based traffic spectra 181
A.2 Traffic spectra aggregation into FHWA classes 181
A.3 Traffic spectra within FHWA class for each road type 182
A.4 Axle group-weighted traffic spectra (classes 1 to 4) 182
A.5 Axle group-weighted traffic spectra (classes 7 to 10) 182
A.6 Axle group-weighted traffic spectra (classes 11 to 16) 183

B.1 Single axle load distributions of vehicle classes 4 and 5 – October . . . 186
B.2 Single axle load distributions of vehicle classes 6 and 8 – October . . . 187
B.3 Single axle load distributions of vehicle classes 9 and 11 – October . . . 187
B.4 Tandem axle load distributions – October 188
B.5 Tridem axle load distributions – October 188
B.6 Single axle load distributions of vehicle classes 4 and 5 – November . . 189
B.7 Single axle load distributions of vehicle classes 6 and 8 – November . . 189
B.8 Single axle load distributions of vehicle classes 9 and 11 – November . . 190
B.9 Tandem axle load distributions – November 190
B.10 Single axle load distributions of vehicle classes 4 and 5 – December . . 191
B.11 Single axle load distributions of vehicle classes 6 and 8 – December . . 191
B.12 Single axle load distributions of vehicle classes 9 and 11 – December . . 192
B.13 Tandem axle load distributions – December 192
B.14 Tridem axle load distributions – December 193
B.15 Single axle load distributions of vehicle classes 4 and 5 – November . . 197
B.16 Single axle load distributions of vehicle classes 6 and 8 – November . . 197
B.17 Single axle load distributions of vehicle classes 9, 10, and 11 – November 198
B.18 Tandem axle load distributions of vehicle classes 6 and 8 – November . 198
B.19 Tandem axle load distributions of vehicle classes 9 and 10 – November 199

B.20 Tridem axle load distributions – November 199
B.21 Quad axle load distribution – November 200
B.22 Single axle load distributions of vehicle classes 4 and 5 – December . . 200
B.23 Single axle load distributions of vehicle classes 6 and 8 – December . . 201
B.24 Single axle load distributions of vehicle classes 9, 10, and 11 – December 201
B.25 Tandem axle load distributions of vehicle classes 6 and 8 – December . 202
B.26 Tandem axle load distributions of vehicle classes 9 and 10 – December 202
B.27 Tridem axle load distributions – December 203
B.28 Quad axle load distribution – December 203

C.1 PavMe main interface 208
C.2 The LTPP InfoPave section for the download of the climate datasets . 210
C.3 The climate module in the PavME Software 211
C.4 The materials module in the PavME Software 212
C.5 Resilient modulus input interface in PavME 213
C.6 PavMe interface for the transfer and damage functions calibration . . . 213
C.7 The traffic module in the PavME Software 214
C.8 The traffic module in the PavME Software: single axle load distribution factors 214

List of Tables

3.1 Minimum Sample Size (Number of Days per Year) to Estimate the Normalized Axle-Load Distribution—WIM Data [4] 35
3.2 Suggested default values for the average number of single, tandem, and tridem axles per truck class, [3] 35
3.3 Traffic volume – base year information sources for different input levels 37
3.4 Raw data sources and spatial scale for the vehicle class distribution . . 38
3.5 Truck Traffic Classes, [3] 38
3.6 Typical vehicle class distributions associated with each TTC, [3] 39
3.7 Layout of the axle load distribution table for the single axle group . . . 41
3.8 Raw data sources for general traffic inputs 41
3.9 Recommended code values, [3] 45
3.10 Testing temperatures and loading frequencies for mixture and binder characterization, [3] 47
3.11 Binder tests and conversion to viscosity, [3] 47
3.12 Characterization of the asphalt mixture for Input Level 2, [3] 49
3.13 Recommended ranges of the Poisson's ratio as a function of temperature at Input Level 2C, [3] 51
3.14 Typical values of the Poisson's ratio as a function of temperature at Input Level 3, [3] 52
3.15 Typical ranges and values of Poisson's ratio for Input Level 3, [3] . . . 55
3.16 Poisson's ratio for bedrock materials at different Input Levels 56
3.17 Modulus of elasticity for bedrock materials at different Input Levels . . 57

5.1 Meteorological variables used for the climatic characterization 63
5.2 New approach for traffic input levels 94

6.1 Summary of the active WIM stations all year round 117
6.2 Detailed count of passages for the A3 motorway traffic 118

6.3 Directional and lane distribution factors for the A3 motorway traffic . . 118
6.4 Vehicle class distribution for the A3 motorway traffic 119
6.5 Number of axles per truck for the A3 motorway traffic 119
6.6 Monthly Adjustment Factors for the A3 motorway traffic 120
6.7 Vehicle class distribution for the SS45bis highway traffic 124
6.8 Number of axles per truck for the SS45bis highway traffic 124
6.9 Monthly Adjustment Factors for the SS45bis highway traffic 125
6.10 CNR-based axle per truck definition 134
6.11 WC1 – Dynamic modulus data expressed in MPa 134
6.12 WC1 – Dynamic modulus data expressed in psi 135
6.13 WC3 – Dynamic modulus data expressed in MPa 135
6.14 WC3 – Dynamic modulus data expressed in psi 135
6.15 Complex modulus measured at 1.59 Hz loading frequency 135
6.16 Mixture-specific coefficients 136
6.17 Global calibration coefficients 137
6.18 Sensitivity analysis matrix – Trento section 138
6.19 Sensitivity analysis matrix – Napoli section 139
6.20 Climate sensitivity analysis matrix 139

A.1 CNR-based axle load distributions for single, tandem, and tridem groups – Rural motorways 184
A.2 CNR-based axle load distributions for single, tandem, and tridem groups – Two-lane tourist highways 185

B.1 Single axle load distribution factors for August, October, November, December 194
B.2 Tandem axle load distribution factors for August, October, November, December 195
B.3 Tridem axle load distribution factors for August, October, November, December 196
B.4 Single axle load distribution factors for October, November, December 204
B.5 Tandem axle load distribution factors for October, November, December 205
B.6 Tridem axle load distribution factors for October, November, December 206
B.7 Quad axle load distribution factors for October, November, December . 207

Listings

A.1 Python script for ERA5 data processing 158
A.2 Python script for WIM data filtering and FHWA vehicle classification . 165
A.3 Python script for axle-load distribution generation 173

Introduction

A rigorous and valuable national pavement design approach should fulfil two main requirements. First, its outcomes must be demonstrable and replicable, in accordance with the scientific method. Second, the approach should address contemporary challenges related to climate change and resource scarcity, which have led to the adoption of innovative materials and technologies. Therefore, flexibility is essential to accommodate different input data depending on the specific design case, and purely empirical methods should be replaced by mechanistic-empirical ones.

Over the years, several national organisations and private companies have proposed mechanistic-empirical approaches for the design of asphalt and concrete pavements. This is the case for the Asphalt Institute method (USA), the Shell method (The Netherlands), the Austroads method (Australia), the LCPC-SETRA method (France), the DMRB method (United Kingdom), the BRRC method (Belgium), and the South African Mechanistic Design Method (SAMDM).

To date, no Italian organization has developed a national mechanistic-empirical design procedure for pavements. The adoption of different and inconsistent design methods across the country prevents a rational definition of the final pavement structure. For this reason, the development of a unified and rigorous design approach in Italy is highly desirable.

This thesis is structured as follows.

Chapter 1 provides an overview of the methodologies that are currently employed for pavement design in Italy, highlighting the need for a mechanistic-empirical design approach for the Country.

Chapter 2 describes the MEPDG framework, developed on the basis of the NCHRP 1-37A Project, [3].

Chapter 3 provides a description of the input requirements of the method, along with their processing within the MEPDG.

Chapter 4 is a review of the current literature about the approach to the MEPDG out-

side the US, and in Italy.
Chapter 5 presents a proposal for a framework for the local implementation of MEPDG for the Italian context. The term "implementation" is intended to refer to the initial step in the broader process of full implementation, which includes local calibration as its final stage.
Chapter 6 illustrates the sensitivity analysis carried out for two case studies using the proposed framework to assess the impact of different traffic descriptions and material performance in specific climate conditions.
Chapter 7 reports the results of the sensitivity analysis and discusses the implications of the findings.
Chapter 8 highlights the main limitations of the study, together with recommendations for future work.

The approach offered by MEPDG represents one of several valid mechanistic–empirical design methodologies and is not intended to be the ultimate one.

All the analyses and investigations carried out in the present work concern new flexible pavements only. The analysis of new and rehabilitated rigid pavements, as well as rehabilitated flexible pavements, is beyond the scope of this thesis.

The aim of this thesis is to make a first step toward the adoption of an Italian mechanistic–empirical design procedure. The work is not exhaustive in this regard, as the transfer functions implemented in the analyses are not locally calibrated to Italian conditions.

From a cultural viewpoint, the ultimate goal is to encourage the scientific community to reflect on whether current practices can be improved.

The outcomes of this work may lead to two main paths to be followed at the same time in the future. The first is the calibration of the transfer functions for local Italian conditions. The second is a possible agreement with Applied Research Associates (ARA) to develop a modified version of the PavME software capable of accommodating Italian traffic input data and, ultimately, promoting the full implementation of the software as part of a new Italian pavement design approach.

Chapter 1

The current Italian practice for pavement design

In the absence of a unified national pavement design methodology, the Italian design practice relies on a combination of technical guidelines, empirical procedures, and engineering experience. Among the available references, the Italian Pavement Catalog ([7]), published by the National Research Council (NRC), is one of the most widely used tools for the preliminary definition of pavement structures.

The catalog provides a set of predefined pavement sections associated with different traffic categories and subgrade conditions. Although some rational tools were used to design the pavement sections, the approach itself is empirical because the input data on climate, traffic, and materials are not treated as case-specific, and their variability is overlooked. Rather, a set of typical traffic spectra based on the road category is provided, as shown in fig. 1.1

	Tipo di veicolo															
Tipo di strada	1	2	3	4	5	6	7	8	9	10	11	12	13	14	15	16
1) autostrade extraurbane	12.2	----	24.4	14.6	2.4	12.2	2.4	4.9	2.4	4.9	2.4	4.9	0.10	----	----	12.2
2) " urbane	18.2	18.2	16.5	----	----	----	----	----	----	----	----	----	1.6	18.2	27.3	----
3) strade extr. principali e secondarie a forte traffico	----	13.1	39.5	10.5	7.9	2.6	2.6	2.5	2.6	2.5	2.6	2.6	0.5	----	----	10.5
4) strade extraurb. second. ordin.	----	----	58.8	29.4	----	5.9	----	2.8	----	----	----	----	0.2	----	----	2.9
5) " extr. second.-turistiche	24.5	----	40.8	16.3	----	4.15	----	2	----	----	----	----	0.05	----	----	12.2
6) " urbane di scorrimento	18.2	18.2	16.5	----	----	----	----	----	----	----	----	----	1.6	18.2	27.3	----
7) " " di quartiere e locali	80	----	----	----	----	----	----	----	----	----	----	----	----	20	----	----
8) corsie preferenziali	----	----	---	----	----	----	----	---	----	----	---	----	----	47	53	----

Figure 1.1: Typical vehicle class distribution for each road category, [7]

Sixteen heavy vehicle classes are considered in the catalog, provided in fig. 1.2.

Tipo di veicolo	N° Assi	Distribuzione dei carichi per asse in KN
1) autocarri leggeri	2	↓10 ↓20
2) " "	"	↓15 ↓30
3) autocarri medi e pesanti	"	↓40 ↓80
4) " " "	"	↓50 ↓110
5) autocarri pesanti	3	↓40 ↓80 ↓80
6) " "	"	↓60 ↓100 ↓100
7) autotreni e autoarticolati	4	↓40 ↓90 ↓80 ↓80
8) " "	"	↓60 ↓100 ↓100 ↓100
9) " "	5	↓40 ↓80 ↓80 ↓80 ↓80
10) " "	"	↓60 ↓90 ↓90 ↓100 ↓100
11) " "	"	↓40 ↓100 ↓80 ↓80 ↓80
12) " "	"	↓60 ↓110 ↓90 ↓90 ↓90
13) mezzi d'opera	"	↓50 ↓120 ↓130 ↓130 ↓130
14) autobus	2	↓40 ↓80
15) "	2	↓60 ↓100
16) "	2	↓50 ↓80

Figure 1.2: Truck classes, number of axles, and load distribution on each axle, [7]

Traffic volume is discretized into six groups by passages of heavy vehicles on the most loaded lane, as illustrated in fig. 1.3.

Livello di traffico	Numero di veicoli commerciali
1°	400.000
2°	1.500.000
3°	4.000.000
4°	10.000.000
5°	25.000.000
6°	45.000.000

Figure 1.3: Traffic volume on the most loaded lane, [7]

Climate data for flexible pavement design include the seasonal average temperature, the seasonal average daily temperature range, the seasonal average solar radiation, and the annual average wind speed. The climate conditions are considered representative of central Italy for locations at elevations below 100 m.

	TEMPERATURA MEDIA STAG. DELL'ARIA (°C)	MEDIA STAGION. ESCURS. TERMICA GIORNALIERA (°C)	RADIAZIONE SOLARE MEDIA STAG. (Kcal/m^2,d)	VELOCITA' DEL VENTO MEDIA ANNUA (km/h)
INVERNO	4.5	6	2718	13
PRIMAVERA	11.5	7.5	5785	
ESTATE	22.0	10.6	3547	
AUTUNNO	14.0	8.3	6507	

Figure 1.4: Prevailing climate conditions of central Italy, [7]

The asphalt concrete characterization accounts for the volumetric properties (namely, the particle size distribution, the percent binder content by weight of the mixture, and the air voids from the Marshall mix design) and the Marshall stability and stiffness.

The characterization is based on the layer type (wearing course, binder course, or base course) and four levels of traffic volume (from light to very high) other than those presented in fig. 1.3. The unbound materials are characterized using the California Bearing Ratio (CBR). The characterization of asphalt concrete and unbound materials recommended in the catalog is summarized in fig. 1.5.
Subgrade is assumed to perform according to three levels of bearing capacity:

- $M_r = 30\,\text{MPa}$,
- $M_r = 90\,\text{MPa}$, or
- $M_r = 150\,\text{MPa}$.

Conglomerato bituminoso per strato di usura

traffico	granulometria	bitume	stabilità Marshall (75 colpi)		rigidezza Marshall	vuoti residui Marshall
(1)	(2)	(%)	(Kg)	(daN)	(Kg/mm)	(%)
PP	fig. 1	4.5÷6	≥1100	≥1080	300÷450	4÷6
P	"	"	≥1100	≥1080	300÷450	4÷6
M	"	"	≥1000	≥980	>300	3÷6
L	"	"	≥1000	≥980	>300	3÷6

Densità in opera (rispetto alla densità Marshall) ≥ 97%

Conglomerato bituminoso per strato di collegamento

traffico	granulometria	bitume	stabilità Marshall (75 colpi)		rigidezza Marshall	vuoti residui Marshall
(1)	(2)	(%)	(Kg)	(daN)	(Kg/mm)	(%)
PP	fig.2	4.5÷5.5	≥1000	≥980	300÷450	3÷6
P	"	"	≥1000	≥980	300÷450	3÷6
M	"	4÷5.5	≥ 900	≥880	>300	3÷7
L	"	"	≥ 900	≥880	>300	3÷7

Densità in opera (rispetto alla densità Marshall) ≥ 98%

Conglomerato bituminoso per strato di base

traffico	granulometria	bitume	stabilità Marshall (75 colpi)		rigidezza Marshall	vuoti residui Marshall
(1)	(2)	(%)	(Kg)	(daN)	(Kg/mm)	(%)
PP	fig.3	4÷5	≥800	≥780	>250	4÷7
P	"	"	≥800	≥780	"	"
M	"	3.5÷4.5	≥700	≥690	"	"
L	"	"	≥700	≥690	"	"

Densità in opera (rispetto alla densità Marshall) ≥ 98%

Misto granulare non legato

CBR (dopo 4gg di immersione in acqua)	CBR ≥ 30%
Densità (rispetto alla densità AASHTO modificata)	≥ 98%

Figure 1.5: Physical and mechanical properties of materials, [7]

The structural design of the catalog solutions was then performed according to the methodology of the "AASHTO Guide for Design of Pavement Structures", which is empirical by definition, and the multi-layer elastic theory, which provides the rational basis. However, the actual structural design procedure used remains unclear.

By way of example, fig. 1.6 shows the available pavement sections for rural motorways, to be selected according to the subgrade bearing capacity and the traffic volume class.

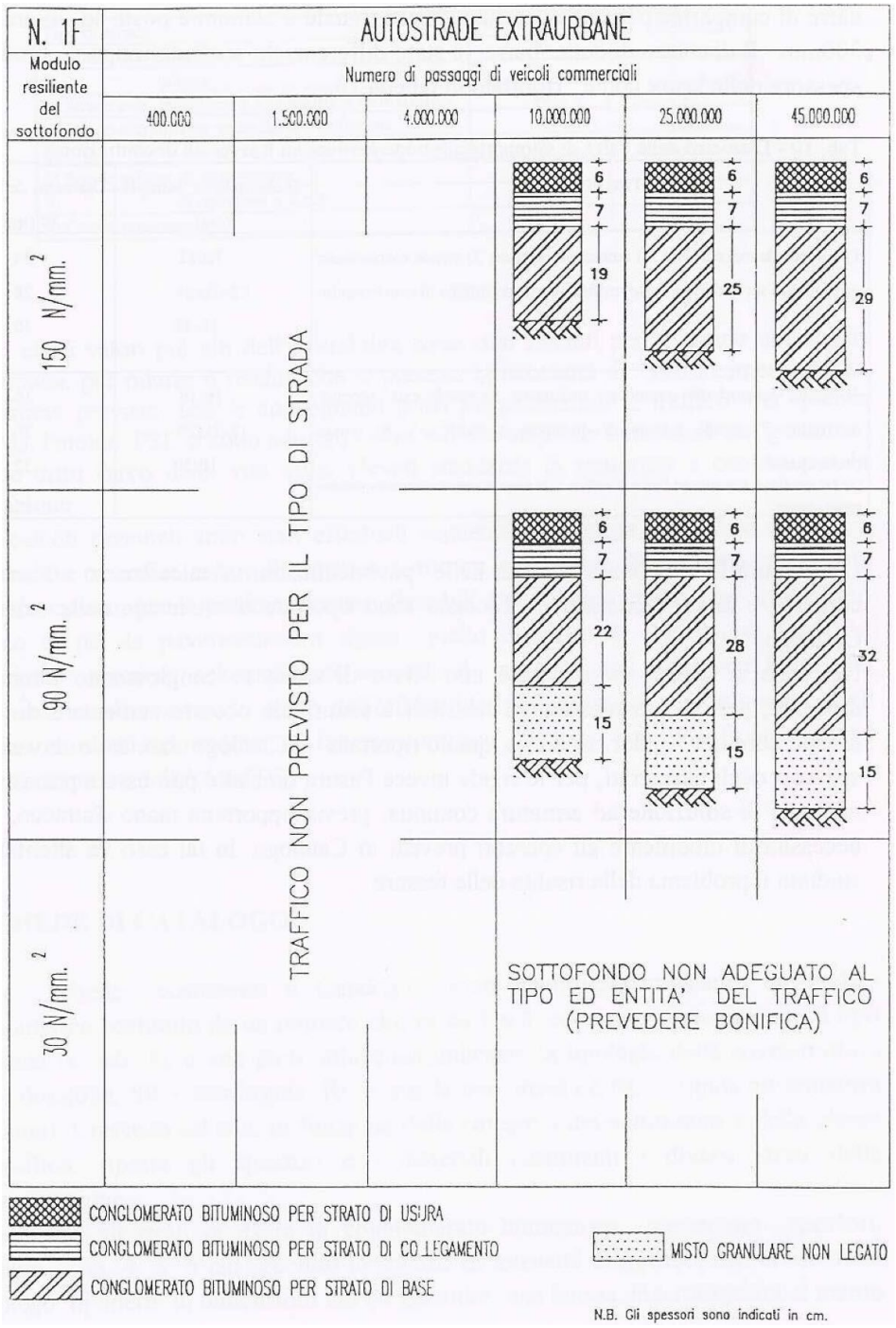

Figure 1.6: Catalog page for rural motorways, [7]

An issue that needs to be highlighted is that the NRC catalog dates back to 1985. This point makes the assumption and guidelines provided in such a document obsolete. This is especially true, provided that this methodology is mainly empirical rather than rational. As a consequence, it does not account for the differences that occurred over

30 years in terms of materials properties, traffic characterization, climate change, and design needs.

In addition, current practice often relies on Equivalent Single Axle Loads (ESALs) to characterize traffic. The load equivalency factor enables a damage-based design framework; however, it cannot represent the actual traffic load spectra experienced by the pavement.

Despite the availability of different tools, the current Italian practice cannot be considered a fully mechanistic–empirical design framework. Instead, pavement design is often based on a combination of catalog solutions, empirical relationships, and engineering judgment, rather than on a unified methodology that can account for the variability and specificity of key design inputs to explicitly predict pavement performance.

This lack of a consistent mechanistic–empirical framework highlights the need for a more structured approach to pavement design in the Italian context. In this regard, the Mechanistic–Empirical Pavement Design Guide (MEPDG) serves as a potential reference framework for developing a performance-based pavement design methodology.

Chapter 2

The MEPDG and NCHRP 1-37A Project

The design approach for road pavement design is an iterative process according to the MEPDG. The same flowchart is implemented in the AASHTOWare Pavement Mechanistic Empirical Design Software, which is owned by AASHTO and developed by ARA.

The aim of the algorithm is to assess whether the trial section is verified for both the loading and thermal distress over the selected design life. Specifically, the loading distresses under analysis for flexible pavements are alligator cracking, which includes bottom-up and top-down fatigue cracking, and rutting. On the other hand, thermal cracking is the non-loading-related distress for HMA pavements. The pavement section is verified if failure due to any of the aforementioned distresses occurs no earlier than the end of the design life.

The starting point of the algorithm is the trial design configuration for the road section. The designer may choose the number of bound and unbound layers, as well as their mechanical and volumetric properties, according to other mechanistic-empirical design procedures, a design catalogue, or their own experience.

Regarding flexible pavements, the [4] suggests limiting the initial number of layers to no more than 7 (3 HMA layers, an unbound aggregate base, a stabilized subgrade or improved embankment, the subgrade layer, and a rigid layer) to optimize the number of inputs to enter.

The second piece of information needed to run the algorithm is a set of input data on materials, climatic conditions, and traffic loads. These are specific to the design in question to ensure an accurate definition of the final section. The quality of the outcome is strictly related to the specification of the input data.

In summary, two pieces of information are provided: the trial design configuration and the input data. The input data refer to traffic, climate, and materials, and are classified using a hierarchical approach. Three input levels are identified for the traffic and material data categories. The higher the input level, the higher the accuracy of the modeling output. The choice of the input level depends on the strategic importance of the project and the relevance of the parameter, since the time and economic burden of collecting more accurate input data is higher. The designer may select a combination of input levels for the three categories because the computational algorithm for distress and damage is the same regardless of the input level selected.

When the algorithm runs, a sequence of calculations is performed based on the inputs. Here is the heart of the mechanistic-empirical method. The initial part of the process is a rational or mechanistic analysis of the pavement section. A structural analysis is carried out to obtain the responses in terms of stresses, strains, and deflections at several critical points within the sections. The structural model used to analyze flexible pavements is Burmister's multi-layered elastic theory. The outcomes of the structural analysis serve as inputs to the next module, which computes the effective damage level for each distress. The damage and transfer functions empirically relate the pavement's structural responses to its damage level.

The ultimate goal is to model how pavement damage develops over time as the number of load repetitions increases. The result is the trend of damage over time, rather than its instantaneous value at the end of the design life. The process is an advantage of the method because it actually accumulates damage as it occurs in the field. The way in which damage accumulation is carried out depends on the type of distress considered and will be discussed later; in any case, time and depth discretizations of the pavement are applied.

Moreover, the International Roughness Index (IRI) is calculated as a function of its initial value, and the distresses mentioned above.

The ultimate verification of the trial section is probabilistic rather than deterministic: a reliability analysis is performed. The trial design is approved if the probability that the final distress or IRI is below its threshold value is at least equal to the selected reliability level.

In the end, if the trial configuration is not verified, it must be modified and the analysis iterated again. The adjustment of the trial section usually concerns the number of layers and their thicknesses.

The procedure stops when verification is successful and all structural requirements

are met.

2.1 Time and pavement structure discretizations

Both temporal and depth discretizations are applied in the pavement model to evaluate distress. In particular, time discretization governs the handling of temperature data, which must be properly accounted for because it influences the variability of the time- and depth-dependent behavior of the HMA dynamic modulus and the resilient modulus of unbound layers.

The time for fatigue cracking and rutting evaluation is discretized differently from thermal cracking.

Because thermal cracking is intrinsic and closely related to the bitumen's failure temperature under tensile stress, an hourly time discretization is adopted for this distress. Thus, the stresses are computed hourly.

On the other hand, despite the dependence of loading crack and rut development on temperature, a monthly time discretization optimizes both computational load and accuracy. The base unit of one month is changed to 15 days during freeze/thaw periods to account for the rapid changes in the pavement's material properties.

This approach allows for capturing the damage caused by these extreme temperatures that may occur in a given month. If the average temperature value were considered, the evaluation of the distress would be oversimplified, and the results may be biased.

Specifically, the monthly temperatures are assumed to be normally distributed, as shown in fig. 2.1. Then, the Gaussian distribution is divided into 5 quintiles, each corresponding to 20% of the frequency distribution, and distresses are calculated as a function of the quintile's value of temperature.

In each quintile calculation, one-fifth of the total monthly truck traffic is considered. There is no tie between the normal distribution of temperatures and the distribution of traffic.

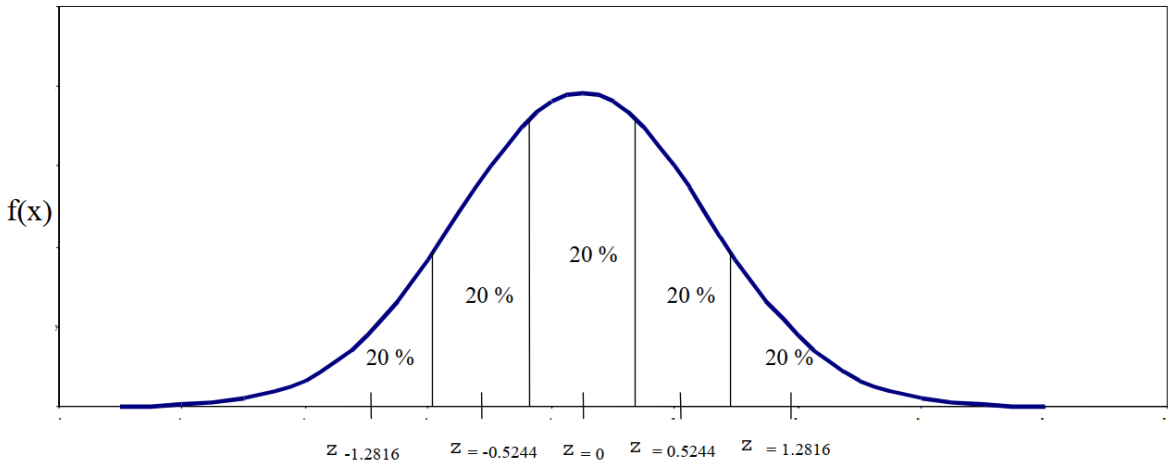

Figure 2.1: Temperature distribution for a given analysis period, [4]

The basic layout of pavement structure consists of three main layers. From the top, namely:

1. hot mix asphalt, including the wearing course, the binder course, and the base course;
2. granular material, often consisting of the base and the subbase layers;
3. subgrade layer.

Each of the aforementioned layers is divided into sub-layers. The structural responses are calculated in each sub-layer. In this way, it is possible to describe how stresses and strains develop within the pavement depth. Therefore, stresses and strains can be expressed as functions of pavement depth.

As a result of the joint time and depth discretizations:

$$E^* = f(\text{Temperature}, \text{Depth}) \Rightarrow \begin{cases} \varepsilon_{t,\text{fatgue}} = f(\text{Depth}) \\ \varepsilon_{c,\text{rutting}} = f(\text{Depth}) \end{cases} \tag{2.1}$$

$$M_R = f(\text{Temperature}, \vartheta = f(\text{Depth})) \Rightarrow \varepsilon_{c,\text{rutting}} = f(\text{Depth})$$

For completeness and accuracy, it is worth noting that the modulus of the asphalt layers also depends on the loading frequency. Moreover, the dynamic modulus is used to compute the creep compliance and the fracture parameter related to thermal cracking

distress, which will be discussed later. Therefore,

$$E^* = f(\text{Temperature}, \omega, \text{Depth}) \Rightarrow \begin{cases} \varepsilon_{t,\text{fatgue}} = f(\text{Depth}) \\ \varepsilon_{c,\text{rutting}} = f(\text{Depth}) \\ \text{Fracture parameter A} \\ m = \left| \frac{d\log D(t)}{d\log t} \right| \end{cases} \tag{2.2}$$

$$M_R = f(\text{Temperature}, \vartheta = f(\text{Depth})) \Rightarrow \varepsilon_{c,\text{rutting}} = f(\text{Depth})$$

2.2 Transfer functions and calibration coefficients for damage calculation

Three distresses are taken into consideration for the analysis of flexible pavements:

- fatigue cracking, including both
  - bottom-up cracking, also known as alligator cracking;
  - top-down cracking, also known as longitudinal.
- rutting;
- thermal cracking.

While fatigue cracking and rutting are caused by vehicle loading, thermal cracking is a non-load-related distress that occurs solely due to thermal action.

2.2.1 Transfer functions and damage accumulation: fatigue cracking

In the case of bottom-up fatigue cracking, the control parameter is the principal horizontal tensile strain at the bottom of the asphalt layer in the most critical transverse position. For each axle group (single, tandem, tridem, quad), the tensile strain is calculated under each axle and under the midway between two consecutive axles.

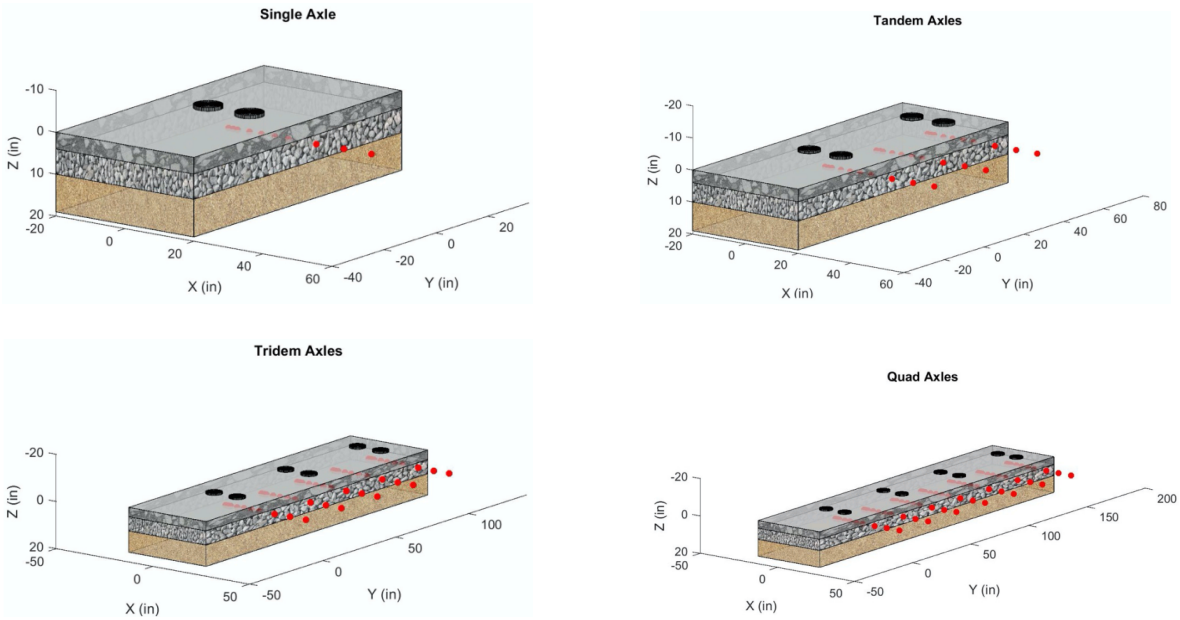

Figure 2.2: Transverse positions for tensile strain calculation, [21]

In the case of top-down cracking, the control parameter is the principal horizontal tensile strain at the top of the asphalt layer in the most critical transverse position. To this extent, the same rationale as bottom-up cracking critical positions applies to the different axle groups.

Once the tensile strains mentioned above are calculated, they are entered into the damage function that correlates distress with actual damage. Thus, the allowable number of axle-load applications is determined as follows:

$$N_{f-HMA} = k_{f1}\,(C)\,(C_h)\,\beta_{f1}\,(\epsilon_t)^{k_{f2}\beta_{f2}}\,(E_{HMA})^{k_{f3}\beta_{f3}} \tag{2.3}$$

where

- $N_{f\text{-}HMA}$ is the allowable number of axle-load applications for the flexible pavement in question;
- ϵ_t is the tensile strain at the critical locations, calculated by the structural response model, [in/in];
- E_{HMA} is the dynamic modulus of the hot mix asphalt measured in compression, [psi];
- $k_{f1} = 0.007566, k_{f2} = 3.9492, k_{f3} = 1.281$ are global field calibration coefficients;

- $\beta_{f1}, \beta_{f2}, \beta_{f3}$ are local field or mixture-specific calibration coefficients, set to 1.0 for global calibration purposes;
- $C = 10^M$, where
  - $M = 4.84 \left(\frac{V_{be}}{V_a + V_{be}} - 0.69 \right)$, where
    - V_{be} is the effective asphalt content by volume, [%];
    - V_a is the percent air voids in the hot mix asphalt mixture, [%];
- C_H is a thickness correction term depending on the type of cracking. Specifically, let H_{HMA} be the total thickness of the hot mix asphalt layer:
  - $C_H = \frac{1}{0.000398 + \frac{0.003602}{1 + e^{\left(11.02 - 3.49\, H_{HMA}\right)}}}$ for bottom-up (alligator) cracking;
  - $C_H = \frac{1}{0.01 + \frac{12.00}{1 + e^{\left(15.676 - 2.8186\, H_{HMA}\right)}}}$ for top-down (longitudinal) cracking.

The number of load repetitions thus calculated becomes the denominator of the incremental damage function, expressed as follows:

$$\Delta DI = \frac{n}{N_{all,f}} \tag{2.4}$$

where n is the actual number of load applications during the service life of the pavement.

The incremental damage function is implemented by considering a "multi-shell" discretization, which develops on several levels, listed below:

- years of service life (20, as a rule of thumb), t;
- climatic periods within a year (usually corresponding to the months), m;
- climatic quintiles, q;
- truck type according to the FHWA vehicle classification, k;
- axle type, a;
- axle load interval, l;
- wheel wonder quintiles, w.

The result is the expected cumulative damage at the end of the pavement's service life:

$$DI = \sum_{t=1}^{Years} \sum_{m=1}^{12} \sum_{q \in Q_{climate}}^{5} \sum_{k \in K_{truck}}^{10} \sum_{a \in A_{axle}} \sum_{l \in L_{load}} \sum_{y \in Y_{wander}}^{5} \frac{n_{t,m,q,k,a,l,y}}{N_{t,m,q,k,a,l,y}} \tag{2.5}$$

The relation considered so far is the Miner's law of damage accumulation, which linearly relates cumulative damage to loading repetitions, as shown in fig. 2.3.

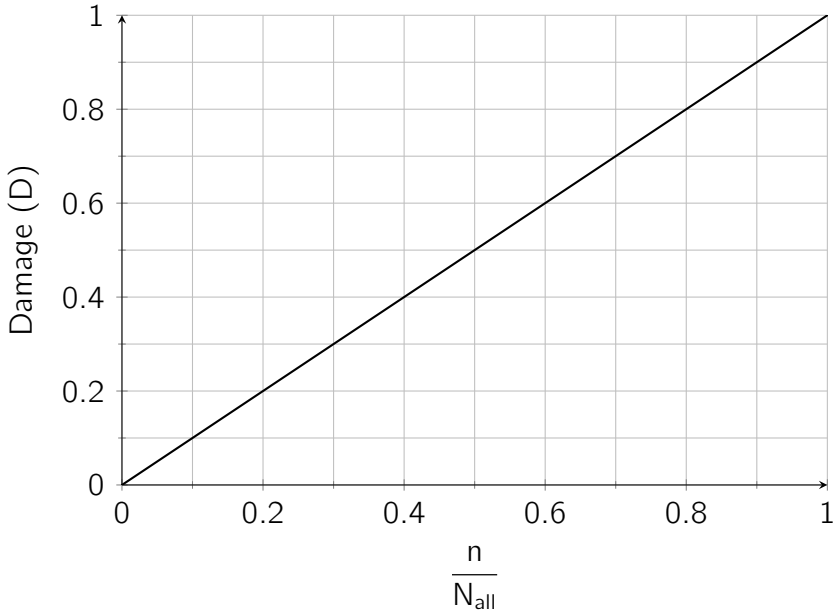

Figure 2.3: Linear damage accumulation according to the Miner's law

The Miner's law is not representative of the actual damage evolution that occurs in the field because it overlooks both aging effects and the ease of crack propagation rather than crack initiation. A more accurate representation of damage evolution is shown in figs. 2.4 and 2.5.

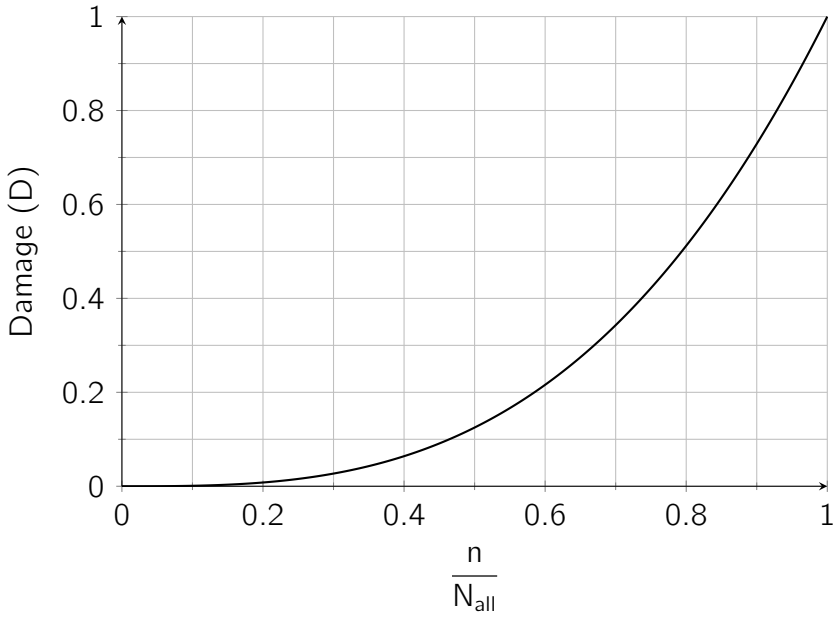

Figure 2.4: In-field actual damage accumulation for bottom-up fatigue cracking

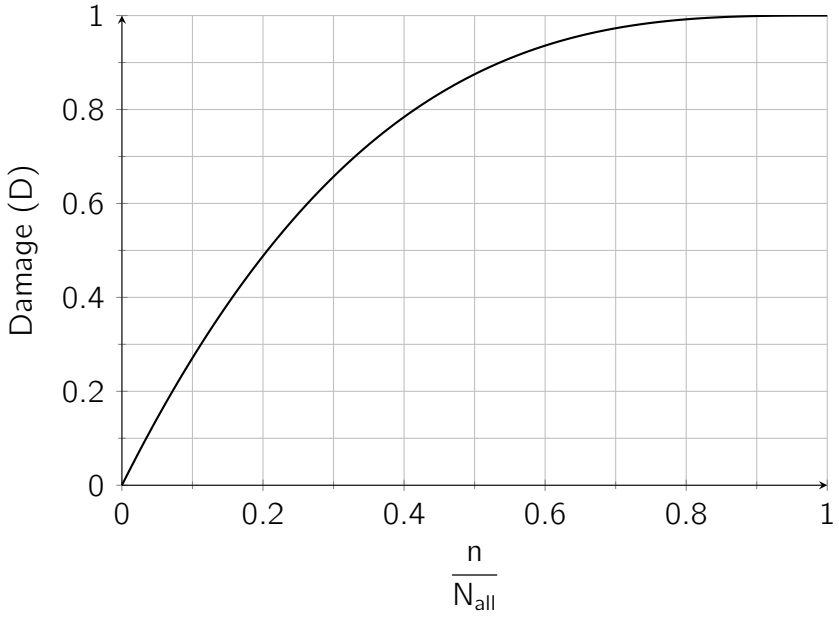

Figure 2.5: In-field actual damage accumulation for top-down fatigue cracking

In order to compensate for the lack of accuracy of the Miner's law in the prediction of the actual damage level, the cumulative damage DI thus calculated enters the fatigue cracking transfer function aimed at measuring the severity of the distress in terms of percent of lane area affected by cracks or total length of the cracks, in case of bottom-up or top-down propagation, respectively.

Specifically, for bottom-up or alligator cracking:

$$FC_{bu} = \left(\frac{1}{60}\right)\left(\frac{C_4}{1 + e^{\left(C_1 C_1^* + C_2 C_2^* \log(DI_{bu} \cdot 100)\right)}}\right) \tag{2.6}$$

where

- FC_{bu} is the area of alligator cracking that initiates at the bottom of the HMA layers calculated over the total lane area, [%];
- DI_{bu} is the cumulative damage index at the bottom of the HMA layers;
- $C_1 = 1.00, C_2 = 1.00, C_4 = 6000$ are transfer function regression constants;
- $C_1^* = -2C_2^*$
- $C_2^* = -2.40874 - 39.748\left(1 + H_{HMA}\right)^{-2.856}$

For top-down or longitudinal cracking, on the other hand:

$$FC_{td} = 10.56\left(\frac{C_4}{1 + e^{\left(C_1 - C_2 \log(DI_{td})\right)}}\right) \tag{2.7}$$

where

- FC_{td} is the length of longitudinal cracks that initiate at the top of the HMA layer, [ft/mi];
- DI_{td} is the cumulative damage index at the top of the HMA surface;
- $C_1 = 7.00, C_2 = 3.5, C_4 = 1000$ are transfer function regression constants.

The transfer function regression constants represent the goal of the MEPDG calibration effort to network and context-specific conditions.

2.2.2 Transfer functions and equivalent cycles approach: rutting

The total rut depth is given by the superposition of the effects of permanent deformations occurring in each layer of the pavement:

$$\Delta_p = \Delta_{p,HMA} + \Delta_{p,unbound} \tag{2.8}$$

where

- $\Delta_{p,HMA}$ is the depth of the rut that occurs in the hot mix asphalt layers, [in];
- $\Delta_{p,unbound}$ is the depth of the rut that occurs in the unbound layers, [in].

In the case of rutting, the control parameter is the permanent plastic deformation calculated at the mid-depth of each layer or sub-layer of the pavement structure. For the subgrade, permanent deformation is calculated at the surface and at a depth of 6 in. below the surface.

The depth of the rut in the hot mix asphalt layers is modeled as follows:

$$\Delta_{p,HMA} = \epsilon_{p,HMA} \cdot h_{HMA} \tag{2.9}$$

$$\frac{\epsilon_{p,HMA}}{\epsilon_{r,HMA}} = k_z \cdot \beta_{1r} \cdot 10^{k_{1r}} \cdot T^{\beta_{2r} k_{2r}} \cdot N^{\beta_{3r} k_{3r}} \tag{2.10}$$

where

- $\epsilon_{p,HMA}$ is the accumulated permanent or plastic axial strain in the HMA layer or sublayer, [in/in];
- $\epsilon_{r,HMA}$ is the resilient or elastic strain calculated by the structural response model at the mid-depth of each HMA layer or sublayer, [in/in];
- h_{HMA} is the thickness of the HMA layer or sublayer, [in];
- N is the number of axle load repetitions;
- T is the mix or pavement temperature, [°F];
- k_z is a depth confinement factor, which depends on the depth below the surface (D, [in]), and on the total HMA thickness (H_{HMA}, [in])

$$k_z = \big(C_1 + C_2 D\big) 0.328196^D \tag{2.11}$$

$$C_1 = -0.1039\big(H_{HMA}\big)^2 + 2.4868 H_{HMA} - 17.342 \tag{2.12}$$

$$C_2 = 0.0172\big(H_{HMA}\big)^2 - 1.7331 H_{HMA} + 27.428 \tag{2.13}$$

- $k_{1r} = -3.35412$, $k_{2r} = 0.4791$, $k_{3r} = 1.5606$ are globald field calibration parameters;
- β_{1r}, β_{2r}, β_{3r} are local or mixture field calibration constants, set to 1.0 for global calibration purposes.

In particular, while the formula in eq. (2.9) is the transfer function for rutting in the HMA layer, the formula in eq. (2.10) is the corresponding damage function.

The depth of the rut in the unbound layers is modeled as follows:

$$\Delta_{p,unbound} = \epsilon_{p,unbound} \cdot h_{unbound} \tag{2.14}$$

$$\epsilon_{p,unbound} = \beta_{s1} \cdot k_{s1} \cdot \epsilon_v \cdot h_{unbound} \cdot \left(\frac{\epsilon_0}{\epsilon_r}\right) \cdot e^{-\left(\frac{\rho}{n}\right)^{\beta}} \tag{2.15}$$

where

- $\epsilon_{p,unbound}$ is the permanent or plastic strain in the unbound layer or sublayer, [in/in];
- n is the number of axle load repetitions;
- ϵ_0 is the intercept determined from laboratory repeated load permanent deformation tests, [in/in];
- ϵ_r is the resilient strain imposed in the laboratory test to obtain the ϵ_0, β, and ρ, [in/in];
- ϵ_v is the average vertical resilient or elastic strain in the unbound layer or sublayer calculated by the structural response model, [in/in];
- β is a parameter dependent on the moisture content of the soil (W_c, [%])

$$\beta = 10^{-0.31119-0.017638\,W_c} \tag{2.16}$$

- ρ is a parameter dependent on β, on the resilient modulus of the unbound material (M_r, [psi]), and on coefficients $a_1 = 0.15$, $a_9 = 20.0$, $b_1 = 0.0$, and $b_2 = 0.0$

$$\rho = 10^9 \left(\frac{\ln\left(\frac{a_1 M_r^{b_1}}{a_9 M_r^{b_2}}\right)}{1 - 10^{\,9\beta}} \right)^{1/\beta} \tag{2.17}$$

- $h_{unbound}$ is the thickness of the unbound layer or sublayer, [in];
- k_{s1} is a global calibration coefficient ($k_{s1} = 2.03$ for granular materials, $k_{s1} = 1.35$ for fine-grained materials);
- β_{s1} is the local calibration constant, set to 1.0 for global calibration purposes.

In particular, while the formula in eq. (2.14) is the transfer function for rutting in the unbound layer, the formula in eq. (2.15) is the corresponding damage function.

Permanent deformation does not accumulate linearly with increasing loading cycles, so the strain-hardening approach must be used to calculate it. The strain-hardening approach can be implemented using the equivalent cycles method.

The application of the equivalent cycles approach in the HMA layer is illustrated in fig. 2.6: for each climatic period or month, the permanent deformation is calculated based on the actual temperature conditions. Let $n_{t,i-1}$ be the actual number of loading cycles, and $\epsilon_{p,i-1}$ be the total plastic strain at the end of the sub-season i-1: these quantities are retrieved on the transfer function curve related to the temperature T_{i-1} of the sub-season i-1. The plastic strain at the beginning of the next sub-season i is retrieved on the curve for the new prevailing conditions, and depends on the initial equivalent loading cycles $n_{t\text{-}equiv,i}$ for sub-season i, calculated from the following equation:

$$n_{t-equiv,i} = \left(\frac{\epsilon_{p,i-1}}{k_z \epsilon_{v,i} 10^{k_{1r}} T_i^{k_{2r}}} \right)^{\frac{1}{k_{3r}}} \tag{2.18}$$

By adding the actual number of load repetitions for season i (n_i) to the initial number of equivalent loading cycles ($n_{t\text{-}equiv,i}$), one can estimate the total plastic strain at the end of the climatic period ($\epsilon_{p,i}$).

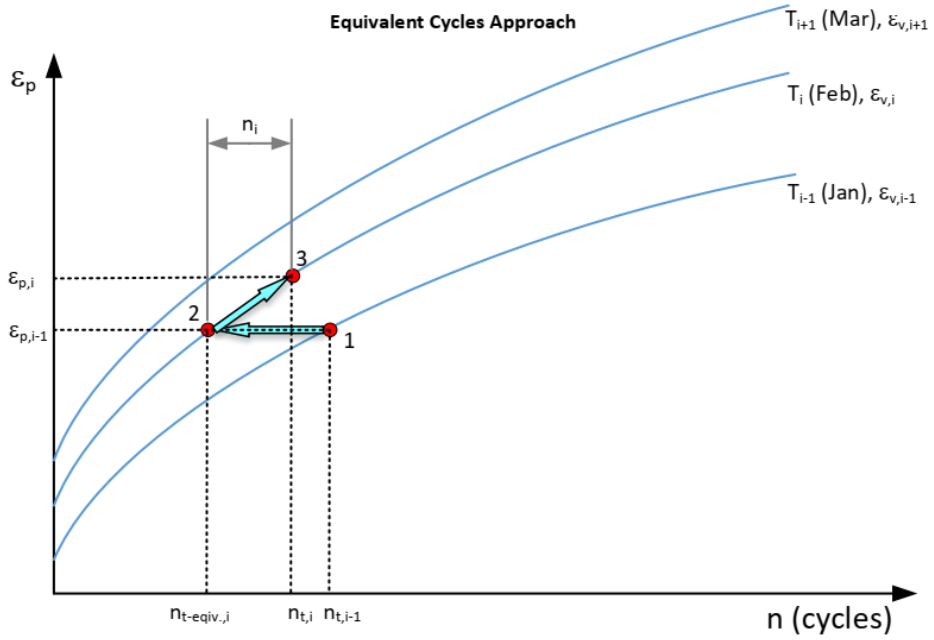

Figure 2.6: Equivalent cycles approach for the calculation of the plastic deformation in the HMA layer, [21]

The same rationale applies to the calculation of permanent deformation in the unbound layers, provided that the temperature is implicitly accounted for in the material's resilient modulus.

2.2.3 Transfer functions and crack propagation: thermal cracking

In the case of thermal cracking, the focus is on the depth of the crack in the hot-mix asphalt layer and its evolution over the pavement's service life. The computation of the crack depth is carried out on a daily and incremental basis:

$$C_0(t_{day}+1) = C_0(t_{day}) + \Delta C \tag{2.19}$$

where

- t_{day} is the time, [days];
- C_0 is the crack depth, [in];
- ΔC is the change in the crack depth due to a cooling cycle in a day, [in].

The incremental crack depth is calculated by means of the simplified Paris Law, which models the crack growth mechanism and is intended to function as both the damage and transfer equation for thermal cracking:

$$\Delta C = A \cdot \left(\Delta K\right)^n \tag{2.20}$$

where

- A is a fracture parameter for the HMA mixture, calculated as follows

$$A = k_t \beta_t \, 10^{\left[4.389 - 2.52 \log\left(E_{HMA}\sigma_m n\right)\right]} \tag{2.21}$$

  where

  - k_t is the global calibration coefficient;
  - β_t is the local or mixture calibration coefficient;
  - E_{HMA} is the indirect tensile modulus, [psi];
  - σ_m is the mixture tensile strength, [psi];

- n is another fracture parameter for the HMA mixture

$$n = 0.8\left[1 + \frac{1}{m}\right] \tag{2.22}$$

where m is derived from the creep compliance curve from laboratory testing:

$$m = \left|\frac{d\log D(t)}{d\log t}\right| \tag{2.23}$$

- ΔK change in the stress intensity factor, K, due to a cooling cycle

$$\Delta K = K_{max} - K_{min} \tag{2.24}$$

where K_{max} and K_{min} are the daily maximum and minimum stress intensity factors at depth of the crack tip, determined according to the corresponding values of daily maximum and minimum viscoelastic thermal stress σ_{max} and σ_{min}:

$$K_{min/max} = \sigma_{min/max}\left(0.45 + 1.99 \cdot C_0^{0.56}\right) \tag{2.25}$$

It is worth mentioning that while the stress intensity factors are calculated daily, the viscoelastic thermal stresses are calculated hourly, in line with the time discretization introduced in section 2.1. Once the maximum and minimum viscoelastic thermal stresses σ_{max} and σ_{min} are defined for the day under analysis, they are plugged into eq. (2.25). The viscoelastic stress response to the thermal strain is computed through the convolution integral between the relaxation modulus and the strain rate functions, in order to account for the deformation history and the relaxation properties of the mixture:

$$\sigma(t_r) = \left(E * \frac{\partial \epsilon}{\partial \tau}\right)(t_r) = \int_0^{t_r} E(t_r - \tau)\frac{\partial \epsilon}{\partial \tau}\, d\tau \tag{2.26}$$

By applying the linear law of thermal contraction, eq. (2.26) becomes

$$\sigma(t_r) = \int_0^{t_r} E(t_r - \tau) L_{HMA}\frac{\partial T}{\partial \tau}\, d\tau \tag{2.27}$$

where L_{HMA} is the thermal contraction coefficient of the material.
Finally, the evaluation of the observed amount of thermal cracking in ft/mi is probabilistic

rather than deterministic:

$$TC = \beta_{t1}\mathcal{N}\left[\frac{1}{\sigma_d}\log\left(\frac{C_d}{H_{HMA}}\right)\right] \tag{2.28}$$

where

- β_{t1} is a regression coefficient determined through global calibration;
- $\mathcal{N}$[z] is the standard normal distribution evaluated at z;
- σ_d is the standard deviation of the log of the depth of cracks in the pavement, [in];
- C_d is the crack depth, [in];
- H_{HMA} is the thickness of the HMA layers, [in].

2.3 Output and iterative process: the reliability analysis

Once the evolution of distress over the service life has been evaluated, the indicators are combined into the International Roughness Index, which measures the perceived discomfort caused by irregularities on the pavement surface. The IRI is calculated through the formula

$$IRI = IRI_0 + C_1 \cdot RD + C_2 \cdot FC_{total} + C_3 \cdot TC + C_4 \cdot (SF) \tag{2.29}$$

where

- IRI_0 is the initial IRI value after construction, and when the pavement is opened to traffic - the "base year" time, [in/mi];
- RD is the average rut depth, [in];
- FC_{total} is the percent area of fatigue cracking with respect to the total lane area:

$$FC_{total}[\%] = FC_{bu}[\%] + \frac{FC_{td}[ft/mi] \cdot 1[ft] \cdot Section\ Length[mi]}{Lane\ Area[ft^2]} \cdot 100 \tag{2.30}$$

- TC is the length of thermal cracking, [ft/mi];

- SF is the site factor, calculated in accordance to the following equation:

$$SF = Age^{1.5}\{\ln\left[(Precip+1)\,(FI+1)\,p_{02}\right]\} + \{\ln\left[(Precip+1)\,(PI+1)\,p_{200}\right]\} \tag{2.31}$$

  where

  - Age is the pavement age, [year];
  - PI is the plasticity index of the soil;
  - FI is the average annual freezing index, [°F days];
  - Precip is the average annual precipitation or rainfall, [in];
  - p_{02} is the percent passing the 0.02 mm sieve, [%];
  - p_{200} is the percent passing the 0.075 mm sieve, [%]

- $C_1 = 40.0, C_2 = 0.400, C_3 = 0.008, C_4 = 0.015$ are calibration factors.

The calibration factors represent the goal of the MEPDG calibration effort to network and context-specific conditions.

A reliability analysis is carried out to assess the validity of the trial design. The reliability level is intended to be the probability that the design will perform its intended function over the service life, that is, the probability of the distress or the IRI index being lower than a selected threshold:

$$R = P[Distress\ or\ IRI < Critical\ Distress\ or\ IRI] \tag{2.32}$$

Reliability values are statistically determined by various agencies and then selected by the designer based on the strategic importance of the pavement under analysis. The higher the reliability level, the lower the probability of failure and, consequently, the more conservative the design assumptions.

The normal distribution of the distress and the IRI values is considered

$$IRI \sim \mathcal{N}(\mu_{IRI}, s^2_{IRI}) \tag{2.33}$$

$$Distress \sim \mathcal{N}(\mu_d, s^2_d) \tag{2.34}$$

From a statistical view point, eq. (2.32) becomes

$$\begin{cases} IRI_{R=50\%} + z_R \cdot s_{IRI} < IRI_{threshold} \\ Distress_{R=50\%} + z_R \cdot s_d < Distress_{threshold} \end{cases} \tag{2.35}$$

where z_R is the z-score value, which depends on the selected reliability level. As illustrated in fig. 2.7, $R = P[z < z_R]$.

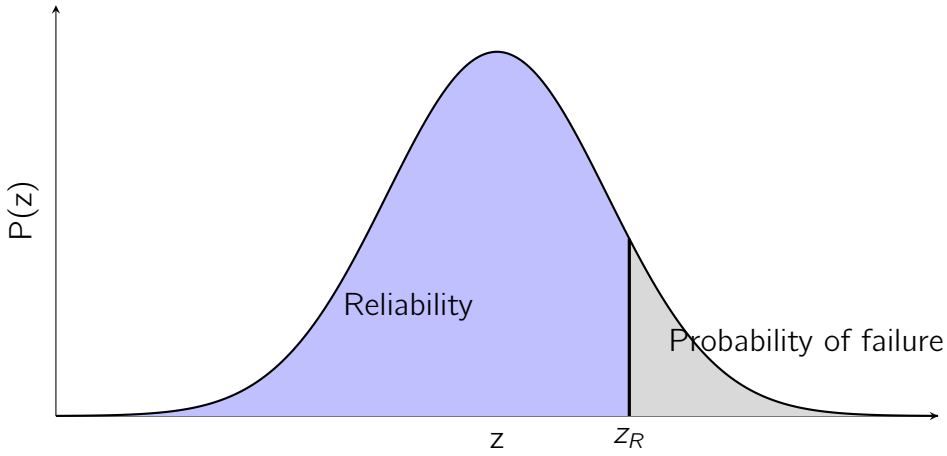

Figure 2.7: Standard Normal PDF and z-score

If the conditions in eq. (2.35) are met, the trial section is verified, and the design iterative process stops. If not, the trial section is modified, and a new iteration is performed.

Chapter 3

Requirements and processing for the input data within the MEPDG framework

3.1 Climate input data

The climate information required by the MEPDG is expressed in Imperial units. Such data are among the inputs to the Enhanced Integrated Climate Model (EICM), a program that simulates variations in the properties of pavements and subgrade materials as a function of temperature and moisture trends with depth and over time.

The inputs listed below should cover one design life cycle (i.e., 20 years):

- hourly air temperature, [K];
- hourly precipitation, [in];
- hourly wind speed, [mi/h];
- hourly sunshine percentage, [%];
- hourly relative humidity, [%].

Sunshine data are intended as complementary to cloud cover, measured as a percentage. The cloud cover is the portion of sky covered by clouds, expressed as a percentage (0 % = clear sky, 100 % = fully covered sky).

$$\text{Sunshine (\%)} = 100 - \text{Cloud Cover (\%)}$$

The algorithm embedded in the EICM is presented hereafter.

3.1.1 The heat transfer model for frost-action and temperature-related effects

Dempsey and Thompson [9] introduced the heat-transfer model that is currently embedded in the EICM. The model aims to simulate temperature trends within the pavement depth and, ultimately, detect freeze-thaw cycles. A one-dimensional, forward-finite-difference, heat transfer model was developed for this purpose. The hypothesis of one-dimensional heat transfer is supported by the fact that the depth of the frost penetration is small when compared to the pavement's width.

The finite-difference pavement system used in the heat-transfer model is illustrated in fig. 3.1.

The pavement section is discretised into 41 volume elements, each represented by the corresponding node at its mid-depth. Specifically,

- node 1 lies on the pavement's surface and the corresponding volume is one-half of a normal element;
- nodes 2 through 37 are identified as "normal nodes" and the thickness of their volume elements is ΔX;
- nodes 38, 39, and 40 are identified as "termination nodes" and the thickness of their volume elements is ΔW. The discretisation is rougher because the temperature is more stable with increasing pavement depth, and Y is the pavement depth beyond which the ground temperature is essentially constant for simulation purposes. In particular, setting $\Delta W = 3\Delta X$ is a worthwhile compromise between two effects:
    - the computational load is decreased;
    - the computational error is increased by a minimum amount (less than 1%).
- node 41 is a constant temperature node that simulates the heat transfer between the pavement and the interior of the earth.

Heat transfer within the pavement system is governed by the conduction phenomenon, which is modeled by the one-dimensional, second-order Fourier partial differential equation for conductive heat transfer:

$$\frac{\partial^2 T}{\partial x^2} = \frac{1}{\alpha}\frac{\partial T}{\partial t} \tag{3.1}$$

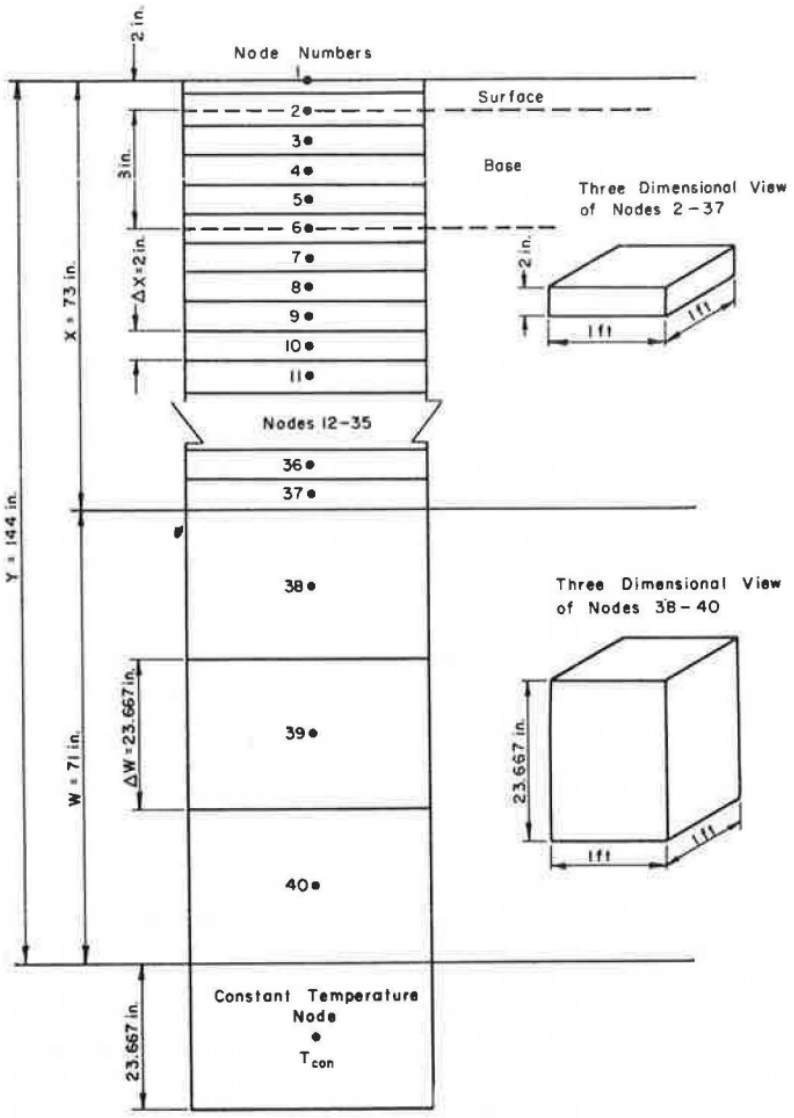

Figure 3.1: Finite difference pavement section, [9]

By applying a finite difference approximation to both time and space variables, (3.1) can be replaced by

$$\frac{T_{n-1} + T_{n+1} - 2T_n}{\Delta x^2} = \frac{1}{\alpha} \frac{T'_n - T_n}{\Delta t} \tag{3.2}$$

where the thermal diffusivity is

$$\alpha = \frac{K}{C\gamma} = \frac{K}{Q} \tag{3.3}$$

including:

- the thermal conductivity K, [Btu/(h · ft · °F)]
- the heat capacity Q, [Btu/(ft^3·°F)], obtained by the product of
    - the unit weight γ, [lb/ft^3], and
    - the specific heat capacity C, [Btu/(lb · °F)].

Equation (3.2) becomes then

$$\frac{K}{\Delta x}(T_{n-1} - T_n) + \frac{K}{\Delta x}(T_{n+1} - T_n) = \frac{\gamma C \Delta x}{\Delta t}(T'_n - T_n) \tag{3.4}$$

In the end, the simulation of the temperature trend is performed for successive (i.e. "forward") time intervals. Indeed, the temperature of a specific node at time t + Δt is computed as a function of the temperature of the node itself and the temperature of the adjacent nodes at time t:

$$T'_n = T_n(t + \Delta t) = f(T_{n-1}(t),\, T_n(t),\, T_{n+1}(t)) \tag{3.5}$$

Equation (3.1) is a second-order Partial Differential Equation (PDE) in the spatial domain, so two spatial boundary conditions are needed to solve it.

Node 1 and node 41 represent the boundary conditions of the finite element system. Namely, node 41 provides a Dirichlet boundary condition since T_{con} is a variable input parameter as a function of the geographical area:

$$T(x = x_{max}) = T_{const} \tag{3.6}$$

On the other hand, the meteorological parameters are introduced, and the energy balance is performed at node 1; hence, node 1 provides a Neumann boundary condition.

The energy balance at node 1 includes three heat components, as the heat transfer caused by transpiration, condensation, evaporation, and sublimation is neglected:

- convection between the pavement surface and air, Q_c;
- radiation between the pavement surface and air, Q_{rad};
- conduction between node 1 and the pavement beneath, Q_g.

$$Q_{rad} + Q_c + Q_g = 0 \tag{3.7}$$

The radiation component involves the shortwave and the long-wave contributions:

$$Q_{rad} = Q_{short} + Q_{long} \tag{3.8}$$

The short-wave component is

$$Q_{short} = Q_{incident} - Q_{reflected} = a \cdot Q_{incident} = a \cdot R^* \cdot \left(A + B \frac{S}{100} \right) \tag{3.9}$$

where

- $Q_{incident}$ is the incident short-wave radiation on the surface;
- a is the surface short-wave absorptivity;
- S is the sunshine percentage;
- R^* is the extraterrestrial radiation, whose trend is assumed to be parabolic from the time of sunrise to the time of sunset for a specific location, as plotted in fig. 3.2.

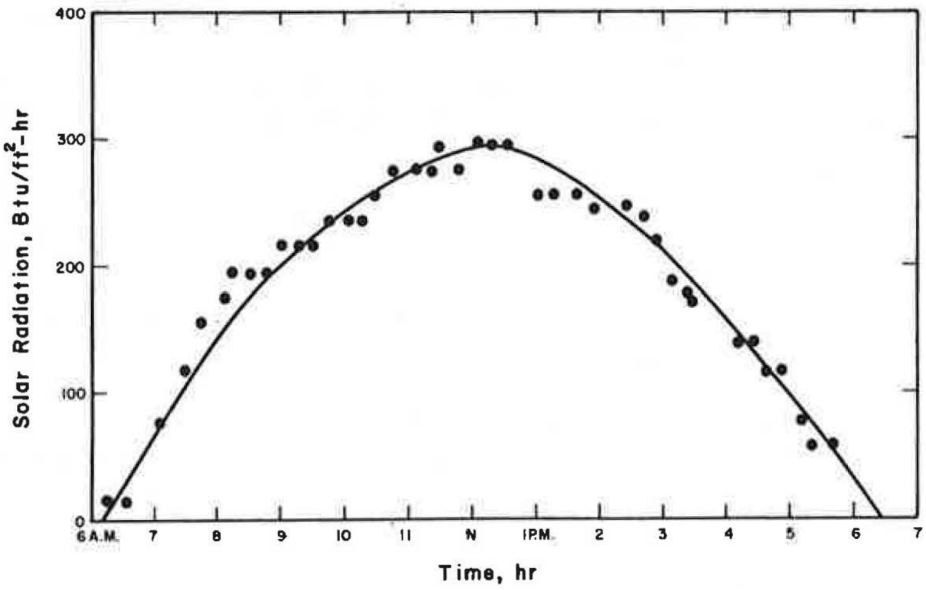

Figure 3.2: Variation in solar intensity, [9]

The long-wave component consists of the radiation emitted by the pavement and the radiation emitted by the atmosphere

$$Q_{long} = Q_{atmosphere} - Q_{pavement} = \left(1 - N\frac{W}{100}\right) \cdot (Q_z - Q_x) \tag{3.10}$$

where

- $1 - N\frac{W}{100}$ is the cloud-base correction factor, depending on the percentage of cloud cover $W = 100 - S$;
- Q_z and Q_x are the radiation emitted, respectively, by the atmosphere and the pavement with no correction for cloud cover.

The convection component of the heat transfer balance linearly depends on the difference between the air temperature T_{air} and the surface temperature T_1:

$$Q_c = H \cdot (T_{air} - T_1) \tag{3.11}$$

The convection coefficient H is estimated according to the following empirical formula:

$$H = 122.93 \left\{0.00144\, T_m^{0.3}\, U^{0.7} + 0.00097 \left(T_1 - T_{air}\right)^{0.3}\right\} \tag{3.12}$$

where

- T_{air} and T_1 are expressed in Celsius degrees,
- T_m is the average of T_{air} and T_1 in Kelvin degrees,
- U is the wind velocity in m/s.

The conduction component is modeled by the one-dimensional, first-order Fourier partial differential equation for conductive heat:

$$Q_g = -K \frac{\partial T}{\partial x} \tag{3.13}$$

By replacing eqs. (3.8), (3.11) and (3.13) in (3.7), one can retrieve the Neumann condition in the final form:

$$Q_{rad} + Q_c = -K \frac{\partial T}{\partial x} \tag{3.14}$$

Equation (3.1) is a first-order PDE in the time domain, so an initial condition is needed to solve it. The initial condition is represented by the temperature trend within the pavement system at time t_0, which is obtained by initiating the simulation some weeks earlier than t_0. The very first simulation is performed by assuming a feasible initial temperature trend, and, as the iterations succeed, the model will converge to an accurate estimation of the initial condition.

The final Initial-Boundary Value Problem is

$$\begin{cases} \dfrac{\partial T(x,t)}{\partial t} = \alpha \dfrac{\partial^2 T(x,t)}{\partial x^2}, & x \in (0, x_{max}),\ t > t_0 \\ T(x, t_0) = T_0(x), & x \in [0, x_{max}] \\ T(x_{max}, t) = T_{con}, & t > 0 \\ Q_{rad} + Q_c = -K \dfrac{\partial T(0,t)}{\partial x}, & t > 0 \end{cases} \tag{3.15}$$

The heat transfer model thus presented overlooks the effects of precipitation and moisture infiltration, both on heat fluxes and on the mechanical properties of granular materials. Although the goal of the NCHRP 1-37A project was to incorporate the moisture effect into pavement design and into the EICM, the research is still ongoing.

The ultimate goal of the heat transfer model is to identify the freeze-thaw cycles. A freeze-thaw cycle occurs when the pavement's temperature ranges between 30 °F and 32 °F (-1.1 °C and 0 °C, respectively) for a sufficient period of time. This temperature

range is named "freezing zone". Latent heat exchange occurs during phase transitions, which are isothermal processes. Therefore, the heat capacity is artificially increased in the freezing zone to simulate the lag in the temperature variation, as represented in fig. 3.3:

$$C_f = \frac{144\, w\, \gamma_d}{200\, \gamma} \tag{3.16}$$

The latent heat capacity in (3.16) is a function of the moisture content w, the dry density γ_d, and the unit weight γ.

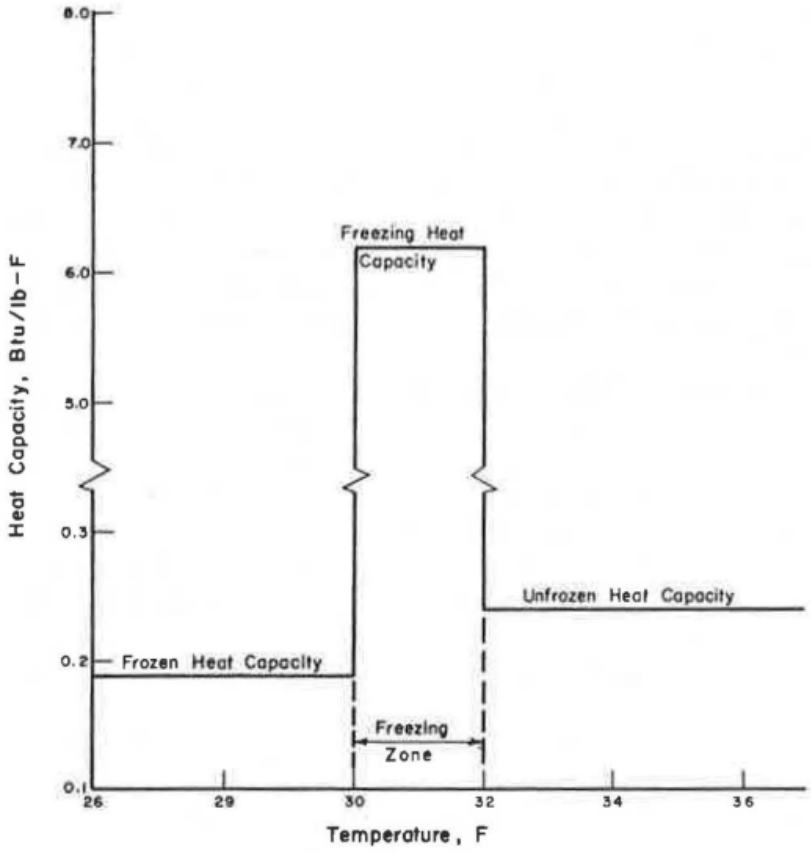

Figure 3.3: Effect of the temperature on the heat capacity, [9]

3.2 Traffic input data

The MEPDG does not utilize any equivalency factor, such as the Equivalent Single Axle Load (ESAL) or the Axle Load Equivalency Factor (ALEF), for traffic characterization. Rather, the effort aims at a more realistic description of the vehicular flow by means of the actual spectra.

The Federal Highway Administration (FHWA) vehicle classification includes thirteen

classes of light and heavy vehicles, as shown in figure 3.4. Because of the results of AAHSTO 93 road tests, the rationale in the design approach is accounting for heavy vehicles only. Therefore, ten truck classes - from class 4 to 13 - are embedded in the design methodology: each of them can be modeled according to specific axle types and loads.

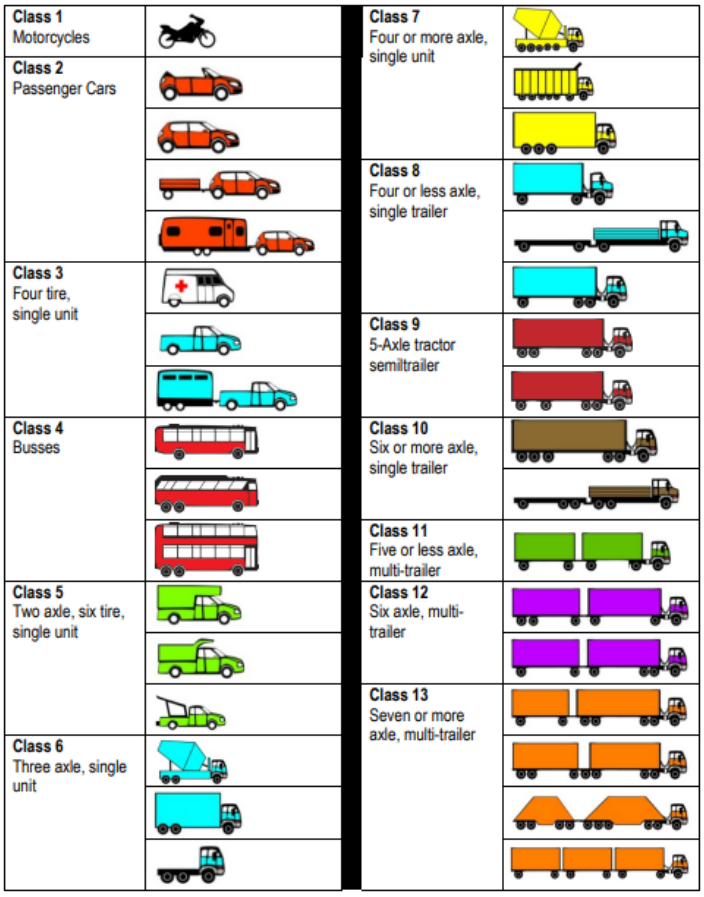

Figure 3.4: FHWA vehicle classification scheme [17]

Traffic data can be collected through weight-in-motion (WIM) stations and automatic vehicle classification (AVC) devices. The sampling may be performed according to the desired level of confidence and accuracy, as shown in table 3.1.

Standard Error (±%)	Level of Confidence (%)				
	80	90	95	97.5	99
20	1	1	1	1	1
10	1	1	2	2	3
5	2	3	5	7	10
2	8	19	30	43	61
1	32	74	122	172	242

Table 3.1: Minimum Sample Size (Number of Days per Year) to Estimate the Normalized Axle-Load Distribution—WIM Data [4]

Level 1 traffic input data consists of observations from WIM stations and AVC devices located on nearby segments of the design highway, assuming that no major intersections or features are affecting its traffic stream.

Level 2 traffic input data consists of observations from WIM stations and AVC devices located within the same region as the design infrastructure.

Level 3 traffic input data consists of default values estimated using a database developed in the framework of the Long-Term Pavement Performance (LTPP) program, as reported in table 3.2.

Truck Class	Single	Tandem	Tridem	Quad
4	1.62	0.39	0.00	0.00
5	2.00	0.00	0.00	0.00
6	1.02	0.99	0.00	0.00
7	1.00	0.26	0.83	0.00
8	2.38	0.67	0.00	0.00
9	1.13	1.93	0.00	0.00
10	1.19	1.09	0.89	0.00
11	4.29	0.26	0.06	0.00
12	3.52	1.14	0.06	0.00
13	2.15	2.13	0.35	0.00

Note: The number of quad axles per truck class is 0.00 because too few were counted in the LTPP traffic database.

Table 3.2: Suggested default values for the average number of single, tandem, and tridem axles per truck class, [3]

For level 1 and level 2 inputs, the amount of data used in the analysis should be adequate and statistically significant. Therefore, the collection of such data should be

performed over several years and be representative of the change in the traffic trend over time.

Two main assumptions are used for traffic characterization within the MEPDG framework:

1. the Average Annual Daily Truck Traffic (AADTT) may be subjected to both annual and monthly variation by means of the Growth Factor (GF) and the Monthly Adjustment Factor (MAF), respectively;

2. all statistics related to the axle load distribution within each class (namely, the axle load distributions for each axle type and vehicle class, and the axles per truck) remain constant in the design life of the pavement.

The variability of the AADTT over the week may be considered to improve the accuracy in the determination of the input itself. However, such fluctuations are overlooked in the computational process.

The data required for the pavement structural design are grouped into four types, which will be detailed in the following sections. The groups are:

- traffic volume – base year information;
- traffic volume adjustment factors;
- axle load distribution factors;
- general traffic inputs.

3.2.1 Traffic volume – base year information

"Base year" refers to the time when the pavement under design is opened to traffic. Thus, the statistics reported below do not include the effects generated by the construction equipment and vehicles:

- two-way Average Annual Daily Truck Traffic (AADTT);
- number of lanes in the design direction;
- percent trucks in the design direction;
- percent trucks in the design lane;

- truck operational speed, [mph].

Input Level	Data Source
Input Level 1	Direct measurements from WIM, AVC, or traffic counts for the project location
	Locally calibrated traffic models
Input Level 2	Direct measurements from WIM, AVC, or traffic counts at the regional level
	Traffic models calibrated at the regional level
Input Level 3	Direct measurements from WIM, AVC, or traffic counts at the national level
	Values estimated from other data (e.g., AADTT estimated from AADT and percentage of heavy vehicles) or based on engineering judgment
	Default values provided by the MEPDG based on data from the LTPP (Long-Term Pavement Performance) program managed by FHWA

Table 3.3: Traffic volume – base year information sources for different input levels

3.2.2 Traffic volume adjustment factors

For flexible pavement design, the information required is:

- the vehicle class distribution;
- traffic growth factors;
- monthly adjustment factors.

Furthermore, hourly adjustment factors are required for rigid pavement design.

The raw data sources and scales used to determine the vehicle class distribution are reported in table 3.4.

	Input Level 1	Input Level 2	Input Level 3
Source	WIM, AVC, traffic counts (an adequate amount of collected data is required)	WIM, AVC, traffic counts (an adequate amount of collected data is required)	WIM, AVC, traffic counts, engineering estimates
Scale	Local	Regional	National

Table 3.4: Raw data sources and spatial scale for the vehicle class distribution

At Input Levels 1 and 2, the vehicle class distribution is determined by normalizing the number of vehicles over the total amount within each truck class.
The NCHRP 1-37A Project identified 17 Truck Traffic Classes (TTC), each describing a predominant fleet composition in the stream, as shown in table 3.5.

Buses in Traffic Stream	Commodities being Transported by Type of Truck		TTC Group No.
	Multi-Trailer	Single-Trailers and Single-Units	
Low to none (<2%)	Relatively high amount of multi-trailer trucks (>10%)	Predominantly single-trailer trucks	5
		High percentage of single-trailer trucks, but some single-unit trucks	8
		Mixed truck traffic with a higher percentage of single-trailer trucks	11
		Mixed truck traffic with about equal percentages of single-unit and single-trailer trucks	13
		Predominantly single-unit trucks	16
	Moderate amount of multi-trailer trucks (2-10%)	Predominantly single-trailer trucks	3
		Mixed truck traffic with a higher percentage of single-trailer trucks	7
		Mixed truck traffic with about equal percentages of single-unit and single-trailer trucks	10
		Predominantly single-unit trucks	15
Low to moderate (>2%)	Low to none (<2%)	Predominantly single-trailer trucks	1
		Predominantly single-trailer trucks, but with a low percentage of single-unit trucks	2
		Predominantly single-trailer trucks with a low to moderate amount of single-unit trucks	4
		Mixed truck traffic with a higher percentage of single-trailer trucks	6
		Mixed truck traffic with about equal percentages of single-unit and single-trailer trucks	9
		Mixed truck traffic with a higher percentage of single-unit trucks	12
		Predominantly single-unit trucks	14
Major bus route (>25%)	Low to none (<2%)	Mixed truck traffic with about equal single-unit and single-trailer trucks	17

Table 3.5: Truck Traffic Classes, [3]

Then, each class was associated with a typical vehicle-class distribution, as described in table 3.6.

TTC Group	TTC Description	Vehicle/Truck Class Distribution (percent)									
		4	5	6	7	8	9	10	11	12	13
1	Major single-trailer truck route (type I)	1.3	8.5	2.8	0.3	7.6	74.0	1.2	3.4	0.6	0.3
2	Major single-trailer truck route (Type II)	2.4	14.1	4.5	0.7	7.9	66.3	1.4	2.2	0.3	0.2
3	Major single- and multi- trailer truck route (Type I)	0.9	11.6	3.6	0.2	6.7	62.0	4.8	2.6	1.4	6.2
4	Major single-trailer truck route (Type III)	2.4	22.7	5.7	1.4	8.1	55.5	1.7	2.2	0.2	0.4
5	Major single- and multi- trailer truck route (Type II).	0.9	14.2	3.5	0.6	6.9	54.0	5.0	2.7	1.2	11.0
6	Intermediate light and single-trailer truck route (I)	2.8	31.0	7.3	0.8	9.3	44.8	2.3	1.0	0.4	0.3
7	Major mixed truck route (Type I)	1.0	23.8	4.2	0.5	10.2	42.2	5.8	2.6	1.3	8.4
8	Major multi-trailer truck route (Type I)	1.7	19.3	4.6	0.9	6.7	44.8	6.0	2.6	1.6	11.8
9	Intermediate light and single-trailer truck route (II)	3.3	34.0	11.7	1.6	9.9	36.2	1.0	1.8	0.2	0.3
10	Major mixed truck route (Type II)	0.8	30.8	6.9	0.1	7.8	37.5	3.7	1.2	4.5	6.7
11	Major multi-trailer truck route (Type II)	1.8	24.6	7.6	0.5	5.0	31.3	9.8	0.8	3.3	15.3
12	Intermediate light and single-trailer truck route (III)	3.9	40.8	11.7	1.5	12.2	25.0	2.7	0.6	0.3	1.3
13	Major mixed truck route (Type III)	0.8	33.6	6.2	0.1	7.9	26.0	10.5	1.4	3.2	10.3
14	Major light truck route (Type I)	2.9	56.9	10.4	3.7	9.2	15.3	0.6	0.3	0.4	0.3
15	Major light truck route (Type II)	1.8	56.5	8.5	1.8	6.2	14.1	5.4	0.0	0.0	5.7
16	Major light and multi-trailer truck route	1.3	48.4	10.8	1.9	6.7	13.4	4.3	0.5	0.1	12.6
17	Major bus route	36.2	14.6	13.4	0.5	14.6	17.8	0.5	0.8	0.1	1.5

Table 3.6: Typical vehicle class distributions associated with each TTC, [3]

At Input Level 3, the designer is required to select one or more classes that best describe the expected traffic flow for the infrastructure of interest. When more than one class is selected within the TTC, the corresponding distributions are to be combined accordingly.

Traffic growth factors may be estimated from short or continuous duration traffic counts. However, such an assessment is likely to be biased; therefore, the growth rate should ideally be obtained through a rigorous traffic analysis.
As previously mentioned, the growth factors are used to evaluate changes in truck traffic over time. Three formulations may be adopted for this purpose:

1. no growth:

$$AADTT_{YEAR_X} = 1.0 \cdot AADTT_{YEAR_1} \tag{3.17}$$

2. linear growth:

$$AADTT_{YEAR_X} = GR \cdot YEAR_X + AADTT_{YEAR_1} \tag{3.18}$$

3. compound growth:

$$AADTT_{YEAR_X} = AADTT_{YEAR_1} \cdot GR^{YEAR_X} \tag{3.19}$$

where

- $\text{AADTT}_{\text{YEAR}_X}$ is the AADTT at age X;
- GR is the traffic growth rate;
- $\text{AADTT}_{\text{YEAR}_1}$ is the base year AADTT.

The monthly adjustment factor is calculated for each truck class as the related proportion of AADTT for every month of the year:

$$MAF_m = \frac{AMDTT_m}{\sum_{m=1}^{12} AAMTT_m} \cdot 12 = \frac{AMDTT_m}{AADTT} \cdot 12 \tag{3.20}$$

where

- MAF_m is the monthly adjustment factor for month m;
- AMDTT_m is the Average Monthly Daily Truck Traffic for month m.

Although the monthly proportion of the AADTT may vary from year to year, these values are assumed to remain constant over the design life.

3.2.3 Axle load distribution factors

Each axle group is associated with its own discretization into loading bins:

- single axles: 3,000 lb to 40,000 lb at 1,000-lb intervals;
- tandem axles: 6,000 lb to 80,000 lb at 2,000-lb intervals;
- tridem and quad axles: 12,000 lb to 102,000 lb at 3,000-lb intervals.

For each axle type (single, tandem, tridem, and quad) within each vehicle class (x), the axle load distribution represents the percentage of total axle repetitions within each loading interval (c). In other words, each factor for the specific x vehicle class is derived as the number of passages within a specific loading bin, normalized over the total number of passages for the vehicle class in question:

Truck class	2500 ÷ 3500 lb	3500 ÷ 4500 lb	4500 ÷ 5500 lb	5500 ÷ 6500 lb	...
3	$\frac{N_{x,c}}{\sum_{x,c} N_{x,c}} \cdot 100$				
4					
5					
6					
...					

Table 3.7: Layout of the axle load distribution table for the single axle group

The only way to retrieve the axle load distribution factors is to collect traffic data using WIM stations over a sufficiently long period. That data must be processed to populate the axle load distribution table for Input Levels 1 and 2. If the collection of direct observations is unavailable, default values retrieved from the LTPP program are suggested for Input Level 3.

3.2.4 General traffic inputs

This type of information is embedded in the computational process to define the details related to loading and its configuration.

The source for the raw data at each input level is reported in table 3.8.

	Input Level 1	**Input Level 2**	**Input Level 3**
Source	Direct measurements on the project road (not possible for new pavements)	Average values at the regional scale for infrastructures with similar characteristics	Average values at the national scale for infrastructures with similar characteristics Default values

Table 3.8: Raw data sources for general traffic inputs

The input data belonging to this section can be further subdivided into three groups referred to, respectively:

- the axle configuration;
- the lateral wander;
- the wheelbase.

The inputs used to refine the axle configuration include the average axle width, tire pressure, dual-tire spacing, and axle spacing for multiple axle groups.

The data used to describe the lateral wander involves the design lane width, the traffic wander standard deviation, and the mean wheel location.
The mean wheel location is defined as the distance from the outer edge of the wheel to the pavement marking; hence, it is a proxy for the prevailing loading location. However, stresses and strains are sensitive to both the actual loading location and the interactions between loads applied by different wheels on the same axle. The wander standard deviation allows for a more accurate consideration of the actual loading location.

The wheelbase is related to the prevailing configurations of trucks, with short, medium, and long axle spacings. Indeed, the required data include the average spacing of long, medium, and short axles, as well as the percentage of trucks with long, medium, and short axles.

Finally, the axle configuration is further detailed by the number of axles per truck, defined for each axle type within each truck class. This statistic is obtained by processing the WIM or AVC traffic data for Input Levels 1 and 2. When these data are unavailable, typical values may be used instead.

3.2.5 Traffic input data processing

Let m, a, x, and c denote, respectively, the month of the year, the axle type, the truck class, and the loading bin. For each month, the following steps are taken to calculate the total number of passages for the axle type associated with a specific loading bin.

1. The number of truck passages for the x class is calculated as:

$$N_x = AAMTT_m \cdot P_D \cdot P_L \cdot N_m \cdot P_x \tag{3.21}$$

where

- P_L is the lane distribution factor;
- P_D is the direction distribution factor;

- P_x is the percentage of vehicles belonging to the x class;
- N_m is the number of days in the m month;
- $AAMTT_m$ is the Annual Average Monthly Truck Traffic for the m month, calculated as

$$AAMTT_m = AADTT_{YEAR_X} \cdot MAF_m \tag{3.22}$$

2. The number of axle passages for each a-type axle and x class is calculated as:

$$N_{a,x} = N_x \cdot APT_{a,x} \tag{3.23}$$

where $APT_{a,x}$ is the amount of a-type axle per truck in the x class.

3. The number of axle passages for each a-type axle, x class, and c loading bin is calculated as:

$$N_{c,a,x} = N_{a,x} \cdot ALDF_{c,a,x} \tag{3.24}$$

where $ALDF_{c,a,x}$ is the Axle Load Distribution Factor corresponding to the c lading bin of the x class and the a-type axle.

4. The total number of axle passages for each a-type axle, and c loading bin over all the truck classes is calculated as:

$$N_{c,a}^{TOT} = \sum_{x=4}^{13} N_{c,a,x} \tag{3.25}$$

As a result, the monthly axle type-based number of passages is discretized into the specific loading bins to derive $N_{c,single}^{TOT}$, $N_{c,tandem}^{TOT}$, $N_{c,tridem}^{TOT}$, $N_{c,quad}^{TOT}$, and to match, in the end, the time discretization whereof in section 2.1.

3.3 Materials input data

3.3.1 HMA input data for the Master Curve

The MEPDG modeling approach for the asphalt mixture master curve is driven by the Global Aging System (GAS), regardless of the Input Level used. Hence, the GAS is introduced below, while the procedures for the different input levels will be discussed afterwards.

3.3.1.1 The Global Aging System for aging simulation

The Global Aging System is a sub-model used for mixture aging estimation. The model hypothesizes that the aging of the binder phase is representative of the aging of the mix. The aging of the bitumen is simulated by a gradual increase in its viscosity, which is reflected in the properties of the entire mixture. As a matter of fact, the time and depth dependent viscosity $\eta = \eta(t_{service}, z)$ is used to calculate the shift factor of the master curve, as follows:

$$a(T) = a(\eta(t_{service}, z), T) = c(\log \eta - \log \eta_{T_r}) \tag{3.26}$$

where

- c is a mixture-specific fitting parameter;
- η is the viscosity at the temperature of interest, [cP];
- η_{T_r} is the viscosity at the reference temperature, [cP]. The default reference temperature is $T_r = 70°F = 21.1°C$.

The reduced loading time is defined as

$$t_r = \frac{t_{load}}{a(T)} \tag{3.27}$$

and is employed in the mathematical optimization of the final master curve.

The GAS sub-model consists, in turn, of four subsequent sub-sub-models that are updated over time to avoid implementing a stationary, homogeneous dynamic module.

The first step is the "Original to mix or lay down model", which simulates the aging caused by the mixing and compaction effort, to wit, the short-term aging:

$$\log \log(\eta_{t_{service}=0}) = a_0 + a_1 \log \log(\eta_{orig}) \tag{3.28}$$

$$a_0 = 0.054405 + 0.004082 \cdot code \tag{3.29}$$

$$a_1 = 0.972035 + 0.010886 \cdot code \tag{3.30}$$

where

- $\eta_{t_{service}=0}$ is the viscosity after mixing and compaction, [cP];
- η_{orig} is the viscosity of the binder in its original state, right after being produced in the refinery, [cP];

- the code value depends on the hardening ratio (see table 3.9), that is, the ratio of the log-log RTFO viscosity to the log-log original viscosity.

Mix/Lay-Down Hardening Resistance	Expected Hardening Ratio Values	Code Value
Excellent to Good	$HR \leq 1.030$	-1
Average	$1.030 < HR \leq 1.075$	0
Fair	$1.075 < HR \leq 1.100$	1
Poor	$HR > 1.100$	2

Table 3.9: Recommended code values, [3]

For short-term aging not to be considered twice, a_0 and a_1 are to be set to 0 and 1, respectively, when the complex modulus of the binder is measured for the RTFO-aged condition.

The second step consists of the "Surface aging model", which includes the environmental effect for the long-term surface aging:

$$\log\log(\eta_{aged}) = \frac{\log\log(\eta_{t_{service}=0}) + At}{1 + Bt} \tag{3.31}$$

$$A = -0.004166 + 1.41213(C) + (C)\log(Maat) + (D)\log\log(\eta_{t_{service}=0}) \tag{3.32}$$

$$B = 0.197725 + 0.068384\log(C) \tag{3.33}$$

$$C = 10^{274.4946 - 193.831\log(T_R) + 33.9366(T_R)^2} \tag{3.34}$$

$$D = -14.5521 + 10.47662\log(T_R) - 1.88161\log(T_R)^2 \tag{3.35}$$

where

- η_{aged} is the aged vistosity, [cP];
- Maat is the mean annual air temperature, [°F];
- T_R is the Rankine temperature, [°R];
- t is the time in months.

The third step involves adjusting the aged viscosity due to air voids. The air void adjustment factor F_v depends on the percentage of air voids V_a: indeed, air voids affect the amount of oxygen in the mix, which is responsible for its oxidation and aging.

$$\log\log(\eta'_{aged}) = F_v \log\log(\eta_{aged}) \tag{3.36}$$

$$F_v = \frac{1 + 1.0367 \times 10^{-4} \cdot V_a \cdot t}{1 + 6.1798 \times 10^{-4} \cdot t} \tag{3.37}$$

$$V_a = \frac{V_{a,orig} + 0.011 \cdot t - 2}{1 + 4.24 \times 10^{-4} \cdot t \cdot Maat + 1.169 \times 10^{-3} \cdot \left(\frac{t}{\eta_{orig@77°F}} \right)} \tag{3.38}$$

where

- $V_{a,orig}$ is the initial percentage of air voids, [%];
- t is the time in months;
- $\eta_{orig@77°F}$ is the original binder viscosity at 77 °F, [MP].

The fourth and last step of the Global Aging System incorporates the viscosity dependency on depth. Its output is the trend of the viscosity as a function of time and depth in the HMA layer.

$$\eta(t_{service}, z) = \frac{\eta'_{aged}(4 + E) - E(\eta_{t_{service}=0})(1 - 4z)}{4 \cdot (1 + Ez)} \tag{3.39}$$

$$E = 23.83\, e^{-0.0308 \cdot Maat} \tag{3.40}$$

where

- $\eta(t_{service}, z)$ is the aged viscosity at time $t_{service}$ and depth z, [MP];
- z is the depth, [in].

3.3.1.2 Input Level 1

The sources for the Input Level 1 data are summarized in table 3.10.

T [°F]	T [°C]	Mixture E* and δ^1				Binder G* and δ^2
		0.1 Hz	1 Hz	10 Hz	25 Hz	1.59 Hz
10	−12.2	X	X	X	X	
25	−3.9					
40	4.4	X	X	X	X	X
55	12.8					X
70	21.1	X	X	X	X	X
85	29.4					X
100	37.8	X	X	X	X	X
115	46.1					X
130	54.4	X	X	X	X	X

[1] Testing performed in accordance with AASHTO T342, [30].
[2] Testing performed in accordance with AASHTO T315, [26].

Table 3.10: Testing temperatures and loading frequencies for mixture and binder characterization, [3]

Alternatively, the binder can be characterized based on the tests reported in table 3.11.

$$\log \eta = 10.5012 - 2.2601 \log(Pen) + 0.00389 \log(Pen)^2 \tag{3.41}$$

No.	Test	T [°C]	Conversion to viscosity [Poise]
1	Penetration	15	See eq. (3.41)
2	Penetration	25	See eq. (3.41)
3	Brookfield viscosity	60	None
4	Brookfield viscosity	80	None
5	Brookfield viscosity	100	None
6	Brookfield viscosity	121.1	None
7	Brookfield viscosity	135	None
8	Brookfield viscosity	176	None
9	Softening point	Measured	13,000
10	Absolute viscosity	60	None
11	Kinematic viscosity	135	Value × 0.948

Table 3.11: Binder tests and conversion to viscosity, [3]

When the binder is characterized in accordance with table 3.10, its viscosity is obtained as a function of the shear modulus ($|G^*|$, [Pa]), and the phase angle (δ, [°]):

$$\eta = \frac{|G^*|}{10} \left(\frac{1}{\sin \delta} \right)^{4.8628} \tag{3.42}$$

The upper limit for viscosity at low temperatures and high loading rates is 2.7×10^{10} P.

The binder property thus calculated enters the Global Aging System model, which computes viscosity as a function of time and depth. Let $\mathcal{T}_{\text{test}}$ denote the set of temperatures at which the binder is tested. The following empirical log–log linear relationship relates the binder viscosity, expressed in centipoise (cP), to the temperature in Rankine:

$$\log\log\eta = A + VTS\log T_R, \qquad \forall\, T_R \in \mathcal{T}_{\text{test}} \tag{3.43}$$

The regression parameters A and VTS from eq. (3.43) are retrieved by linear interpolation of the experimental viscosity data.

The complex modulus of the asphalt mixture is obtained through laboratory testing, as described in table 3.10. The shift factors are then calculated according to eq. (3.26), and the mathematical optimization of the mixture-specific fitting parameters α, β, δ, γ, c in the following relationship is performed to develop the full master curve.

$$\log(E^*) = \delta + \frac{\alpha}{1 + e^{\beta+\gamma\log t_r}} \tag{3.44}$$

$$t_r = \frac{t_{load}}{a(T)} = \frac{t_{load}}{c(\log\eta - \log\eta_{T_r})} \tag{3.45}$$

The final master curve of the mixture accounts for the depth and the mixture's aging.

3.3.1.3 Input Level 2

The sources for the characterization of the mixture at the Input Level 2 are summarized in table 3.12.

Parameter	Description	Units
η	Binder viscosity	10^6 Poise
ω	Loading rate	Hz
V_a	Air void content	Percent by total mixture volume
$V_{b,\text{eff}}$	Effective asphalt content	Percent by total mixture volume
ρ_{34}	Cumulative percent retained on 3/4 in sieve	Cumulative percent by weight of aggregate
ρ_{38}	Cumulative percent retained on 3/8 in sieve	Cumulative percent by weight of aggregate
ρ_4	Cumulative percent retained on #4 sieve	Cumulative percent by weight of aggregate
ρ_{200}	Percent passing #200 sieve	Percent by weight of aggregate

Table 3.12: Characterization of the asphalt mixture for Input Level 2, [3]

The binder should be tested in accordance with table 3.10. When the results of these tests are not available, the procedures summarized in table 3.11 can be used instead.

The workflow for building the master curve is similar to that implemented when the Input Level 1 is used. First, the viscosity of the original or RTFO-aged binder is calculated with eq. (3.41) or eq. (3.42). The viscosity thus computed is manipulated by the Global Aging System. Then, the regression parameters A and VTS from eq. (3.43) are retrieved by linear interpolation of the experimental viscosity data.

Since no direct testing of the dynamic modulus is required at Input Level 2, the Witczak and Fonseca formula described in [37] is used in the algorithm. The input data for the computation of the dynamic modulus are the properties listed in table 3.12:

$$\begin{aligned}\log(E^*) = {} & 3.750063 + 0.02932\,\rho_{200} - 0.001767\,(\rho_{200})^2 - 0.002841\,\rho_4 \\ & - 0.058097\,V_a - 0.802208\left(\frac{V_{b,eff}}{V_{b,eff}+V_a}\right) \\ & + \frac{3.871977 - 0.0021\,\rho_4 + 0.003958\,\rho_{38} - 0.000017\,(\rho_{38})^2 + 0.005470\,\rho_{34}}{1 + e^{(-0.603313 - 0.313351\log\omega - 0.393532\log\eta)}}\end{aligned} \tag{3.46}$$

The dynamic modulus in eq. (3.46) can be expressed in the form of the sigmoidal function in eq. (3.44) to build the master curve over the entire loading rate domain.

In such a case, the mixture-specific parameters α, β, δ, γ, c are no longer retrieved through mathematical optimization; rather, they depend on the properties summarized in table 3.12.

$$\begin{aligned}\delta = 3.750063 + 0.02932\,\rho_{200} - 0.001767\,(\rho_{200})^2 \\ - 0.002841\,\rho_4 - 0.058097\,V_a - 0.802208\left(\frac{V_{b,eff}}{V_{b,eff}+V_a}\right)\end{aligned} \tag{3.47}$$

$$\alpha = 3.871977 - 0.0021\,\rho_4 + 0.003958\,\rho_{38} - 0.000017\,(\rho_{38})^2 + 0.005470\,\rho_{34} \tag{3.48}$$

$$\beta = -0.603313 - 0.393532\log(\eta_{T_r}) \tag{3.49}$$

$$t_r = \frac{t_{load}}{a(T)} = \frac{t_{load}}{c(\log\eta - \log\eta_{T_r})} \tag{3.50}$$

$$\gamma = 0.313351 \tag{3.51}$$

$$c = 1.255882 \tag{3.52}$$

3.3.1.4 Input Level 3

No testing is required at Input Level 3. The input parameters are the same as those for Input Level 2, but they can be obtained directly from representative data for similar mixtures. Concerning the binder's data, default values are used for the parameters A and VTS from eq. (3.43), based on any of the following information:

- Performance Grade of the asphalt binder;
- Viscosity grade of the asphalt binder;
- Penetration grade of the asphalt binder.

The viscosity is then entered into the Global Aging System, and the time-depth dependent master curve is obtained according to eq. (3.46) and eq. (3.44).

3.3.2 HMA: other properties

To fully characterize the asphalt mixture from mechanical and thermal viewpoints, a set of additional properties is considered.

3.3.2.1 Poisson's ratio

The Poisson's ratio for bituminous mixtures is a dynamic and complex parameter: it depends, indeed, on temperature, loading frequency, and confinement state. Ideally, the dependency of the Poisson's ratio on temperature should be embedded in the algorithm as $\mu = \mu(\mathrm{T})$. In practice, the structural analysis is carried out using Burmister's multi-layered elasticity theory, which neglects the effect of temperature on Poisson's ratio within each layer. The benefit of accurately measuring the Poisson's ratio is not worth the effort. So, Input Level 1 is not implemented in this instance. Input Level 2 and 3 are used instead.

Input Level 2 is further subdivided into:

- level 2A, which estimates the Poisson's ratio at a specific temperature as a function of the dynamic modulus at the same temperature

$$\mu_{HMA} = 0.15 + \frac{0.35}{1 + e^{(a+bE_{HMA})}} \tag{3.53}$$

  where a and b are estimated through regression of laboratory results.

- Level 2B, which estimates the Poisson's ratio at a specific temperature as a function of the dynamic modulus at the same temperature through eq. (3.53), where a and b are typical values.

- Level 2C: the Poisson's ratio is selected by the user among a range of temperature-based typical values, as shown in table 3.13.

Temperature [°F]	**Temperature [°C]**	μ_{range}
< 0	< -17.8	< 0.15
$0 \div 40$	$-17.8 \div 4.4$	$0.15 \div 0.20$
$40 \div 70$	$4.4 \div 21.1$	$0.20 \div 0.30$
$70 \div 100$	$21.1 \div 37.8$	$0.30 \div 0.40$
$100 \div 130$	$37.8 \div 54.4$	$0.40 \div 0.48$
> 130	> 54.4	$0.45 \div 0.48$

Table 3.13: Recommended ranges of the Poisson's ratio as a function of temperature at Input Level 2C, [3]

A temperature-based default value is provided for Poisson's ratio at Input Level 3, as shown in table 3.14.

Temperature [°F]	Temperature [°C]	$\mu_{typical}$
< 0	< -17.8	0.15
$0 \div 40$	$-17.8 \div 4.4$	0.20
$40 \div 70$	$4.4 \div 21.1$	0.25
$70 \div 100$	$21.1 \div 37.8$	0.35
$100 \div 130$	$37.8 \div 54.4$	0.45
> 130	> 54.4	0.48

Table 3.14: Typical values of the Poisson's ratio as a function of temperature at Input Level 3, [3]

3.3.2.2 Additional materials inputs required for climatic modeling

Three thermal properties are required as input data for the heat-transfer model used to simulate the temperature trend in the pavement described in section 3.1.1. All three of them are implemented at Input Level 3. They are listed below, along with their role in the model and recommended values.

- Surface shortwave absorptivity, implemented for the heat transfer balance at node 1 in eq. (3.9). The typical values for this parameter depend on the age of the pavement, and, in turn, on its color. The younger the pavement, the darker its shade, and the greater its shortwave absorption capability:
    - aged, gray colored pavement: $0.80 \div 0.90$;
    - new, black colored pavement: $0.90 \div 0.98$.
- Thermal conductivity (K) and specific heat capacity (C), implemented for the computation of the thermal diffusivity in eq. (3.3). Their default values at Input Level 3 are:
    - $K = 1.25\,\text{Btu}/(\text{h} \cdot \text{ft} \cdot {}^\circ\text{F}) = 2.16\,\text{W}/(\text{m} \cdot \text{K})$
    - $C = 0.28\,\text{Btu}/(\text{lb} \cdot {}^\circ\text{F}) = 1.17\,\text{kJ}/(\text{kg} \cdot \text{K})$

3.3.2.3 Additional materials inputs required for distress and transfer functions

The mechanical and thermal properties described below are indirectly incorporated into the Paris Law for estimating damage caused by thermal action.

Tensile strength is used for the calculation of the fracture parameter in eq. (2.21). It is obtained through laboratory tests at Input Levels 1 and 2, based on the AASHTO T322 test protocol [28].

Tensile strength at Input Level 3 is derived through the regression equation presented below.

$$\begin{aligned} TS =& 7416.712 - 114.016 \cdot V_a - 0.304 \cdot V_a^2 - 122.592 \cdot VFA \\ &+ 0.704 \cdot VFA^2 + 405.71 \cdot \log(Pen_{@77^\circ F}) - 2039.296 \cdot log(A) \end{aligned} \tag{3.54}$$

where

- TS is the indirect tensile strength at 14 °F, [psi];
- V_a is the percentage of air voids, [%];
- VFA is the percentage of voids filled with asphalt in the mix, [%];
- $Pen_{@77^\circ F}$ is the binder penetration at 77 °F, [dmm];
- A is the viscosity-temperature susceptibility intercept from eq. (3.43).

Creep compliance is used to calculate the slope, m, of its log–log versus time curve, as shown in eq. (2.23). Then, the m value is plugged into the fracture parameter, n, in eq. (2.22). Creep compliance is derived through laboratory testing at Input Levels 1 and 2, based on the AASHTO T322 test protocol [28]. Input Level 1 requires the material to be tested at low, intermediate and high temperatures, respectively, corresponding to 4 °F, 14 °F, 32 °F (i.e. −20 °C, −10 °C, 0 °C). Input Level 2 is used when laboratory testing is carried out only at intermediate temperatures.

Creep compliance at Input Level 3 is derived through the regression equation presented below.

$$D(t) = D_1 \cdot t^m \tag{3.55}$$

$$\begin{aligned} \log(D_1) =& -8.524 + 0.01306 \cdot T + 0.7957 \cdot \log(V_a) \\ &+ 2.0103 \cdot \log(VFA) - 1.923 \cdot \log(A) \end{aligned} \tag{3.56}$$

$$\begin{aligned} m =& 1.1628 - 0.00185 \cdot T - 0.04596 \cdot V_a - 0.01126 \cdot VFA \\ &+ 0.00247 \cdot Pen_{@77^\circ F} + 0.001683 \cdot T \cdot (Pen_{@77^\circ F})^{0.4605} \end{aligned} \tag{3.57}$$

where all variables are the same as in eq. (3.54) and T is the temperature at which creep compliance is measured in Fahrenheit degrees.

The linear coefficient of thermal contraction of asphalt concrete is calculated as a function of the HMA volumetric properties, as there are no testing procedures for it to be measured:

$$L_{HMA} = \frac{VMA \cdot B_{bitumen} + V_{AGG} \cdot B_{AGG}}{3 \cdot V_{TOTAL}} \tag{3.58}$$

where

- VMA is the percentage of voids in the mineral aggregate, [%];
- V_{AGG} is the percentage of aggregate in the mix by volume, [%];
- $V_{TOTAL} = 100\%$;
- $B_{bitumen}$ is the volumetric coefficient of thermal contraction of the bitumen, $(3.5 \times 10^{-4}) \div (4.3 \times 10^{-4})$ $^{\circ}C^{-1}$;
- B_{AGG} is the volumetric coefficient of thermal contraction of the aggregate phase, $(21 \times 10^{-6}) \div (37 \times 10^{-6})$ $^{\circ}C^{-1}$.

3.3.3 Input data for unbound granular materials

The unbound granular materials for the base and subbase layers are defined according to the Highway Research Board (HRB) soil classification system described in [24], and belong to the groups A-1, A-2, and A-3. The unbound granular materials for the subgrade are defined according to the HRB classification system and the Unified Soil Classification System (USCS) described in [5], and may belong to any group.

The input data for the unbound granular materials are classified into three groups:

- the pavement response model material inputs;
- the Enhanced Integrated Climatic Model (EICM) material inputs;
- other material properties.

3.3.3.1 Pavement response model material inputs

The pavement response model material inputs include the resilient modulus and Poisson's ratio.

The resilient modulus can be determined through laboratory testing according to AASHTO T307 ([25]) or NCHRP 1-28A ([1]). The stress state applied to the specimen should be representative of the specific in situ conditions of the material, which depend on depth. The experimental data should be fitted to the following generalized constitutive model:

$$M_r = k_1 p_a \left(\frac{\theta}{P_a}\right)^{k_2} \left(\frac{\tau_{oct}}{P_a} + 1\right)^{k_3} \tag{3.59}$$

where

- M_r is the resilient modulus, [psi];
- $\theta = \sigma_1 + \sigma_2 + \sigma_3$ is the bulk stress;
- $\tau_{oct} = \frac{1}{3}\sqrt{(\sigma_1 - \sigma_2)^2 + (\sigma_1 - \sigma_3)^2 + (\sigma_2 - \sigma_3)^2}$ is the octahedral shear stress;
- σ_1, σ_2, σ_3 are the major, intermediate, and minor principal stress, respectively;
- P_a is the atmospherc pressure;
- k_1, k_2, k_3 are the regression constants of the model.

Moreover, the resilient modulus is calculated using empirical correlations with other strength parameters (Input Level 2), or some default values are recommended based on the classification group (Input Level 3). The common practice is to use the empirical formula, which directly relates the resilient modulus to the California Bearing Ratio (CBR):

$$M_r = 2555 \cdot CBR^{0.64} \tag{3.60}$$

In any case and at all Input Levels, the resilient modulus should be carefully selected in consideration of the layout of the entire pavement's section and the possible presence of a shallow bedrock.

The influence of Poisson's ratio on the pavement's structural response is generally limited: Input Levels 1 and 2 may be implemented, but they are not recommended. Hence, Input Level 3 is used (see table 3.15).

Material description	μ_{range}	$\mu_{typical}$
Clay (saturated)	$0.4 \div 0.5$	0.45
Clay (unsaturated)	$0.1 \div 0.3$	0.20
Sandy clay	$0.2 \div 0.3$	0.25
Silt	$0.3 \div 0.35$	0.325
Dense sand	$0.2 \div 0.4$	0.30
Coarse-grained sand	0.15	0.15
Fine-grained sand	0.25	0.25
Bedrock	$0.1 \div 0.4$	0.25

Table 3.15: Typical ranges and values of Poisson's ratio for Input Level 3, [3]

3.3.3.2 EICM material inputs

The hydraulic and physical properties of the unbound granular materials required as inputs for the Enhanced Integrated Climatic Model, along with their Input Levels, are

reported below:

- Plasticity Index, implemented at Input Level 1;
- particle size distribution, implemented at Input Level 1;
- saturated hydraulic conductivity, implemented at Input Levels 1, 2, or 3;
- specific gravity of solids, implemented at Input Levels 1, 2, or 3;
- Optimum Moisture Content and Maximum Dry Density, implemented at Input Levels 1, 2, or 3;
- soil water characteristics curve parameters.

3.3.3.3 Other material properties

The last property for the unbound granular materials is the coefficient of lateral pressure, expressed as

$$k_0 = \frac{\mu}{1-\mu} \tag{3.61}$$

for cohesive materials, and as

$$k_0 = 1 - \sin\phi \tag{3.62}$$

for cohesionless materials.

3.3.4 Input data for bedrock materials

Bedrock can significantly affect the structural response of the pavement section. This is especially true if the bedrock layer is shallow. It is therefore essential to account for its presence in the design stage by means of Poisson's ratio and the modulus of elasticity. Both parameters are implemented at Input Levels 2 or 3, as detailed in tables 3.16 and 3.17.

Material	**Input Level 2**	**Input Level 3**
Solid, massive bedrock	$0.10 \div 0.25$	0.15
Highly fractured, weathered bedrock	$0.25 \div 0.40$	0.30

Table 3.16: Poisson's ratio for bedrock materials at different Input Levels

Material	Input Level 2		Input Level 3	
	ksi	MPa	ksi	MPa
Solid, massive bedrock	750 ÷ 2000	5170 ÷ 13,790	1000	6895
Highly fractured, weathered bedrock	250 ÷ 1000	1720 ÷ 6895	500	3447

Table 3.17: Modulus of elasticity for bedrock materials at different Input Levels

Chapter 4

Full implementation: preliminary implementation vs. calibration

First, it is necessary to define the concept of full implementation of the Mechanistic Empirical Pavement Design Guide. When fully implementing this design methodology, the first step is to select and process the case-specific input data to accurately characterize climate, traffic, and materials. This typically involves defining local climatic databases, characterizing traffic in terms of axle-load spectra, and determining relevant material properties. This phase can be referred to as the preliminary implementation of the MEPDG.

The second step is calibrating the transfer functions to predict distress, which consists of adjusting the local calibration coefficients to minimize the bias between modeled and observed distress values and the variance of the modeled values. The observed distress values can be obtained from the Pavement Management System databases and should include data covering at least one design life cycle. This is needed to calibrate the damage functions across the full domain of loading repetitions and to avoid extrapolation of the model, which is likely to produce inaccurate results. In practice, in the case of flexible pavements, the main objectives of the transfer functions calibration are the C_x coefficients in eqs. (2.6), (2.7) and (2.29).

Both procedures, preliminary implementation and calibration, require a large amount of data. The former requires large climate and traffic datasets, along with a peculiar and broad materials characterization. The latter involves collecting observed distress data over the design life of a significant number of pavement sections within the PMS framework.

Hence, local calibration should not be regarded as an isolated step, but rather as

the final stage of a broader full implementation process. In particular, unless the local input data are first characterized with sufficient accuracy, the minimization of the error between observed and predicted pavement performance may have limited physical meaning. Once both the preliminary implementation and calibration are completed, the MEPDG can be adopted locally as a pavement design methodology.

4.1 The MEPDG in the US

Several US states have implemented the MEPDG or developed a customized mechanistic-empirical design framework. While some Departments of Transportation (DOTs) are still in the preliminary phase, others have reached more advanced stages in calibrating transfer functions to local conditions. Also, some implementations are still research-oriented, whereas others are already employed in the design practice.

By way of example, MEAPA was developed in Michigan, CalME in California, Mn-PAVE in Minnesota, WisPave in Wisconsin, and TxME in Texas.

Nevertheless, the philosophy of this design methodology relies on an ongoing process of calibration. As a matter of fact, the empirical side of the method requires that the damage and transfer function calibration coefficients be periodically recalibrated to account for the adoption of innovative materials and technologies or the review of current technical specifications. Therefore, regardless of the stage, the work is always in progress.

4.2 The MEPDG outside the US

Several studies have investigated the possibility of implementing the Mechanistic–Empirical Pavement Design Guide (MEPDG) outside its original North American context. These efforts generally aim to evaluate the applicability of the methodology under different climatic, traffic, and material conditions, and to explore the possibility of calibrating the distress transfer functions to local conditions. However, the literature indicates that most of these studies are preliminary implementation efforts rather than complete local calibration frameworks.

A common characteristic of many international studies is that the initial focus is placed on adapting the input data required by the MEPDG to local conditions. For example, studies conducted in Chile ([8]) developed local climatic datasets for several

regions, constructed traffic load spectra based on available measurements, and determined mixture master curves in order to reproduce realistic local conditions within the MEPDG framework. Nevertheless, the authors highlight that the calibration results remain preliminary, as the available traffic and climatic data did not always align exactly with the sections used for model validation.

In Qatar, the MEPDG framework was applied using locally representative traffic, climate, and material inputs to evaluate pavement performance and conduct life-cycle cost analyses. However, the study explicitly recognizes that further work is required to perform a proper local calibration of the distress models ([33]). Likewise, applications carried out in Saudi Arabia mainly focused on evaluating the predicted performance of pavement structures under local climatic conditions and identifying discrepancies between predicted and observed distresses, rather than performing a systematic calibration of the transfer functions.

In other contexts, such as Egypt ([34]), the implementation process has focused on developing simplified regional frameworks capable of approximating the behavior predicted by the MEPDG through surrogate models and regional databases. While these approaches represent useful tools for preliminary pavement analysis, they still rely on nationally calibrated distress models and therefore do not constitute a full local calibration of the mechanistic–empirical framework.

Even in studies that attempt a more formal calibration procedure, significant challenges remain. For instance, calibration studies performed in Ontario ([2]) highlight the difficulties associated with constructing consistent calibration databases, particularly with respect to the compatibility between pavement management system data and the distress definitions used within the MEPDG. In many cases, only a limited subset of performance indicators can be used for calibration due to inconsistencies in the available datasets.

Overall, the international literature suggests that the implementation of the MEPDG outside its original inference space typically progresses through preliminary stages focused on adapting and processing local input data. Comprehensive local calibration of the distress transfer functions remains relatively limited, primarily due to the difficulty of obtaining high-quality, internally consistent datasets that describe traffic loading, climatic conditions, material properties, and pavement performance.

4.3 The MEPDG State of the art in Italy

The only study that investigated the possible use of the MEPDG for the Italian case is the one conducted by Prof. Caliendo from Salerno University, [6]. The main implication of this research deals with the implementation of the Italian traffic characterization within the MEPDG framework. Specifically, Prof. Caliendo aggregated the sixteen Italian vehicle classes defined in fig. 1.2 into five of the classes considered in the MEPDG, as illustrated in fig. 4.1.

MEPDG defaults as truck classes			Italian truck classes	
Truck class	Type of vehicle	No. axles	Truck class	Type of vehicle
4	Buses	2 and 3	14 + 15 + 16	2-axle buses
5	Single-unit trucks	2	1 + 2 + 3 + 4	2-axle single-unit trucks
6	Single-unit trucks	3	5 + 6	3-axle single-unit trucks
7	Single-unit trucks	≥ 4	—	—
8	Single trailer trucks	≤ 4	—	—
9	Single trailer trucks	5	9 + 10 + 11 + 12 + 13	3-axle tractor with 2-axle trailer 2-axle tractor with 3-axle trailer
10	Single trailer trucks	≥ 6	—	—
11	Multitrailer trucks	≤ 5	7 + 8	4-axle multitrailer trucks
12	Multitrailer trucks	6	—	—
13	Multitrailer trucks	≥ 7	—	—

Figure 4.1: Aggregation of the Italian CNR-based vehicle classes into the FHWA classes, [6]

Although with some differences in the final output, this framework was replicated in section 5.2.2 for the same purpose.

4.4 Introduction of the MEPDG in the Italian context

In light of everything presented so far, progress in the use of the MEPDG as a design methodology outside the US remains limited. Specifically, the overall maturity level in Italy allows for significant freedom to explore the topic.

As discussed, the first phase of the broader full implementation process stands in the preliminary implementation and development of adequate input data. Therefore, a framework for the Italian implementation of the MEPDG is presented in the following chapter.

Chapter 5

Framework for the local implementation of the MEPDG

In this chapter, the methodology for implementing the MEPDG in the Italian context is outlined. Some recommendations are provided for handling the input data required to implement them in the MEPDG framework. The three modules will be addressed one by one, starting with the climate section, followed by the traffic and materials sections.

5.1 Climate section

The work presented in this section aims to identify a database of modeled climate data suitable for accurately describing Italian conditions with respect to the environmental variables required by the MEPDG. The methodology consists of the statistical analysis of the differences between climate observations and modeled values. The validation procedure is conducted over a 20-year period – from 1st January 2005 to 31st December 2024 – corresponding to the design-life cycle of the pavement. The ultimate goal is to validate a climate database as a reference for climate data in pavement design. Information from models is to be used as an alternative or complementary source to meteorological observations from local weather stations; indeed, measurements cannot be derived homogeneously in space, and are often discontinuous in time.

5.1.1 Available climate data for the local implementation

5.1.1.1 Field observations from weather stations

Climate observations for temperature, wind speed, cloud cover, relative humidity, and precipitation were recorded by the Torino–Caselle airport station and provided by the Italian Air Force (ITAF) upon request. The coordinates of the Torino–Caselle airport weather station are: 45.2025, 7.6494.

The variables of the dataset provided by the ITAF are summarized in table 5.1.

Variable	Description	Unit	Temporal resolution
Wnd F	Wind speed averaged over a 10-minute period, measured in open terrain at approximately 10 m above ground level	kts	Two observations per hour
T	Air temperature measured at approximately 2 m above ground level and rounded to the nearest integer	°C	Two observations per hour
Rel hum	Relative humidity estimated from dew point temperature at approximately 2 m above ground level	%	Two observations per hour
C clds	Total cloud cover expressed in oktas (eighths of the sky dome)	oktas	Irregular observations
PR12a	Accumulated precipitation over the 12-hour interval from 00:00 to 12:00	mm	12-hour accumulation
PR12b	Accumulated precipitation over the 12-hour interval from 12:00 to 24:00	mm	12-hour accumulation

Table 5.1: Meteorological variables used for the climatic characterization

The correlation between the Okta Scale and the percent one is shown below:

- Sky clear: 0 oktas = 0% → Sunshine = 100%
- Few clouds: 1 to 2 oktas = 18.75% → Sunshine = 81.25%
- Scattered: 3 to 4 oktas = 43.75% → Sunshine = 56.25%
- Broken: 5 or 6 or 7 oktas = 75% → Sunshine = 25%
- Overcast: 8 oktas = 100% → Sunshine = 0%

The data were processed to obtain a consistent, hourly-based dataset expressed in International System units. However, the temporal resolution of wind speed and precipitation was retained as originally.

5.1.1.2 Reanalysis models: ERA5 and MERRA-2 datasets

Reanalysis products combine numerical weather prediction models with historical observations through data assimilation techniques in order to generate physically consistent atmospheric datasets over long time periods. Among the most widely used reanalysis databases are ERA5, developed by the European Centre for Medium-Range Weather Forecasts (ECMWF), and MERRA-2, produced by the National Aeronautics and Space Administration (NASA). Both datasets provide long-term, spatially continuous records of meteorological variables.

The two databases differ in the atmospheric model used to produce the climate data and in their spatial resolution. ERA5 uses the Integrated Forecasting System (IFS) model, while MERRA-2 uses the Goddard Earth Observing System (GEOS-5) model. The spatial resolution for the reanalysis data is 0.25°x0.25° for ERA-5, 0.5°x0.625° for MERRA-2. Thus, a 0.1 degree lat-lon grid was used to filter data for a single cell in both ERA5 and MERRA-2 networks.

The cell of interest for the location of the Torino–Caselle airport station was identified in the ERA5 and MERRA-2 networks by the following coordinates: 7.60 W, 45.15 S, 7.70 E, 45.25 N.

Downloading the reanalysis results is a time-consuming and computationally intensive process. This is especially true when dealing with hourly values over such a long time period.

MERRA-2 data can be accessed through NASA's GES DISC data portal upon creating an account. After defining the spatial domain, temporal range, and variables of interest, the portal automatically generates download URLs pointing to the daily NetCDF data files stored on the NASA servers. Such files have to be individually retrieved through the dedicated URLs. This procedure was automated by means of a short script to be run from the Windows Command Prompt, which iterates through the list of URLs contained in the file MERRA_reanalysis.txt and downloads the corresponding NetCDF files:

```
for /F "usebackq delims=" %A in ("MERRA_reanalysis.txt") do curl
--netrc- file "%CD%\_netrc" -b "%CD%\.urs_cookies" -c
```

```
"%CD%\.urs_cookies" -L -O -J "%A"
```

Six variables were selected among three datasets.
The dataset in fig. 5.1 included

- 2-meter air temperature (T2M), [K];
- 10-meter northward wind (V10M), [m/s];
- 10-meter eastward wind (U10M), [m/s];
- surface pressure (PS), [Pa];
- 2-meter specific humidity (QV2M), [kg/kg].

The dataset in fig. 5.2 was used for the total cloud area fraction (CLDTOT), [–].
The dataset in fig. 5.3 was used for the bias-corrected total precipitation (PRECTOTCORR), $\left[\frac{\text{kg}}{\text{m}^2\text{s}}\right]$.

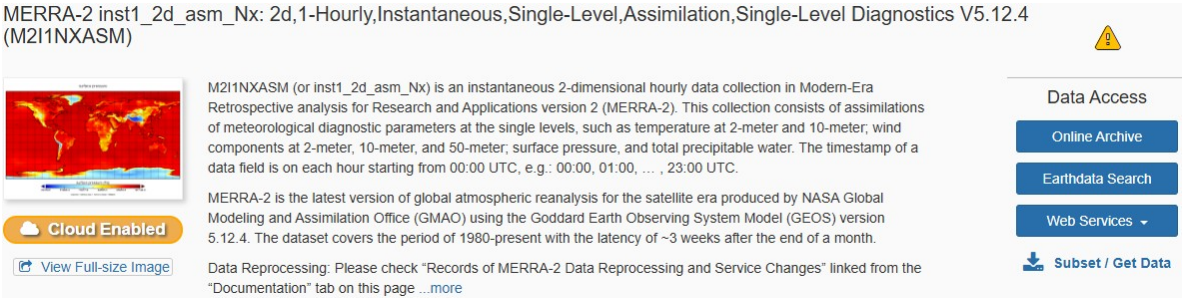

Figure 5.1: MERRA-2 inst1_2d_asm_Nx dataset

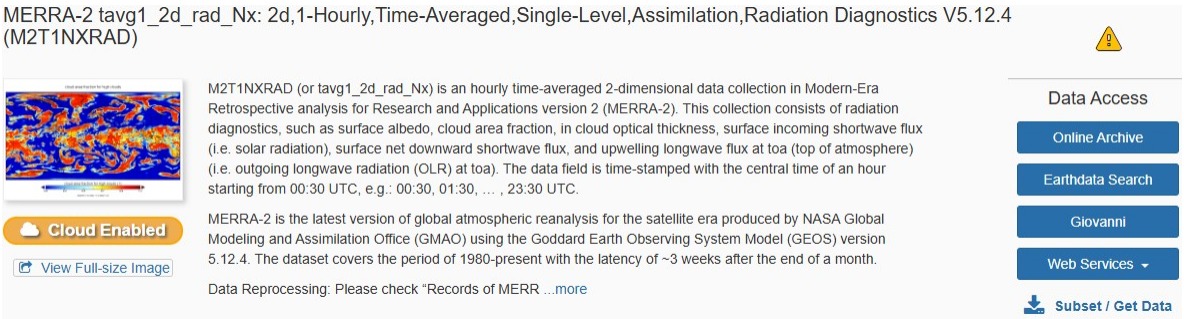

Figure 5.2: MERRA-2 tavg1_2d_rad_Nx dataset

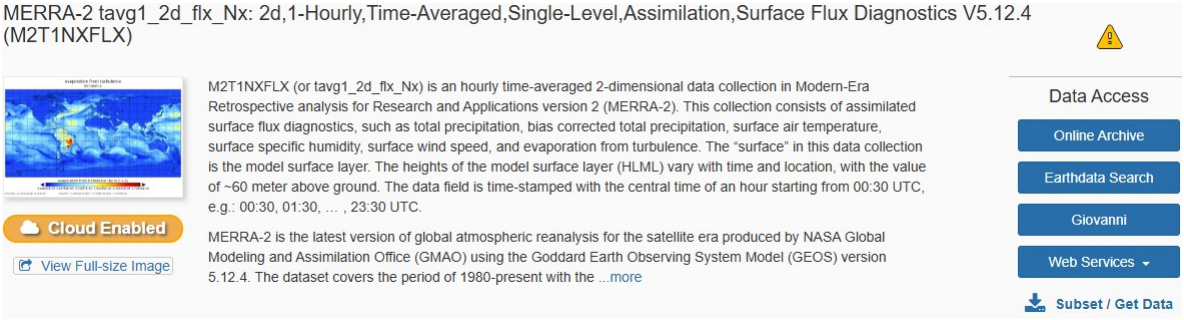

Figure 5.3: MERRA-2 tavg1_2d_flx_Nx dataset

Note that the measurement unit of the bias-corrected total precipitation is nothing but millimeters per second [mm/s], because if $1\,\text{kg} = 1\,\text{dm}^3 = 0.001\,\text{m}^3$ of water is spread over a $1\,\text{m}^2$ surface area, its thickness is 1 mm.

The relative humidity was calculated as the ratio between the actual vapor pressure and the saturation vapor pressure:

$$RH[\%] = 100 \cdot \frac{e(T)}{e(T_s)} \tag{5.1}$$

where

- the Magnus-Tetens equation is utilized to calculate the numerator as a function of the air temperature, T:

$$e(T) = 6.112 \cdot e^{\left(\frac{17.67 \cdot T}{T+243.5}\right)} \tag{5.2}$$

- the Dalton law together with the ideal gas law applies to the denominator, as a function of the specific humidity, q, and the surface pressure, P:

$$e = \frac{q \cdot P}{0.622 + 0.378q} \tag{5.3}$$

ERA5 data are available through the Copernicus Climate Data Store upon creating an account. After defining the spatial domain, temporal range, and variables of interest, the request is processed, and the monthly NetCDF files can then be downloaded. The Copernicus Climate Data Store sets a limit on request size; as a consequence, the temporal domain of each request cannot exceed 3 months, which makes the overall download process time-consuming.

The variables selected from the ERA5 database, along with their label and measurement unit, are listed below:

- 2m temperature (t2m), [K];
- 2m dewpoint temperature (d2m), [K];
- 10m u-component of wind (u10), [m/s];
- 10m v-component of wind (v10), [m/s];
- total precipitation (tp), [m];
- total cloud cover (tcc), [-].

The relative humidity was calculated as the ratio between the actual vapor pressure and the saturation vapor pressure:

$$RH[\%] = 100 \cdot \frac{e(T)}{e(T_s)} \tag{5.4}$$

where the Magnus-Tetens equation (5.2) is utilized to calculate the numerator and the denominator as a function of, respectively, the actual air temperature, T, and the dew-point temperature, T_s.

5.1.2 Processing and statistical comparison of climatic data

The three aforementioned datasets were standardized to the same layout for comparison.

Several challenges were encountered when working with the MERRA-2 and the measured data, while the ERA5 dataset was more straightforward to handle.

Specifically, the in situ observations were incomplete over the 20-year analysis period because the ITAF-managed meteorological station was inactive during some time frames. In particular, only some random rows in the dataset included the cloud cover index, which was absent from March 2009 onward. Moreover, cloud cover is reported in Oktas by the AMI, necessitating conversion to percent. The main issue in this regard is that the population of Sunshine data obtained is discrete due to the intrinsic nature of the Okta Scale, whereas the modeled data continuously spans 0% to 100%.
Furthermore, the precipitation observations are cumulative and reported on a 12-hour basis. Therefore, the modeled data for this variable were cumulated on the same time basis for consistency and comparison purposes.

Concerning the MERRA-2 reanalysis model, two main issues arose. First, several duplicates of rows were found in the dataset. Then, some of the relative humidity values were found to exceed 100%, which is physically unrealistic. This may be caused

by the numerical inconsistency between the numerator and the denominator of the relative humidity formula 5.4. As a consequence, the relative humidity values over the threshold were clipped to 100% to allow for a consistent comparison with the other datasets. This issue was not encountered when calculating relative humidity from the ERA5 data, which includes both air temperature and dew-point temperature, thereby allowing the use of the Magnus-Tetens equation above and below the fraction line.

The results of the statistical comparison of MERRA-2 vs. observations and ERA5 vs. observations are presented in the following sections.

5.1.2.1 Temperature

The hourly modeled temperature data were plotted against the measured data to assess their agreement with the equality line (fig. 5.4). For the same purpose, the linear trendline was plotted as well.

The temperature quintiles are the values used in the MEPDG design methodology to compute the pavement's response. Therefore, the same plots were created to compare the temperatures corresponding to the accumulated frequencies of 10, 30, 50, 70, and 90 percent within each month (figs. 5.5 to 5.9).

In figs. 5.4 to 5.9, one can observe that the ITAF station thermometer has a measurement resolution of 0.5 °C, whereas ERA5 and MERRA-2 provide temperature as a continuous variable. These plots show that both models underestimate the temperature data: the slopes of all the trendlines are close to 1, but their intercepts range from -1 to -2. The sole exception is in the comparison of the 2nd quintile values from the MERRA-2 model, where the trendline intercept is nearly +2, indicating an overestimation of these values.

Hourly model-observation differences were aggregated into monthly mean biases and RMSE. The distribution of monthly mean biases and RMSE over the 20-year period was then used to compute the overall mean bias and RMSE, as shown by the dotted line in the graphs in figs. 5.10 and 5.11.

The overall mean bias and RMSE thus calculated are similar in the two cases under analysis, even though the ERA5 model performs slightly better. The overall mean biases are -1.89 °C and -1.79 °C for the MERRA-2 and the ERA5 model-observation differences, respectively. In the same manner, the overall mean RMSE is 2.95 °C and 2.36 °C for the MERRA-2 and the ERA5 model-observation differences, respectively.

In conclusion, the ERA5 reanalysis dataset more accurately predicts actual temperature data.

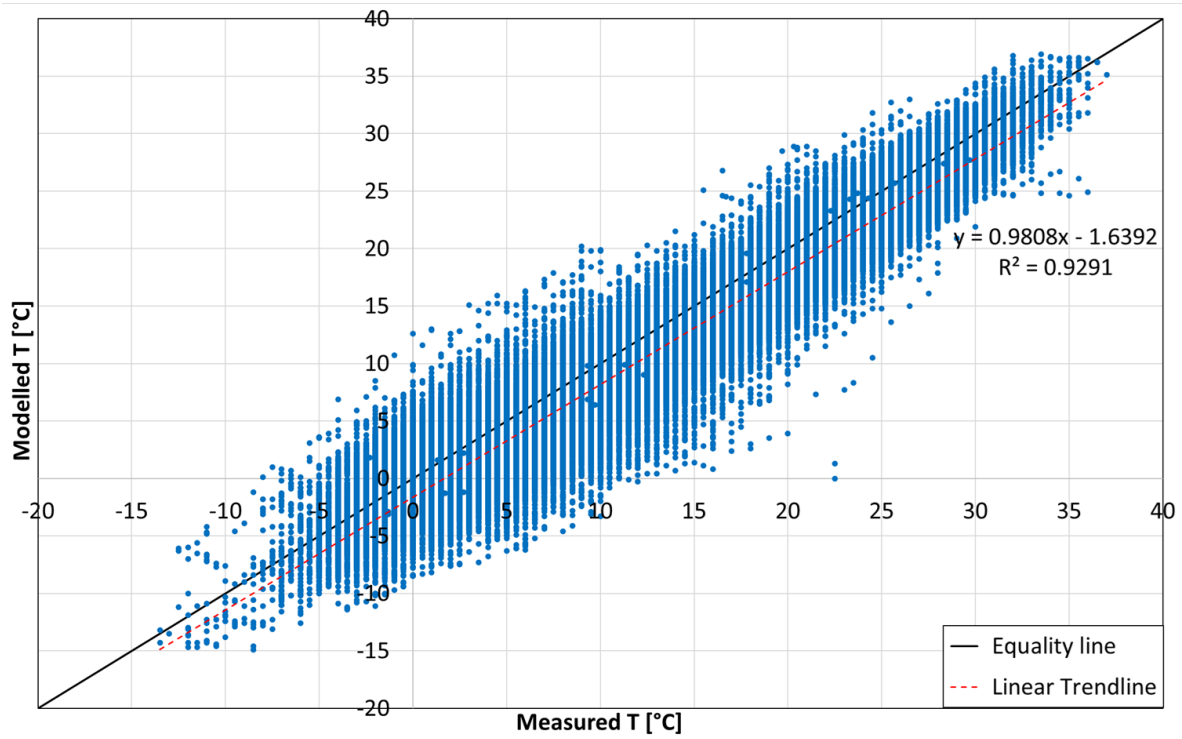

(a) Field observations vs. MERRA-2 model

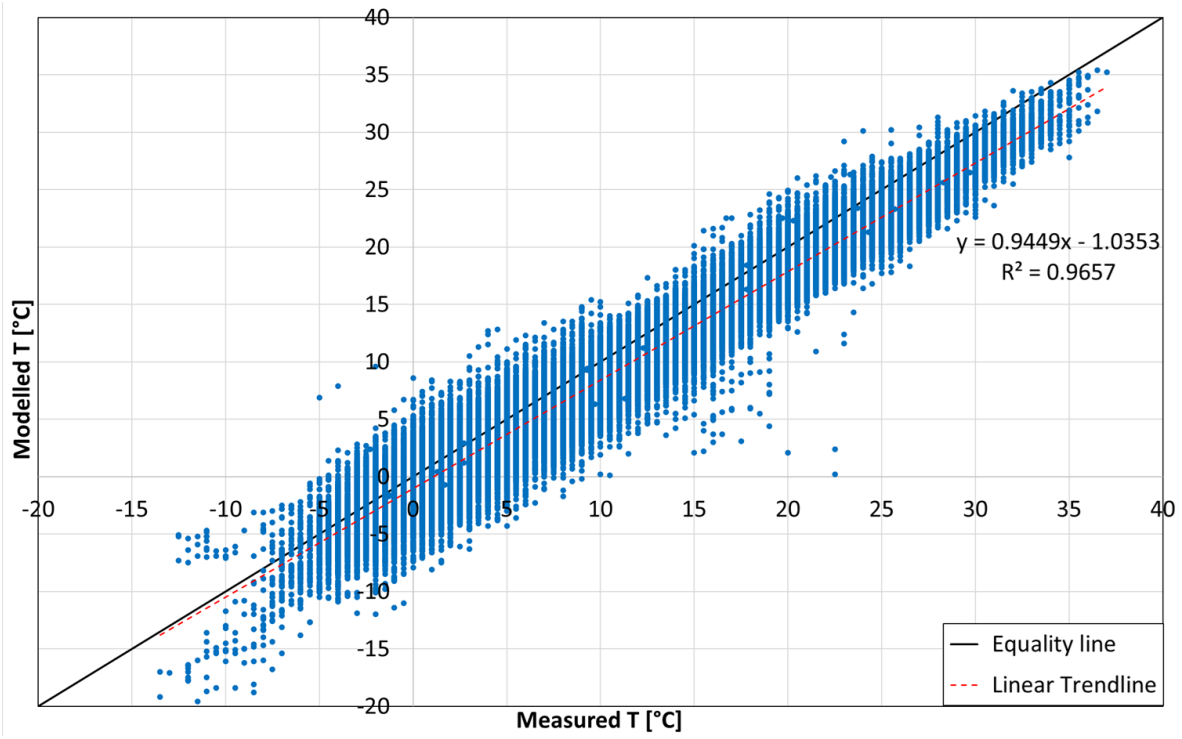

(b) Field observations vs. ERA5 model

Figure 5.4: Comparison between measured and modeled temperature data

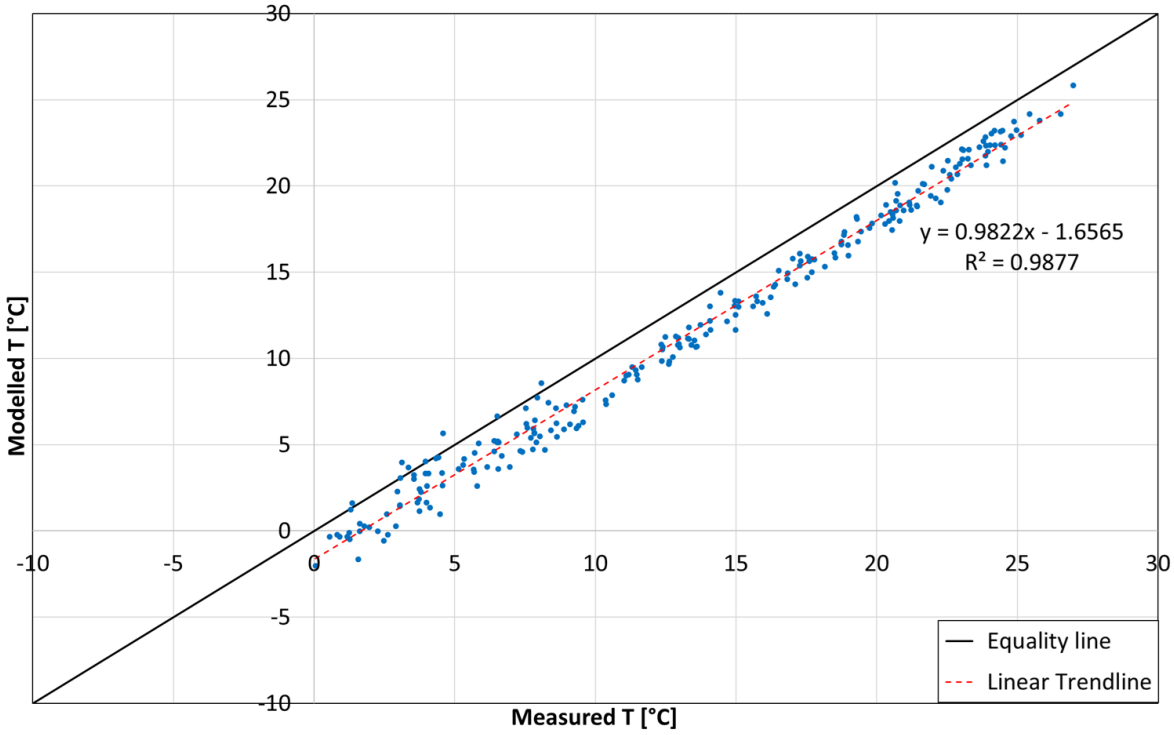

(a) Field observations vs. MERRA-2 model

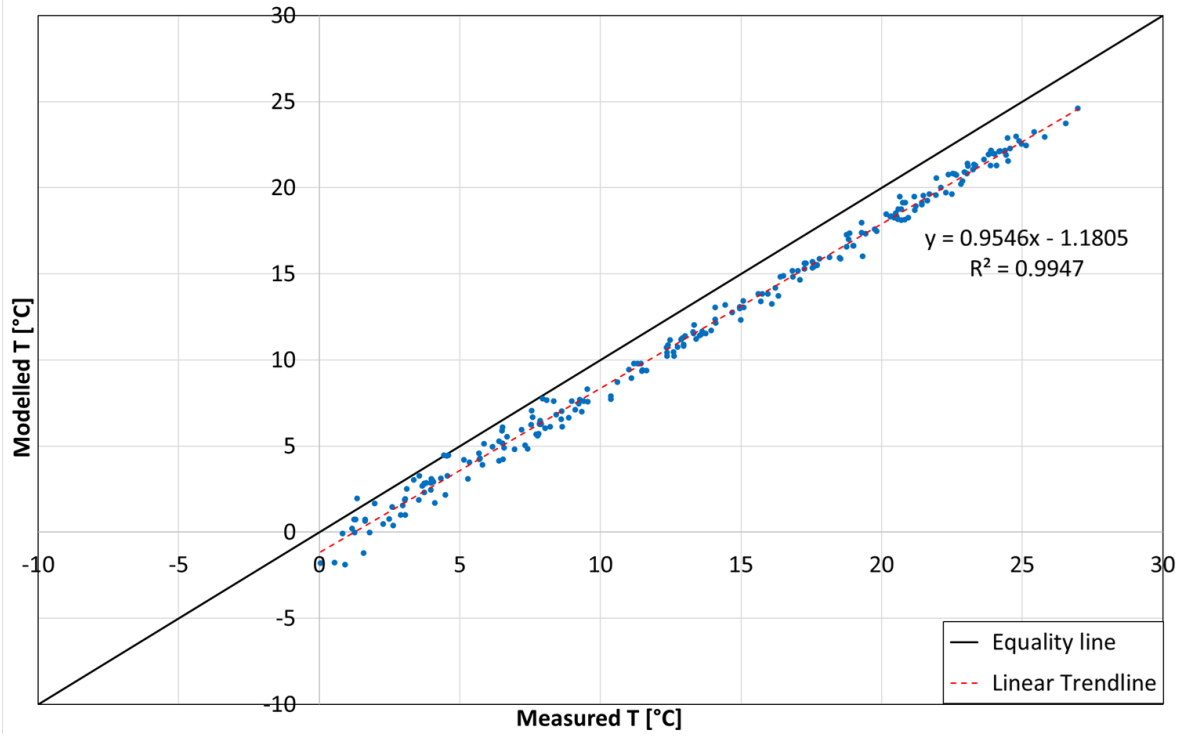

(b) Field observations vs. ERA5 model

Figure 5.5: Comparison between measured and modeled temperature data for the 1st quintile

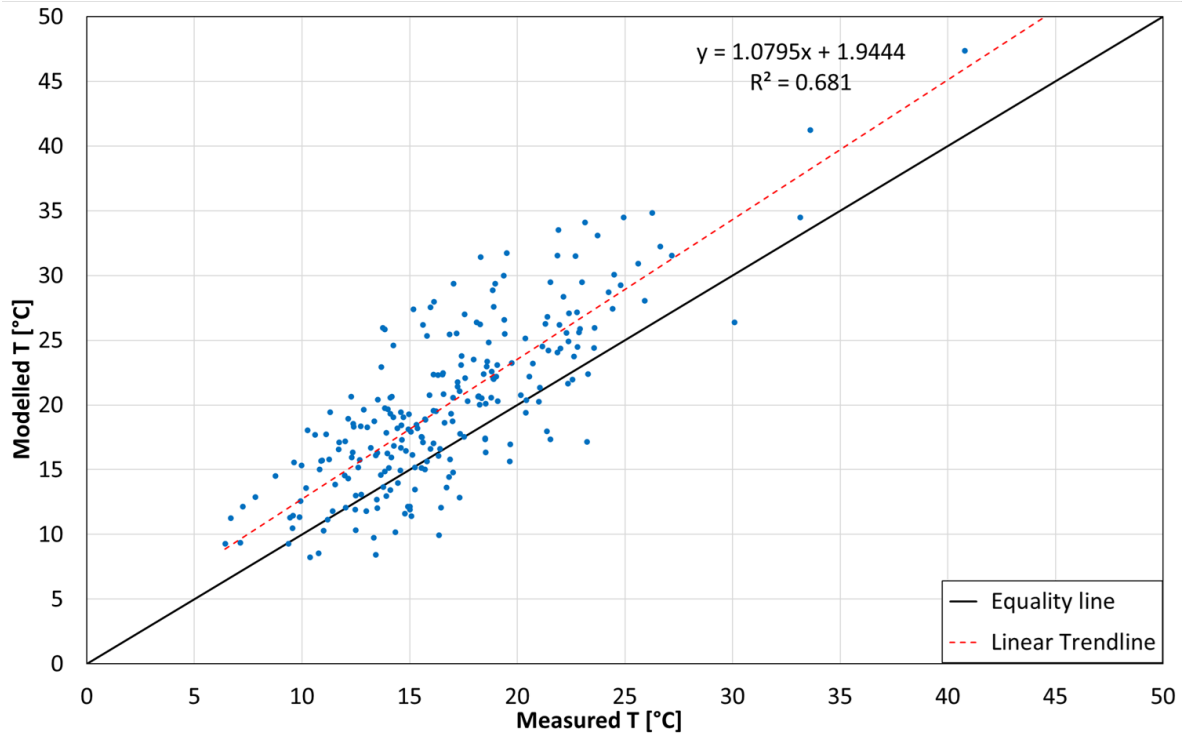

(a) Field observations vs. MERRA-2 model

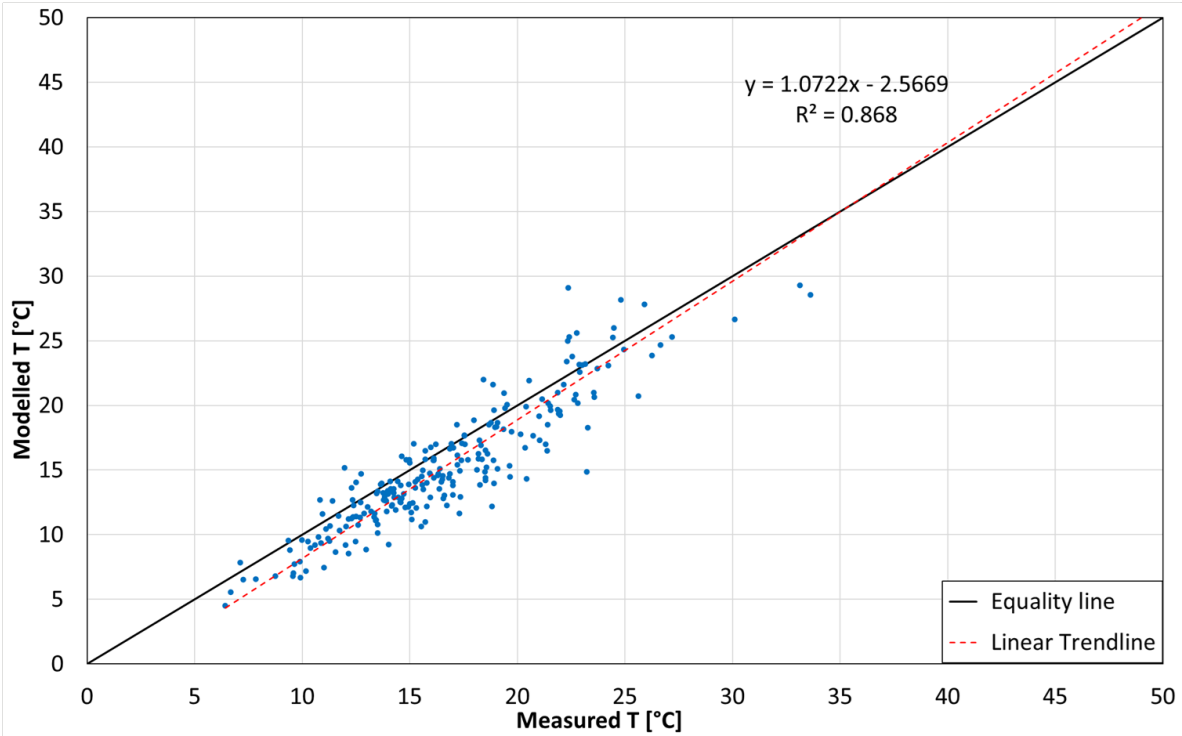

(b) Field observations vs. ERA5 model

Figure 5.6: Comparison between measured and modeled temperature data for the 2nd quintile

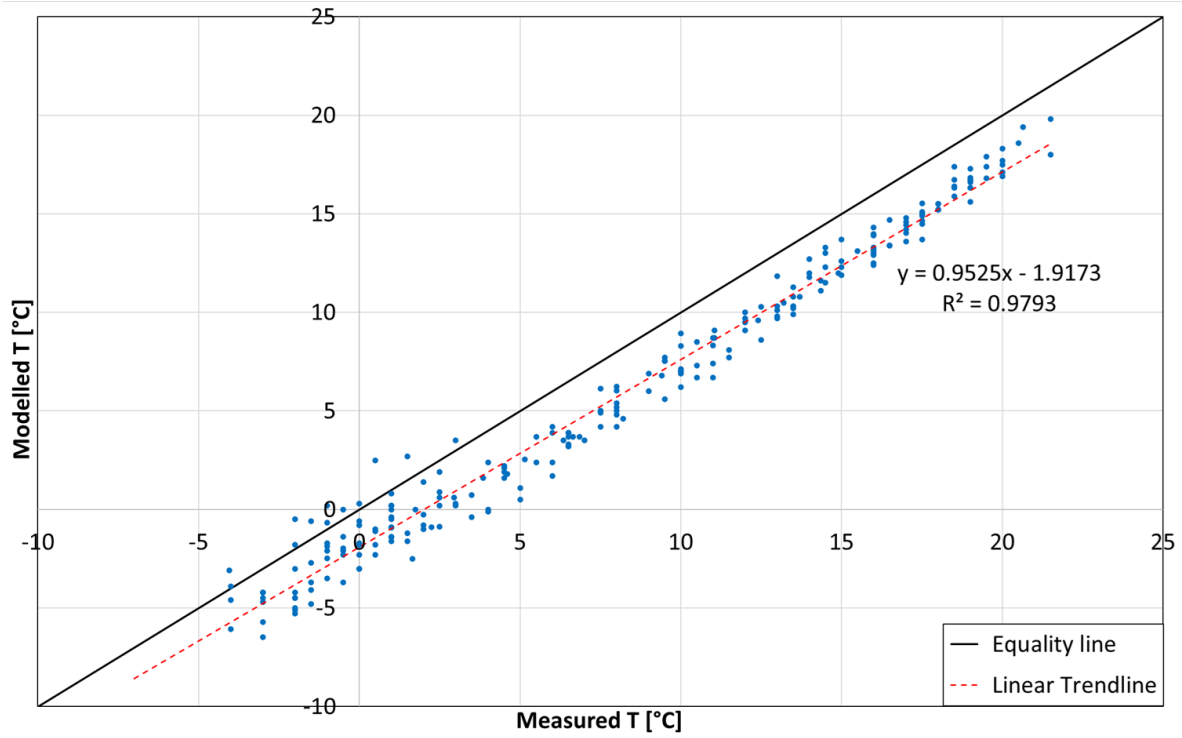

(a) Field observations vs. MERRA-2 model

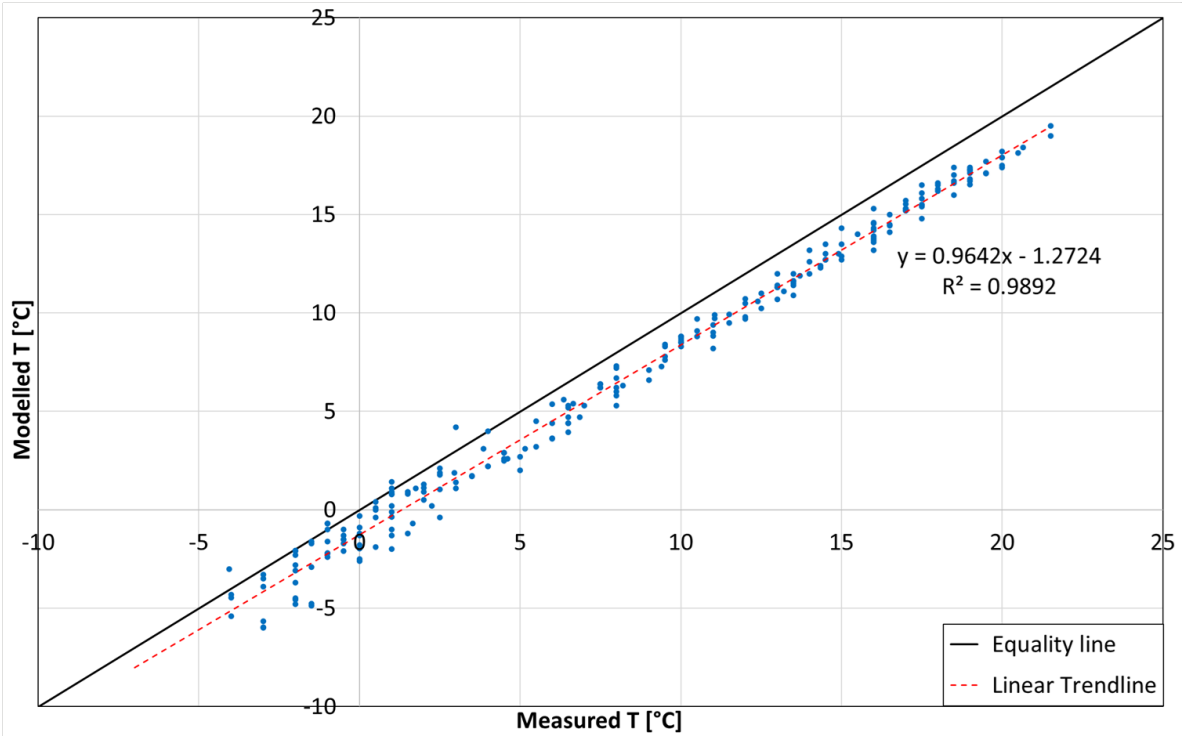

(b) Field observations vs. ERA5 model

Figure 5.7: Comparison between measured and modeled temperature data for the 3rd quintile

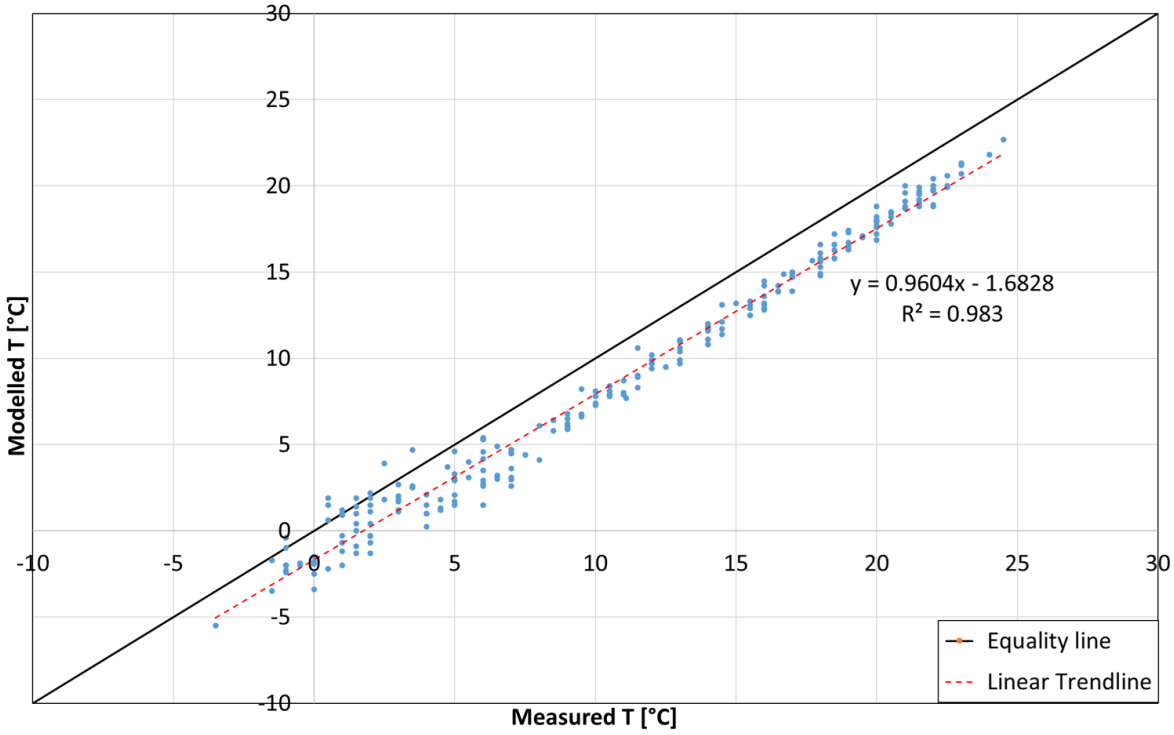

(a) Field observations vs. MERRA-2 model

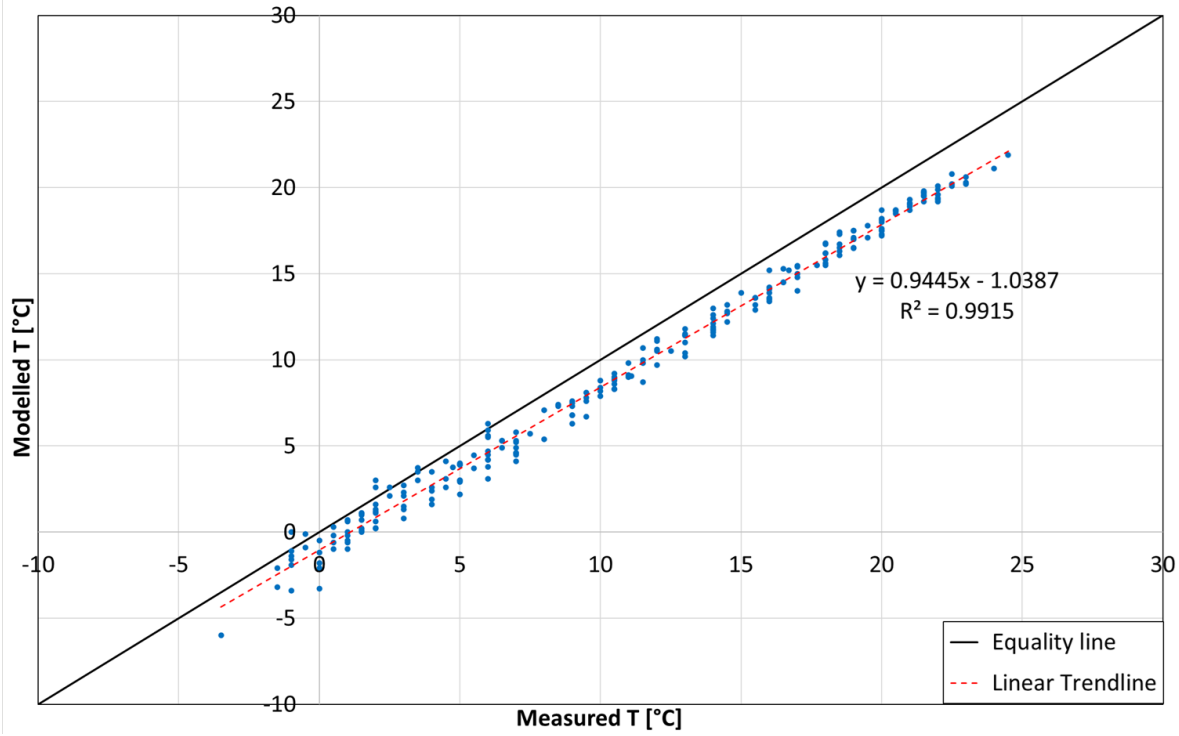

(b) Field observations vs. ERA5 model

Figure 5.8: Comparison between measured and modeled temperature data for the 4th quintile

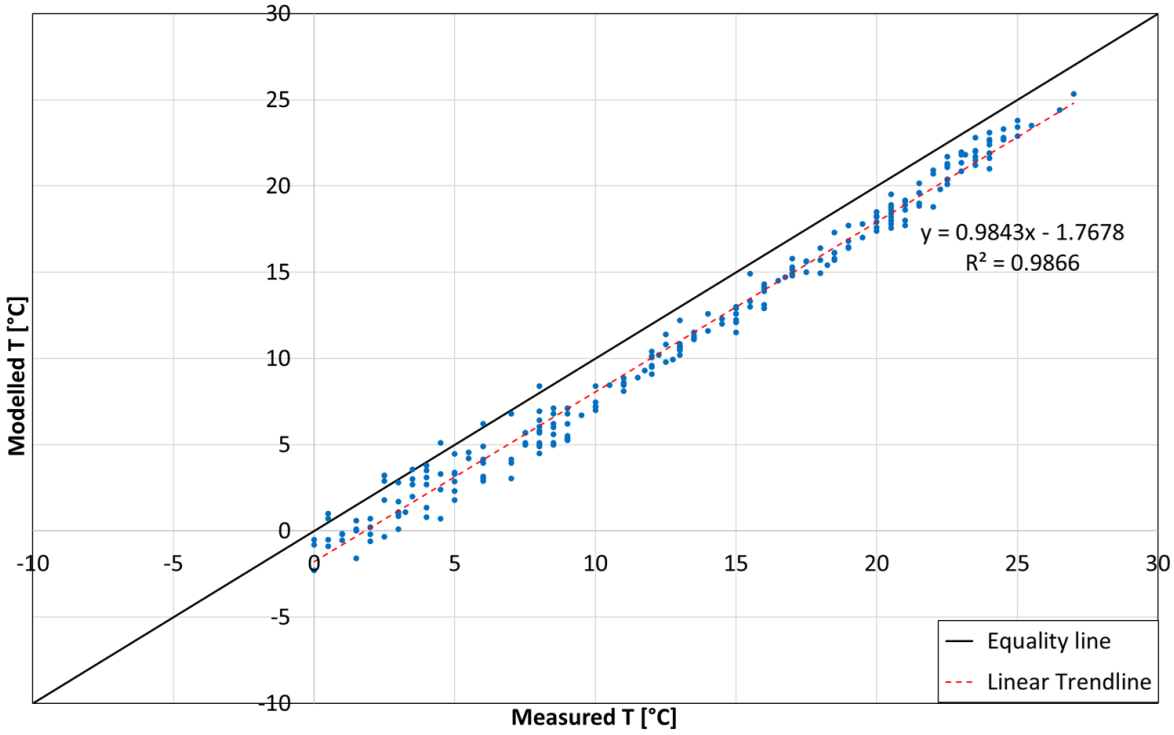

(a) Field observations vs. MERRA-2 model

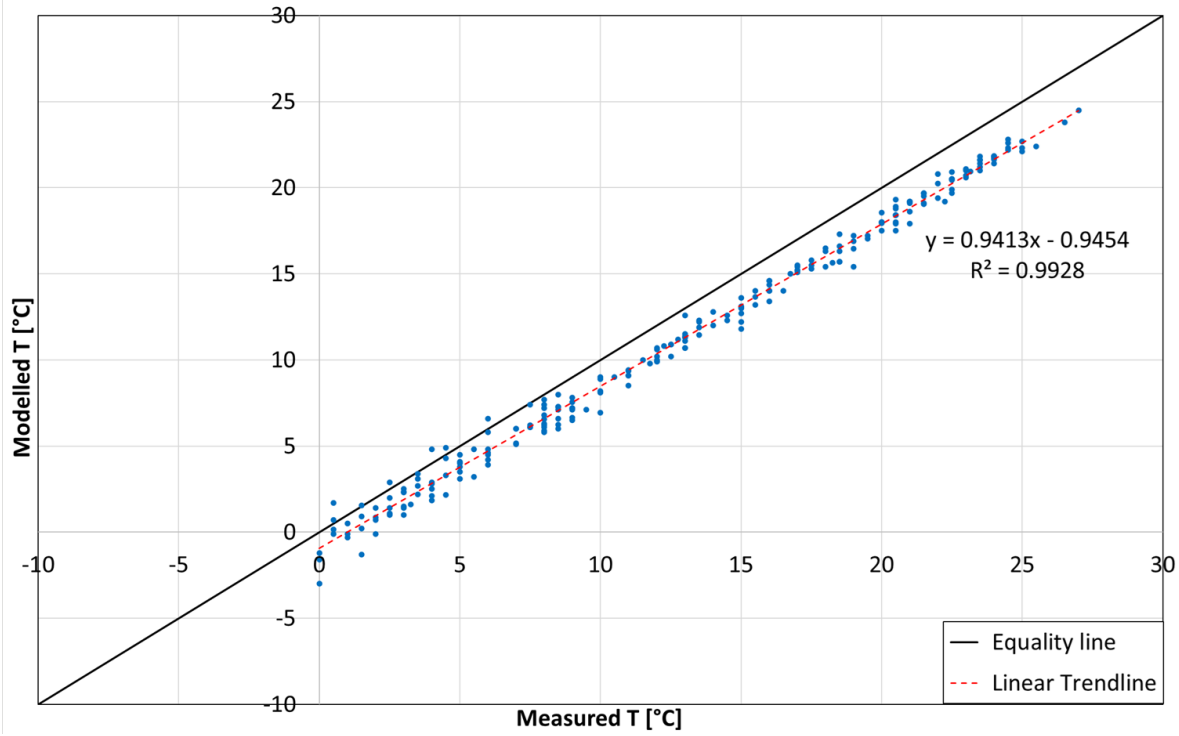

(b) Field observations vs. ERA5 model

Figure 5.9: Comparison between measured and modeled temperature data for the 5th quintile

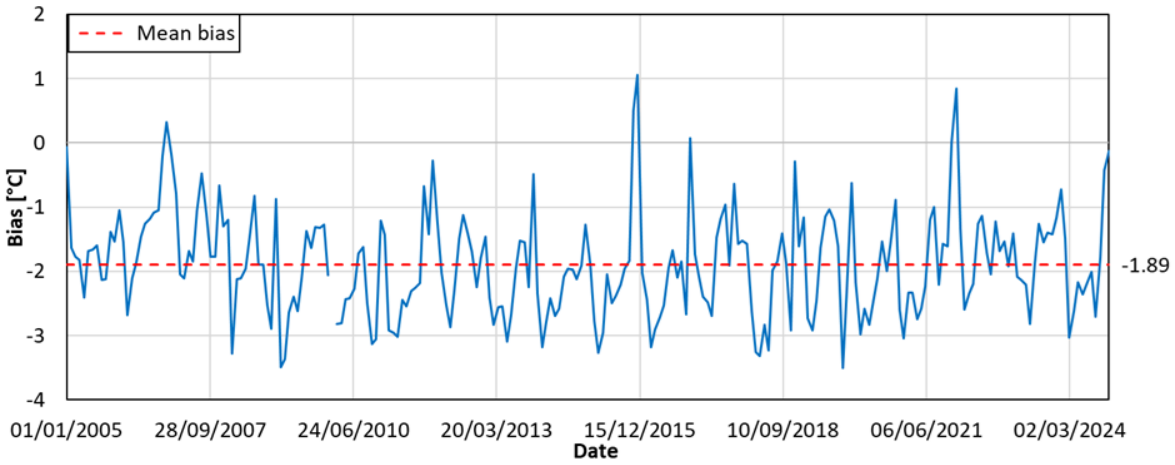

(a) Field observations vs. MERRA-2 model

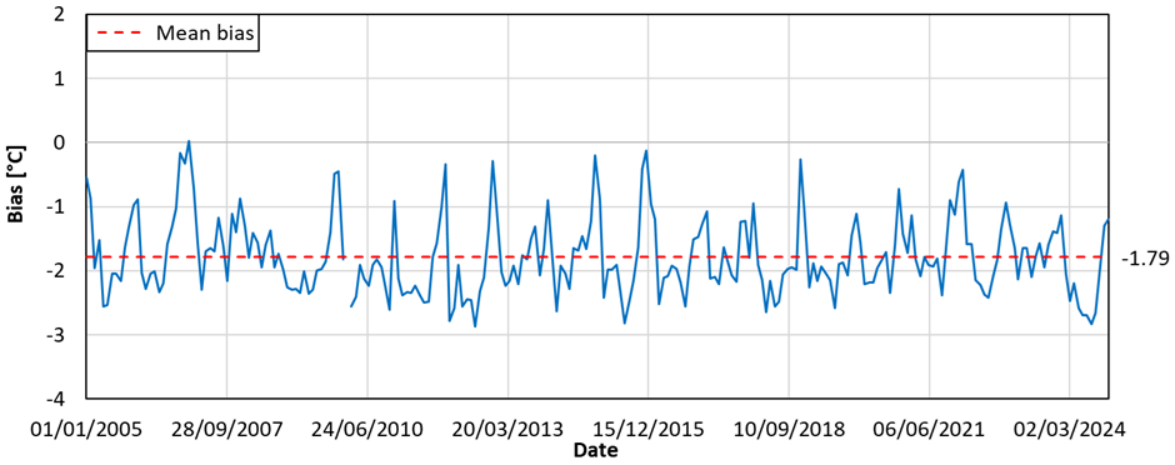

(b) Field observations vs. ERA5 model

Figure 5.10: Trend of the monthly mean bias for temperature

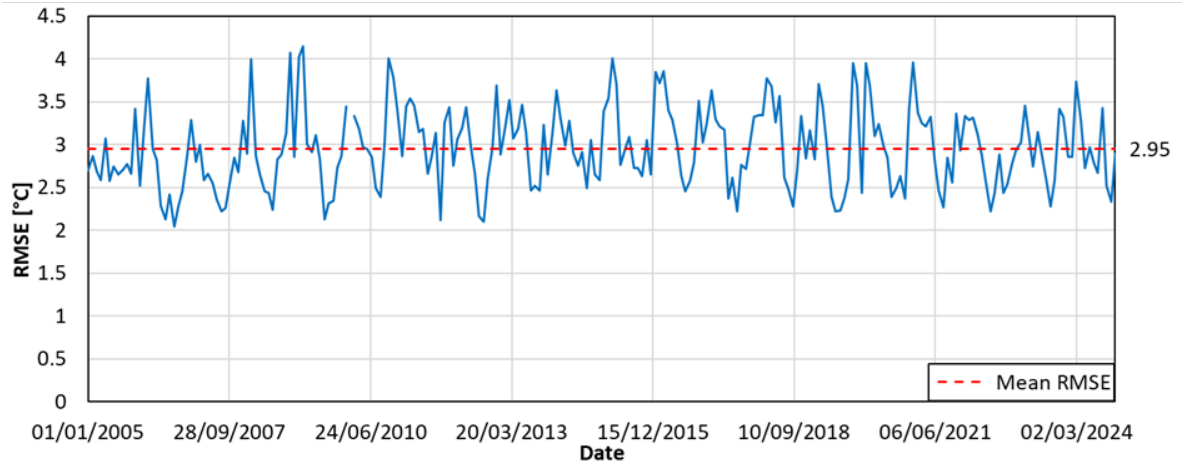

(a) Field observations vs. MERRA-2 model

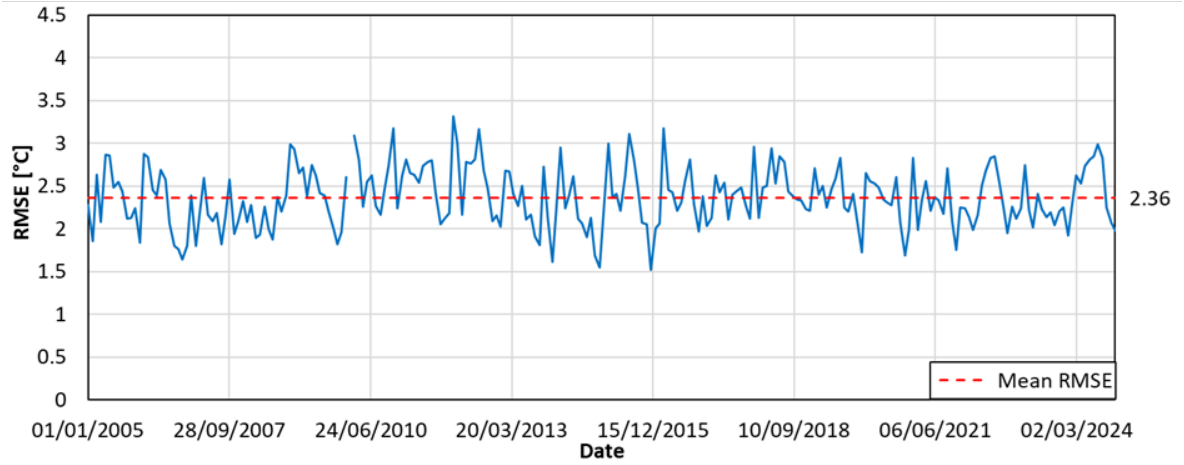

(b) Field observations vs. ERA5 model

Figure 5.11: Trend of the monthly mean RMSE for temperature

5.1.2.2 Wind speeed

The hourly modeled temperature data were plotted against the measured data to assess their agreement with the equality line (fig. 5.12). For the same purpose, the linear trendline was plotted as well.
These scatter plots show that the correlation between modeled and measured wind speed data is very poor in both cases. The slopes of the trendlines are far from those of the equality lines.
At first glance, the MERRA-2 dataset appears evenly distributed around the equality line, whereas the ERA5 dataset underestimates the measured values. This observation is confirmed by the next plots.

Hourly model-observation differences were aggregated into monthly mean biases and RMSE. The distribution of monthly mean biases and RMSE over the 20-year period was then used to compute the overall mean bias and RMSE, as shown by the dotted line in the graphs in figs. 5.13 and 5.14.
As stated above, the overall mean bias of the ERA5 estimates is negative and worse than that of MERRA-2. However, the trends in fig. 5.13 show a significant variability in the monthly mean bias over the analysis period, which explains why the overall mean RMSEs are 5.08 km/h and 5.12 km/h for MERRA-2 and ERA5, respectively.

In conclusion, both models show poor correlation with the observations.

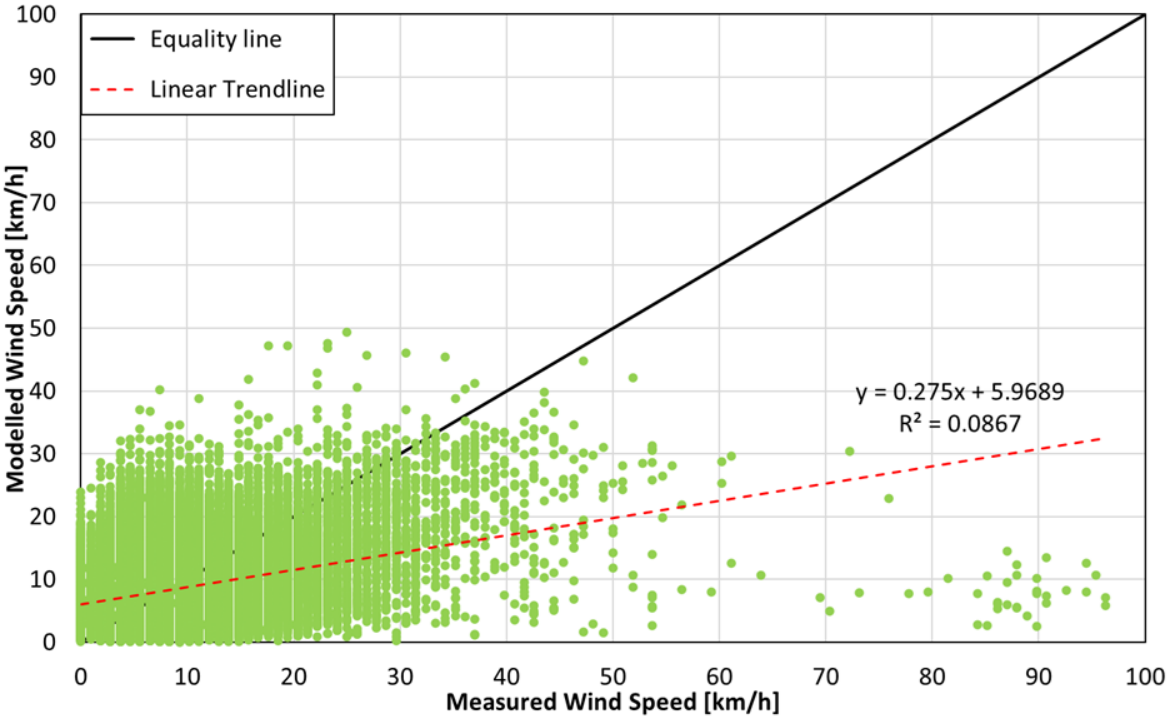

(a) Field observations vs. MERRA-2 model

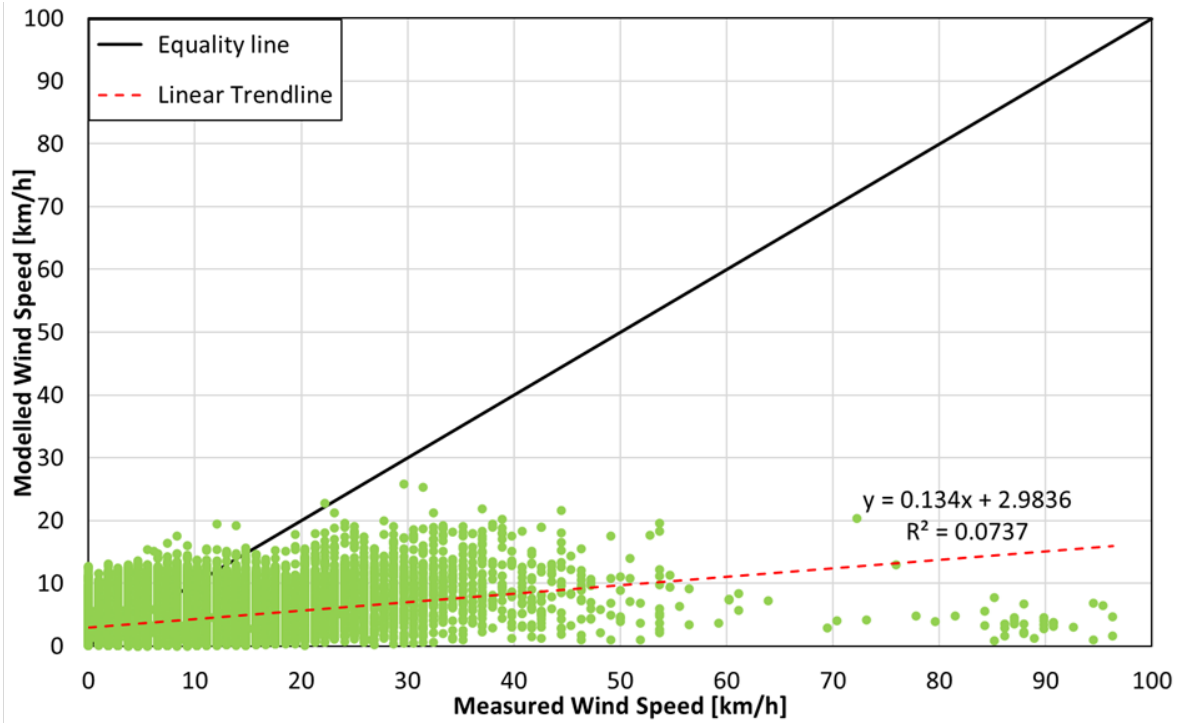

(b) Field observations vs. ERA5 model

Figure 5.12: Comparison between measured and modeled wind speed data

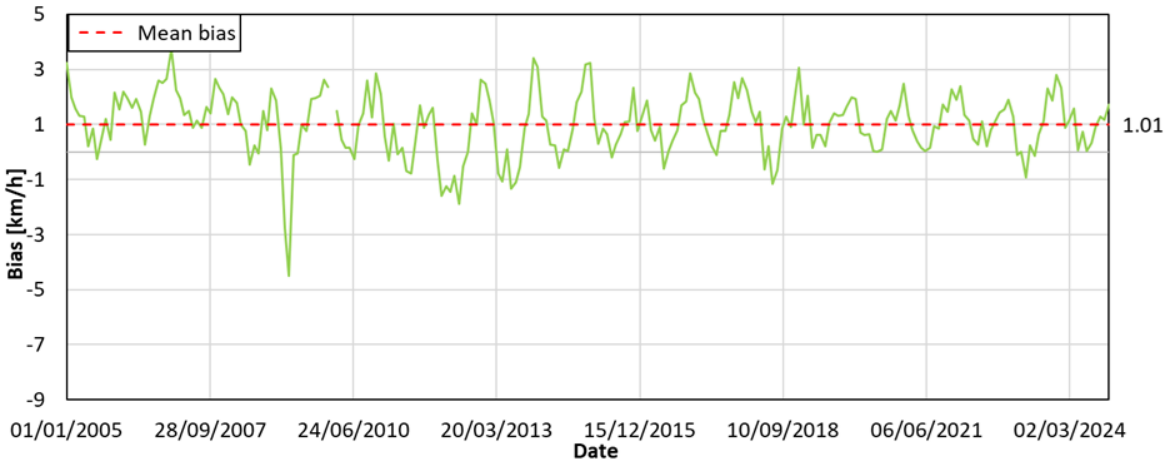

(a) Field observations vs. MERRA-2 model

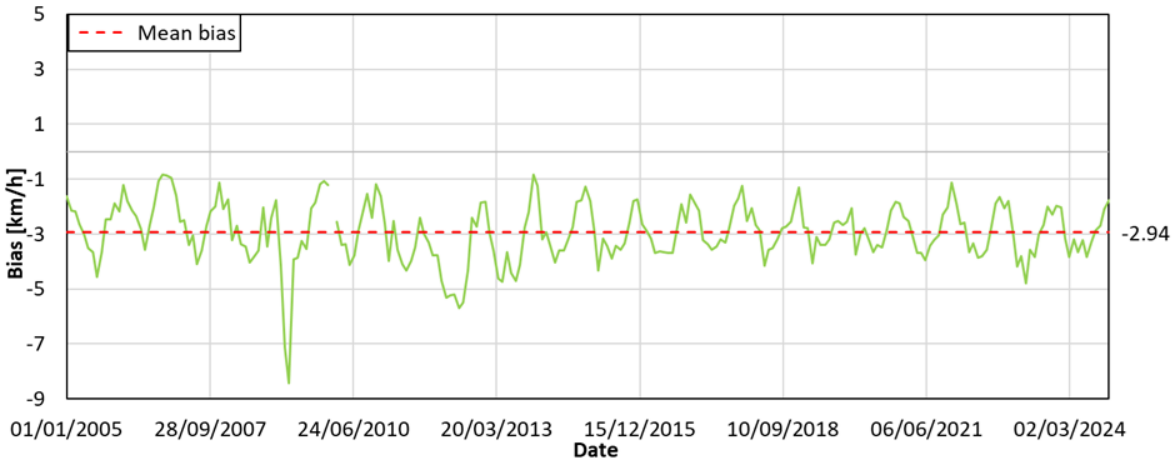

(b) Field observations vs. ERA5 model

Figure 5.13: Trend of the monthly mean bias for wind speed

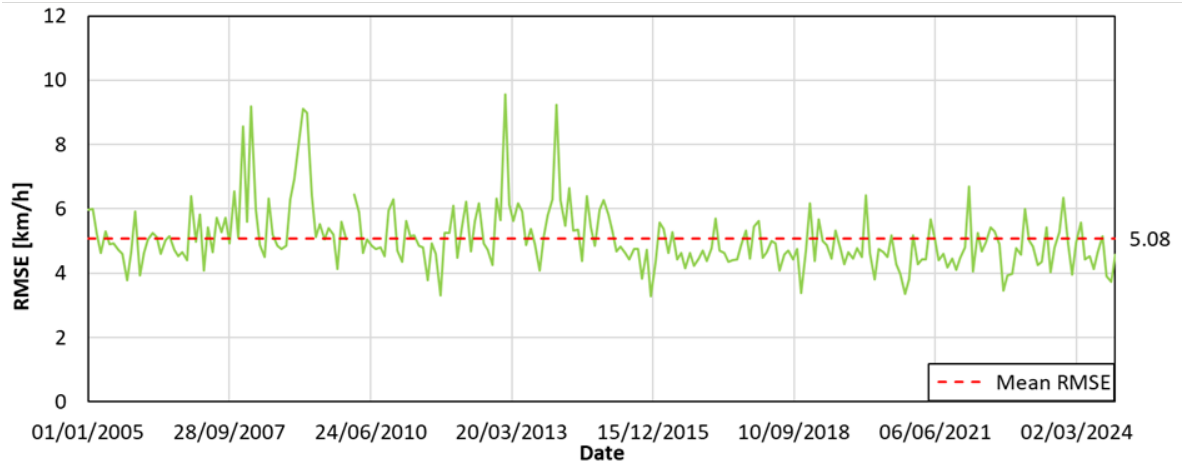

(a) Field observations vs. MERRA-2 model

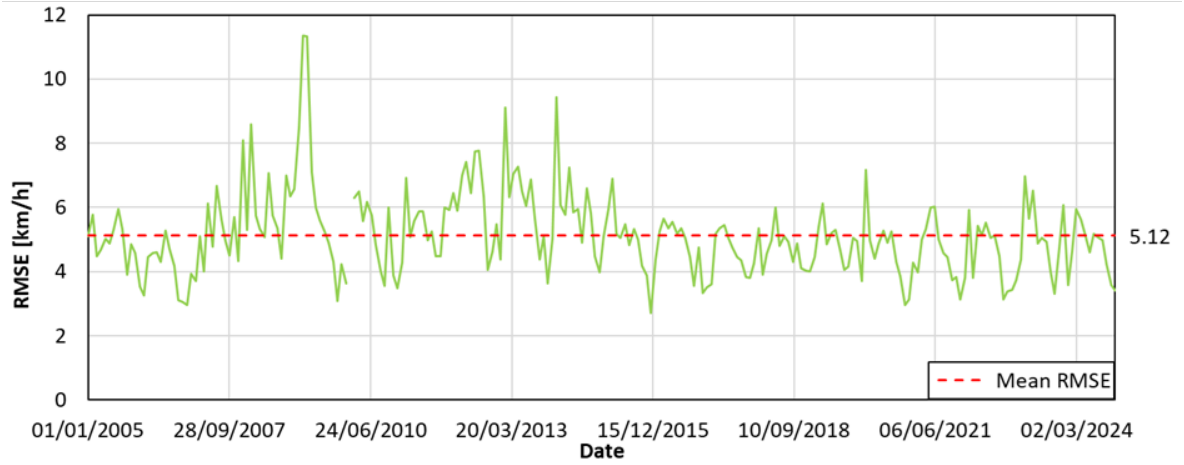

(b) Field observations vs. ERA5 model

Figure 5.14: Trend of the monthly mean RMSE for wind speed

5.1.2.3 Sunshine

The hourly modeled temperature data were plotted against the measured data to assess their agreement with the equality line (fig. 5.15). As previously mentioned, the cloud cover data are recorded in Oktas by the ITAF; in contrast, the modeled values do not belong to a discrete population. This leads to the graph layout shown in fig. 5.15. In this specific case, the linear trendline was not plotted for clear reasons.

Hourly model-observation differences were aggregated into monthly mean biases and RMSE. The distribution of monthly mean biases and RMSE over the 20-year period was then used to compute the overall mean bias and RMSE, as shown by the dotted line in the graphs in figs. 5.13 and 5.14.

In these plots, the lack of in-field observations since 2009 is pointed out.

In conclusion, the comparison between the modeled and measured data is pointless for this quantity; accordingly, the Sunshine variable will be excluded from the following considerations.

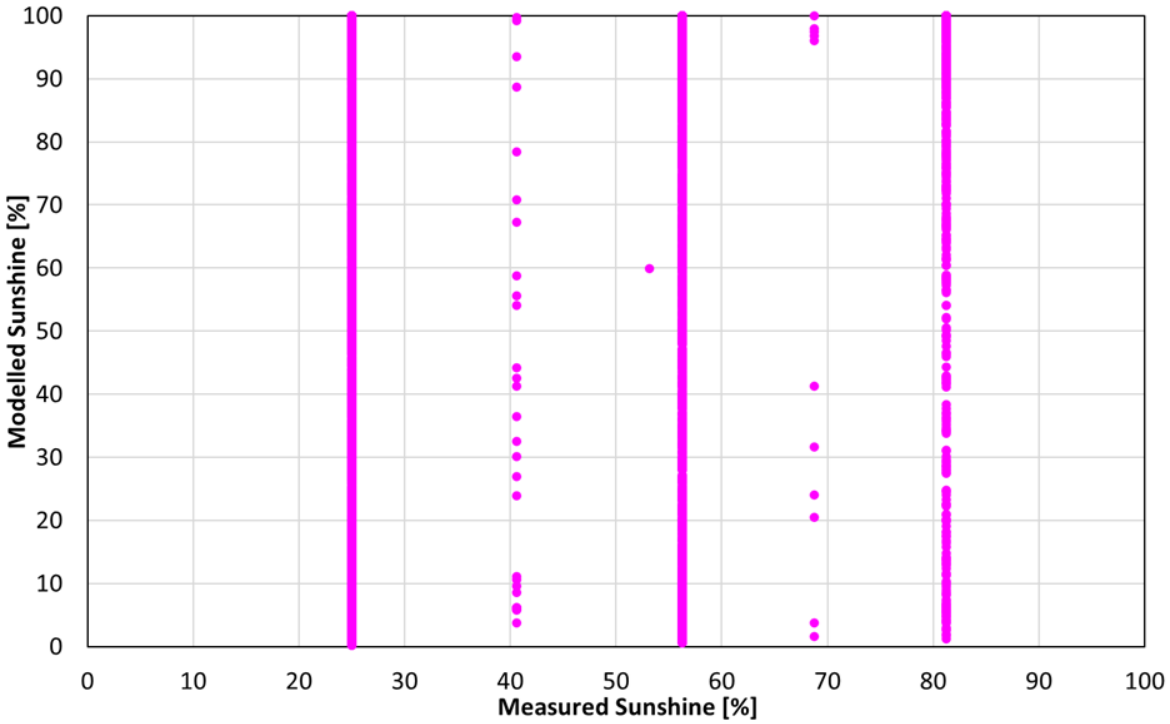

(a) Field observations vs. MERRA-2 model

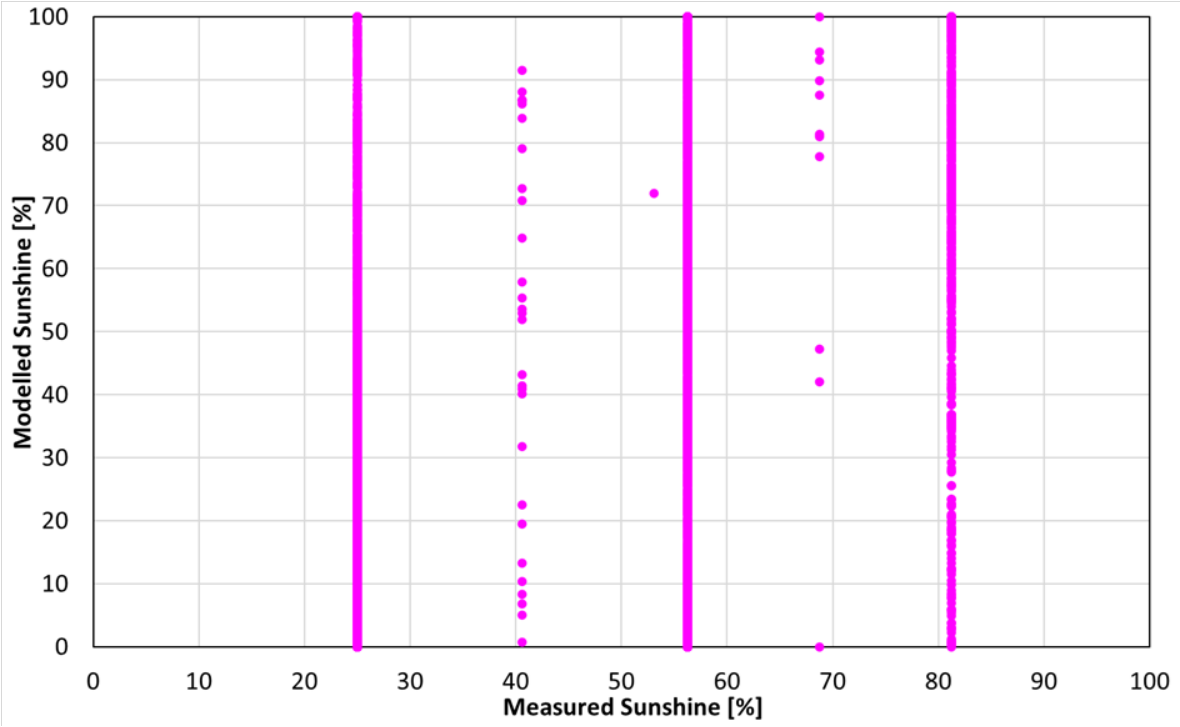

(b) Field observations vs. ERA5 model

Figure 5.15: Comparison between measured and modeled sunshine data

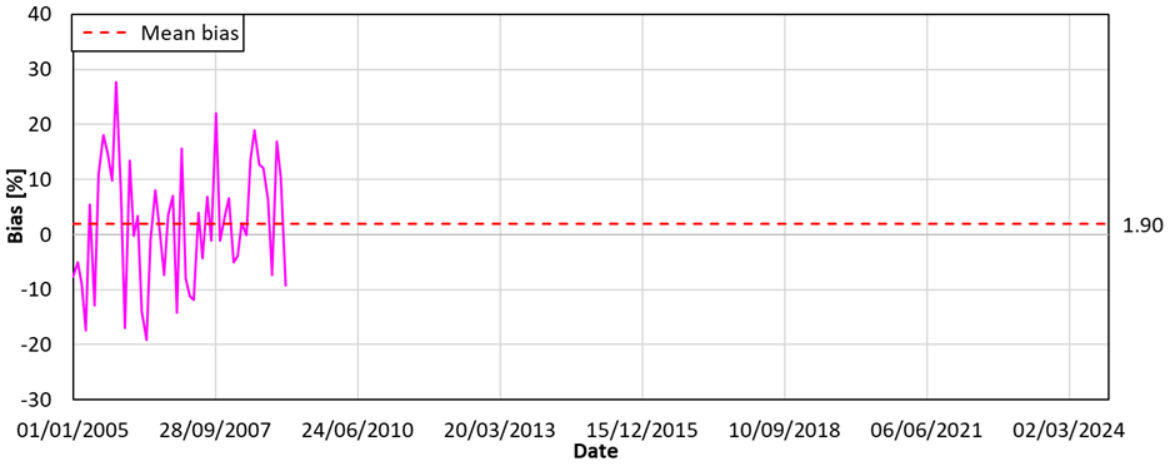

(a) Field observations vs. MERRA-2 model

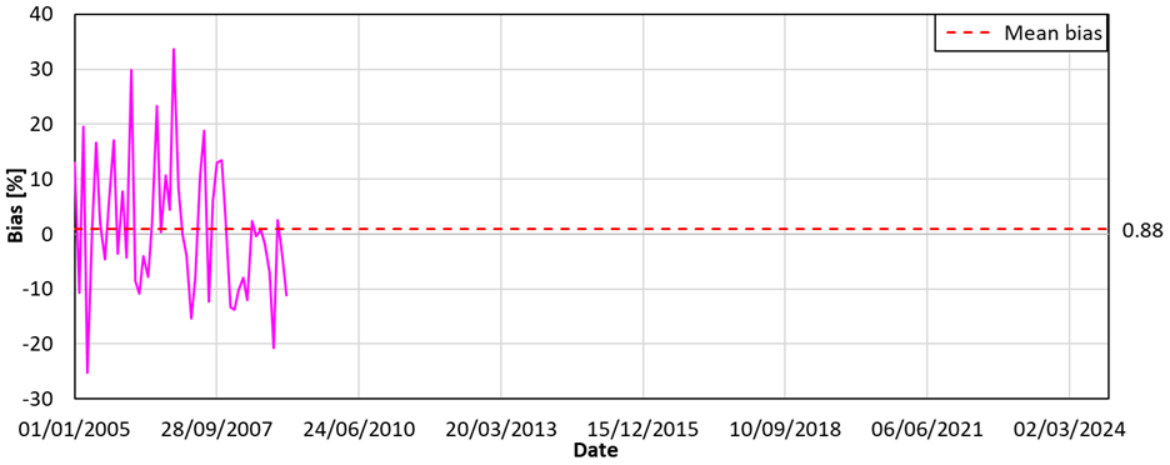

(b) Field observations vs. ERA5 model

Figure 5.16: Trend of the monthly mean bias for sunshine

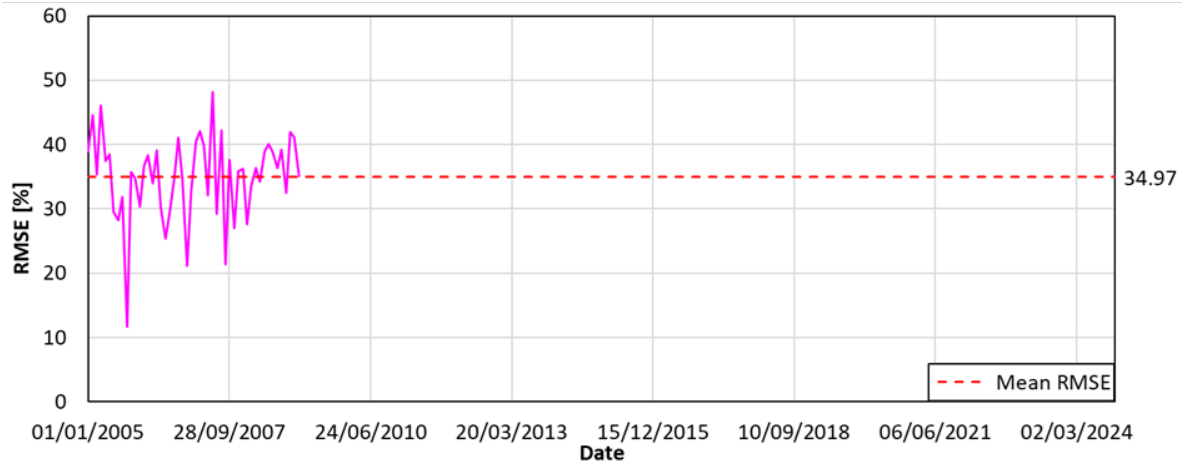

(a) Field observations vs. MERRA-2 model

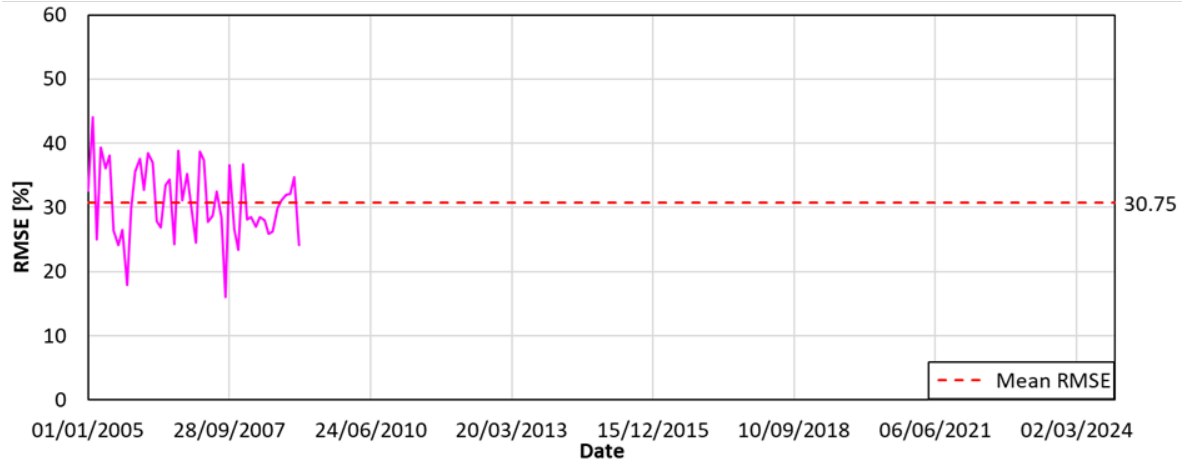

(b) Field observations vs. ERA5 model

Figure 5.17: Trend of the monthly mean RMSE for sunshine

5.1.2.4 Precipitation

The hourly modeled temperature data were plotted against the measured data to assess their agreement with the equality line (fig. 5.18). For the same purpose, the linear trendline was plotted as well.
These scatter plots show that the correlation between modeled and measured wind speed data is poor in both cases. The slopes of the trendlines are far from those of the equality lines.
At first glance, the ERA5 dataset appears slightly more evenly distributed around the equality line, whereas the MERRA-2 dataset underestimates the measured values.

Hourly model-observation differences were aggregated into monthly mean biases and RMSE. The distribution of monthly mean biases and RMSE over the 20-year period was then used to compute the overall mean bias and RMSE, represented by the dotted line in the graphs shown in figs. 5.19 and 5.20.
Unlike what seems to be shown in fig. 5.18, the overall mean biases and RMSEs suggest that the MERRA-2 dataset is more accurate in predicting the actual 12-hour cumulated precipitation values. As a matter of fact, the overall mean biases in fig. 5.19 are -0.17 mm and 0.92 mm for MERRA-2 and ERA5, respectively. Nevertheless, the variability of the MERRA-2 monthly mean biases is lower than that of ERA5, and the temporal trend is even smoother. As a result, as shown in fig. 5.18, the overall mean RMSE is lower for MERRA-2 than ERA5.

In conclusion, the MERRA-2 reanalysis dataset more accurately predicts actual precipitation.

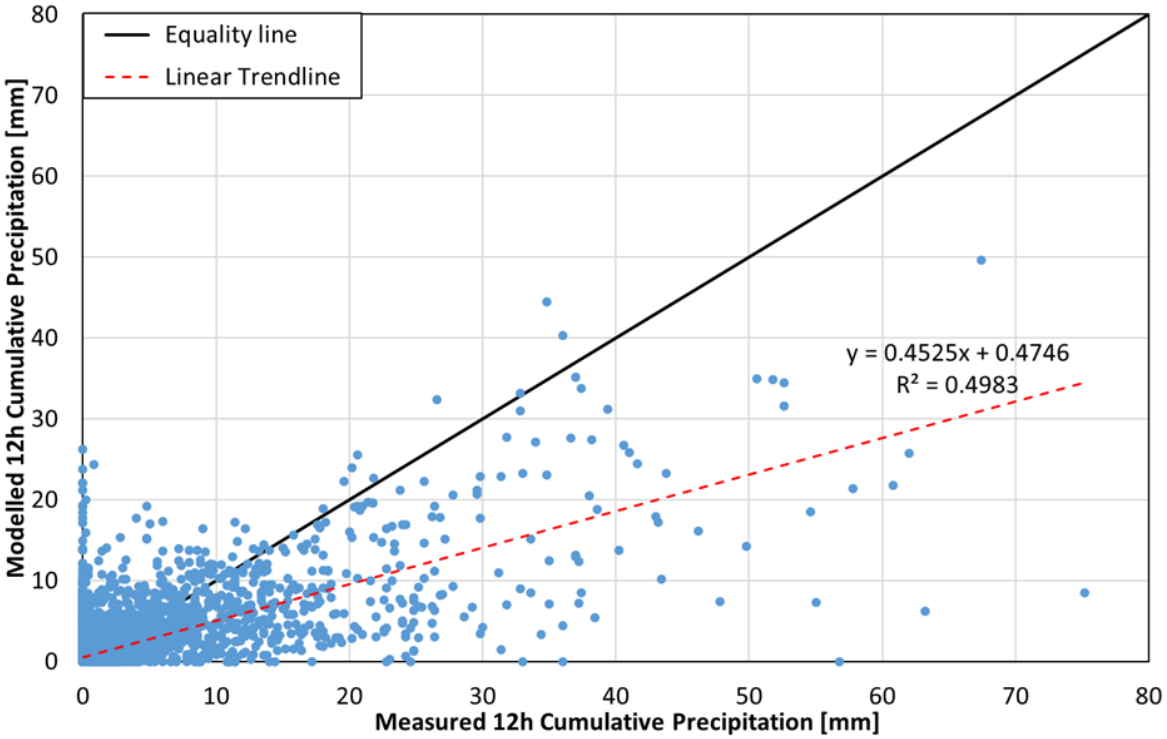

(a) Field observations vs. MERRA-2 model

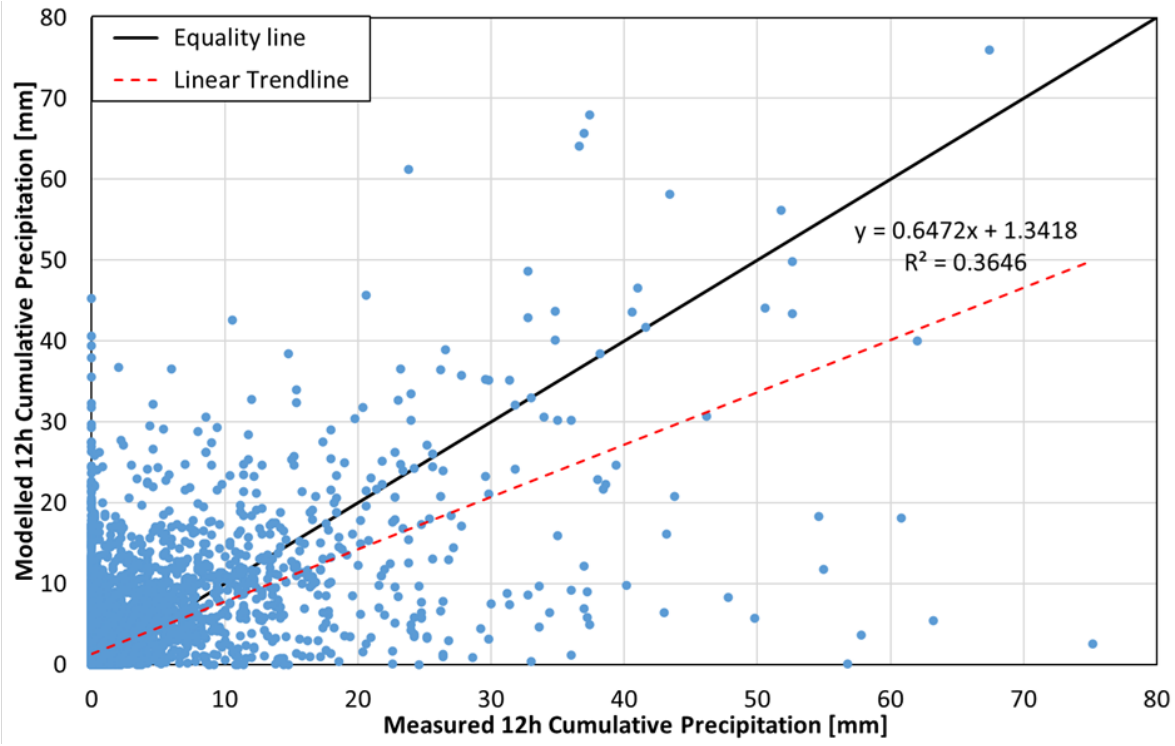

(b) Field observations vs. ERA5 model

Figure 5.18: Comparison between measured and modeled precipitation data

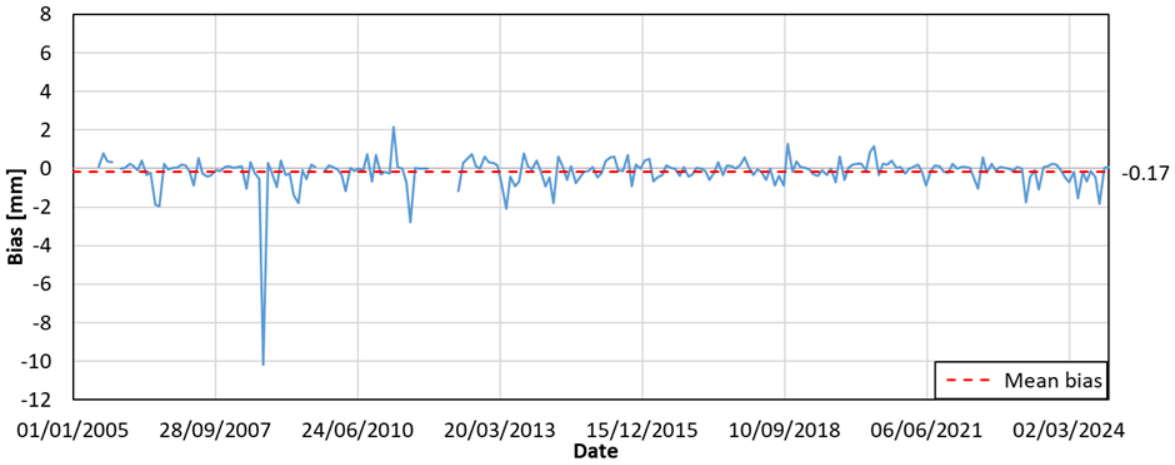

(a) Field observations vs. MERRA-2 model

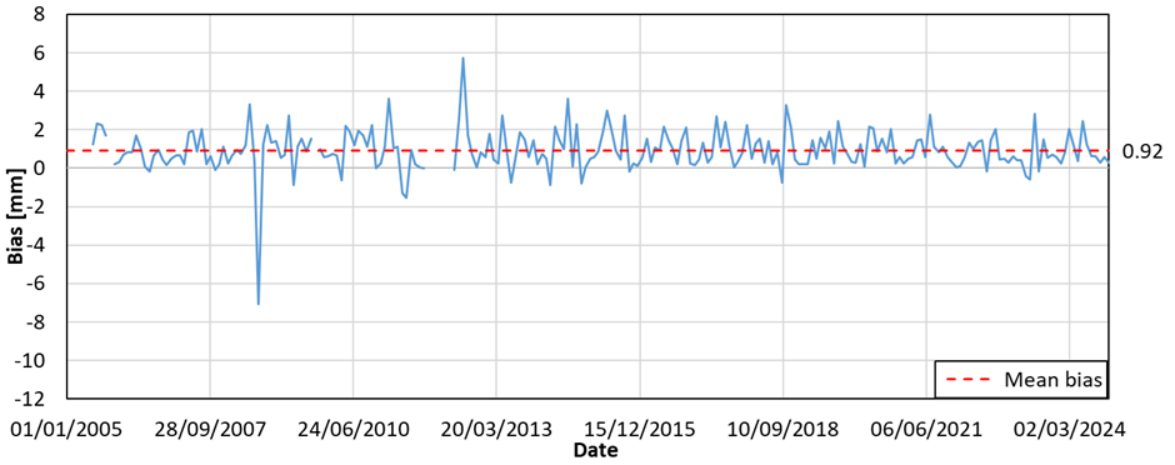

(b) Field observations vs. ERA5 model

Figure 5.19: Trend of the monthly mean bias for precipitation

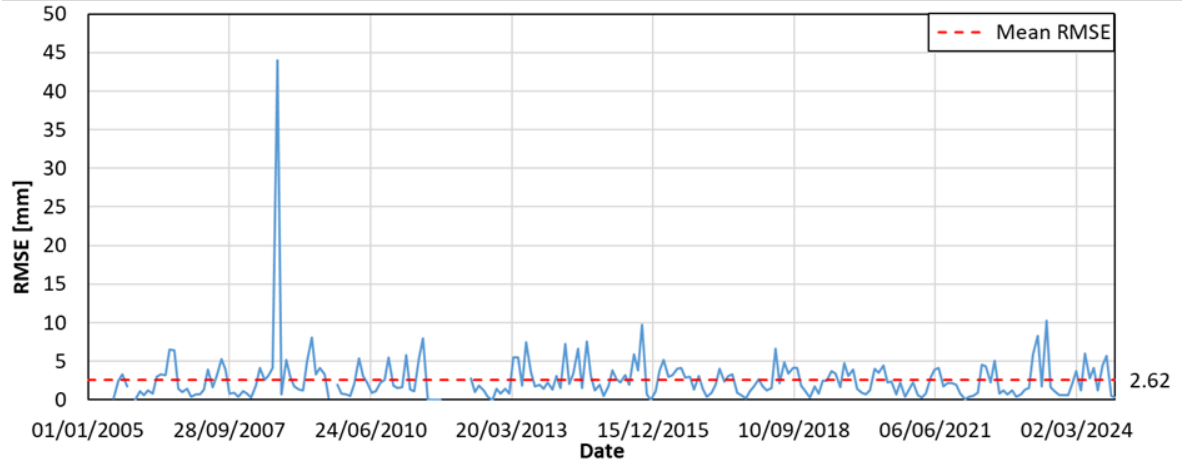

(a) Field observations vs. MERRA-2 model

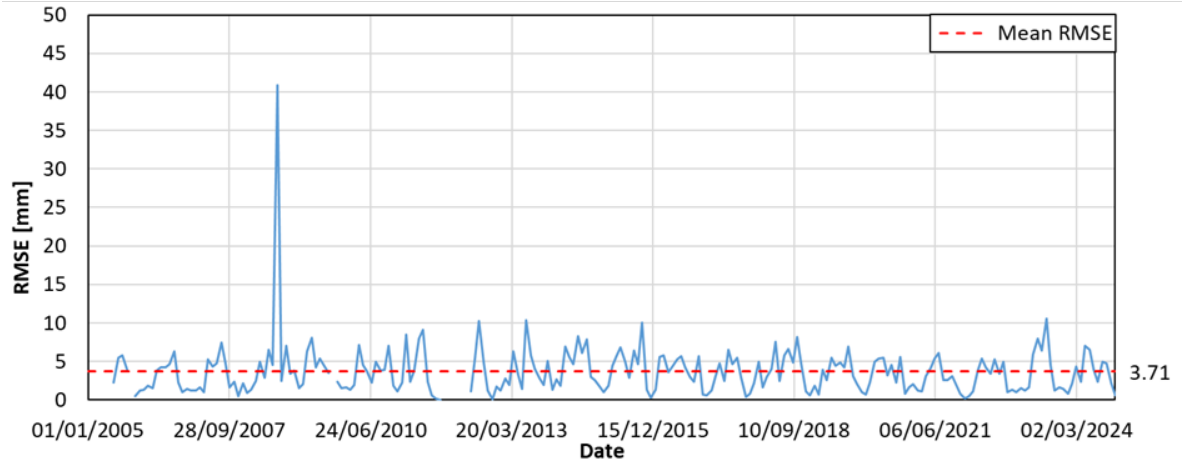

(b) Field observations vs. ERA5 model

Figure 5.20: Trend of the monthly mean RMSE for precipitation

5.1.2.5 Relative humidity

The hourly modeled temperature data were plotted against the measured data to assess their agreement with the equality line (fig. 5.21). For the same purpose, the linear trendline was plotted as well.
These scatter plots show that the correlation between modeled and measured wind speed data is average in both cases. The slopes of the trendlines are neither far nor similar to those of the equality lines. The trendline equations are similar, even though the values predicted by the MERRA-2 reanalysis model are more dispersed than those from ERA5.

Hourly model-observation differences were aggregated into monthly mean biases and RMSE. The distribution of monthly mean biases and RMSE over the 20-year period was then used to compute the overall mean bias and RMSE, as shown by the dotted line in the graphs in figs. 5.22 and 5.23.
The trends in fig. 5.22 show a significant variability in the monthly mean bias over the analysis period, which explains why the overall mean RMSEs are 14.77 % and 11.03 % for MERRA-2 and ERA5, respectively.

In conclusion, both models are poorly correlated with the observations. Still, the ERA5 dataset is the best for relative humidity.

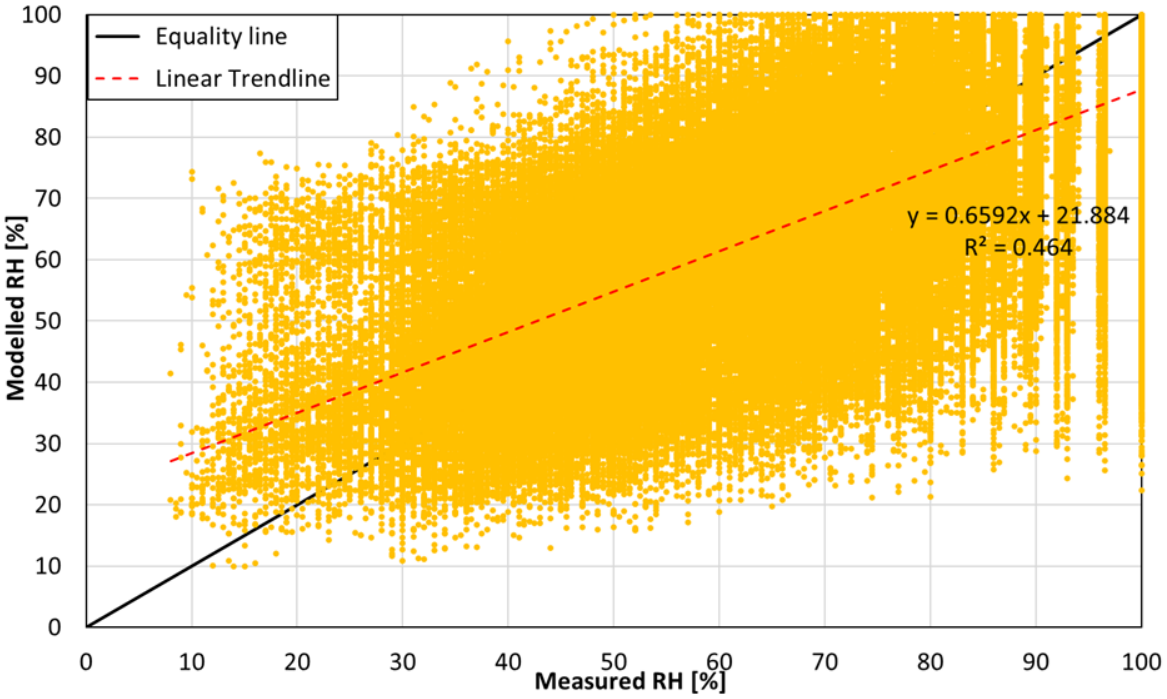

(a) Field observations vs. MERRA-2 model

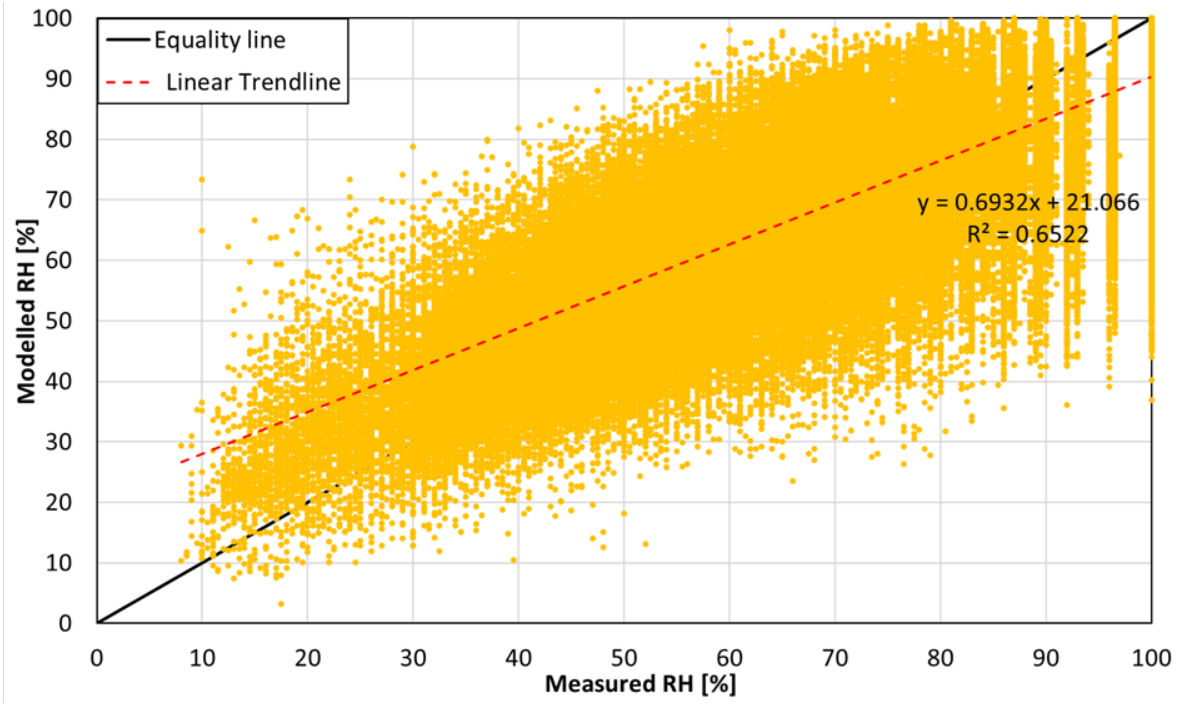

(b) Field observations vs. ERA5 model

Figure 5.21: Comparison between measured and modeled RH data

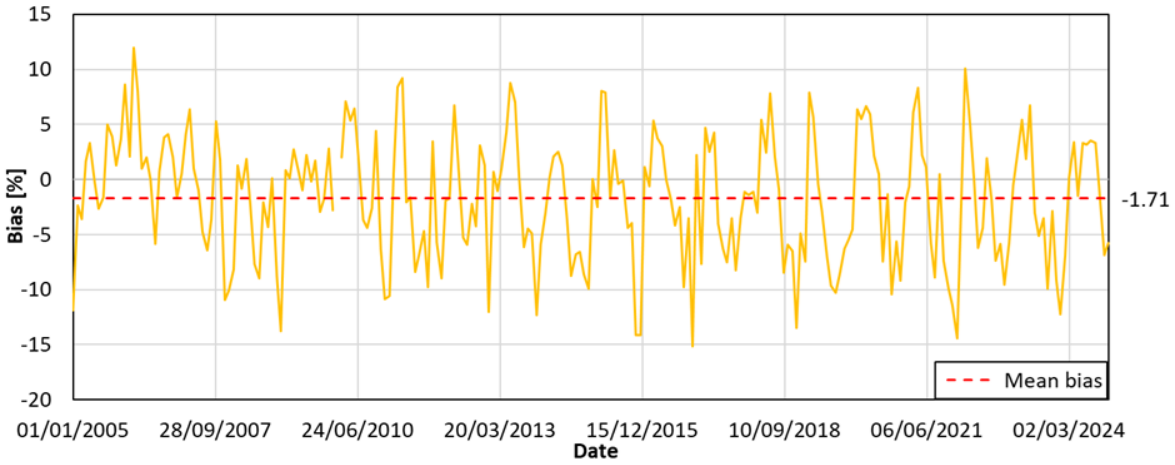

(a) Field observations vs. MERRA-2 model

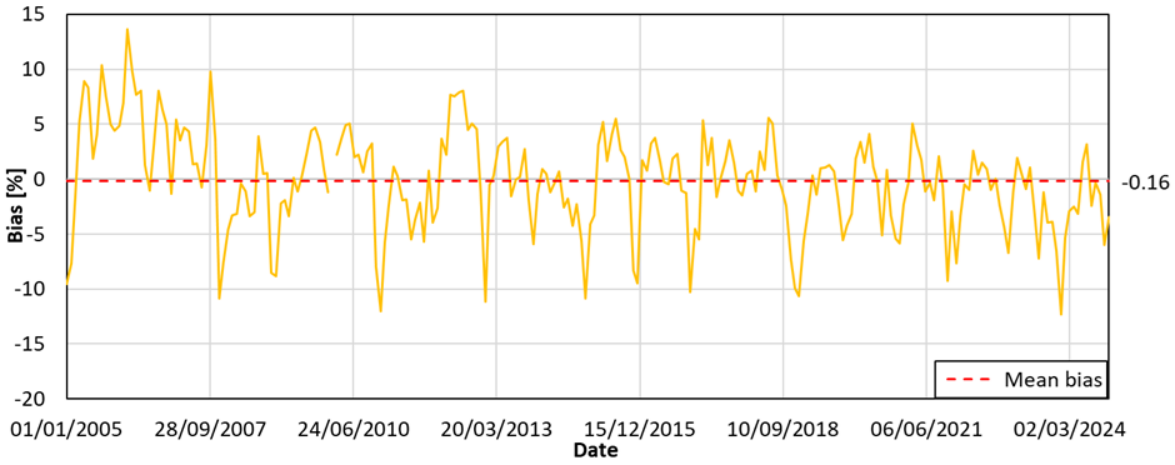

(b) Field observations vs. ERA5 model

Figure 5.22: Trend of the monthly mean bias for RH

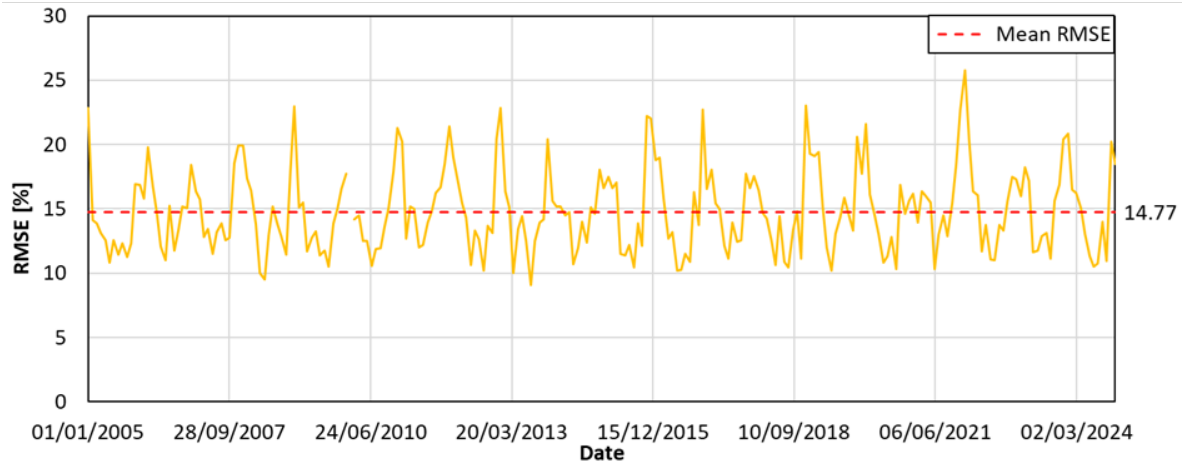

(a) Field observations vs. MERRA-2 model

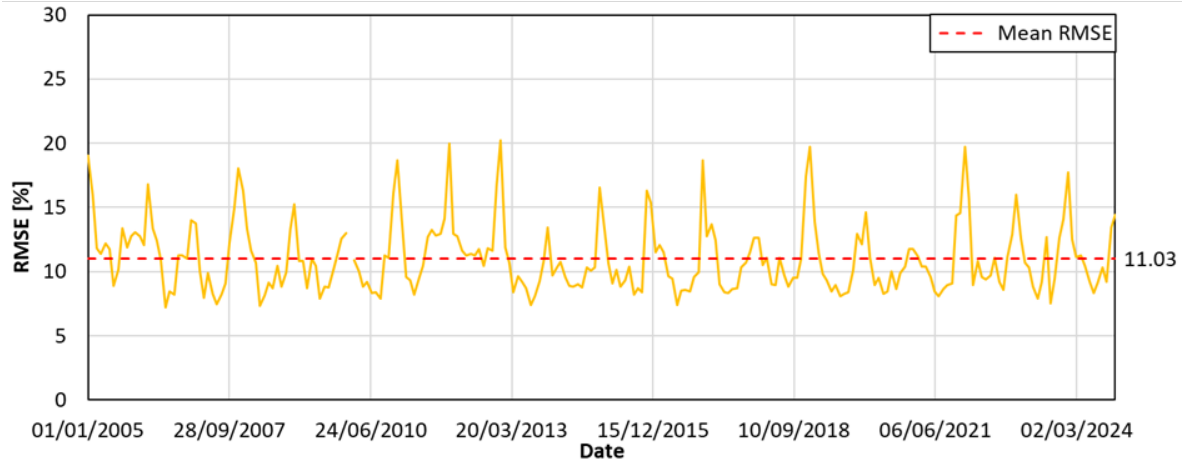

(b) Field observations vs. ERA5 model

Figure 5.23: Trend of the monthly mean RMSE for RH

5.1.3 Final considerations

A summary of the overall mean biases and RMSEs for the five variables under analysis is reported below.

	Dataset	T [°C]	WS [km/h]	Sun [%]	Prec [mm]	RH [%]
Bias	**MERRA-2**	-1.89	1.01	1.9	-0.17	-1.71
	ERA5	-1.79	-2.94	0.88	0.92	-0.16
RMSE	**MERRA-2**	2.95	5.08	34.97	2.62	14.77
	ERA5	2.36	5.12	30.75	3.71	11.03

As discussed earlier, the final assessment of the reanalysis model's accuracy overlooks the Sunshine data. Regarding the wind speed variable, neither model proved more accurate than the other. On the other hand, the ERA5 dataset yielded more accurate predictions for temperature and relative humidity, whereas the MERRA-2 modeled data better represent precipitation.

Although the comparison does not identify a dataset that consistently outperforms the others across all variables, ERA5 performs better on the majority of variables considered in the analysis. In addition, ERA5 provides a higher spatial resolution than MERRA-2, which is advantageous for representing local climatic conditions.

For these reasons, the ERA5 reanalysis dataset is recommended as the reference climatic database for implementing the MEPDG framework in the Italian context.

The Python script developed for processing ERA5 raw climate data is shown in Code A.1.

5.2 Traffic section

5.2.1 Traffic input levels: a new approach for the Italian implementation

Although input levels for both materials and traffic are formally defined in the MEPDG, they serve different purposes. In the case of materials, some physical and mechanical properties are required; thus, the input levels assess the expected accuracy of the data. On the other hand, the data necessary on the traffic side are neither physical nor mechanical properties, yet they are aggregated descriptors of the traffic to serve.

Therefore, the traffic input levels indicate the scale and source of the information, rather than the expected accuracy of the data. In particular, default values are suggested as input level 3: these values have been developed through a statistical traffic analysis of actual weight-in-motion data collected during the LTTP program. That being the case, their implementation in the US context is meaningful. Instead, the input level 3 identified in the MEPDG should not be implemented in the Italian context, as the original background of these statistics is likely inconsistent with the local one.

For this reason, an alternative to the default traffic information embedded in the MEPDG is needed: in view of the implementation in the Italian context, a new data-source-based approach to the traffic input levels is hereafter proposed.

Three categories of variables can be identified concerning traffic information:

- traffic count;
- vehicle classification;
- axle weights.

Knowledge of all three variables mentioned above enables full characterization of the roadway traffic. In fact, the AADTT – and possibly related statistics, such as the lane distribution factor and direction distribution factor – and MAF can be derived from the traffic count. Additionally, the vehicle class distribution comes from the vehicle classification; the number of axles per truck is obtained by considering the traffic count and vehicle classification. Finally, the axle load distribution can be retrieved from the axle weight data.

Regarding the new data-source-based approach to the traffic input levels, the sources of the three categories of information are summarized in table 5.2.

Input Level	**Traffic count**	**Vehicle classification**	**Axle weights**
1	WIM	WIM	WIM
2	AVC/Camera	AVC/Camera	CNR
3	Manual	CNR	CNR

Table 5.2: New approach for traffic input levels

Input level 1 is to be implemented when weight-in-motion data is available for the infrastructure in question or its feeder connectors. All input data are derived from field observations. Input level 1 is thought to provide the highest form of detail and accuracy.

Input level 2 is suggested when traffic count and vehicle classification for the infrastructure in question or its feeder connectors are available by means of AVC devices or cameras. The axle load distribution tables are the default ones from the CNR catalog. Input Level 2 represents a compromise between direct observations and standard assumptions.

Input level 3 is suggested when the output of manual vehicle count for the infrastructure in question or its feeder connectors is available, but no other direct observation can be obtained. The axle weights and vehicle classification tables are the default ones from the CNR catalog, while the axle per truck table comes from a theoretical definition of the traffic class itself. Input Level 3 is expected to be the least accurate level of characterization, yet it enables the use of information other than direct observation.

5.2.2 Traffic data processing

The workflow for implementing Italian traffic according to the new approach is outlined in this section.

The axle configuration of the vehicles is defined by a vector of digits, whose coding convention was proposed by [18]. Each axle corresponds to a digit: "1" is for a single axle, "2" is for an axle belonging to a tandem group, "3" is for an axle belonging to a tridem group, while "4" to "7" are for axles belonging to a multi-axle system of four, five, six, and seven axles. By way of example, the vector [1 1 3 3 3 0 0 0 0 0] indicates a five-axle vehicle with two single axles and one tridem axle group, while the vector [1 2 2 1 3 3 3 0 0 0] corresponds to a seven-axle truck with one single axle, followed by a tandem group, another single axle, and a tridem group.

First, the sixteen Italian classes defined in the Italian Catalog of Road Pavements are mapped to the ten FHWA classes based on the truck axle configuration in terms of number of axles and axle type, and on the truck vehicle type, following [6]. Specifically, six out of ten FHWA classes are crowded by the Italian ones:

- buses of Italian classes 14, 15, and 16 were found to be equivalent to two-axle buses of FHWA class 4;
- light, medium, and heavy trucks of Italian classes 1, 2, 3, and 4 were found to be equivalent to single-unit, two-axle trucks of FHWA class 5;
- heavy trucks of Italian classes 5 and 6 were found to be equivalent to single-unit, three-axle trucks of FHWA class 6;

- truck-trailers and semi-trailers of Italian classes 7 and 8 were found to be equivalent to single-trailer, four-axle trucks of FHWA class 8;
- truck-trailers and semi-trailers of Italian classes 9 and 10 were found to be equivalent to five-axle tractor semi-trailer trucks of FHWA class 9;
- truck-trailers and semi-trailers of Italian classes 11 and 12, and construction trucks of the Italian class 13, were found to be equivalent to multi-trailer trucks of FHWA class 10.

The correspondence identified in this thesis is slightly different from that obtained by prof. Caliendo in the previous work performed. Indeed, although Italian classes 9, 10, 11, 12, and 13 feature five-axle trucks, the axle layout of classes 9 and 10 (i.e., [1 2 2 2 2 0 0 0 0 0]) is not the same as that of classes 11, 12, and 13 (i.e., [1 1 3 3 3 0 0 0 0 0]). Therefore, these classes were assigned to two separate FHWA classes (namely, classes 9 and 11) to account for the different types of axle groups, as the number of axles per truck plays an important role in the MEPDG framework.

If needed, the remaining FHWA classes may be employed to include those vehicle types overlooked in the Italian classification system but still traveling in the Italian road network.

A graphical and color-coded representation of the class mapping is shown in fig. 5.24.

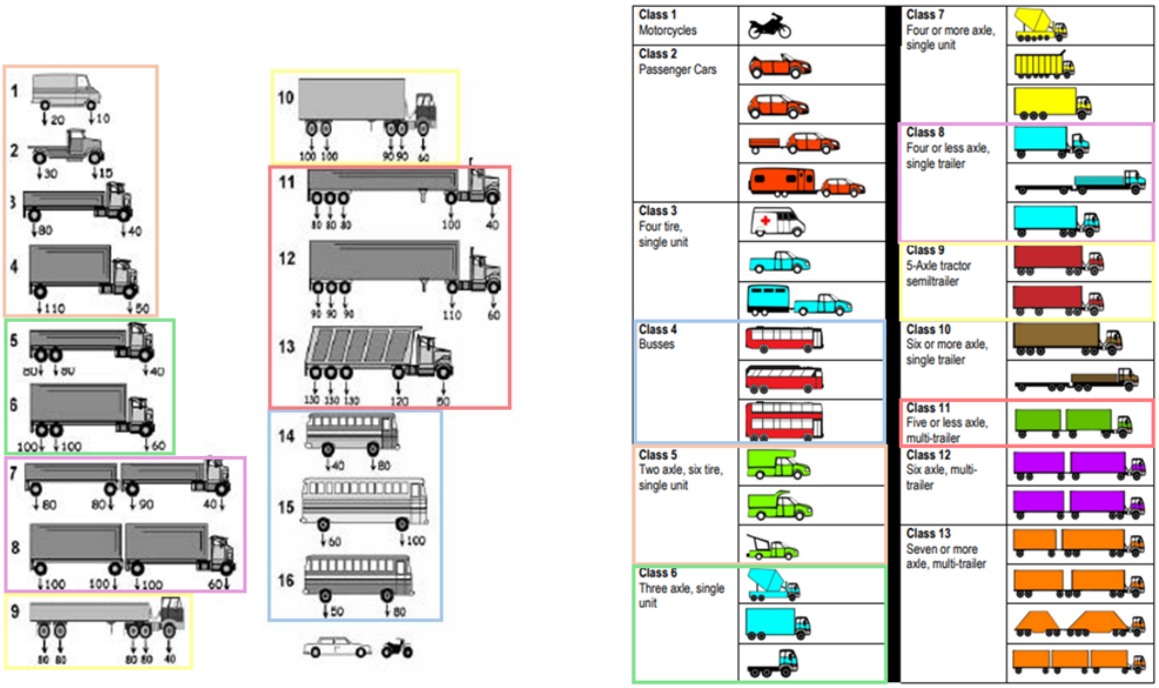

Figure 5.24: Italian to FHWA class mapping

The procedure branches off in three directions, according to the input level considered. The workflows for each of the three input levels are described hereafter.

5.2.2.1 WIM data processing for the new Input Level 1

The following step consists of the weight-in-motion data processing to exclude the light vehicles from the dataset. Here, an assumption is made: the light vehicles are identified as those whose wheelbase is less than 3 m. As a result, the traffic count is obtained.

Subsequently, the remaining heavy vehicles are aggregated into the six FHWA truck classes mentioned above. The truck aggregation into FHWA classes is performed based on the axle number, axle type, and vehicle configuration; that is, vehicles with 3 and 4 axles are entered in classes 6 and 8, respectively. Two-axle vehicles may fall into either class 4 or 5: to assess this, the wheelbase is used as a classification criterion, and it is assumed that two-axle trucks whose wheelbase is less than 5 m are allocated to class 5, while the remaining ones are considered to be buses and fall into class 4. Similarly, five-axle vehicles may belong to either class 9 or 11: to discriminate between them, the trucks featuring the [1 2 2 2 2 0 0 0 0 0] axle layout are grouped in class 9, and those featuring the [1 1 3 3 3 0 0 0 0 0] axle layout are grouped in class 11. In this way, the vehicle classification is derived.

Finally, each axle is assigned to the appropriate load bin according to its axle load. As a result, the category of variable related to axle weights is assessed too.

The Python code developed for these purposes is reported in chapter A.

5.2.2.2 AVC or camera data analysis for the new Input Level 2

The information obtained through AVC devices or cameras is to be analyzed to classify vehicles based on the same rationale as for Input Level 1. Thus, the traffic count and vehicle classification are straightforward.

As mentioned, the axle weights are the CNR standard ones. The detailed procedure to derive the CNR-based axle load distributions is outlined in chapter A.

5.2.2.3 Manual traffic count for the new Input Level 3

The CNR vehicle class distribution is applied to the AADTT originating from the manual truck count to retrieve the vehicle classification variable.
The axle weights are the CNR standard ones, just as in Input Level 2.

5.3 Materials section

In this section, the calibration procedures for the damage functions are addressed. Finally, a set of local standards is provided for the testing procedures necessary to implement the MEPDG in the Italian context.

5.3.1 Mixture-specific calibration for the damage models

The implementation of the MEPDG to local conditions involves the calibration of the β parameters incorporated in the distress damage functions presented in eqs. (2.3), (2.10), (2.15) and (2.20). The β parameters are representative of the actual performance of the material in question against the specific damage considered, which the other mechanical properties are not capable of properly characterizing.
It is essential to clarify that the calibration introduced in this section is material-specific, as it does not deal with the calibration of the transfer function presented in eqs. (2.6), (2.7) and (2.14), which is network and context-specific instead.
The material-specific calibration of the damage functions is performed independently on the MEPDG, while the calibration of the actual transfer functions aims at minimizing

the bias and the standard deviation between the modeled and measured values of the damage. In this regard, the transfer functions were included in the MEPDG to dispose of some in-field variables that could be measured in the framework of the Pavement Management System, and allow for the calibration of their coefficients. The common practice in the PMS is to periodically record the entity and severity of the in-field distress: as a matter of fact, the procedure is carried out regardless of the material properties of the section under analysis. Hence, the calibration of the transfer functions is carried out by setting the β parameters of the damage functions to 1.

It is worthwhile mentioning that the calibration procedures hereafter relate to the hot mix asphalt layer only. Therefore, it will be referred to as mixture-specific calibration.

The ultimate goal of the mixture-specific calibration is the development of a consistent materials library of calibration coefficients, and to use them to address their effect on the damage evolution in the same section, and at equal climate and traffic conditions. The consistency of the library lies in the procedures used to test different materials for the same parameter. For the comparison between the β factors to be meaningful, it is recommended that the observed property – which is used as a proxy for the distress in question – is investigated with the same experimental procedure for all materials belonging to the library.

5.3.1.1 Fatigue cracking model

The goal of the calibration of the fatigue cracking model is to retrieve the β coefficients of the fatigue line in eq. (2.3). The fatigue line can be experimentally obtained according to two procedures: the push-pull or pull-pull test and the cyclic loading fatigue test in different configurations (such as the 4-point bending test, described in [27]). Regarding the former procedures, it is worth noting that the AASHTO-standardized procedure is the pull-pull test described in [32], while the push-pull test protocol remains unofficial; however, the common practice among DOTs is to use the procedure they consider most appropriate. The reference study used for this thesis ([22]) employs the push-pull paradigm.

Although the two protocols are implemented for the same purpose in this context, they investigate different behaviors. The pull-pull or push–pull configuration characterizes the intrinsic constitutive behavior of the asphalt mixture under uniform cyclic loading, analyzing the actual visco-elastic response through the C-S curve. In contrast, the 4-point bending test evaluates the flexural structural response under a non-uniform stress state.

As highlighted in [22], the push-pull test is suitable for the Visco-Elastic Continuum Damage (VECD) modeling, since it produces a uniform uniaxial stress–strain state. Through calibration of the VECD model, the C-S curve of the material can be obtained, where C is the pseudo-stiffness, and S is the damage parameter. The form of the C-S curve may be selected among the following alternatives:

$$C = e^{aS^b} \tag{5.5}$$

$$C = C_{10} - C_{11}S^{C_{12}} \tag{5.6}$$

where a, b, C_{10}, C_{11}, and C_{12} represent the outputs of the VECD calibration effort.

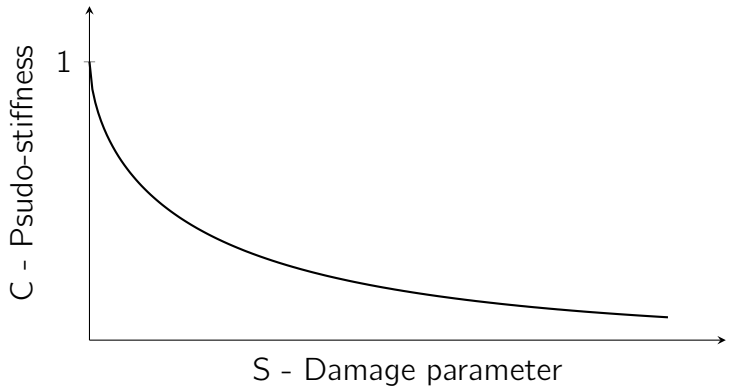

Figure 5.25: Exponential trend of the C–S curve in the VECD model

The philosophy of VECD modeling is that the C-S curve, once calibrated, is independent of temperature, loading magnitude, and rate, and it is also intended to be material-specific. Therefore, the fatigue behavior of the material can be simulated and extrapolated outside the temperature and loading domain in which the VECD was originally calibrated.
Practically, the failure criterion for the C-S curve is determined, and the number of cycles is modeled accordingly for several initial microstrain values. The ordered pairs (ϵ, N_f) thus obtained are interpolated, and the fatigue line in the form

$$N_f = A\,\epsilon^{-B} \tag{5.7}$$

is found. It follows that when implementing the VECD modeling, the fatigue line can be obtained with a limited number of laboratory tests, namely those necessary to calibrate the VECD model itself.

On the other hand, the result of each 4-point bending test is a single ordered pair (ϵ, N_f) for specific temperature and loading conditions. Several laboratory tests at different initial microstrain values are therefore necessary to model the full fatigue line.

In the end, both experimental procedures feature advantages and drawbacks. Although when implementing the push-pull protocol the number of tests to perform is limited, the computational burden of fitting the fatigue line in addition to calibrating the VECD model is greater than that of the linear interpolation necessary when the 4-point bending test is performed instead.

Regardless of the procedure adopted, the fatigue line retrieved through linear interpolation features the same form as the one proposed in eq. (2.3):

$$\begin{cases} N_f = k_{f1}\,(C)\,(C_h)\,\beta_{f1}\,(\epsilon_t)^{k_{f2}\beta_{f2}}\,(E_{HMA})^{k_{f3}\beta_{f3}} \\ N_f = A\,(\epsilon_t)^{-B} \end{cases} \tag{5.8}$$

The goal of the calibration procedure is to minimize the difference between the measured number of loading cycles to failure obtained with eq. (5.7), and the modeled one obtained through eq. (2.3). Both equations indirectly include the dependency on temperature and loading frequency in the tensile strain and the dynamic modulus. As a matter of fact, the dynamic modulus E_{HMA} is determined at a specific temperature and, from the mathematical viewpoint, is not an independent variable in the system. It follows that the measured data and the modeled ones should be referred to a set of different temperature and loading frequency values for the calibration of β_{f1}, β_{f2}, β_{f3} to be meaningful.

5.3.1.2 Rutting model

Two testing procedures can be used to measure the variables for the calibration of the rutting damage function: the Repeated Load Permanent Deformation test, according to AASHTO T378 [31], and the Hamburg Wheel-Tracking Test, according to AASHTO T324 [29]. The method selected in this work is the first one, and the calibration workflow is proposed in [35]. The Repeated Load Permanent Deformation test is performed on a cylindrical sample subjected to repeated haversine loading.

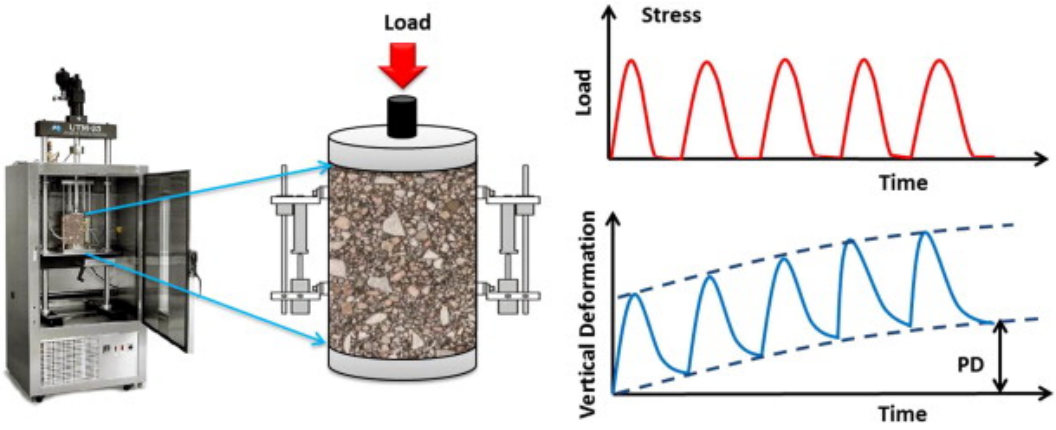

Figure 5.26: RLPD test configuration, [38]

The output is the amount of plastic deformation as a function of the number of loading cycles:

$$\epsilon_p = \epsilon_p(N) \tag{5.9}$$

It follows that the ϵ_p-N plot can be obtained: such a graph, if represented in the log – log scale, identifies three stages.

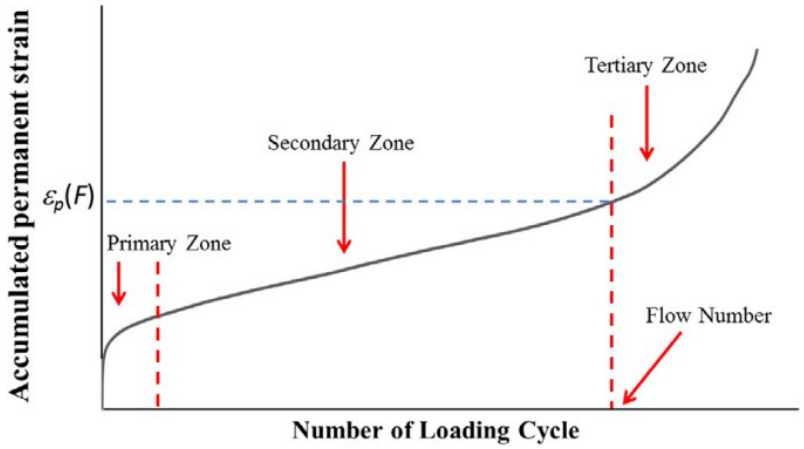

Figure 5.27: ϵ_p-N plot, [38]

In the primary stage, the slope is high but shows a decreasing trend. In the secondary stage, the accumulation of permanent deformation is almost linear: the viscoplastic behavior of the mixture is enclosed in this phase, and the inclination of the curve is an indicator of the rutting rate. In the tertiary stage, the permanent deformation increases at a higher rate, and the mixture approaches the state of failure. The number of loading cycles that marks the transition between the secondary and tertiary stage is identified as the Flow Number (FN).

The RLPD test has to be performed at a single reference temperature. The ordered pairs (N,ϵ_p) from the secondary stage are used to perform a bi-logarithmic linear regression and minimize the difference between the linear branch of the curve and the damage function in eq. (2.10). By taking the logarithm of both sides, the eq. (2.10) can be linearized and take the same form as the secondary branch:

$$\begin{cases} \log \epsilon_{p,HMA} = \log \epsilon_{r,HMA} + \log \beta_{1r} + k_{1r} + \beta_{2r} k_{2r} \log T + \beta_{3r} k_{3r} \log N \\ \log \epsilon_{p,HMA} = I + \alpha \log N \end{cases} \tag{5.10}$$

where

- the depth confinement factor (k_z) is set to 1 to account for laboratory conditions;
- the resilient strain can be calculated from the laboratory results for the dynamic modulus.

$$\epsilon_r = \frac{1}{|E^*|}(\sigma_1 - 2\nu\sigma_3) \tag{5.11}$$

The intercept and angular coefficient of the line can be calculated. At this stage of the calibration process, $\beta_{r2} = 1$ since the analysis is carried out for a single temperature. The mixture-specific coefficients β_{r1}, β_{r3} are obtained accordingly.
Then, the ϵ_p-N curve related to the testing reference temperature is shifted according to the same rationale as that of the time-temperature superposition (TTS) principle. The approach, shown in fig. 5.28 and previously described and validated in [20], can be defined as a "temperature-number of cycles superposition principle". The permanent strain developed for a given number of loading cycles at the desired temperature is the same as that developed for the reduced number of loading cycles (N_r) at a reference temperature.

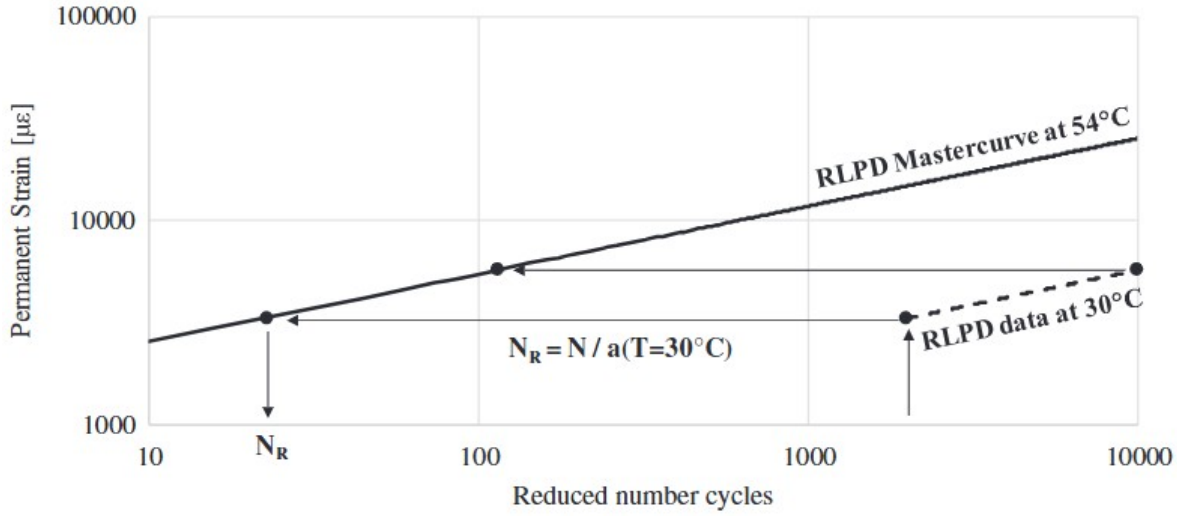

Figure 5.28: RLPD curve horisontal shifting, [35]

The reduced number of loading cycles is computed by applying a temperature-based shift factor, according to the Arrhenius equation:

$$\log\left[a(T)\right] = \frac{\Delta E_a}{19.14714\left(\frac{1}{T} - \frac{1}{T_r}\right)} \tag{5.12}$$

$$N_r = \frac{N}{a(T)} \tag{5.13}$$

where

- T is the test temperature, K;
- T_r is the reference temperature, K;
- ΔE_a is the activation energy and is treated as a fitting parameter.

Once the full RLPD master curve has been obtained, the β coefficients have to be recalibrated to account for the applied shift. Since the shift is a horizontal translation, the angular coefficient α is the same, and so is β_{r3}. Consequently, β_{r1} and β_{r2} are recalculated, and the final set of calibration coefficients is determined.

It should be noted that the damage function in eq. (2.10) is representative of the in-field conditions, where the material is in its confined state. For the sake of consistency, the [35] recommends that the RLPD test simulate the same conditions and be performed in the confined state. In the same way, the dynamic modulus in eq. (5.11) refers to the material in its confined condition, and the dynamic modulus test is recommended to be

performed accordingly, as described in the AASHTO T378 Standard. Conversely, when the dynamic modulus is intended as the primary input, it has to be representative of the material in its unconfined state to avoid the effect of the confinement being considered twice.

5.3.1.3 Thermal cracking model

The Thermal Cracking Model (TCMODEL) implemented in the MEPDG is highly sensitive to the fracture parameter n and the binder's Performance Grade ([23]). By changing the low PG by one grade, the modeled amount of thermal cracking unrealistically fluctuates between its minimum and maximum values. This makes the TCMODEL inaccurate in predicting the in-field damage when implemented as is. The local or mixture-specific calibration coefficient β_t was included in the MEPDG framework to adjust the sensitivity of the TCMODEL when other conditions than the prevailing ones are met.

It should be noted that, originally, the goal of the calibration of the thermal cracking model was the β_t parameter in eq. (2.21), since the k_t parameter was intended as the output of the global calibration effort. Practically, the calibration parameter that the PavME Software refers to is $k = k_t\beta_t$. Hence, the common practice is to focus on k rather than β_t. By way of example, a predictive equation for the mixture-specific k coefficient was determined in [23] through the Multi-Gene Genetic Programming (MGGP) approach. The equation includes the linear and non-linear effects of multiple variables – the design traffic, the pavement thickness, the optimal binder content and target air voids in the job mix formula, the low PG temperature, the slope of the logarithm of modulus versus temperature (SLE) – on the calibration coefficient. This makes it capable of accounting for the distinctive features of the mixture in question for the State of Michigan or other nations where similar mix-design procedures and materials properties are encountered.

It is recommended that other Countries develop their specific calibration procedure for the thermal cracking parameter or use the aforementioned equation by simply recalibrating its coefficients.

5.3.2 Italian Standards for the materials characterization

In this section, a summary of the official AASHTO-standardized protocols for material characterization is provided; these norms serve as the primary reference for the MEPDG implementation. However, a set of European or Italian standards for laboratory testing

is provided as part of the framework for the local implementation of the MEPDG. The experimental procedures that follow refer to both the direct input data for material properties and the tests required to calibrate the β coefficients in the damage functions.

5.3.2.1 Experimental procedures for the input variables determination

In consideration of section 3.3, Input Level 1 is suitable for four types of material properties, listed below:

- the dynamic modulus of the mixture, E*;
- the complex modulus and the phase angle of the binder, G* and δ;
- the indirect tensile strength, σ_t;
- the creep compliance, D(t);
- the resilient modulus, M_r.

These variables can be measured through laboratory tests and directly incorporated into the methodology. When the raw data for Input Level 1 are not available, Pseudo Level 1 is recommended instead. Pseudo Level 1 is an artificial implementation of Input Level 1, in which the unknown variable is determined using formulations developed and calibrated for the specific context and material type. Such estimation of the material property is thought to be performed outside the MEPDG. The parameter thus determined is then incorporated into the design methodology as Input Level 1, although it was not obtained through direct experimental testing. The rationale of Pseudo Level 1 is similar to that of Input Level 2 or 3, since it entails the use of some empirical approaches. However, the correlations involved in Input Level 2 and 3 are not mixture or context-specific, which makes the use of Pseudo Level 1 more accurate. If neither Input Level 1 nor Pseudo Level 1 is applicable, one can fall back on Level 2 and 3.

The AASHTO and reference local standards related to the aforementioned variables are provided, as follows:

- the dynamic modulus of the mixture (E*) can be measured in unconfined conditions based on AASHTO T342 ([30]) or EN 12697-26 ([14]), in the DTC-CY configuration;
- the complex modulus and phase angle of the binder (G* and δ) can be measured based on AASHTO T315 ([26]) or EN 14770 ([16]);

- the indirect tensile strength (σ_t) can be measured based on AASHTO T322 ([28]) or EN 12697-23 ([12]);
- the creep compliance, D(t) can be measured based on AASHTO T322 ([28]);
- the resilient modulus (M_r) can be measured based on AASHTO T307 ([25]) or EN 13286-7 ([10]).

The only local reference standard to determine the creep compliance, D(t), through laboratory testing is the CNR n. 106 norm, [7]. Since this document dates back to 1985, it may be considered outdated, and its use is not recommended. A suitable alternative to direct testing is the Pseudo Level 1 implementation for creep compliance. The dynamic modulus and creep compliance are dual properties of the material; specifically, the relation between the complex modulus and the complex compliance was defined in [36]:

$$E^*(\omega)D^*(\omega) = 1 \tag{5.14}$$

Moreover, the creep compliance D(t) can be obtained through the interconversion of the complex compliance $D^*(\omega)$ by employing the Prony series, similar to what is shown in [21] on the complex modulus side.

5.3.2.2 Experimental procedures for the damage functions calibration

In this section, the set of original AASHTO standards related to the testing procedures for damage function calibration is summarized. If available, the corresponding European Norm (EN) is also provided. Four experimental protocols can be employed for this purpose:

- the push-pull or pull-pull test, which can be performed according to AASHTO T411 ([32]) or EN 12697-26 ([14]), in the DTC-CY configuration;
- the fatigue test in several configurations, which can be performed according to AASHTO T321 ([27]) or EN 12697-24 ([13]);
- the Repeated Load Permanent Deformation test in the confined condition, which can be performed according to AASHTO T378 ([31]) or EN 12697-25 ([11]);
- the Hamburg Wheel-Tracking test, which can be performed according to AASHTO T324 ([29]) or EN 12697-22 ([15]).

To date, no European or Italian Standard outlines any experimental procedure for determining the dynamic modulus in the confined configuration. This variable is necessary for the calibration of the rutting damage model, as detailed in section 5.3.1.2. Hence, a consistent research direction would be the development of a triaxial dynamic modulus configuration, conceptually aligned with the DTC-CY loading scheme prescribed by EN 12697-26, for the direct characterization of the confined mixture stiffness under a representative stress state.

Chapter 6

Case studies

The objective of this work is twofold:

1. the preliminary implementation of the MEPDG in the Italian context based on the framework recommended in chapter 5;

2. a sensitivity analysis on traffic, climate, and materials input data.

It is essential to clarify that the case studies presented in this thesis are intended for demonstration purposes, as they are not meant to be actual pavement designs. The main goal of the sensitivity analysis is to investigate the effect of the input data variability and peculiarity on the design output. As a matter of fact, the transfer functions used to design the pavement sections have not been calibrated to local conditions, and the calibration coefficients are the default values suggested by the MEPDG. Therefore, the results of the analysis are to be interpreted in a comparative context, rather than in absolute terms.

Finally, this work focuses on the analysis of two main pavement distresses: bottom-up fatigue cracking and rutting.

The case studies concern two existing road infrastructures:

1. the SS45bis highway, located in Trento, and

2. the A3 motorway, located in Napoli.

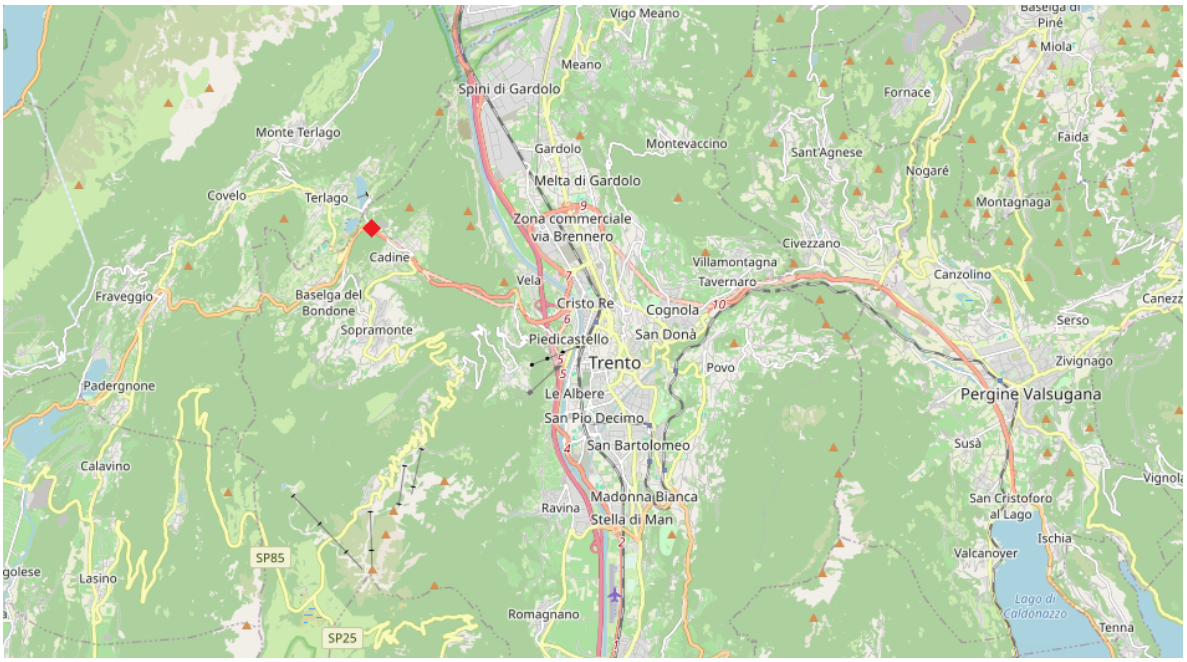

Figure 6.1: The SS45bis highway (TN). Source: OpenStreetMap

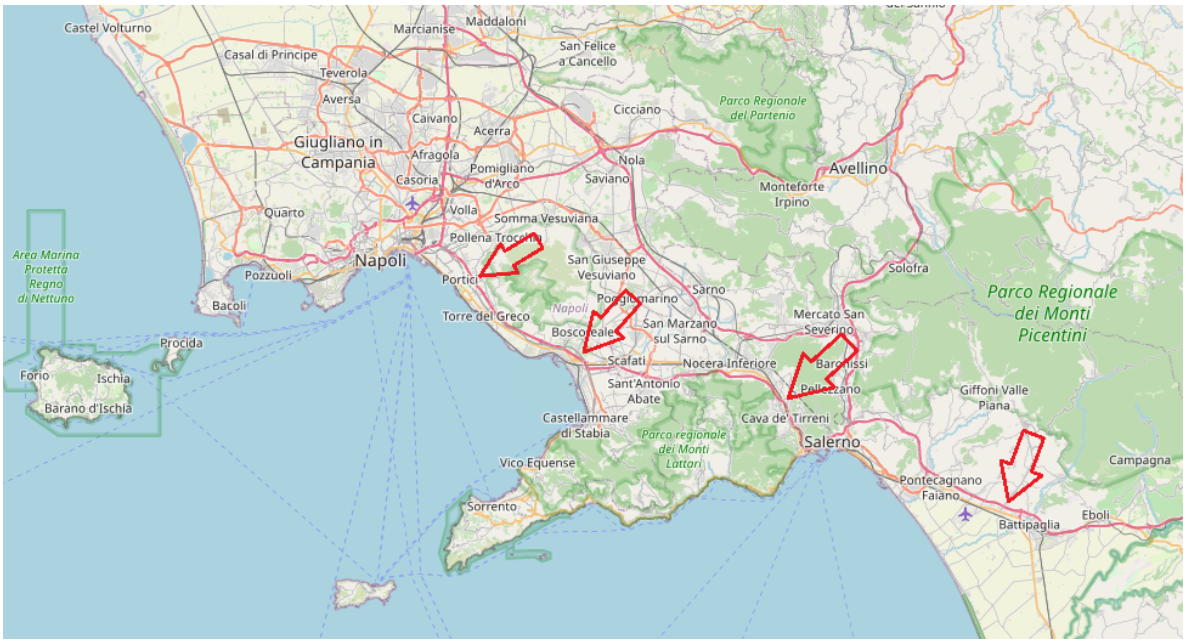

Figure 6.2: The A3 motorway (NA). Source: OpenStreetMap

In both cases, location-specific input data for traffic and climate were used, while the same types of material were considered.

6.1 The AASHTOWare Pavement ME Design software

The software used for the design is AASHTOWare PavME Design, developed by Applied Research Associates (ARA) on behalf of AASHTO.

Figure 6.3: AASHTOWare PavME Design logo

The Software was built upon the MEPDG and NCHRP mechanistic-empirical pavement design workflow to employ material properties, axle-load spectra, and climate data to calculate pavement responses and predict pavement distress and smoothness loss over the design life.

The user must provide the input data, including possible calibration parameters, in the Software-specific format, and the analysis is then run according to the MEPDG workflow. The main output of the analysis is a report that collects the plots showing the evolution of distress over time.

A user guide to the PavME Design software is presented in chapter B.

6.2 Data for the local implementation and sensitivity analysis

6.2.1 Climate data

Climate data from 1st January 2005 to 31st December 2024 for the design location were downloaded from the ERA5 database as described in section 5.1 and processed as per the procedure and codes presented in Code A.1.

The coordinates of the two locations under analysis are: 46.0917, 11.0591 (Trento), 40.6864, 14.7687 (Napoli). The cell of interest was identified in the ERA-5 network by the following coordinates:

- 11.0 W, 46.0 S, 11.1 E, 46.1 N for Trento;
- 14.7 W, 40.6 S, 14.8 E, 40.7 N for Napoli.

The outputs of the climate data processing are summarized below (figs. 6.4 to 6.8 for Trento, figs. 6.9 to 6.13 for Napoli), on a monthly basis for graphical reasons, although they were derived and used on an hourly basis.

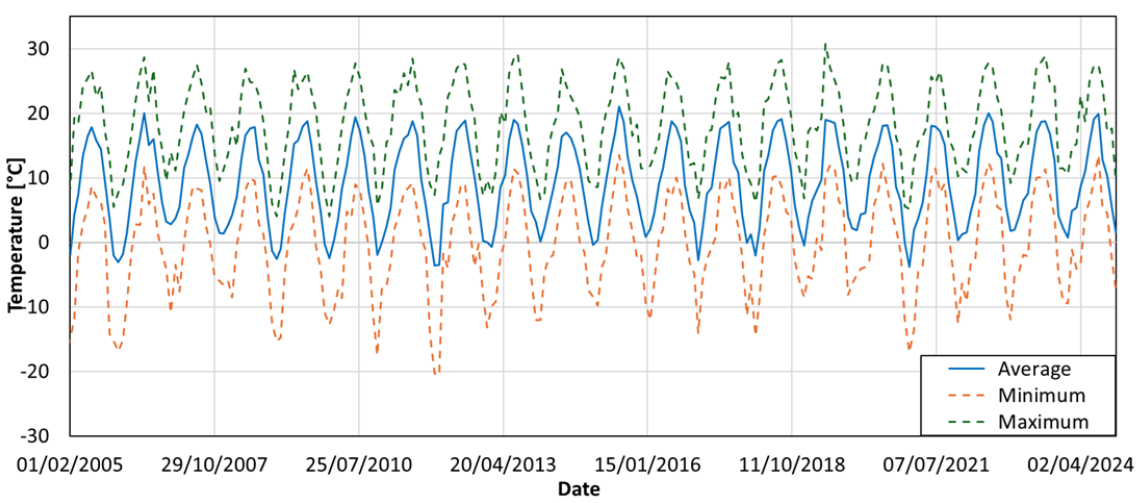

Figure 6.4: Monthly temperature summary – Trento

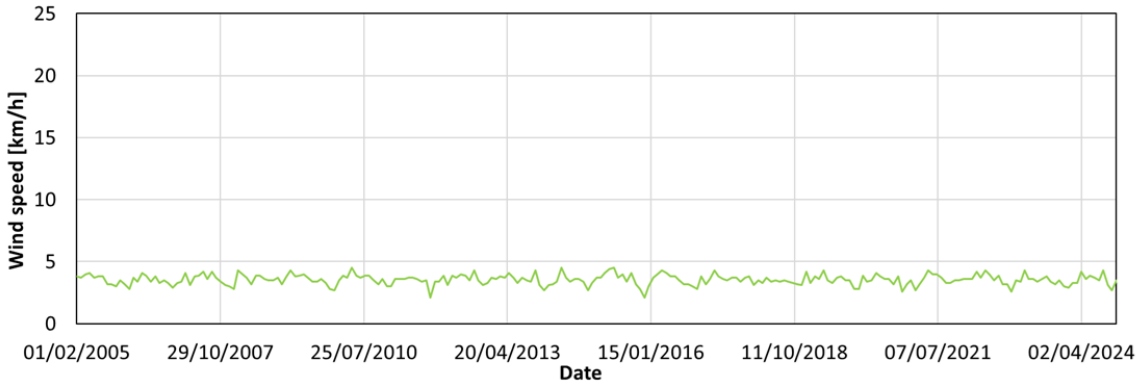

Figure 6.5: Monthly wind speed summary – Trento

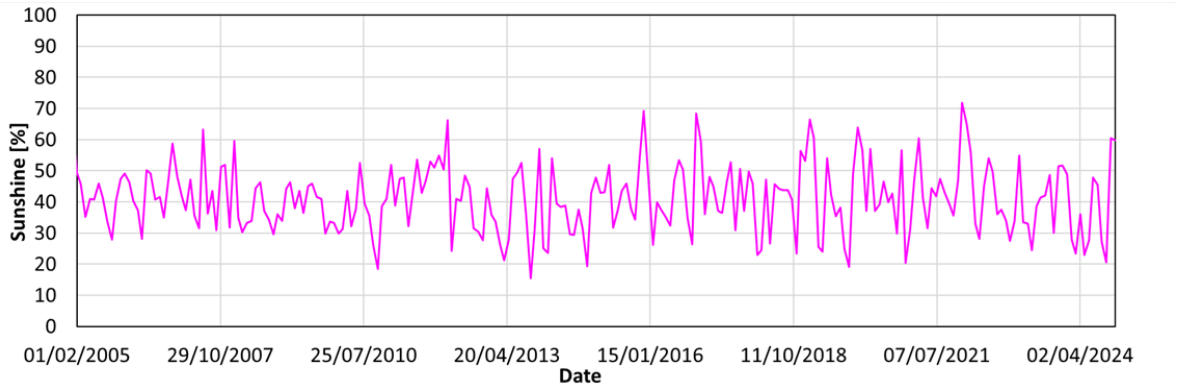

Figure 6.6: Monthly sunshine summary – Trento

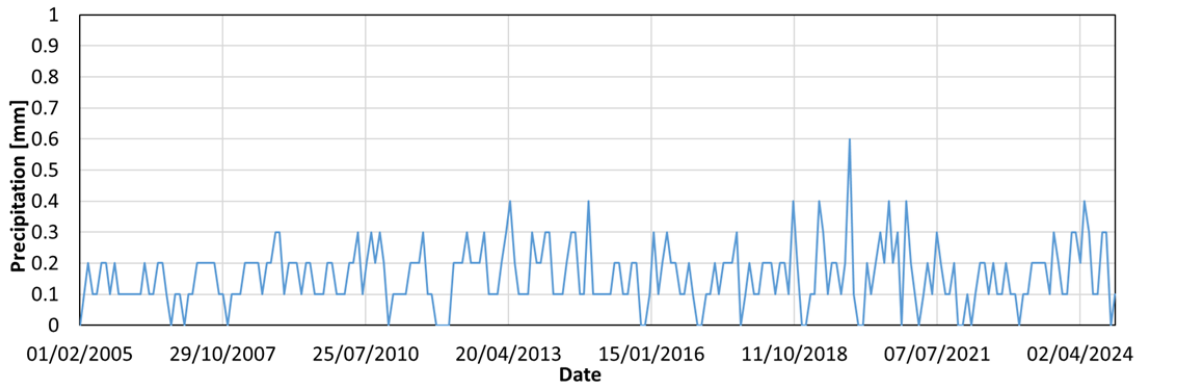

Figure 6.7: Monthly precipitation summary – Trento

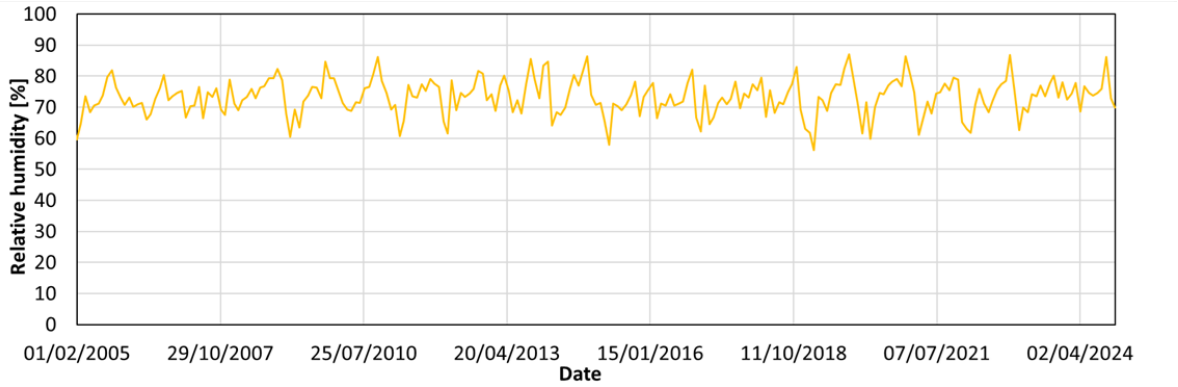

Figure 6.8: Monthly RH summary – Trento

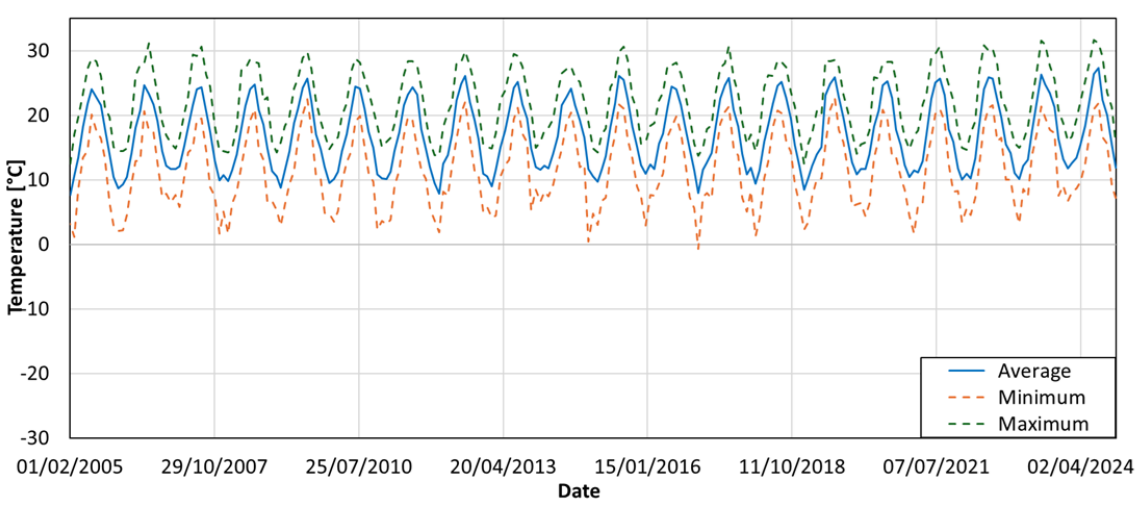

Figure 6.9: Monthly temperature summary – Napoli

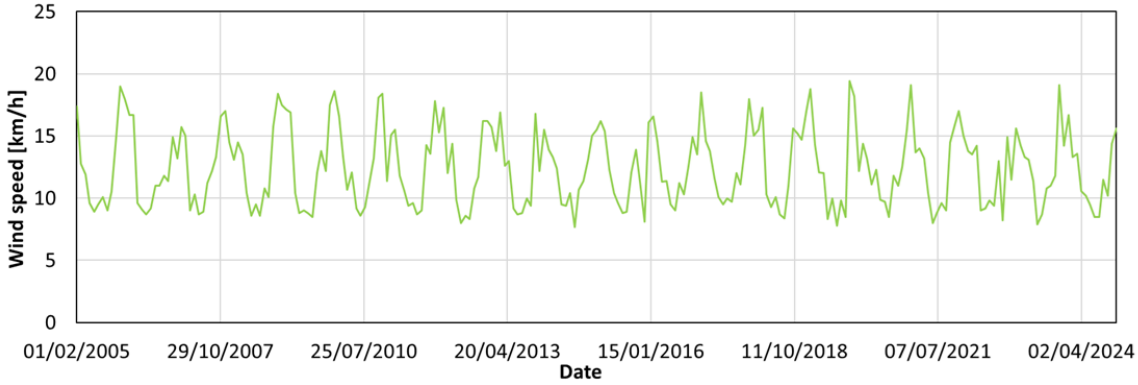

Figure 6.10: Monthly wind speed summary – Napoli

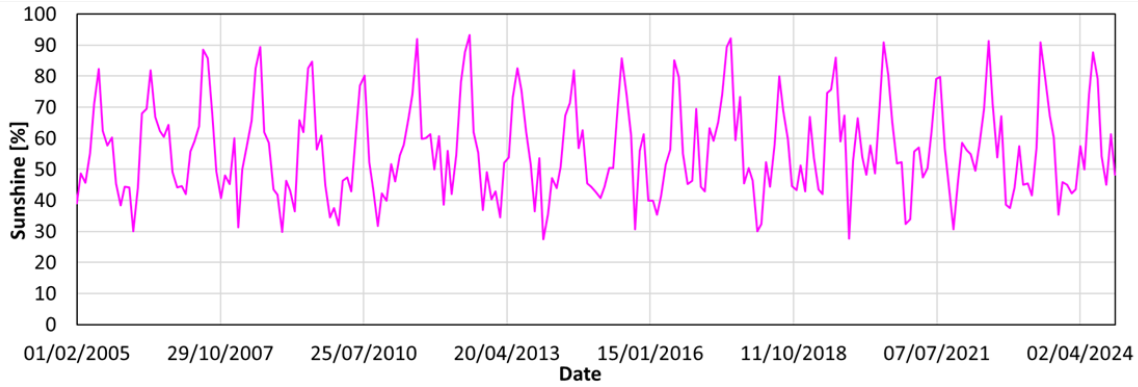

Figure 6.11: Monthly sunshine summary – Napoli

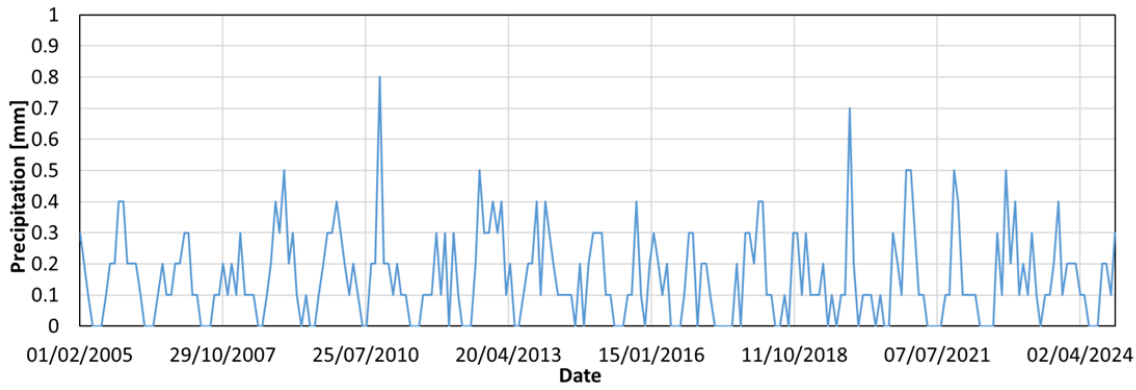

Figure 6.12: Monthly precipitation summary – Napoli

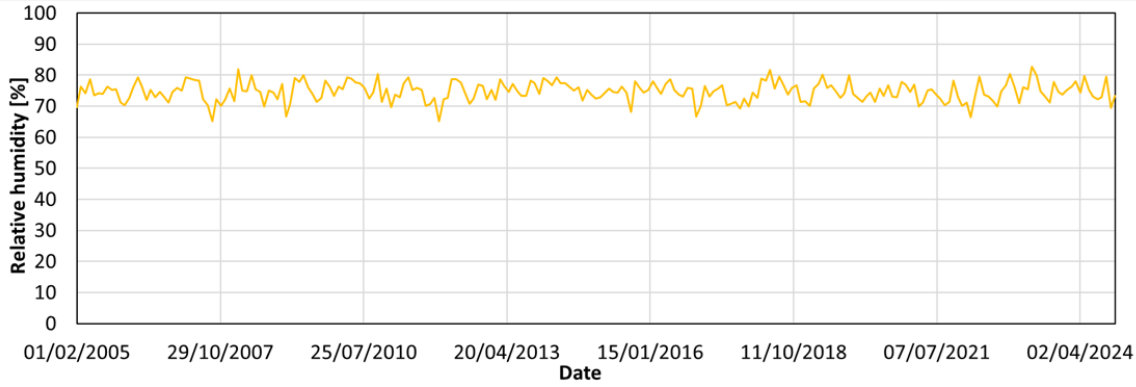

Figure 6.13: Monthly RH summary – Napoli

Then, the ERA5 climate files were converted to the HCD (Hourly Climate Data) format using the Imperial system of units. The original HCD file for the project location was downloaded from the LTPP InfoPave portal and then overwritten with the ERA5 data. The HCD file thus obtained was loaded into the Software.

6.2.2 Traffic data

Data from WIM stations were used to characterize traffic in the two case studies. Such data were used to implement the three traffic input levels reported in table 5.2.

6.2.2.1 Input Level 1: the Salerno to Napoli A3 motorway

Sixteen WIM stations have been installed along the A3 motorway, as shown in fig. 6.14; the collected data were published by Università degli Studi di Napoli Federico II and the Autostrade per l'Italia group, [18].

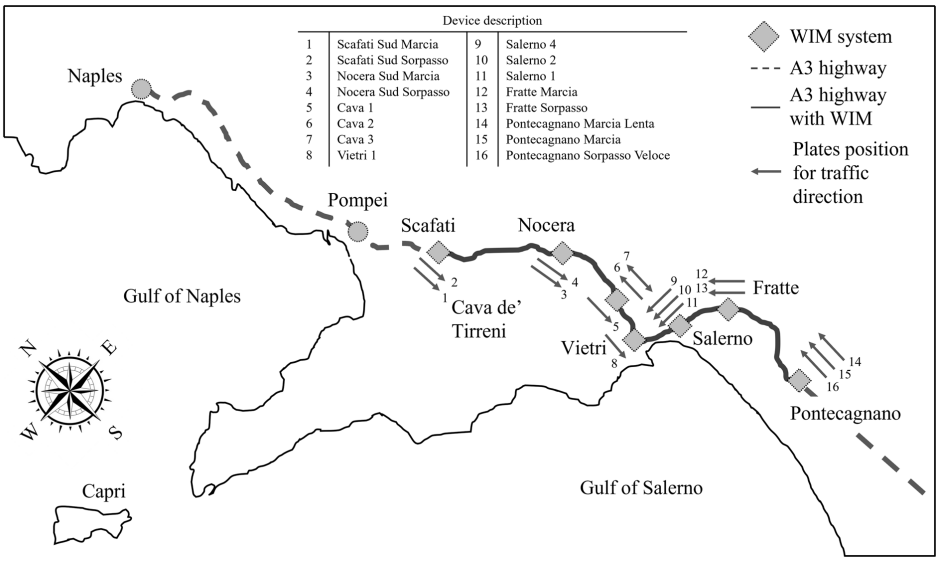

Figure 6.14: Location of the WIM devices on the A3 motorway, [18]

The WIM database was published after a data-cleaning procedure. In this regard, it is worth mentioning that multiple passages by the same vehicle on the same trip were filtered out, as the system included a series of automatic license plate recognition (ALPR) cameras.

Although observations were collected from February 2021 to January 2022, the WIM station system was fully operational in August, October, November, and December. The data recorded by some stations along the infrastructure are not available for the remaining months, as shown in table 6.1. Consequently, the information from these four months was considered representative of the entire year and propagated evenly over the eight missing months as follows:

- the August data was considered representative of the traffic in January and May;
- the October data was considered representative of the traffic in February and June;
- the November data was considered representative of the traffic in March and July;
- the December data was considered representative of the traffic in April and September.

The amount of available data enables estimation of the normalized axle-load distribution at the $95\% \pm 1\%$ confidence level, as shown in table 3.1.

WIM Device		02/21	03/21	04/21	05/21	06/21	07/21	08/21	09/21	10/21	11/21	12/21	01/22
#	Name												
1	Scafati Sud Marcia	☐	☐	☐	☐	☐	☐	☒	☒	☒	☒	☒	☒
2	Scafati Sud Sorp.	☐	☐	☐	☐	☐	☐	☒	☒	☒	☒	☒	☒
3	Nocera Sud Marcia	☐	☐	☐	☐	☐	☐	☒	☒	☒	☒	☒	☒
4	Nocera Sud Sorp.	☐	☐	☒	☐	☐	☐	☒	☐	☒	☒	☒	☒
5	Cava 1	☐	☐	☐	☒	☒	☒	☒	☒	☒	☒	☒	☒
6	Cava 2	☐	☐	☐	☒	☒	☒	☒	☒	☒	☒	☒	☒
7	Cava 3	☐	☐	☐	☒	☒	☒	☒	☒	☒	☒	☒	☒
8	Vietri 1	☒	☒	☐	☒	☒	☒	☒	☒	☒	☒	☒	☒
9	Salerno 4	☐	☐	☐	☐	☒	☒	☒	☒	☒	☒	☒	☒
10	Salerno 2	☐	☐	☐	☒	☒	☒	☒	☒	☒	☒	☒	☒
11	Salerno 1	☒	☒	☒	☒	☒	☒	☒	☒	☒	☒	☒	☒
	SAM - Salerno 1	☐	☐	☐	☐	☐	☐	☐	☐	☐	☐	☐	☒
12	Fratte Marcia	☐	☐	☐	☐	☐	☐	☒	☒	☒	☒	☒	☒
13	Fratte Sorpasso	☐	☐	☐	☐	☐	☐	☒	☒	☒	☒	☒	☒
14	Pontecagnano Marcia Lenta	☐	☐	☐	☐	☐	☐	☒	☒	☒	☒	☒	☒
15	Pontecagnano Marcia	☐	☐	☐	☐	☐	☐	☒	☒	☒	☒	☒	☐
16	Pontecagnano Sorp. Veloce	☐	☐	☐	☐	☐	☐	☒	☒	☒	☒	☒	☐

Table 6.1: Summary of the active WIM stations all year round

Finally, the information collected by the "Cava 3" device was omitted from the analysis, because the station operates in both directions and the counts are aggregated into a single total in the dataset. In other words, it was assumed that the directional distribution factor is not affected by the "Cava 3" count.

A summary of the traffic analysis results is presented below. This input data was fed into PavME Design for pavement design.

The vehicle count over the four months, in both directions, is 1788749, which sums to a yearly total of 5366247. The AADTT is 14702 veh/day. The most trafficked direction is from Salerno to Napoli: the direction distribution factor is $P_D = 61.65\%$, and the lane distribution factor is $P_L = 55.69\%$. Three lanes in the Salerno-to-Napoli direction were considered for these calculations and as input in the design process. These results were derived by considering the detailed count of passages in table 6.2 separately between the two directions. A summary of these calculations is shown in table 6.3.

WIM Device		Passages Count				Lane
#	Name	Aug-21	Oct-21	Nov-21	Dec-21	
1	**Scafati Sud Marcia**	50543	58307	50161	47793	1
2	**Scafati Sud Sorpasso**	44091	40047	35506	32657	2
3	**Nocera Sud Marcia**	20622	20653	19936	24291	1
4	**Nocera Sud Sorpasso**	11018	9303	10009	13651	2
5	**Cava 1**	36066	33688	32385	30630	1
6	**Cava 2**	25335	18212	14696	15771	2
7	**Cava 3**	–	–	–	–	3
8	**Vietri 1**	11396	12001	20655	20489	1
9	**Salerno 4**	26587	22182	16679	18362	1
10	**Salerno 2**	3406	4432	3869	3685	2
11	**Salerno 1**	13397	22593	20740	18705	3
	SAM - Salerno 1	0	0	0	0	
13	**Fratte Marcia**	37489	46307	41136	43485	1
14	**Fratte Sorpasso**	14279	11304	14542	13898	2
15	**Pontecagnano Marcia Lenta**	71778	72333	73136	70719	1
16	**Pontecagnano Marcia**	65872	68445	64479	20930	2
17	**Pontecagnano Sorp. Veloce**	45061	31658	27427	19922	3

Table 6.2: Detailed count of passages for the A3 motorway traffic

Direction	Passages count				P_D	P_L
	Lane 1	Lane 2	Lane 3	Total		
Napoli → Salerno	489616	196282	–	685898	38.35%	71.38%
Salerno → Napoli	614207	289141	199503	1102851	61.65%	55.69%

Table 6.3: Directional and lane distribution factors for the A3 motorway traffic

More analysis outputs are shown in the following tables: vehicle class distribution (table 6.4), number of axles per truck (table 6.5), and monthly adjustment factors (table 6.6).

Vehicle Class	Vehicle Count	Distribution [%]
4	75405	4.21
5	1340843	74.96
6	51798	2.90
7	0	0.00
8	104554	5.85
9	14026	0.78
10	0	0.00
11	202123	11.30
12	0	0.00
13	0	0.00
Total	1788749	100.00

Table 6.4: Vehicle class distribution for the A3 motorway traffic

Vehicle Class	Single	Tandem	Tridem	Quad
4	2.00	0.00	0.00	0.00
5	2.00	0.00	0.00	0.00
6	1.28	0.89	0.00	0.00
7	0.00	0.00	0.00	0.00
8	2.19	0.98	0.01	0.00
9	2.33	1.04	0.00	0.00
10	0.00	0.00	0.00	0.00
11	2.00	0.00	1.00	0.00
12	0.00	0.00	0.00	0.00
13	0.00	0.00	0.00	0.00

Table 6.5: Number of axles per truck for the A3 motorway traffic

MONTH	Class 4	Class 5	Class 6	Class 7	Class 8	Class 9	Class 10	Class 11	Class 12	Class 13
January	0.81	1.12	0.88	1.00	0.77	0.91	1.00	0.84	1.00	1.00
February	1.12	1.04	1.07	1.00	1.12	1.06	1.00	1.07	1.00	1.00
March	1.12	0.96	1.06	1.00	1.12	1.09	1.00	1.13	1.00	1.00
April	0.95	0.86	0.97	1.00	0.99	0.94	1.00	0.96	1.00	1.00
May	0.81	1.15	0.91	1.00	0.77	0.91	1.00	0.84	1.00	1.00
June	1.12	1.04	1.07	1.00	1.12	1.06	1.00	1.07	1.00	1.00
July	1.12	0.96	1.06	1.00	1.12	1.09	1.00	1.13	1.00	1.00
August	0.81	1.15	0.91	1.00	0.77	0.91	1.00	0.84	1.00	1.00
September	0.95	0.86	0.97	1.00	0.99	0.94	1.00	0.96	1.00	1.00
October	1.12	1.04	1.07	1.00	1.12	1.06	1.00	1.07	1.00	1.00
November	1.12	0.96	1.06	1.00	1.12	1.09	1.00	1.13	1.00	1.00
December	0.95	0.86	0.97	1.00	0.99	0.94	1.00	0.96	1.00	1.00

Table 6.6: Monthly Adjustment Factors for the A3 motorway traffic

The axle load distributions related to August are presented in figs. 6.15 to 6.19. For additional details and the complete results of the analysis, see chapter B.

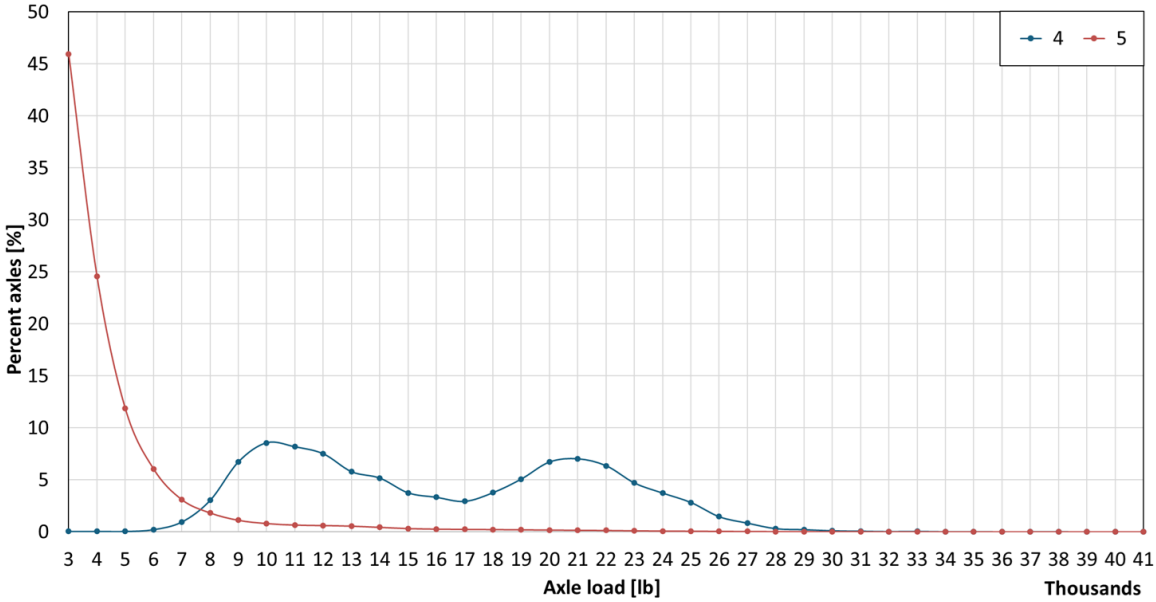

Figure 6.15: Single axle load distributions of vehicle classes 4 and 5 – August

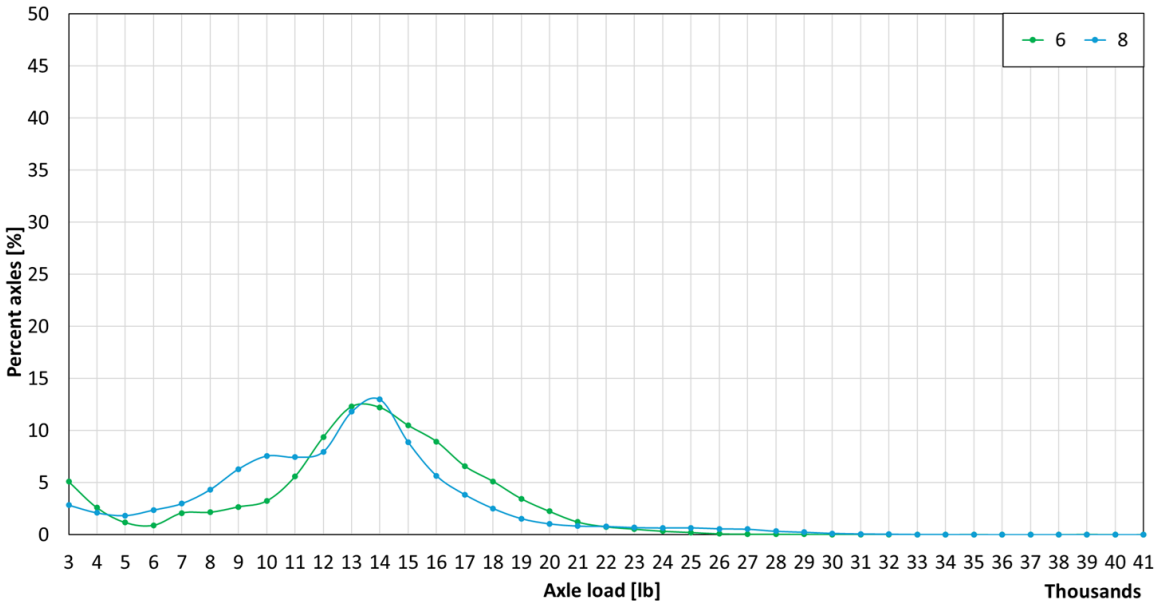

Figure 6.16: Single axle load distributions of vehicle classes 6 and 8 – August

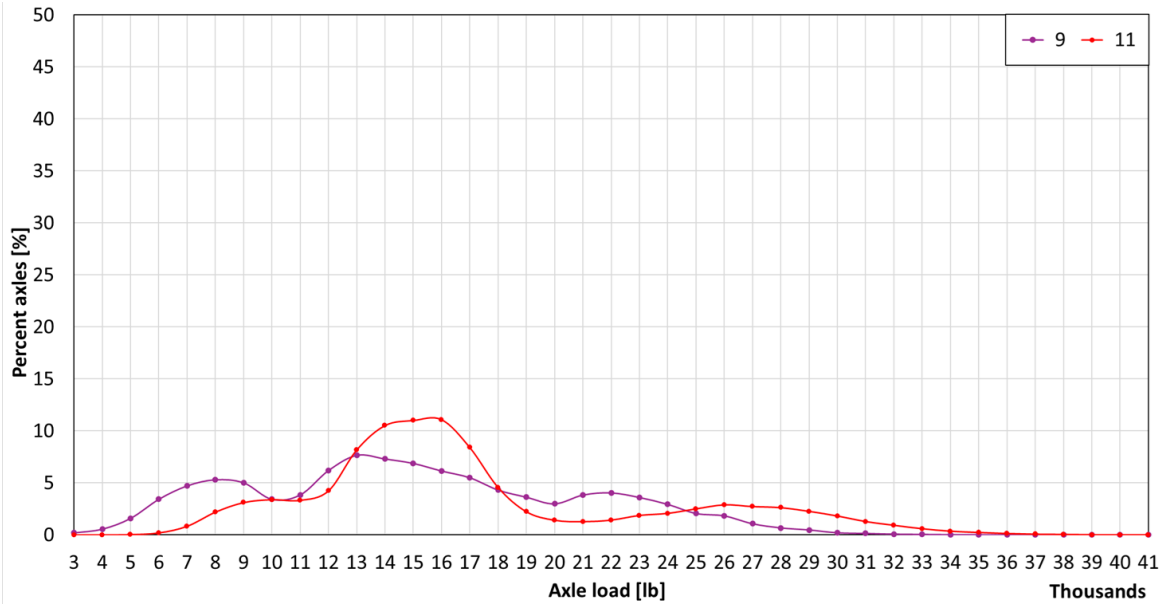

Figure 6.17: Single axle load distributions of vehicle classes 9 and 11 – August

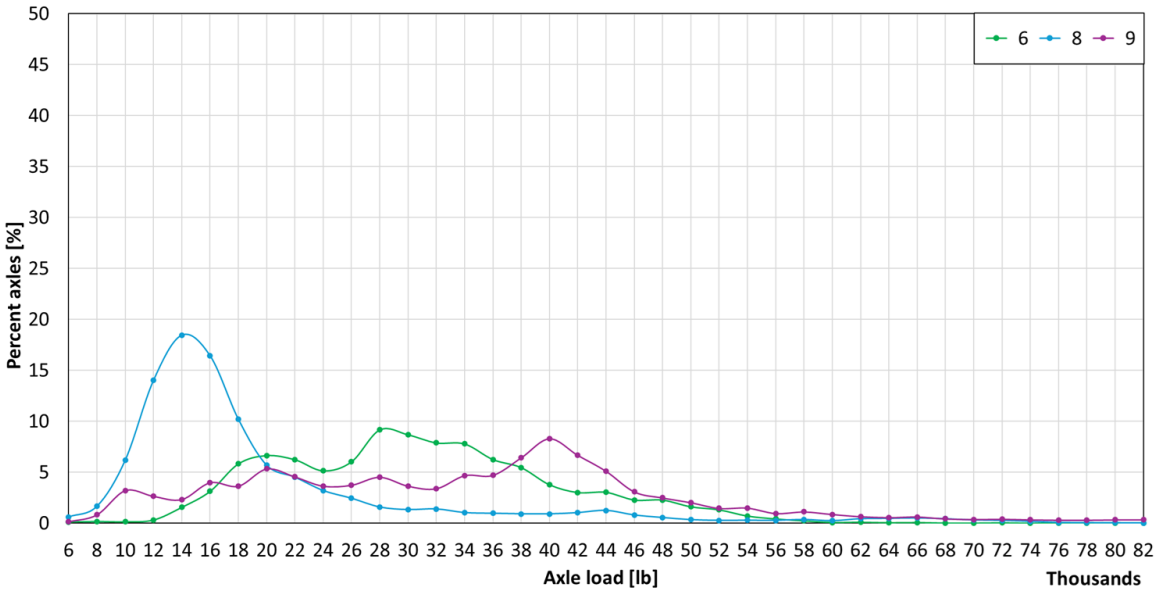

Figure 6.18: Tandem axle load distributions – August

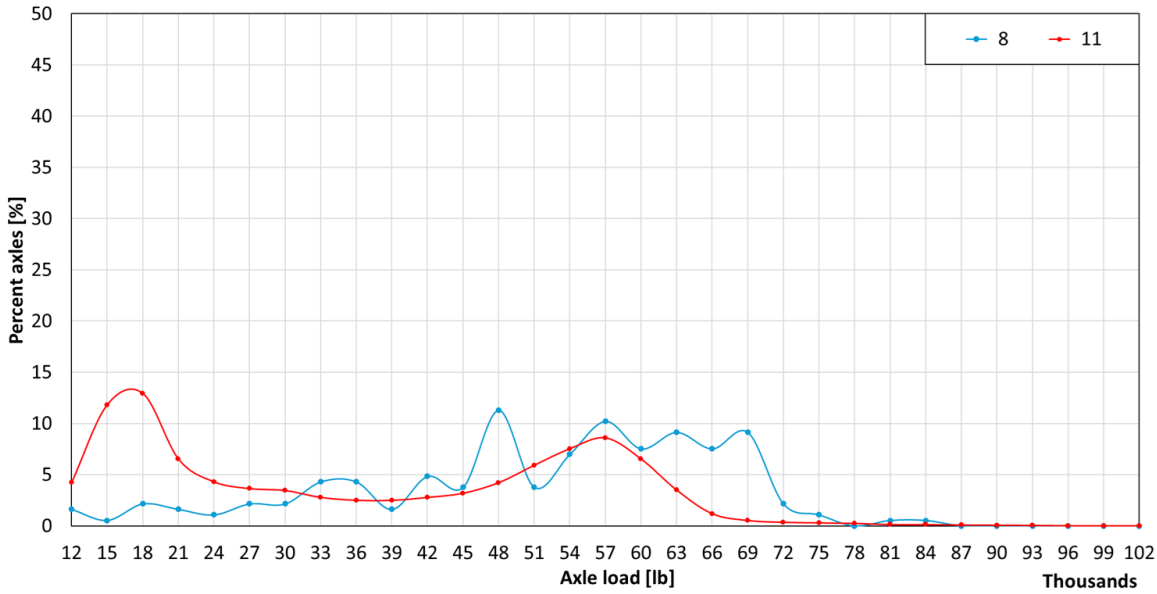

Figure 6.19: Tridem axle load distributions – August

6.2.2.2 Input Level 1: the SS45bis highway in Trento

The weight-in-motion station on this highway is managed by the Trento Province and was installed by the Bisonte by iWiM company, which provided data for October, November, and December 2025.

Data processing was more straightforward, as only one WIM device installed in one

lane was involved in the measurements. Therefore, neither a data-cleaning procedure nor the calculation of the distribution factors was necessary.

Similarly to the Napoli case, the available information from the three months was considered representative of the entire year and propagated evenly over the nine missing months as follows:

- the October data was considered representative of the traffic in January, April, and July;
- the November data was considered representative of the traffic in February, May, and August;
- the December data was considered representative of the traffic in March, June, and September.

The amount of available data enables estimation of the normalized axle-load distribution at the $93\% \pm 1\%$ confidence level, as shown in table 3.1.

Since the WIM device detected some six-axle vehicles and classified them as valid, it was necessary to include an additional vehicle class besides the six identified in section 5.2.2. Thus, FHWA vehicle class 10 identifies six-axle vehicles with either of the following configurations: [1 2 2 3 3 3 0 0 0 0] or [1 1 4 4 4 4 0 0 0 0].

A summary of the traffic analysis results is presented below: vehicle class distribution (table 6.7), number of axles per truck (table 6.8), and monthly adjustment factors (table 6.9). This input data was fed into PavME Design for pavement design.

The vehicle count over the three months is 129529, which sums to a yearly total of 518116. The AADTT is 1419 veh/day.

Vehicle Class	Vehicle Count	Distribution [%]
4	7546	5.83
5	100264	77.41
6	5296	4.09
7	0	0.00
8	5811	4.49
9	1491	1.15
10	539	0.40
11	8582	6.63
12	0	0.00
13	0	0.00
Total	129529	100.00

Table 6.7: Vehicle class distribution for the SS45bis highway traffic

Vehicle Class	Single	Tandem	Tridem	Quad
4	2.00	0.00	0.00	0.00
5	2.00	0.00	0.00	0.00
6	1.34	0.83	0.00	0.00
7	0.00	0.00	0.00	0.00
8	2.15	0.89	0.02	0.00
9	2.61	1.00	0.00	0.00
10	1.88	1.69	0.16	0.05
11	2.00	0.00	1.00	0.00
12	0.00	0.00	0.00	0.00
13	0.00	0.00	0.00	0.00

Table 6.8: Number of axles per truck for the SS45bis highway traffic

MONTH	Class 4	Class 5	Class 6	Class 7	Class 8	Class 9	Class 10	Class 11	Class 12	Class 13
January	1.08	1.24	1.24	1.00	1.41	1.13	1.03	1.24	1.00	1.00
February	0.97	0.90	0.92	1.00	0.85	0.91	1.10	1.00	1.00	1.00
March	0.95	0.86	0.84	1.00	0.74	0.96	0.87	0.76	1.00	1.00
April	1.08	1.24	1.24	1.00	1.41	1.13	1.03	1.24	1.00	1.00
May	0.97	0.90	0.92	1.00	0.85	0.91	1.10	1.00	1.00	1.00
June	0.95	0.86	0.84	1.00	0.74	0.96	0.87	0.76	1.00	1.00
July	1.08	1.24	1.24	1.00	1.41	1.13	1.03	1.24	1.00	1.00
August	0.97	0.90	0.92	1.00	0.85	0.91	1.10	1.00	1.00	1.00
September	0.95	0.86	0.84	1.00	0.74	0.96	0.87	0.76	1.00	1.00
October	1.08	1.24	1.24	1.00	1.41	1.13	1.03	1.24	1.00	1.00
November	0.97	0.90	0.92	1.00	0.85	0.91	1.10	1.00	1.00	1.00
December	0.95	0.86	0.84	1.00	0.74	0.96	0.87	0.76	1.00	1.00

Table 6.9: Monthly Adjustment Factors for the SS45bis highway traffic

The axle load distributions related to October are presented in figs. 6.20 to 6.26. For additional details and the complete results of the analysis, see chapter B.

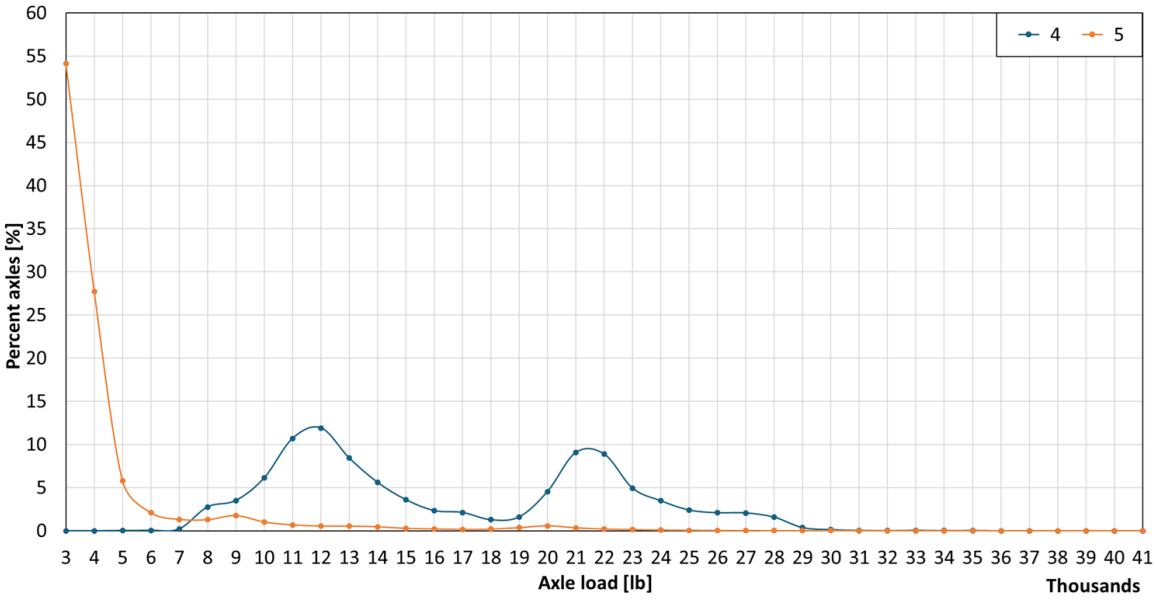

Figure 6.20: Single axle load distributions of vehicle classes 4 and 5 – October

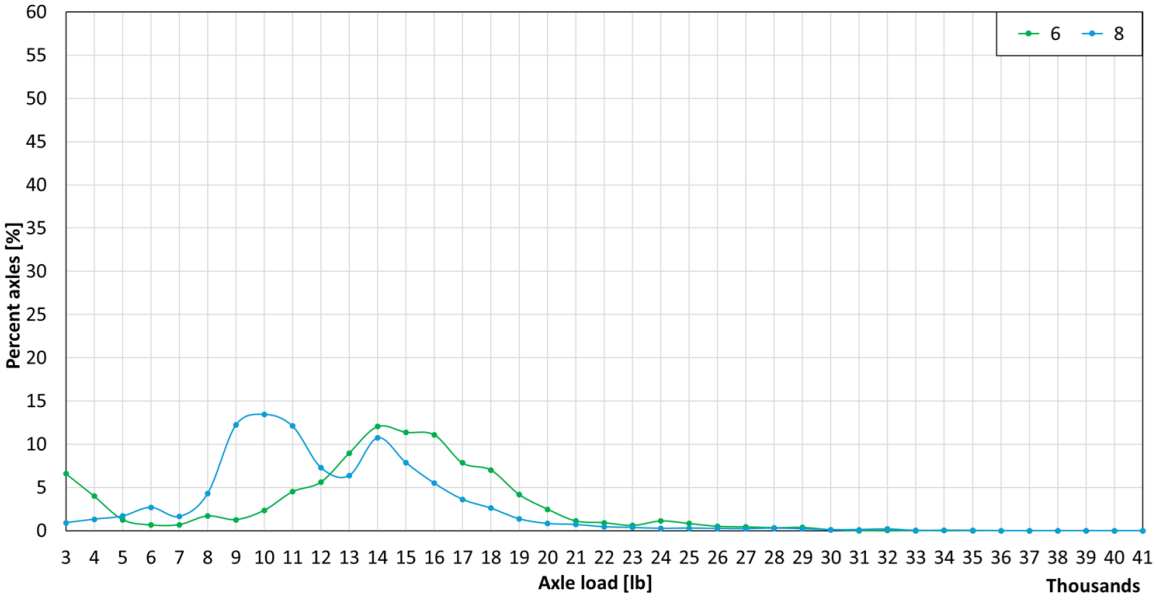

Figure 6.21: Single axle load distributions of vehicle classes 6 and 8 – October

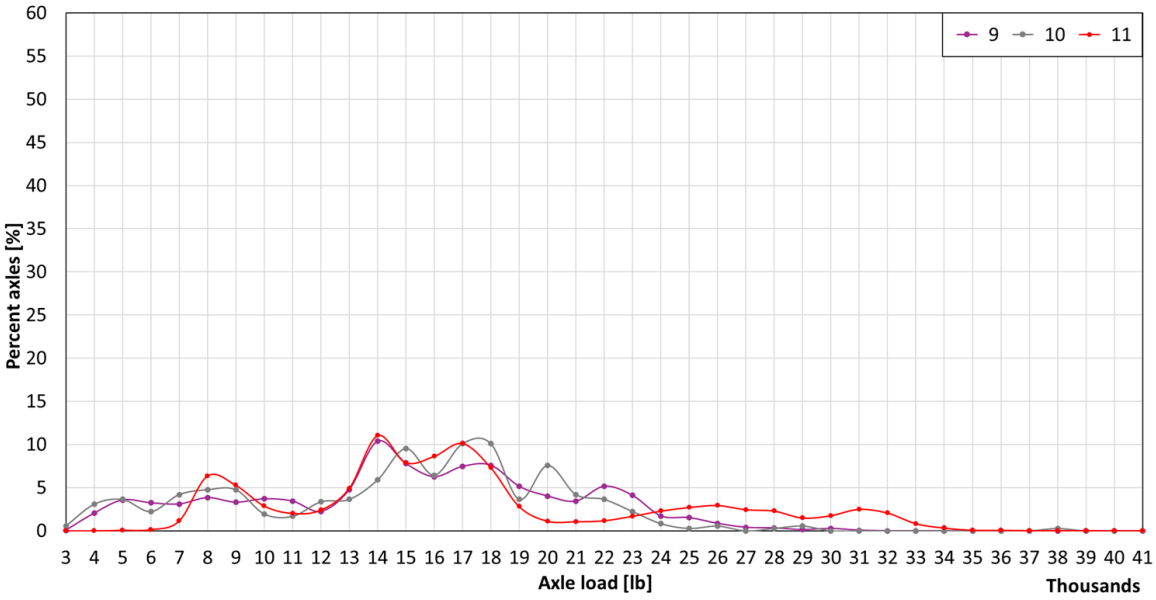

Figure 6.22: Single axle load distributions of vehicle classes 9, 10, and 11 – October

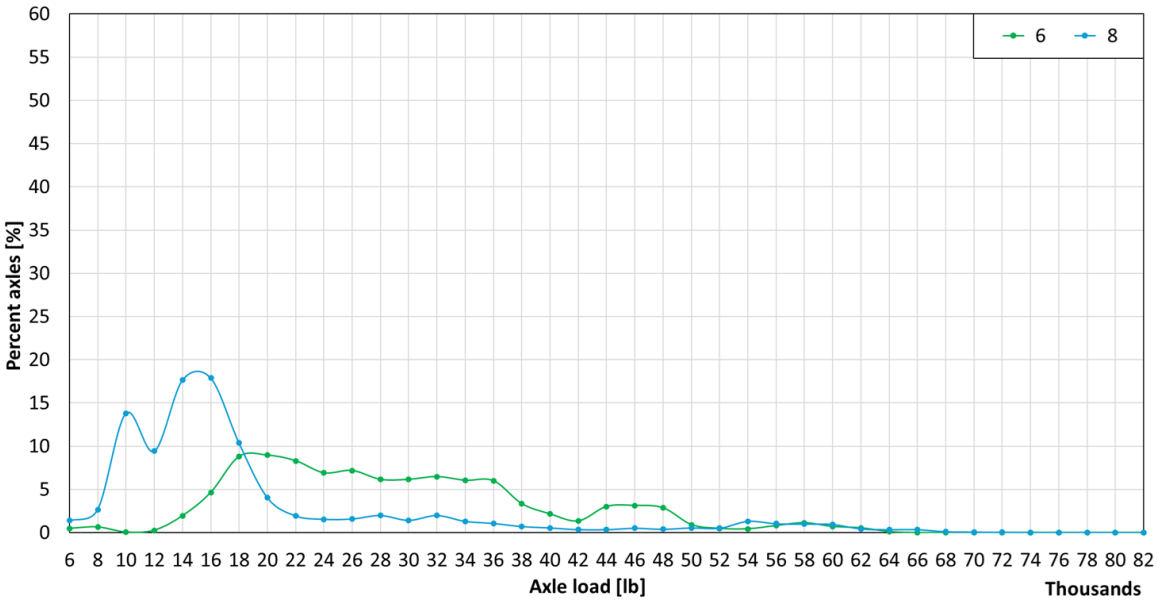

Figure 6.23: Tandem axle load distributions of vehicle classes 6 and 8 – October

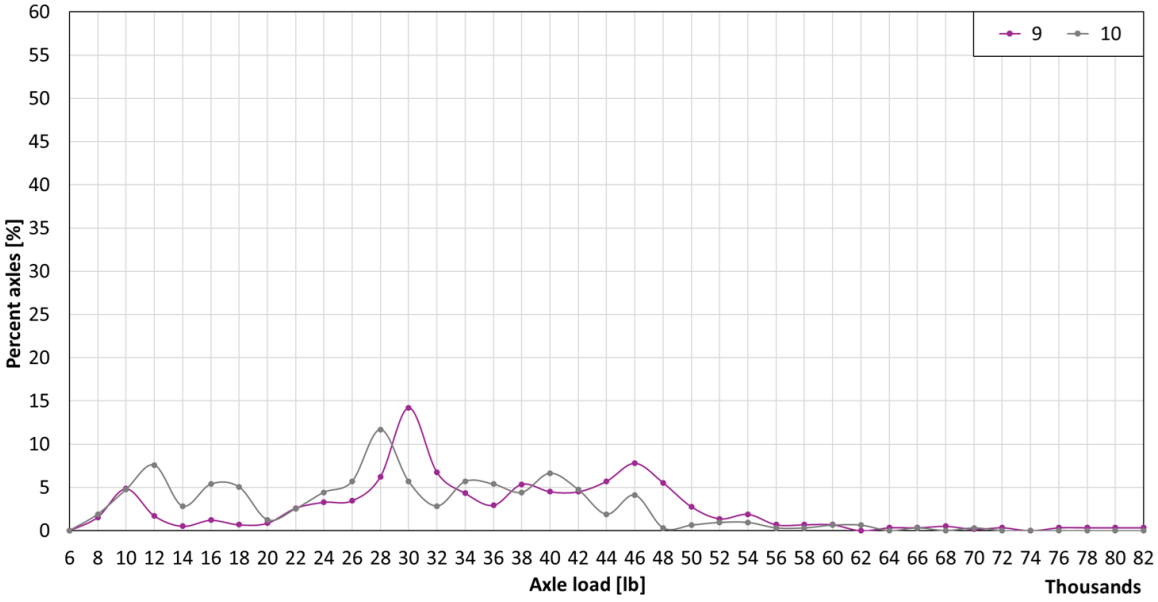

Figure 6.24: Tandem axle load distributions of vehicle classes 9 and 10 – October

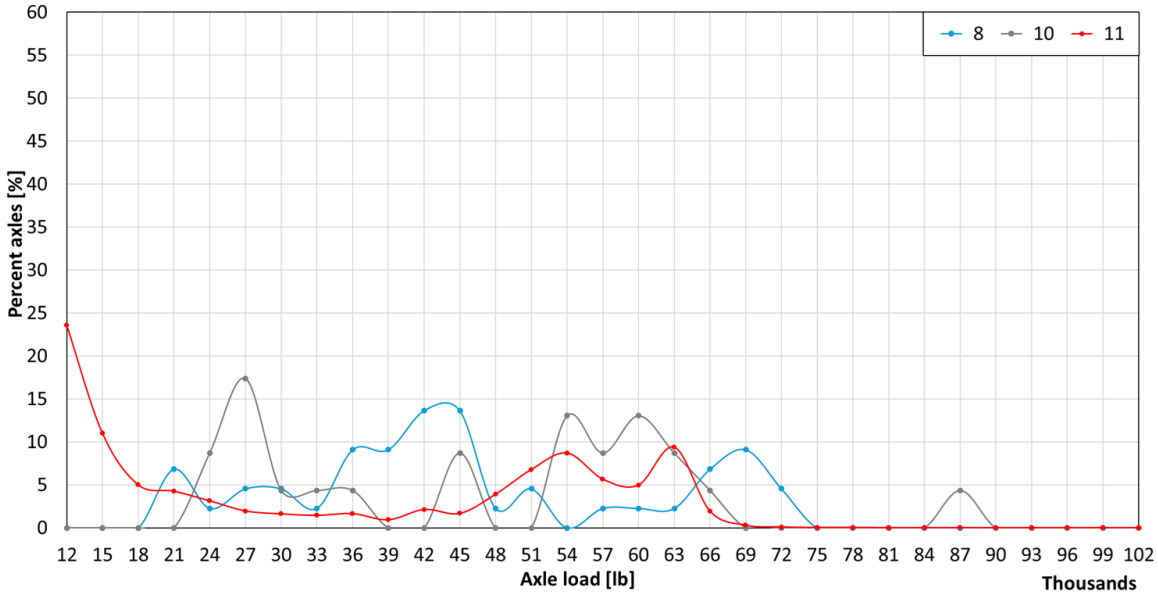

Figure 6.25: Tridem axle load distributions – October

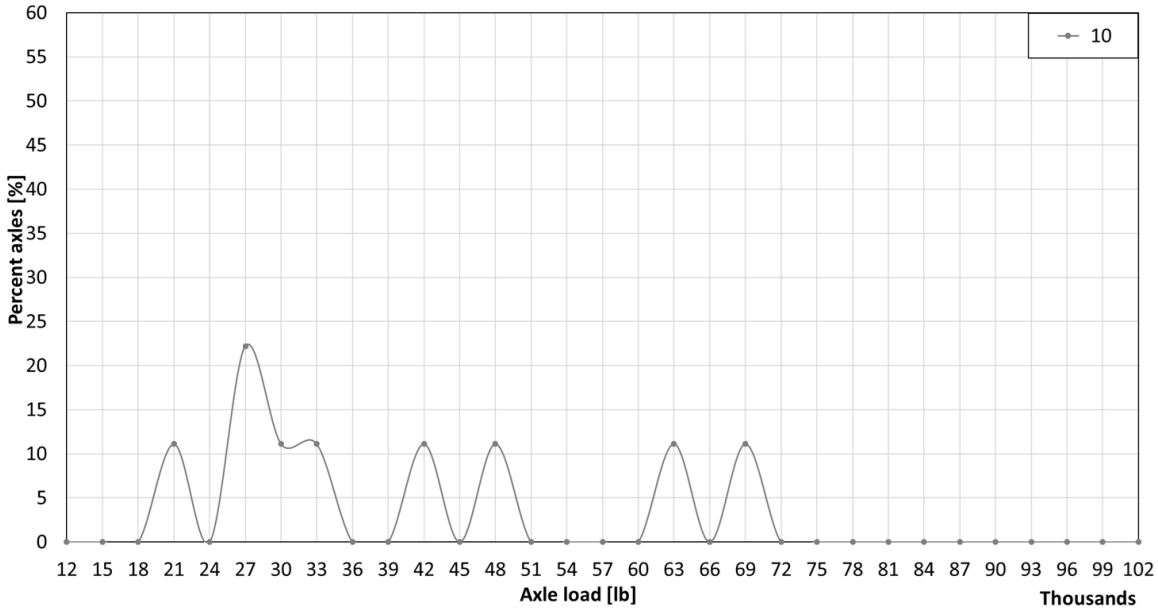

Figure 6.26: Quad axle load distribution – October

6.2.2.3 Input Levels 2 & 3

The statistics proposed in the CNR catalog were used to partially characterize traffic at Input Level 2 and 3, as discussed in section 5.2.1. In this regard, the A3 motorway was classified as a rural motorway (item #1 in fig. 1.1), while the SS45bis highway was classified as a two-lane tourist highway (item #5 in fig. 1.1). Therefore, the vehicle

class distribution was selected accordingly in fig. 1.1; the axle load distributions are those in tables A.1 and A.2 for the A3 motorway and the SS45bis highway, respectively, and are graphed in figs. 6.27 to 6.36.

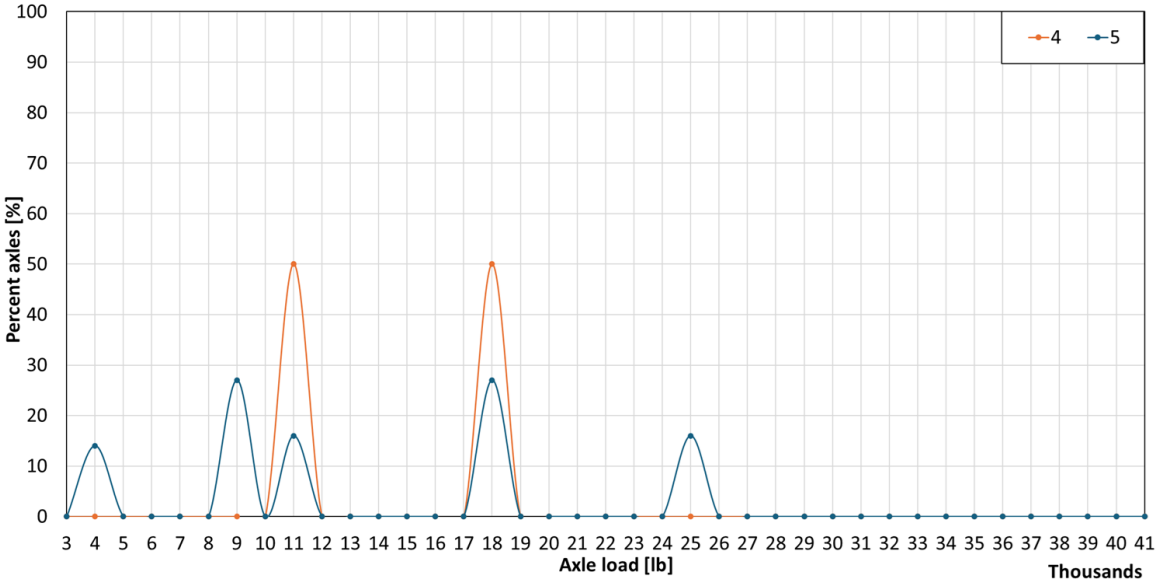

Figure 6.27: Single axle load distributions of vehicle classes 4 and 5 – Napoli

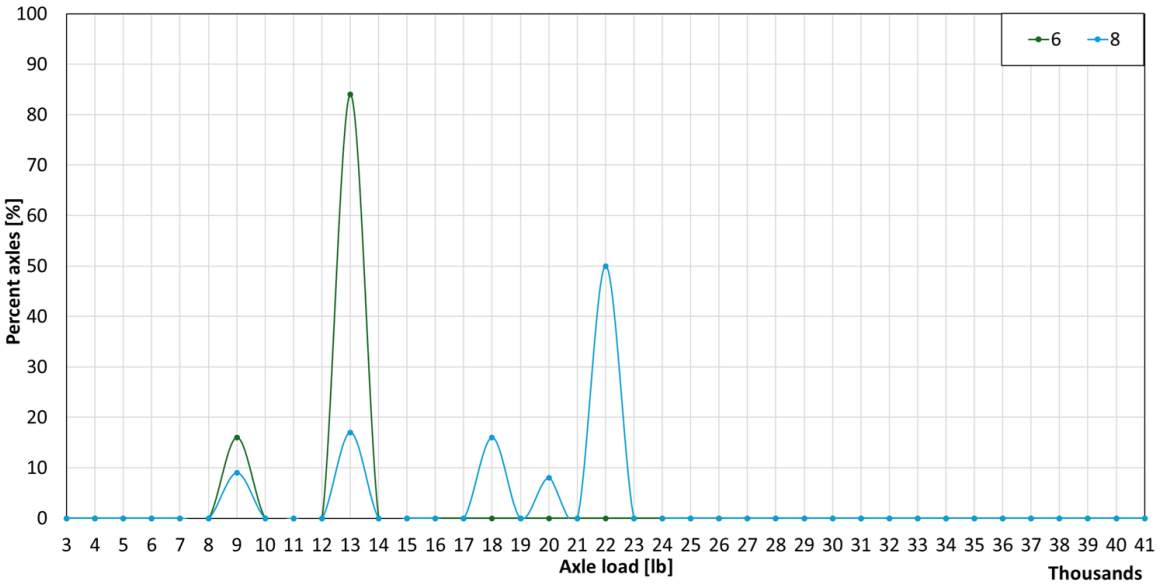

Figure 6.28: Single axle load distributions of vehicle classes 6 and 8 – Napoli

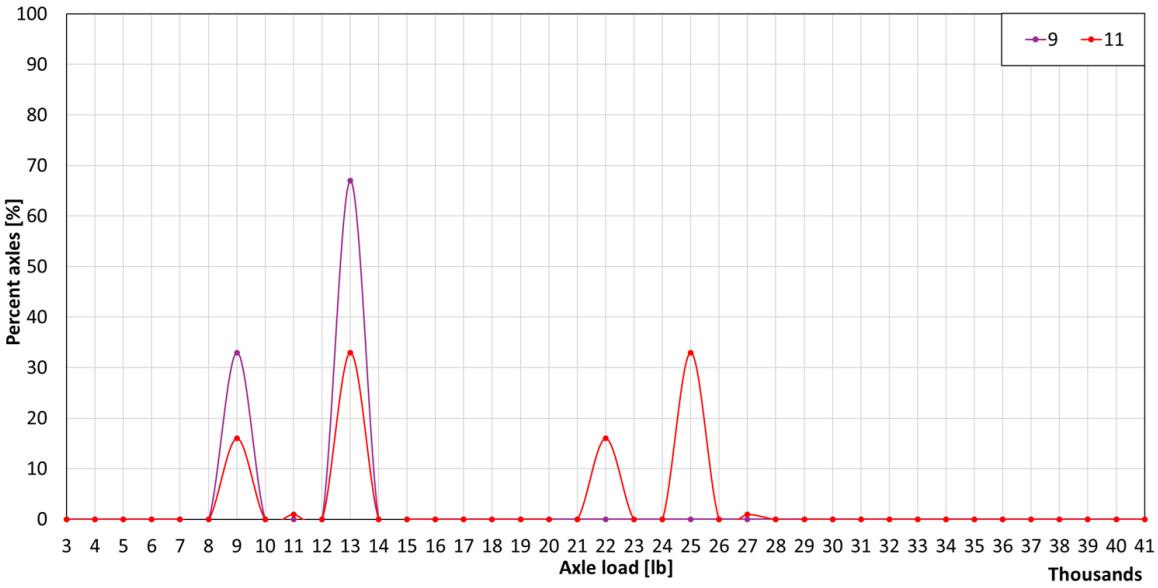

Figure 6.29: Single axle load distributions of vehicle classes 9 and 11 – Napoli

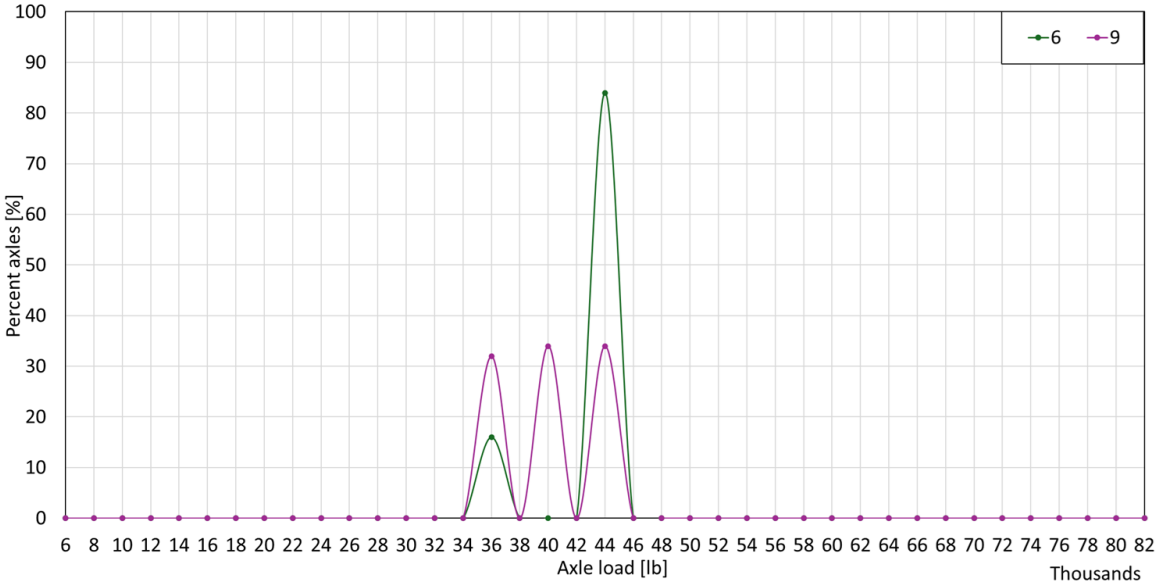

Figure 6.30: Tandem axle load distributions – Napoli

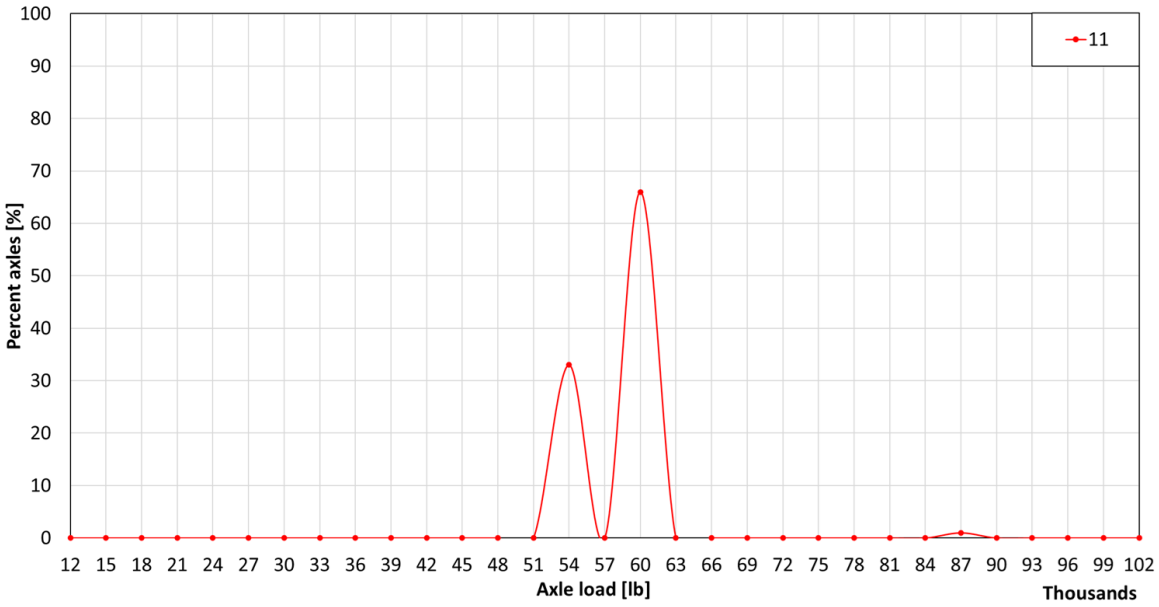

Figure 6.31: Tridem axle load distributions – Napoli

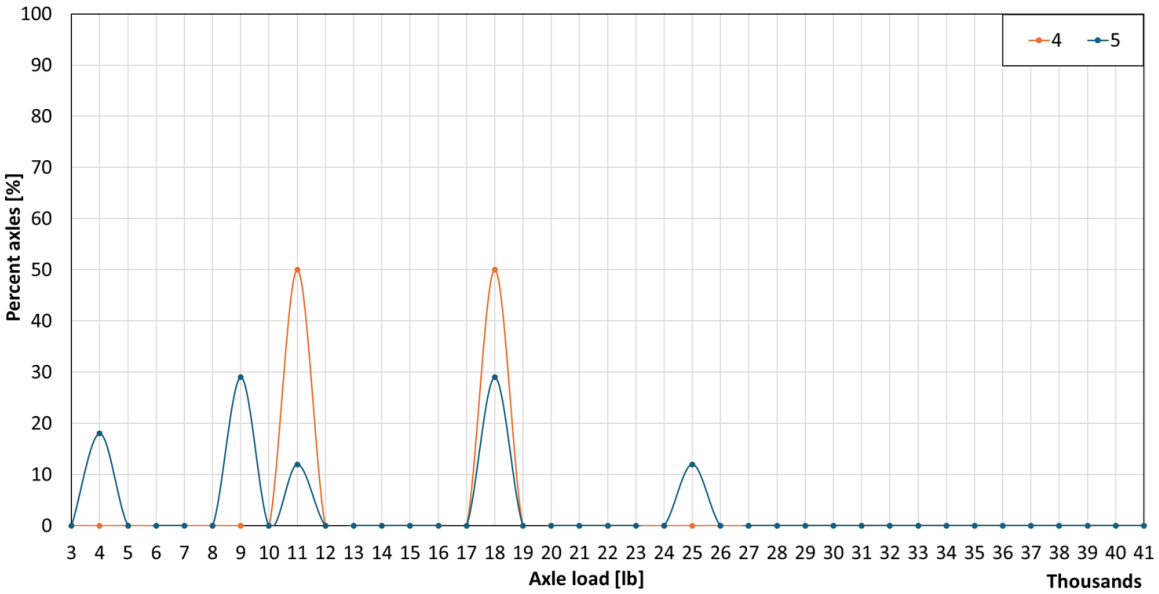

Figure 6.32: Single axle load distributions of vehicle classes 4 and 5 – Trento

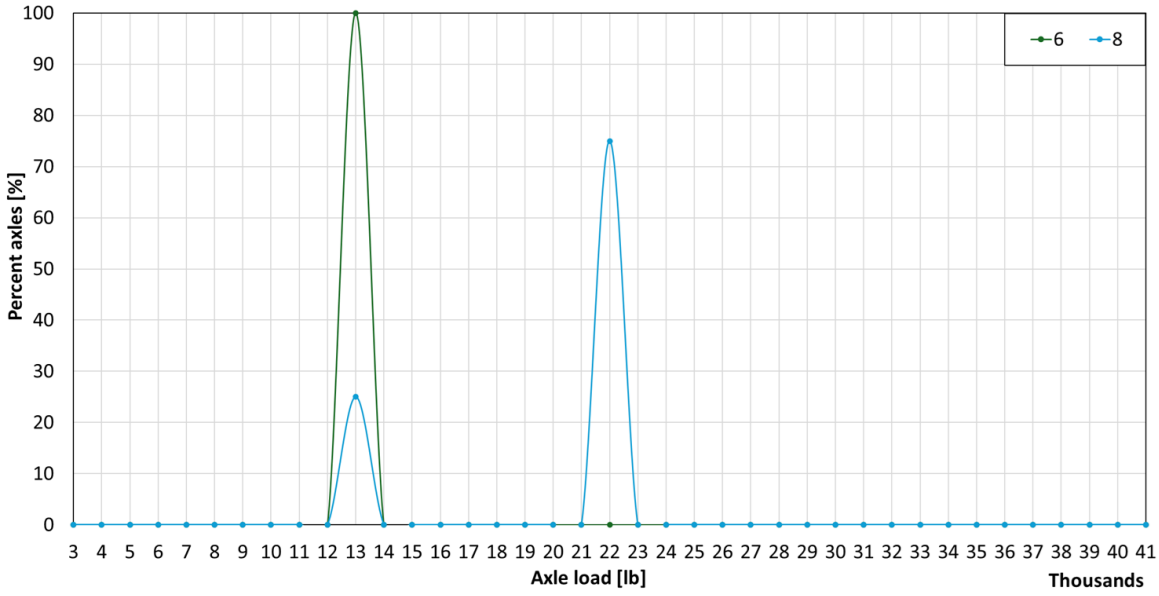

Figure 6.33: Single axle load distributions of vehicle classes 6 and 8 – Trento

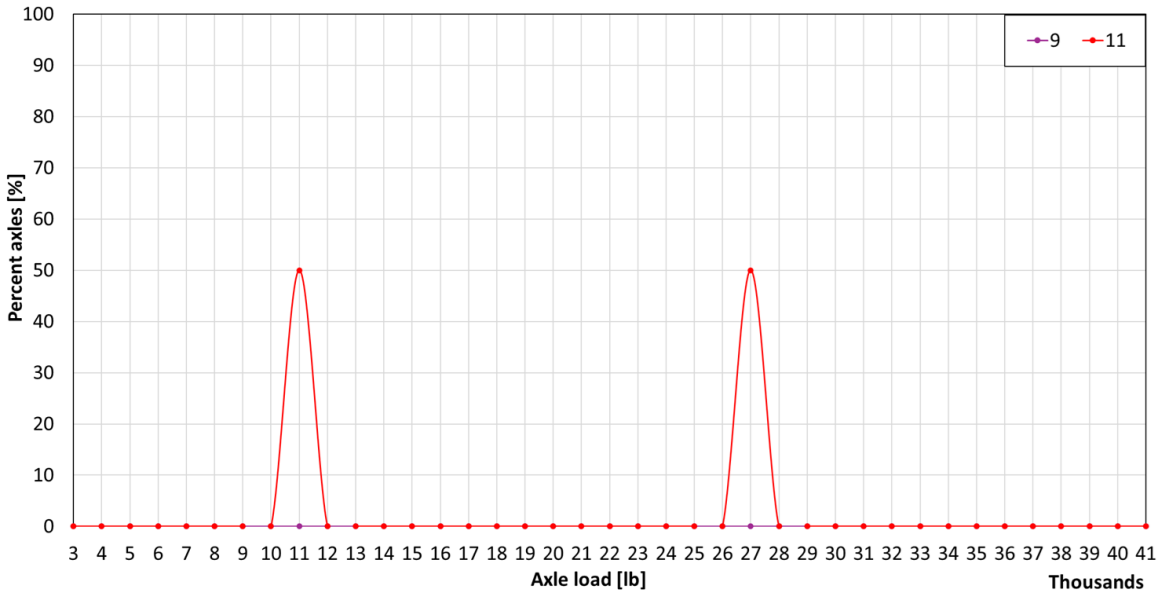

Figure 6.34: Single axle load distributions of vehicle classes 9 and 11 – Trento

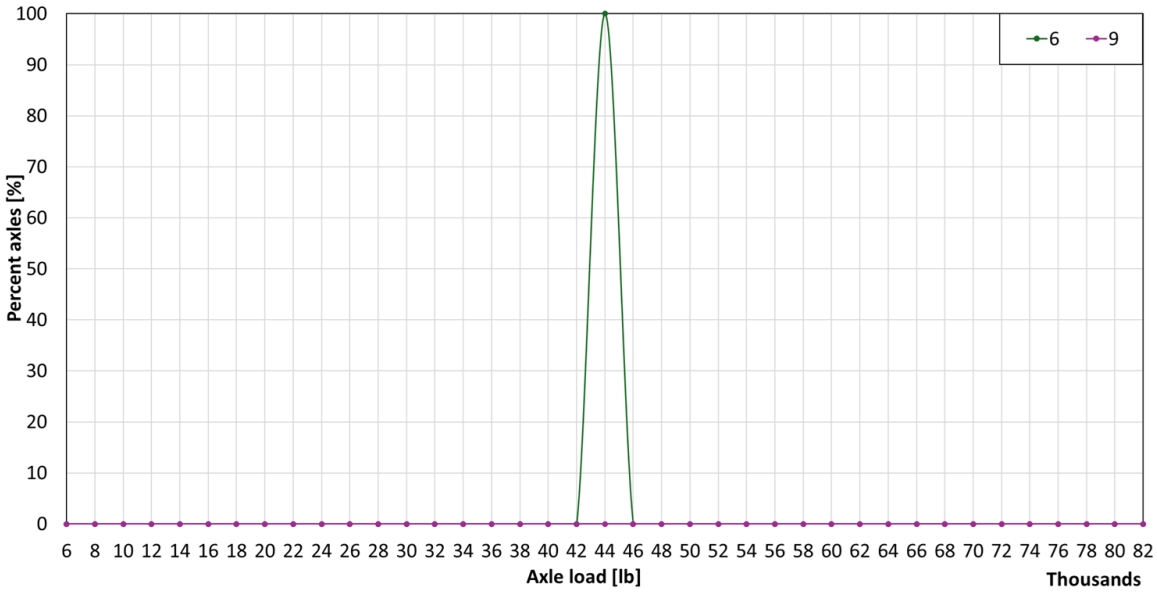

Figure 6.35: Tandem axle load distributions – Trento

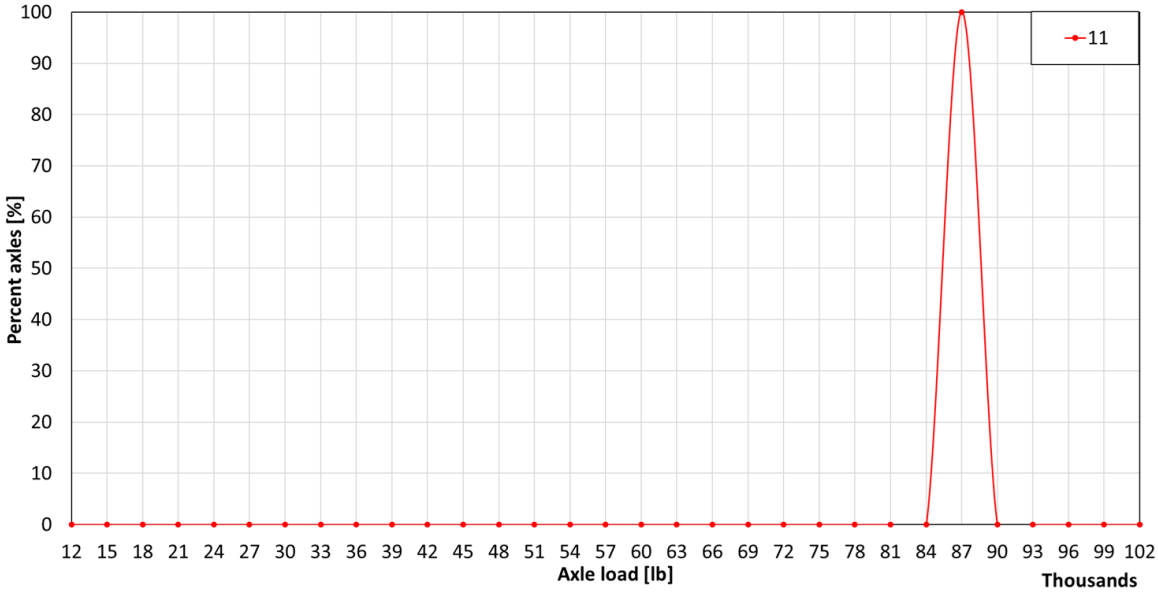

Figure 6.36: Tridem axle load distributions – Trento

The number of axles per truck was determined by the CNR vehicle class configuration, as shown in table 6.10.

Vehicle Class	Single	Tandem	Tridem	Quad
4	2.00	0.00	0.00	0.00
5	2.00	0.00	0.00	0.00
6	1.00	1.00	0.00	0.00
7	0.00	0.00	0.00	0.00
8	4.00	0.00	0.00	0.00
9	1.00	2.00	0.00	0.00
10	0.00	0.00	0.00	0.00
11	2.00	0.00	1.00	0.00
12	0.00	0.00	0.00	0.00
13	0.00	0.00	0.00	0.00

Table 6.10: CNR-based axle per truck definition

The AADTT for Input Levels 2 and 3 is ideally the same as that for Input Level 1. The same applies to the monthly adjustment factors for Input Level 2 only, because it is assumed that the manual vehicle count required by Input Level 3 may not be conducted on a sufficiently large time scale for the calculation of MAF to be meaningful.

6.2.3 Materials data

The effort on the materials input side focused on the asphalt mixture. Since not enough data on Italian mixtures were available, two dummy materials were used to implement the MEPGD and conduct the sensitivity analysis. The mixtures in question are the items labeled "WC1" and "WC3" in [19].

The mechanical properties included as input data for the analysis are reported in tables 6.11 to 6.14.

T [°C]	Frequency [Hz]				
	0.1	**1**	**5**	**10**	**25**
4	9797.2	13874.7	16648.1	17841.9	19348.7
20	2609.3	4910.9	7097.5	8202.5	9877.8
40	612.5	1140.6	1909.2	2405.4	3190.0
54	394.5	563.2	821.5	1007.3	1313.0

Table 6.11: WC1 – Dynamic modulus data expressed in MPa

T [°F]	Frequency [Hz]				
	0.1	1	5	10	25
39	1420961.1	2012361.4	2414608.1	2587757.3	2806295.1
68	378446.1	712267.3	1029409.6	1189667.6	1432661.1
104	88842.9	165428.2	276899.6	348869.8	462669.7
130	57219.2	81682.7	119142.6	146097.3	190428.1

Table 6.12: WC1 – Dynamic modulus data expressed in psi

T [°C]	Frequency [Hz]				
	0.1	1	5	10	25
4	8758.9	12374.1	14828.2	15897.7	17255.0
20	2324.5	4339.0	6253.8	7222.1	8627.1
40	522.6	1005.0	1706.2	2141.9	2843.1
54	318.1	479.4	732.4	909.1	1194.8

Table 6.13: WC3 – Dynamic modulus data expressed in MPa

T [°F]	Frequency [Hz]				
	0.1	1	5	10	25
39	1270375.5	1794715.1	2150647.6	2305775.0	2502632.3
68	337137.0	629317.9	907043.9	1047477.8	1251262.4
104	75796.9	145758.9	247467.5	310649.8	412352.9
130	46142.5	69533.0	106227.3	131849.4	173284.2

Table 6.14: WC3 – Dynamic modulus data expressed in psi

The data for the binder used to mix the two materials are summarized in table 6.15.

T [°C]	T [°F]	$\lvert G^* \rvert$ [Pa]	δ [°]
5	41	30903644.5	37.70
20	68	2813056.6	55.68
35	95	227659.6	63.93
35	95	199151.7	62.59
60	140	10347.2	59.97
80	176	1751.4	61.78

Table 6.15: Complex modulus measured at 1.59 Hz loading frequency

Additional volumetric properties included as input data are:

- the percent of bitumen by weight in the mix, corresponding to $P_b = 4.0\%$ for WC1 and $P_b = 4.8\%$ for WC3;
- the air voids percentage, set to 7% as per in-situ conditions.

The remaining mechanical and volumetric properties, not outlined above, for bound and unbound layers were incorporated into the analysis using their MEPDG default values.

Since the scenarios are intended as a dummy design, the layout selected for the pavement section is not meant to be real. For the sake of simplicity and comparison purposes, the pavement sections feature three layers:

- the hot-mix asphalt layer;
- a unbound granular base;
- the semi-infinite subgrade.

The resilient modulus of the unbound granular base is calculated for CBR = 30%, as recommended in the CNR catalog, fig. 1.5:

$$M_r = 2555 \cdot CBR^{0.64} = 155\,\text{MPa} \tag{6.1}$$

In the same way, the subgrade is assumed to perform its medium-level bearing capacity according to the CNR catalog, thus $M_r = 90\,\text{MPa}$.

The two mixtures of interest were further characterized in terms of performance-to-distress using the mixture-specific calibration coefficients in table 6.16. The damage functions calibrated in this regard are the bottom-up fatigue cracking and rutting ones. According to experimental results, WC1 is expected to perform best against rutting, whereas WC3 is expected to perform best against fatigue cracking.

	Rutting	Fatigue cracking
β_1	1.03235	0.000007
β_2	1.23439	2.057
β_3	0.47584	2.860

(a) WC3

	Rutting	Fatigue cracking
β_1	1.02103	0.000077
β_2	1.05549	1.846
β_3	0.82836	2.422

(b) WC1

Table 6.16: Mixture-specific coefficients

The corresponding global calibration coefficients are the default reported in the MEPDG and in table 6.17.

	Rutting	Fatigue cracking
k_1	-3.35412	0.007566
k_2	0.4791	3.9492
k_3	1.5606	1.281

Table 6.17: Global calibration coefficients

The global calibration coefficient for the damage function related to rutting in unbound layers was assumed to be $k_{s1} = 2.03$. In other words, the unbound layers are hypothesized to be coarse-grained materials.

Finally, the transfer function regression constants for bottom-up fatigue cracking and IRI are the default reported in the MEPDG:

- $C_1 = 1.00, C_2 = 1.00, C_3 = 6000$ for bottom-up fatigue cracking;
- $C_1 = 40.0, C_2 = 0.400, C_3 = 0.008, C_4 = 0.015$ for IRI.

6.3 The sensitivity analysis matrix

The sensitivity analysis matrix involves 13 scenarios and is structured as follows. Two main sections are identified, one for each case study: Trento and Napoli. Each section is then branched into the sensitivity analysis groups dedicated to traffic and materials.

The scenario labels follow the structure *Site–Material–Traffic*, where

- *Site* is the code of the Province of interest (either TN for Trento or NA for Napoli);
- *Material* identifies the asphalt mixture configuration;
- *Traffic* identifies the traffic input level according to the new approach introduced in table 5.2.

By way of example, TN-WC1-IL1 represents the Trento section analyzed using the WC1 mixture and traffic Input Level 1.

The matrices are presented in tables 6.18 and 6.19: such tables show the division between the scenarios dedicated to traffic (#1, 2, 3 for Trento, #8, 9, 10 for Napoli) and materials (#4, 5, 6, 7 for Trento, #11 for Napoli) sensitivity analysis.

To avoid redundancy, an extensive material sensitivity analysis was conducted only for Trento. In this regard, the performances of WC3 were investigated in scenario #4. A similar analysis was performed for both WC1 and WC3 in scenarios #5 and 6, where the performances-to-distress of the mixtures were overlooked, that is, the mixture-specific coefficients were set to 1. As a result, the damage functions were implemented artificially using a non-performance-oriented approach, such as that proposed in the Asphalt Institute Guide.
Finally, the combination of WC1 and WC3 is used in scenarios #7 and 11.

#	**Scenario**	**Materials**	**Traffic**	**Climate**
1	TN-WC1-IL1	WC1	Trento IL1	Trento
2	TN-WC1-IL2	WC1	Trento IL2	Trento
3	TN-WC1-IL3	WC1	Trento IL3	Trento
4	TN-WC3-IL1	WC3	Trento IL1	Trento
5	TN-WC1-β=1-IL1	WC1, β=1	Trento IL1	Trento
6	TN-WC3-β=1-IL1	WC3, β=1	Trento IL1	Trento
7	TN-WC1+WC3-IL1	WC1 + WC3	Trento IL1	Trento

Table 6.18: Sensitivity analysis matrix – Trento section

#	Scenario	Materials	Traffic	Climate
8	NA-WC1-IL1	WC1	Napoli IL1	Napoli
9	NA-WC1-IL2	WC1	Napoli IL2	Napoli
10	NA-WC1-IL3	WC1	Napoli IL3	Napoli
11	NA-WC3-IL1	WC1 + WC3	Napoli IL1	Napoli

Table 6.19: Sensitivity analysis matrix – Napoli section

The overall matrix includes two additional scenarios for the climate sensitivity analysis presented in table 6.20. Scenario #12 is the counterpart of scenario #1, artificially designed under Trento climate conditions. The same applies to scenario #13, the counterpart of scenario #8, artificially designed under Napoli climate conditions.

#	Scenario	Materials	Traffic	Climate
12	TN Clim-NA Traf	WC1	Napoli IL1	Trento
13	NA Clim-TN Traf	WC1	Trento IL1	Napoli

Table 6.20: Climate sensitivity analysis matrix

At all traffic input levels, the growth rate was set to 1%, and the linear growth function was selected. Furthermore, the operational speeds were set to 50 mi/h (80 km/h) and 75 mi/h (120 km/h) for Trento and Napoli, respectively.

Finally, the pavement design was performed at a 50% reliability level, and the distress-specific thresholds were set to the default values in the Software for all damage typologies. This decision was made because the reliability parameters require local calibration within the MEPDG, as do the transfer functions, and this was not performed. Consequently, a reliability level of 50% serves as a neutral baseline for all scenarios.

Chapter 7

Results and discussion

The results are presented hereafter either as damage curves produced by the PavME analysis or as pavement sections optimized iteratively against the distress under analysis. The damage categories examined are bottom-up fatigue cracking and total rutting. For the sake of completeness, the IRI plots are reported as well. However, care shall be taken with this indicator because the formula includes a term related to thermal cracking damage (TC), whose damage function was not subjected to mixture-specific calibration.

7.1 Traffic sensitivity analysis

The pavement section was optimized for scenarios #1 and #8, which serve as the base or reference scenario for the traffic sensitivity analysis of Trento and Napoli, respectively. That is to say that the same section as scenario #1 was used to analyze scenarios #2 and #3, and the same applies to the Napoli counterpart. Hence, the results of the sensitivity analysis are presented in terms of damage and IRI evolution over time for the same section under different traffic load characterizations, namely, Input Levels 1, 2, and 3.

7.1.1 Trento

The optimized section for the base scenario is provided in fig. 7.1. The leading distress is bottom-up fatigue cracking (see fig. 7.2), which is consistent with the expected performance of WC1.

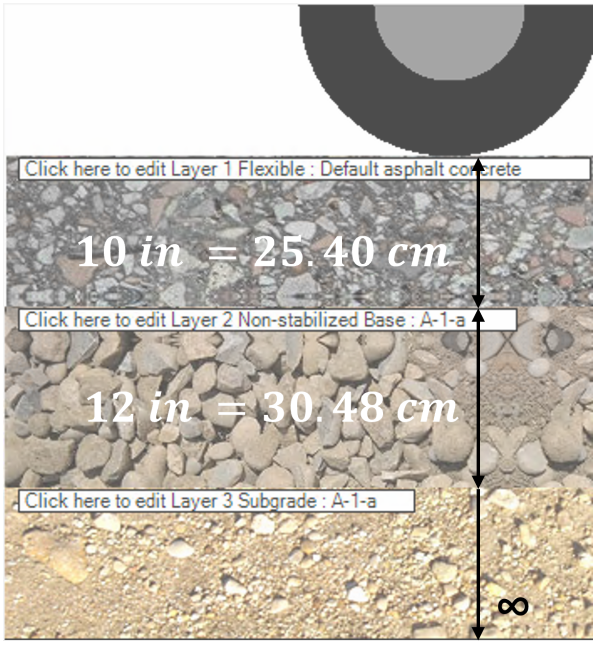

Figure 7.1: Optimized pavement section for Trento base scenario #1

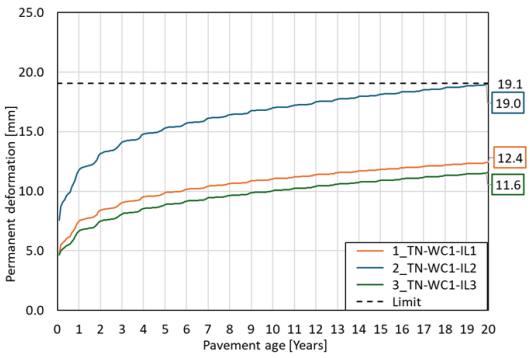

(a) Total rutting

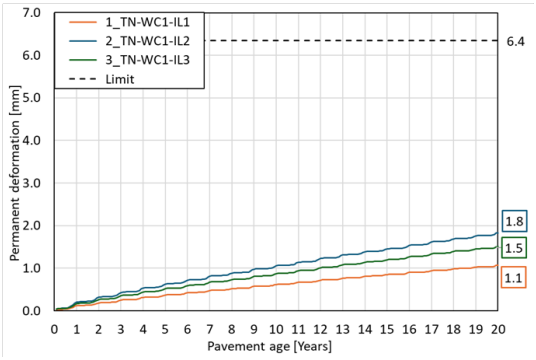

(b) AC rutting

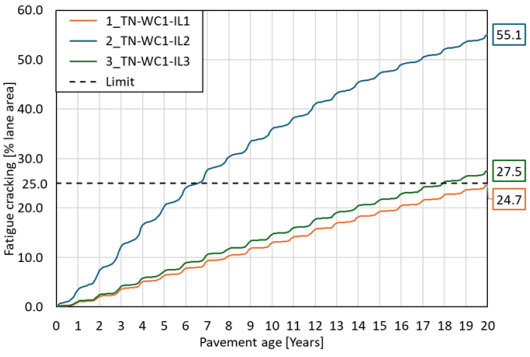

(c) BU fatigue cracking

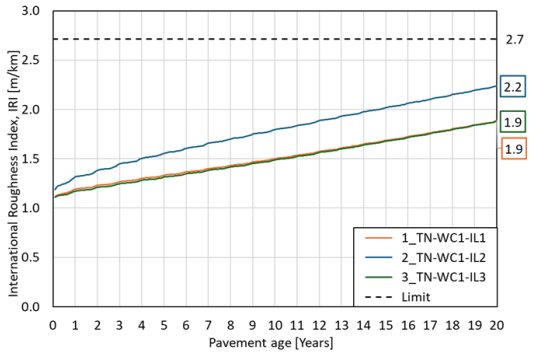

(d) IRI

Figure 7.2: Damage and IRI evolution over time for scenario #1, 2, and 3

7.1.2 Napoli

The optimized section for the base case study is provided in fig. 7.3. The leading distress is bottom-up fatigue cracking (see fig. 7.4), which is consistent with the expected performance of WC1.

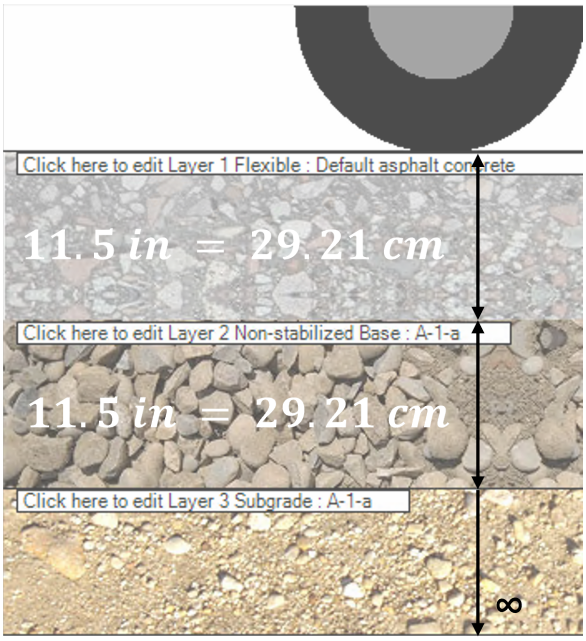

Figure 7.3: Optimized pavement section for Napoli base scenario #8

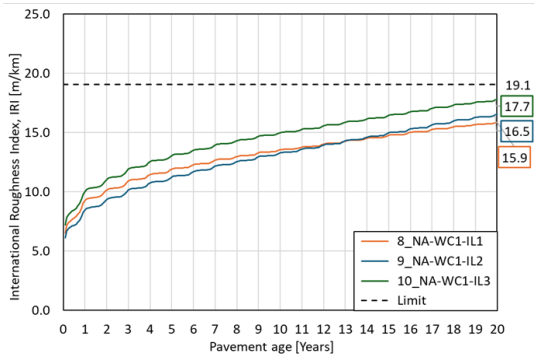

(a) Total rutting

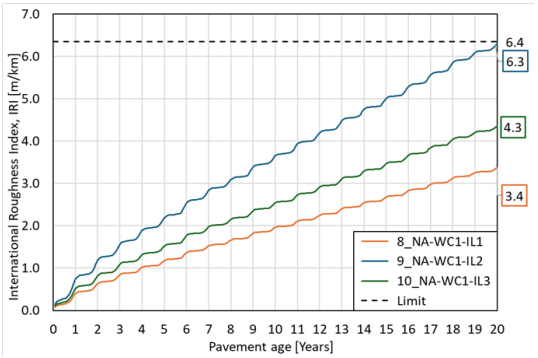

(b) AC rutting

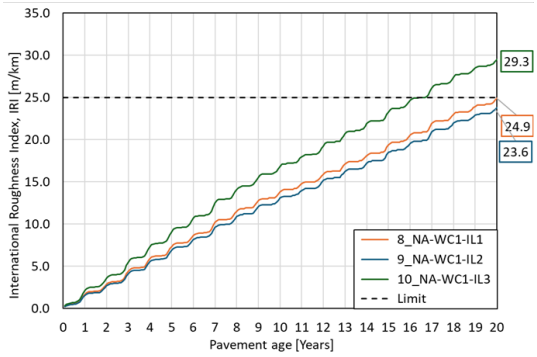

(c) BU fatigue cracking

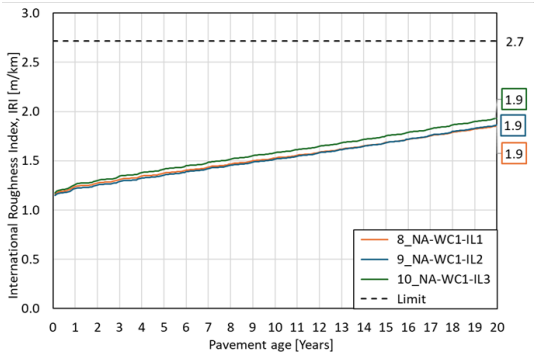

(d) IRI

Figure 7.4: Damage and IRI evolution over time for scenarios #8, 9, and 10

The outcomes presented in figs. 7.2 and 7.4 emphasize that damage and IRI evolution are randomly affected by traffic characterization, that is, by the Input Level implemented. No rationale can be identified to justify the results of the traffic sensitivity analysis. However, adopting the typical traffic statistics proposed in the CNR catalog leads to misdesign of the pavement section, in one way or another, compared to the base scenario.

7.2 Materials sensitivity analysis

The outputs of scenario #4 are obtained with the same section as the base one, fig. 7.1. Hence, fig. 7.5 shows the results of the sensitivity analysis in terms of damage and IRI evolution over time for the same section, with different top-layer materials, namely, WC1 and WC3. The same applies to scenarios #5 and 6 in fig. 7.6.

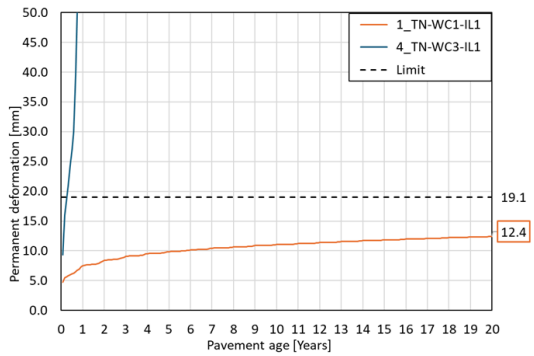

(a) Total rutting

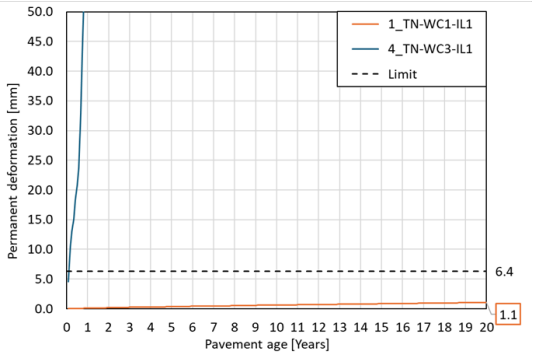

(b) AC rutting

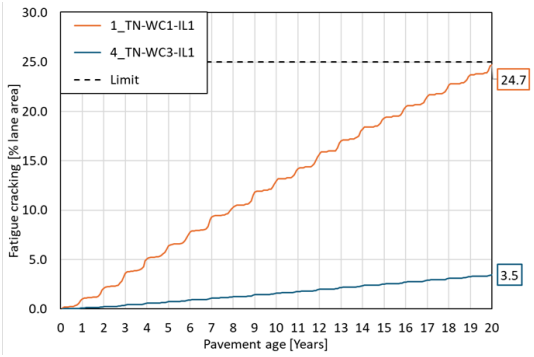

(c) BU fatigue cracking

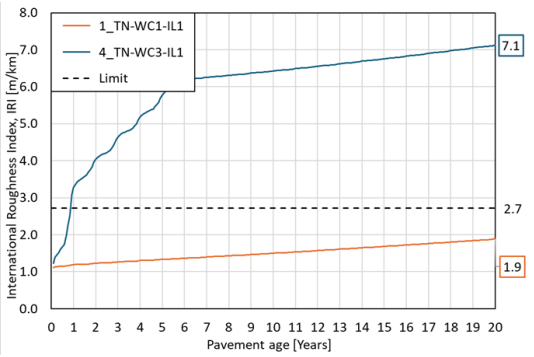

(d) IRI

Figure 7.5: Damage and IRI evolution over time for scenarios #1 and 4

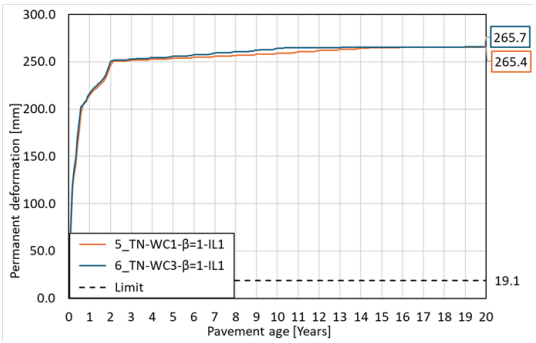

(a) Total rutting

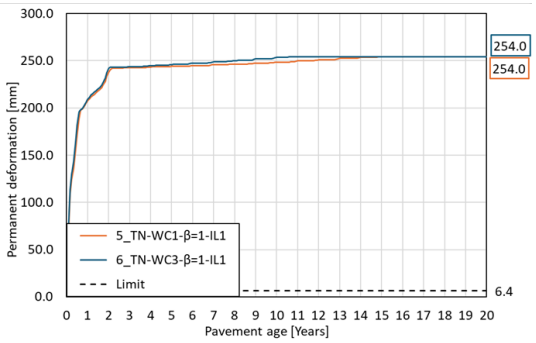

(b) AC rutting

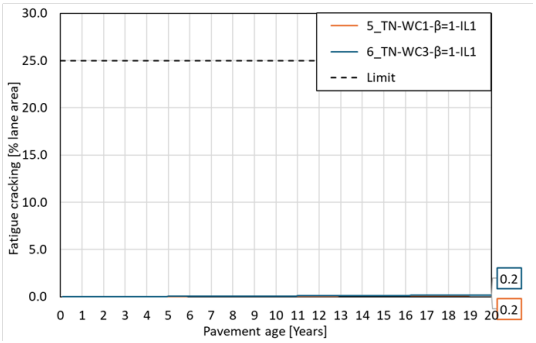

(c) BU fatigue cracking

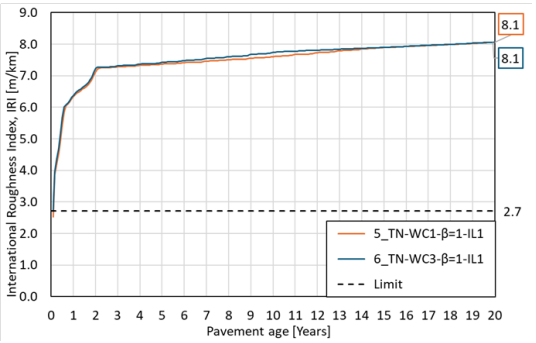

(d) IRI

Figure 7.6: Damage and IRI evolution over time for scenarios #5 and 6

These results highlight the essential role of characterizing materials from a performance perspective, in addition to the more common mechanical and volumetric characterization. In fact, conducting pavement design without considering the mixture's performance leads to a significant underestimation of its impact on damage evolution. When overlooking the performance to rutting and fatigue cracking (scenarios #5 and 6) and considering the sole mechanical and volumetric characterization, no significant difference can be observed in the outputs. Things change when the β factors are calibrated instead (scenarios #1 and 4).

The pavement section was optimized for scenarios #7 and 11, as illustrated in figs. 7.7 and 7.8 respectively.

The PavME software does not allow assigning dedicated β factors to each layer; rather, the set of calibration factors is assigned to all the layers of the material in question, namely, asphalt concrete. Therefore, the rutting-related β factors for WC1 and the fatigue-cracking-related β factors for WC3 were selected for scenarios #7 and 11.

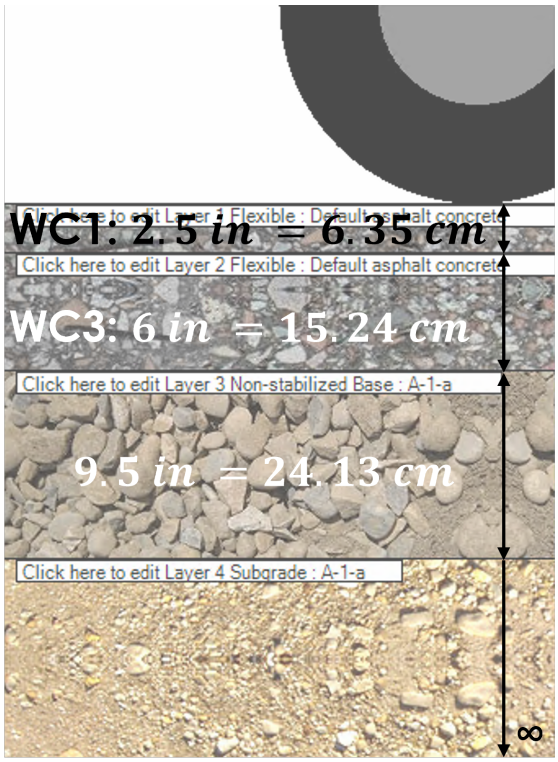

Figure 7.7: Optimized pavement section for scenario #7

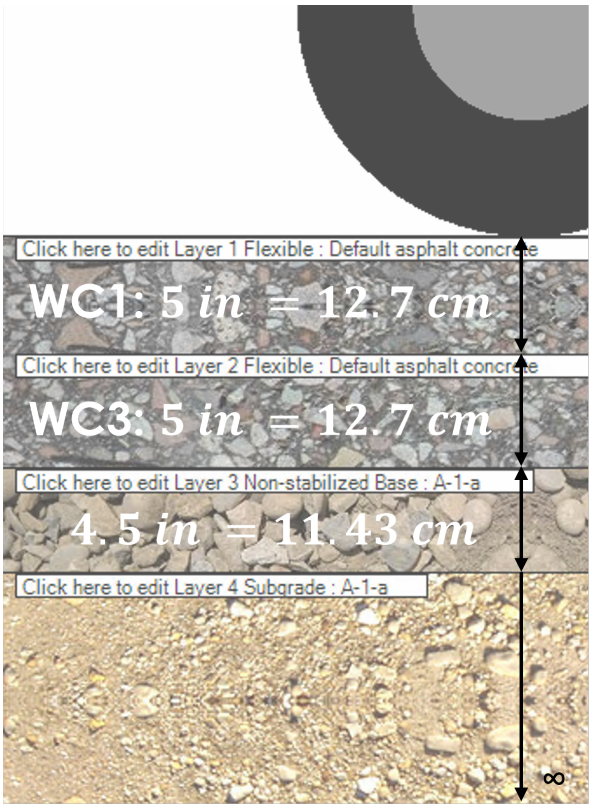

Figure 7.8: Optimized pavement section for scenario #11

These sections indicate that employing a combination of mixtures with different distress profiles by exploiting their performance strengths accordingly – WC1 as top HMA layer, best performing against rutting, and WC3 as bottom HMA layer, best performing against bottom-up fatigue cracking – leads to an overall decrease in the thickness of the layers, thus involving potential economic implications.

As a result, implementing mechanical and physical properties rather than including performance indicators may lead to a simplistic and incomplete characterization of the mixture and, ultimately, to misdesign of the pavement section.

For the sake of completeness, the summary of the distress and IRI evolution over time is presented in figs. 7.9 and 7.10, although here the main interest lies in the pavement section.

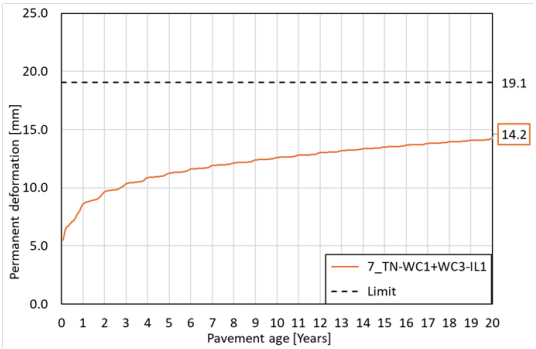

(a) Total rutting

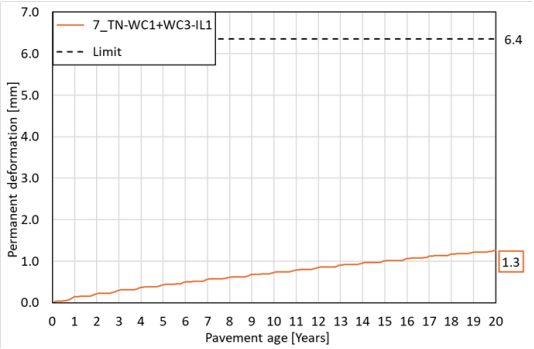

(b) AC rutting

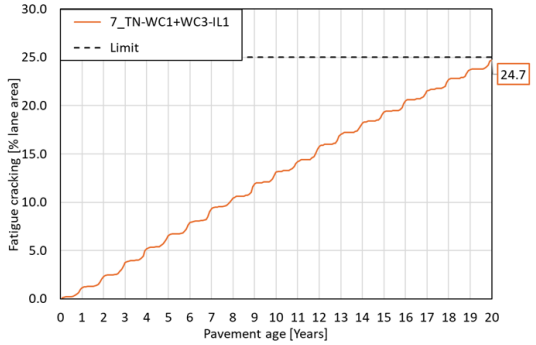

(c) BU fatigue cracking

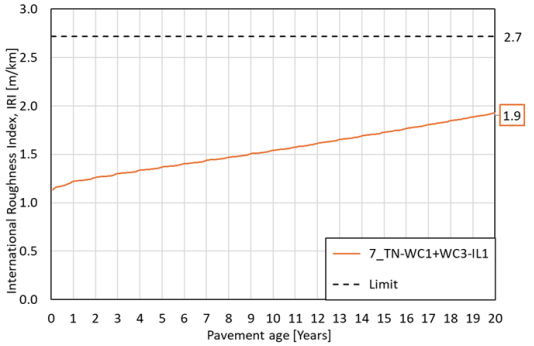

(d) IRI

Figure 7.9: Damage and IRI evolution over time for scenario #7

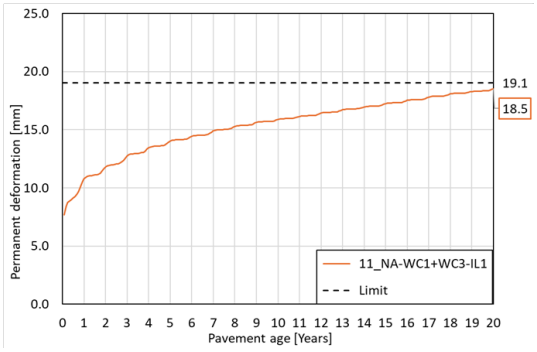

(a) Total rutting

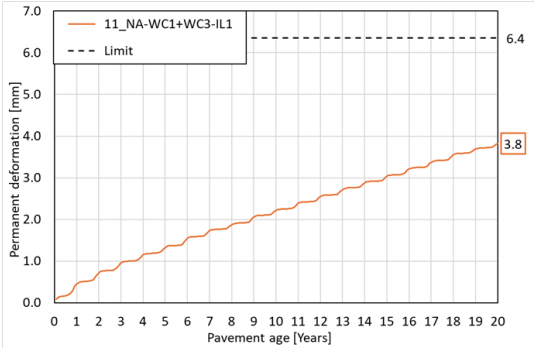

(b) AC rutting

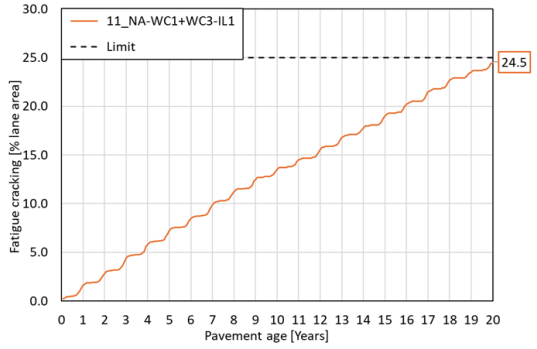

(c) BU fatigue cracking

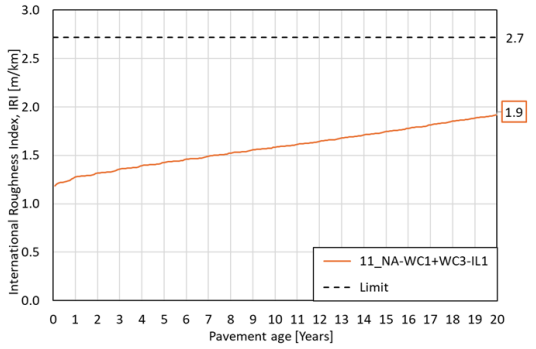

(d) IRI

Figure 7.10: Damage and IRI evolution over time for scenario #11

7.3 Climate sensitivity analysis

The outputs for scenarios #12 and 13 are obtained using the same section as the respective base scenario, figs. 7.1 and 7.3. Hence, figs. 7.11 and 7.12 show the results of the sensitivity analysis in terms of damage and IRI evolution over time for the same section under different climate conditions.

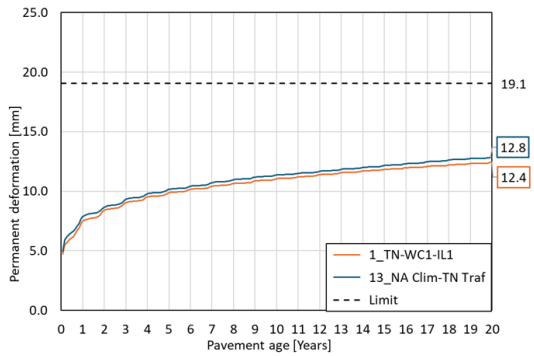

(a) Total rutting

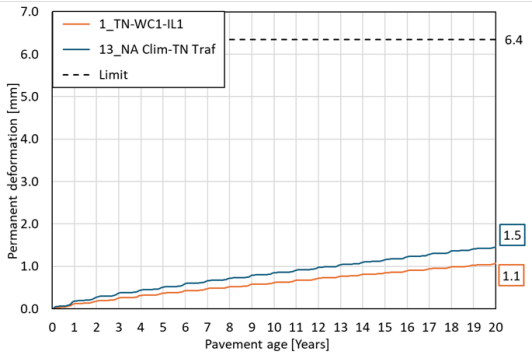

(b) AC rutting

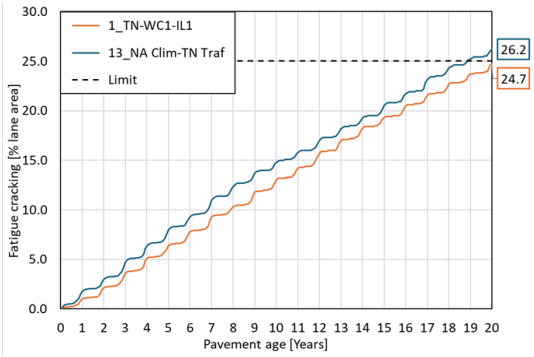

(c) BU fatigue cracking

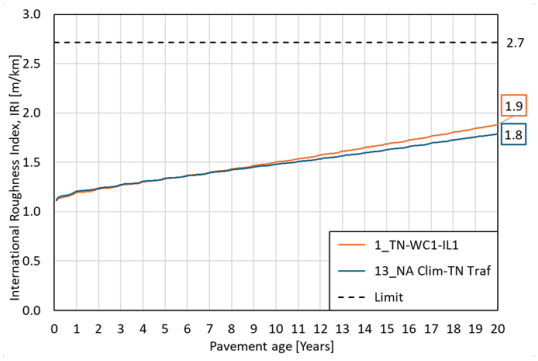

(d) IRI

Figure 7.11: Damage and IRI evolution over time for scenarios #1 and 13

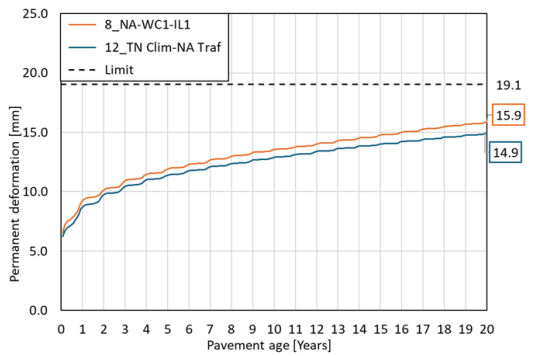

(a) Total rutting

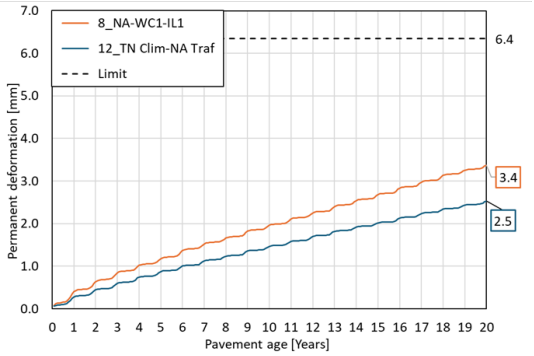

(b) AC rutting

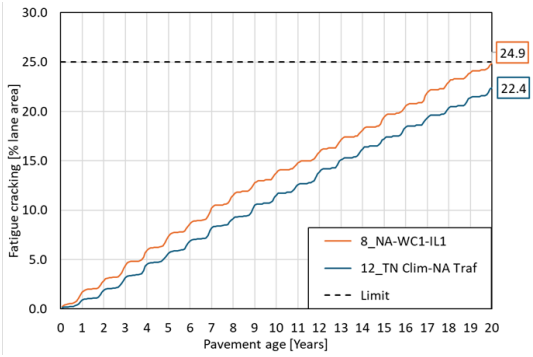

(c) BU fatigue cracking

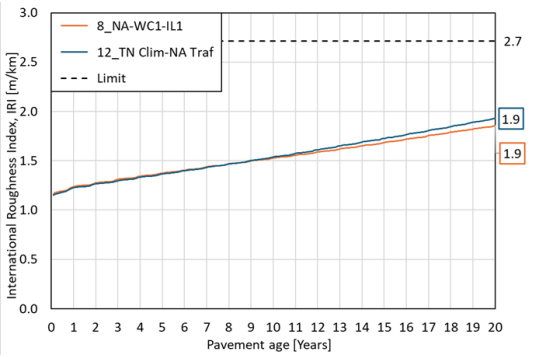

(d) IRI

Figure 7.12: Damage and IRI evolution over time for scenarios #8 and 12

Chapter 8

Conclusions

The product of this research is a framework for the local preliminary implementation of the MEPDG in the Italian context, followed by a demonstration of its use and a sensitivity analysis on the three input data categories.

The results of the sensitivity analysis highlight how input data affects pavement design outputs within the MEPDG framework. In particular, the peculiar and case-specific characterization of traffic, climate data, and material properties significantly influences the evolution of damage.

To sum up, the use of WIM station data, full performance-based material characterization, and comprehensive climate information is encouraged for pavement design purposes within the MEPDG framework.

8.1 Limitations and future work

The present work represents an initial step toward the implementation of a mechanistic–empirical pavement design framework in the Italian context. The limitations of this thesis stem from the exploratory nature of the study and the early stage of development of the research topic. As a matter of fact, the implementation conducted is intended for illustrative purposes and does not represent a fully developed application of the method. Some assumptions were necessary in conducting the sensitivity analysis: the transfer functions were not calibrated to local conditions, and the design sections derived from the procedure are not intended for real-world applications.

An additional limitation of the present work concerns the validation of the ERA5 climatic dataset. The comparison was performed against meteorological data provided by the Italian Air Force; however, this dataset was not fully suitable for validation pur-

poses. In particular, several variables had missing records during the analysis period, and some measurements were not expressed in units directly comparable to those used in ERA5 or MERRA-2. For instance, cloud cover was reported in oktas rather than as a percentage, requiring additional assumptions for data harmonization. As a result, the validation of the reanalysis data should be interpreted with caution. Future work should aim to repeat the validation process using more complete and consistent observational datasets.

The findings of this study suggest that future efforts should prioritize the development of reliable input datasets. Within this process, local calibration should be addressed as a final step, once the input characterization has reached an adequate level of accuracy. Meanwhile, future work should focus on developing a comprehensive, calibration-oriented Pavement Management System (PMS) for the Italian road network. Such a system represents a critical prerequisite for the collection of consistent performance data and, consequently, for the reliable local calibration of mechanistic–empirical models.

Bibliography

[1] Witczak , M. W. Recommended Standard Method for Routine Resilient Modulus Testing of Unbound Granular Base/Subbase Materials and Subgrade Soils. Technical Report NCHRP Project 1-28A, Transportation Research Board, Washington, D.C., 2002.

[2] Ahmed, S., Yuan, X.-X., Lee, W., and Li, N. Local Calibration of Cracking Models in MEPDG for Ontario's Flexible Pavement. Transportation Association of Canada (TAC), 2016.

[3] ERES Consultants Division ARA, Inc. Guide for Mechanistic-Empirical Design of New and Rehabilitated Pavement Structures. Final Report NCHRP Project 1-37A, Transportation Research Board, Washington, D.C., 2004.

[4] American Association. *Mechanistic-Empirical Pavement Design Guide: A Manual of Practice, 2nd Edition*. Washington, DC, 2015.

[5] ASTM International. Standard Practice for Classification of Soils for Engineering Purposes (Unified Soil Classification System).

[6] Ciro Caliendo. Local Calibration and Implementation of the Mechanistic-Empirical Pavement Design Guide for Flexible Pavement Design. *Journal of Transportation Engineering*, 138(3):348–360, March 2012.

[7] Comitato Nazionale delle Ricerche (CNR). Bollettino Ufficiale (Norme tecniche) – A. XIX – N. 106, 1985.

[8] Rodrigo Delgadillo, Carlos Wahr, and Juan Alarcón. Toward Implementation of the Mechanistic-Empirical Pavement Design Guide in Latin America. *Transportation Research Record: Journal of the Transportation Research Board*, 2226:142–148, December 2011.

[9] Barry J Dempsey. A Heat-Transfer Model for Evaluating Frost Action and Temperature-Related Effects in Multilayered Pavement Systems. 1970.

[10] European Committee for Standardization (CEN). EN 13286-7, Unbound and hydraulically bound mixtures – Part 7: Cyclic load triaxial test for unbound mixtures, 2004.

[11] European Committee for Standardization (CEN). EN 12697-25, Bitumunous mixtures – Tests methods – Part 25: Cyclic compression test, 2016.

[12] European Committee for Standardization (CEN). EN 12697-23, Bitumunous mixtures – Tests methods – Part 23: Determination of the indirect tensile strength of bituminous specimens, 2017.

[13] European Committee for Standardization (CEN). EN 12697-24, Bitumunous mixtures – Tests methods – Part 24: Resistance to fatigue, 2018.

[14] European Committee for Standardization (CEN). EN 12697-26, Bitumunous mixtures – Tests methods – Part 26: Stiffness, 2018.

[15] European Committee for Standardization (CEN). EN 12697-22, Bitumunous mixtures – Tests methods – Part 22: Wheel tracking, 2020.

[16] European Committee for Standardization (CEN). EN 14770, Bitumen and bituminous binders – Determination of complex shear modulus and phase ancle – Dynamic Shear Rheometer (DSR), 2023.

[17] Federal Highway Administration (FHWA). *Traffic Monitoring Guide*. U.S. Department of Transportation, Federal Highway Administration, Washington, D.C., December 2022.

[18] Iunio Iervolino, Georgios Baltzopoulos, Antonio Vitale, Antonio Grella, Giovanni Bonini, and Antonio Iannaccone. Empirical distributions of traffic loads from one year of weigh-in-motion data. *Scientific Data*, 10(1):289, May 2023.

[19] Khalifa University of Science and Technology. Performance of bitumen and mixtures based on Superpave design principles. Technical report, Abu Dhabi, 2021.

[20] Sadaf Khosravifar, Intikhab Haider, Zahra Afsharikia, and Charles W. Schwartz. Application of time–temperature superposition to develop master curves of cumulative plastic strain in repeated load permanent deformation tests. *International Journal of Pavement Engineering*, 16(3):214–223, March 2015.

[21] M. E. Kutay and M. Lanotte. Formulations of the pavement performance prediction models in the mechanistic-empirical asphalt pavement analysis (MEAPA) web application. *Michigan State University*, 2020.

[22] M. Emin Kutay and Mike Lanotte. Viscoelastic continuum damage (VECD) models for cracking problems in asphalt mixtures. *International Journal of Pavement Engineering*, 19(3):231–242, March 2018.

[23] Michele Lanotte, M. Emin Kutay, Syed W. Haider, and Gopi Krishna Musunuru. New calibration approach to improve Pavement ME Design thermal cracking prediction: mixture-specific coefficients – the Michigan case study. *Road Materials and Pavement Design*, 21(7):1859–1871, October 2020.

[24] American Association of State Highway and Transportation Officials. M 145-91 (2025) - classification of soils and soil-aggregate mixtures for highway construction purposes, 2025.

[25] American Association of State Highway and Transportation Officials. T 307-99 (2025) – Determining the resilient modulus of soils and aggregate materials, 2025.

[26] American Association of State Highway and Transportation Officials. T 315-24 – Determining the rheological properties of asphalt binder using a dynamic shear rheometer (DSR), 2025.

[27] American Association of State Highway and Transportation Officials. T 321-22 – Determining the fatigue life of compacted asphalt mixtures subjected to repeated flexural bending, 2025.

[28] American Association of State Highway and Transportation Officials. T 322-07 (2020) – Determining the creep compliance and strength of hot mix asphalt (HMA) using the indirect tensile test device, 2025.

[29] American Association of State Highway and Transportation Officials. T 324-23 – Hamburg wheel-track testing of compacted asphalt mixtures, 2025.

[30] American Association of State Highway and Transportation Officials. T 342-22 – Determining dynamic modulus of hot mix asphalt (HMA), 2025.

[31] American Association of State Highway and Transportation Officials. T 378-22 – Determining the dynamic modulus and flow number for asphalt mixtures using the asphalt mixture performance tester (AMPT), 2025.

[32] American Association of State Highway and Transportation Officials. T 411-24 - Determining the damage characteristic curve and failure criterion using small specimens in the asphalt mixture performance tester (AMPT) cyclic fatigue test, 2025.

[33] Husam A. Sadek, Eyad A. Masad, Okan Sirin, Hussain Al-Khalid, Mohammed A. Sadeq, and Dallas Little. Implementation of mechanistic-empirical pavement analysis in the State of Qatar. *International Journal of Pavement Engineering*, 15(6):495–511, July 2014.

[34] Maram Saudy, Tamer Breakah, Mosbeh R. Kaloop, and Sherif El-Badawy. Regional implementation of the mechanistic empirical pavement design and analysis approach: Egyptian case study. *Case Studies in Construction Materials*, 18, July 2023.

[35] Aksel Seitllari, Michele Lanotte, and M. Emin Kutay. Recommended Calibration Procedure of MEPDG Asphalt Rutting Model Using Repeated Load Permanent Deformation and Confined and Unconfined Dynamic Modulus Data. *Journal of Transportation Engineering, Part B: Pavements*, 147(1), March 2021.

[36] Nicholas W. Tschoegl. *The Phenomenological Theory of Linear Viscoelastic Behavior*. Springer, Berlin, Heidelberg, 1989.

[37] M. W. Witczak and O. A. Fonseca. Revised Predictive Model for Dynamic (Complex) Modulus of Asphalt Mixtures. *Transportation Research Record*, 1540(1):15–23, January 1996.

[38] Jun Zhang, Allex Alvarez, Sang Ick Lee, Angela Torres, and Lubinda Walubita. Comparison of flow number, dynamic modulus, and repeated load tests for evaluation of HMA permanent deformation. *Construction and Building Materials*, 44:391–398, July 2013.

Appendix A

Climate and traffic data processing for the local implementation

A.1 ERA5 reanalysis raw data processing

The Python script reported below was used to process hourly ERA5 reanalysis data and generate PavME-compatible climate input files. The workflow includes variable extraction from NetCDF files, unit conversion to imperial units, estimation of relative humidity from air and dew point temperatures, precipitation processing, and export to the HCD format.

```
from pathlib import Path

import numpy as np
import pandas as pd
import xarray as xr

# ============================================================
# CONFIGURATION
# ============================================================

BASE_PATH = Path("path/to/project/folder")
OUTPUT_FILE = BASE_PATH / "ERA5_site_2005_2024_imperial.hcd"

PERIOD_LABELS = [
    "1_JAN_APR",
    "2_MAY_AUG",
```

```
    "3_SEP_DEC",
]

START_YEAR = 2005
END_YEAR = 2024


# ================================================================
# HELPER FUNCTIONS
# ================================================================

def compute_relative_humidity(temp_c: xr.DataArray, dewpoint_c: xr.DataArray) -> xr.DataArray:
    """
    Estimate relative humidity from air temperature and dew point temperature.

    Parameters
    ----------
    temp_c : xarray.DataArray
        Air temperature in degrees Celsius.
    dewpoint_c : xarray.DataArray
        Dew point temperature in degrees Celsius.

    Returns
    -------
    xarray.DataArray
        Relative humidity in percent.
    """
    saturation_vapor_pressure = 6.112 * np.exp((17.67 * temp_c) / (temp_c + 243.5))
    vapor_pressure = 6.112 * np.exp((17.67 * dewpoint_c) / (dewpoint_c + 243.5))
    return 100 * vapor_pressure / saturation_vapor_pressure


def process_era5_period(instantaneous_file: Path, accumulated_file: Path) -> pd.DataFrame:
```

```
    """
    Process one ERA5 period by combining instantaneous and
       accumulated variables.

    The output dataset includes:
    - air temperature [ F ]
    - wind speed [mph]
    - sunshine percentage [%]
    - hourly precipitation [in]
    - relative humidity [%]

    Parameters
    ----------
    instantaneous_file : pathlib.Path
        Path to the ERA5 NetCDF file containing instantaneous
           variables.
    accumulated_file : pathlib.Path
        Path to the ERA5 NetCDF file containing accumulated
           precipitation.

    Returns
    -------
    pandas.DataFrame
        Processed DataFrame for the selected period.
    """
    with xr.open_dataset(instantaneous_file) as ds,
       xr.open_dataset(accumulated_file) as tp_ds:
        # ----------------------------------------------------
        # Meteorological variable calculations
        # ----------------------------------------------------
        temp_c = ds["t2m"] - 273.15
        dewpoint_c = ds["d2m"] - 273.15

        temp_f = temp_c * 9 / 5 + 32
        wind_mph = 3.6 * np.sqrt((ds["u10"] / 1.609) ** 2 +
           (ds["v10"] / 1.609) ** 2)
        sunshine_pct = (1 - ds["tcc"]) * 100
        relative_humidity = compute_relative_humidity(temp_c,
```

```
            dewpoint_c)

        # ----------------------------------------------------
        # Instantaneous variables
        # ----------------------------------------------------
        df_instant = pd.DataFrame(
            {
                "valid_time": ds["valid_time"].values,
                "Temperature": temp_f.values.flatten(),
                "Wind_speed": wind_mph.values.flatten(),
                "Sunshine": sunshine_pct.values.flatten(),
                "RH": relative_humidity.values.flatten(),
            }
        )

        # ----------------------------------------------------
        # Hourly precipitation
        # ----------------------------------------------------
        df_precip = tp_ds["tp"].to_dataframe().reset_index()
        df_precip["Precipitation"] = df_precip["tp"] * 39.37  #
            m -> in

        # Minimum threshold filter
        df_precip.loc[df_precip["Precipitation"] < 0.001,
            "Precipitation"] = 0

        # ----------------------------------------------------
        # Merge and formatting
        # ----------------------------------------------------
        df_final = pd.merge(
            df_instant,
            df_precip[["valid_time", "Precipitation"]],
            on="valid_time",
        )

        df_final["Timestamp"] =
            pd.to_datetime(df_final["valid_time"]
            ).dt.strftime("%Y%m%d%H")
```

```
117
118         df_final = df_final[
119             ["Timestamp", "Temperature", "Wind_speed",
                    "Sunshine", "Precipitation", "RH"]
120         ]
121
122     return df_final
123
124
125 # ================================================================
126 # MAIN PROCESSING WORKFLOW
127 # ================================================================
128
129 def build_era5_dataset(
130     base_path: Path,
131     output_file: Path,
132     start_year: int,
133     end_year: int,
134     period_labels: list[str],
135 ) -> None:
136     """
137     Build the complete ERA5 climate dataset by processing all
            available periods.
138
139     Parameters
140     ----------
141     base_path : pathlib.Path
142         Directory containing the ERA5 NetCDF files.
143     output_file : pathlib.Path
144         Output CSV file path.
145     start_year : int
146         First year to be processed.
147     end_year : int
148         Last year to be processed.
149     period_labels : list[str]
150         List of file suffixes identifying the intra-annual
                periods.
151     """
```

```
    processed_dataframes = []

    for year in range(start_year, end_year + 1):
        for period_label in period_labels:
            instantaneous_file = base_path /
               f"{year}_{period_label}-instant.nc"
            accumulated_file = base_path /
               f"{year}_{period_label}-accum.nc"

            if not instantaneous_file.exists() or not
               accumulated_file.exists():
                continue

            try:
                df_period =
                   process_era5_period(instantaneous_file,
                   accumulated_file)
                processed_dataframes.append(df_period)
                print(f"Processed: {year}_{period_label}")

            except Exception as exc:
                print(f"Error while processing
                   {year}_{period_label}: {exc}")

    # -------------------------------------------------------------
    # Final concatenation and export
    # -------------------------------------------------------------
    if not processed_dataframes:
        print("No data were processed.")
        return

    full_dataset = pd.concat(processed_dataframes,
       ignore_index=True)
    full_dataset = full_dataset.sort_values("Timestamp")

    # Final rounding
    full_dataset["Temperature"] =
       full_dataset["Temperature"].round(1)
```

```
    full_dataset["Wind_speed"] =
        full_dataset["Wind_speed"].round(1)
    full_dataset["Sunshine"] =
        full_dataset["Sunshine"].round(0).astype(int)
    full_dataset["Precipitation"] =
        full_dataset["Precipitation"].round(3)
    full_dataset["RH"] = full_dataset["RH"].round(0).astype(int)

    # Export as comma-separated file without header
    full_dataset.to_csv(
        output_file,
        sep=",",
        index=False,
        header=False,
    )

    print(f"\nExport completed: {output_file}")


# ================================================================
# SCRIPT EXECUTION
# ================================================================

if __name__ == "__main__":
    print("Starting ERA5 climate data processing")
    print("=" * 60)

    build_era5_dataset(
        base_path=BASE_PATH,
        output_file=OUTPUT_FILE,
        start_year=START_YEAR,
        end_year=END_YEAR,
        period_labels=PERIOD_LABELS,
    )

    print("=" * 60)
    print("Processing completed.")
```

Code A.1: Python script for ERA5 data processing

A.2 WIM data processing for the new Input Level 1

The Python script reported below processes monthly WIM datasets. The workflow includes an initial wheelbase-based filter, axle-load conversion from kN to lb, validation against axle-group load thresholds, FHWA vehicle classification, and export of class-specific CSV files and the overall class distribution.

The monthly WIM data in CSV format is the input for the code. It is essential that the following guidelines are met for the code to work properly:

1. the column names in the input file are case sensitive and must be as follows:
    - AxleNumber for the total axle number;
    - MeanAxleDistance for the average wheelbase;
    - AxleLoad_1, AxleLoad_2, ..., AxleLoad_10 for the weights on each axle;
    - MultipleAxleLoad_1, MultipleAxleLoad_2, ..., MultipleAxleLoad_10 for each element belonging to the vector used for the coding convention of the axle configuration.
2. the data format must be consistent:
    - the columns related to weights and distances must contain only numbers. Specifically, the weights are in kilonewtons, and the distances are in meters.
    - the field delimiter must be a comma.

```
import os
from pathlib import Path

import numpy as np
import pandas as pd


# ============================================================
# CONFIGURATION
# ============================================================

BASE_PATH = Path("path/to/project/folder")
INPUT_FOLDER = BASE_PATH / "Raw_Data"
OUTPUT_FOLDER = BASE_PATH / "MEPDG"
```

```
15
16 FILES_TO_PROCESS = ["Month_1", "Month_2", "Month_3"]
17
18 KN_TO_LB = 224.87
19 WHEELBASE_THRESHOLD_M = 3.0
20
21 LOAD_COLUMNS = ["Weight"] + [f"AxleLoad_{i}" for i in range(1,
       11)]
22
23 # Minimum allowable load thresholds for the total axle group
       load [lb]
24 MIN_LOAD_THRESHOLDS_LB = {
25     1: 2500,      # Single axle
26     2: 5000,      # Tandem axle group
27     3: 10500,     # Tridem axle group
28     4: 10500,     # Quad axle group
29 }
30
31 # Maximum allowable load thresholds for the total axle group
       load [lb]
32 MAX_LOAD_THRESHOLDS_LB = {
33     1: 41500,     # Single axle
34     2: 83000,     # Tandem axle group
35     3: 103500,    # Tridem axle group
36     4: 103500,    # Quad axle group
37     5: 103500,
38     6: 103500,
39     7: 103500,
40 }
41
42 FULL_CLASSES_LIST = [f"Class_{i}_FHWA" for i in range(4, 14)]
43
44
45 # ============================================================
46 # VALIDATION FUNCTION
47 # ============================================================
48
49 def is_row_valid(row: pd.Series) -> bool:
```

```
50      """
51      Check whether all axle groups in a vehicle satisfy both the
            minimum and maximum
52      load thresholds.
53
54      Parameters
55      ----------
56      row : pandas.Series
57          Row containing the vehicle record.
58
59      Returns
60      -------
61      bool
62          True if all axle groups satisfy the prescribed limits;
               False otherwise.
63      """
64      num_axles = int(row.get("AxleNumber", 0))
65      if num_axles == 0:
66          return False
67
68      i = 1
69      while i <= num_axles:
70          axle_type_code = int(row.get(f"MultipleAxleLoad_{i}",
               1))
71
72          min_limit = MIN_LOAD_THRESHOLDS_LB.get(axle_type_code,
               2500)
73          max_limit = MAX_LOAD_THRESHOLDS_LB.get(axle_type_code,
               float("inf"))
74
75          current_axle_load = row.get(f"AxleLoad_{i}", 0)
76
77          # Single axle
78          if axle_type_code == 1:
79              group_load = current_axle_load
80              next_index = i + 1
81
82          # Multiple-axle group (e.g., tandem, tridem, quad)
```

```
83          else:
84              group_load = current_axle_load
85              j = i + 1
86
87              while j <= num_axles:
88                  if int(row.get(f"MultipleAxleLoad_{j}", 0)) ==
                        axle_type_code:
89                      group_load += row.get(f"AxleLoad_{j}", 0)
90                      j += 1
91                  else:
92                      break
93
94              next_index = j
95
96          # Group-level validation
97          if group_load < min_limit or group_load > max_limit:
98              return False
99
100         i = next_index
101
102     return True
103
104
105 # ============================================================
106 # MAIN PROCESSING FUNCTION
107 # ============================================================
108
109 def process_wim_file(file_path: Path, output_path: Path) ->
        None:
110     """
111     Process a WIM file for Pavement ME applications.
112
113     The procedure performs:
114     1. Initial filtering based on mean axle distance.
115     2. Load conversion from kN to lb.
116     3. Validation against minimum and maximum axle-group
           thresholds.
117     4. FHWA vehicle classification.
```

```
    5. Export of class distribution and class-specific CSV files.

    Parameters
    ----------
    file_path : pathlib.Path
        Path to the input CSV file.
    output_path : pathlib.Path
        Path to the output directory.
    """
    if not file_path.exists():
        print(f"[WARNING] File not found: {file_path}")
        return

    df = pd.read_csv(file_path, low_memory=False)

    print(f"Processing file: {file_path.name}")
    print(f"Initial number of rows: {len(df)}")

    # ------------------------------------------------------
    # 1. Wheelbase filtering
    # ------------------------------------------------------
    df["MeanAxleDistance"] =
        pd.to_numeric(df["MeanAxleDistance"], errors="coerce")
    df = df[df["MeanAxleDistance"] >
        WHEELBASE_THRESHOLD_M].copy()

    print(
        f"Rows after wheelbase filter "
        f"(MeanAxleDistance > {WHEELBASE_THRESHOLD_M} m):
            {len(df)}"
    )

    # ------------------------------------------------------
    # 2. Load conversion from kN to lb
    # ------------------------------------------------------
    for col in LOAD_COLUMNS:
        if col in df.columns:
```

```
            df[col] = pd.to_numeric(df[col],
                errors="coerce").fillna(0) * KN_TO_LB

    # ----------------------------------------------------------
    # 3. Row filtering based on axle-group load thresholds
    # ----------------------------------------------------------
    df = df[df.apply(is_row_valid, axis=1)].copy()

    print(f"Rows after min/max load threshold filtering:
        {len(df)}")

    # ----------------------------------------------------------
    # 4. FHWA vehicle classification
    # ----------------------------------------------------------
    df["FHWA_Class"] = None

    df.loc[
        (df["AxleNumber"] == 2) & (df["MeanAxleDistance"] >
            5.0),
        "FHWA_Class"
    ] = "Class_4_FHWA"

    df.loc[
        (df["AxleNumber"] == 2) & (df["MeanAxleDistance"] <=
            5.0),
        "FHWA_Class"
    ] = "Class_5_FHWA"

    df.loc[(df["AxleNumber"] == 3), "FHWA_Class"] =
        "Class_6_FHWA"
    df.loc[(df["AxleNumber"] == 4), "FHWA_Class"] =
        "Class_8_FHWA"

    df.loc[
        (df["AxleNumber"] == 5)
        & (df["MultipleAxleLoad_1"] == 1)
        & (
            (df["MultipleAxleLoad_2"] == 2)
```

```
            | (df["MultipleAxleLoad_4"] == 2)
        ),
        "FHWA_Class"
    ] = "Class_9_FHWA"

    df.loc[(df["AxleNumber"] == 6), "FHWA_Class"] =
       "Class_10_FHWA"

    df.loc[
        (df["AxleNumber"] == 5) & (df["MultipleAxleLoad_3"] ==
           3),
        "FHWA_Class"
    ] = "Class_11_FHWA"

    df["FHWA_Class"] = df["FHWA_Class"].fillna("Non_Classified")

    # ---------------------------------------------------------
    # 5. Export class distribution
    # ---------------------------------------------------------
    output_path.mkdir(parents=True, exist_ok=True)

    class_distribution = df["FHWA_Class"].value_counts()
    order_with_non_classified = FULL_CLASSES_LIST +
       ["Non_Classified"]

    distribution_df = (
        class_distribution.reindex(order_with_non_classified,
           fill_value=0)
        .reset_index()
    )
    distribution_df.columns = ["FHWA_Class", "Count"]

    total_classified = distribution_df[
        distribution_df["FHWA_Class"].isin(FULL_CLASSES_LIST)
    ]["Count"].sum()

    distribution_df["Percentage"] = np.where(
        distribution_df["FHWA_Class"] == "Non_Classified",
```

```
            0,
            np.where(
                total_classified > 0,
                distribution_df["Count"] / total_classified * 100,
                0,
            ),
        )

        distribution_df.to_csv(output_path /
           "vehicle_class_distribution.csv", index=False)

        # ----------------------------------------------------
        # 6. Export one CSV file for each FHWA class
        # ----------------------------------------------------
        for vehicle_class in FULL_CLASSES_LIST:
            df_class = df[df["FHWA_Class"] == vehicle_class].copy()

            if not df_class.empty:
                df_class.drop(columns=["FHWA_Class"], inplace=True,
                   errors="ignore")
                df_class.to_csv(output_path /
                   f"{vehicle_class}.csv", index=False)

        print(f"Completed: {file_path.name}")
        print(f"Output directory: {output_path}\n")


# ============================================================
# SCRIPT EXECUTION
# ============================================================

if __name__ == "__main__":
    print("Starting Pavement ME traffic classification")
    print("=" * 60)

    for month in FILES_TO_PROCESS:
        input_file = INPUT_FOLDER / f"{month}.csv"
        monthly_output_folder = OUTPUT_FOLDER / month
```

```
253             process_wim_file(input_file, monthly_output_folder)
254
255     print("=" * 60)
256     print("Processing completed.")
```

Code A.2: Python script for WIM data filtering and FHWA vehicle classification

The Python script reported in Code A.3 derives axle-load distributions from class-specific monthly CSV files, outputs of the Code A.2. The procedure extracts axle-group loads, aggregates tandem, tridem, and quad groups, assigns each load to the corresponding standard MEPDG bin, and exports one distribution file for each axle-group type.

```
1  from pathlib import Path
2
3  import numpy as np
4  import pandas as pd
5
6
7  # ============================================================
8  # CONFIGURATION
9  # ============================================================
10
11 BASE_DIR = Path("path/to/project/folder/MEPDG")
12 FILE_SUFFIXES = ["Month_1", "Month_2", "Month_3"]
13
14 FHWA_CLASSES_ORDERED = [f"Class_{i}_FHWA" for i in range(4, 14)]
15
16 # Standard Pavement ME load bins [lb]
17 LOAD_CLASSES_LB = {
18     "Single": {
19         "start_center": 3000,
20         "end_center": 41000,
21         "step": 1000,
22         "half_step": 500,
23     },
24     "Tandem": {
25         "start_center": 6000,
26         "end_center": 82000,
27         "step": 2000,
```

```
        "half_step": 1000,
    },
    "Tridem": {
        "start_center": 12000,
        "end_center": 102000,
        "step": 3000,
        "half_step": 1500,
    },
    "Quad": {
        "start_center": 12000,
        "end_center": 102000,
        "step": 3000,
        "half_step": 1500,
    },
}


# ============================================================
# HELPER FUNCTIONS
# ============================================================

def map_axle_code_to_string(code: int) -> str:
    """
    Map the axle-group code to the corresponding axle-group
       type.

    Parameters
    ----------
    code : int
        Axle-group code from the WIM dataset.

    Returns
    -------
    str
        Axle-group type.
    """
    if code == 1:
        return "Single"
```

```
    if code == 2:
        return "Tandem"
    if code == 3:
        return "Tridem"
    if code in [4, 5, 6, 7]:
        return "Quad"
    return "Other"


def extract_axle_data(input_file_path: Path, class_name: str)
    -> pd.DataFrame:
    """
    Extract axle-group load data from a class-specific CSV file.

    For multiple-axle groups (e.g., tandem, tridem, quad), the
       total group load
    is obtained by summing the loads of all axles belonging to
       the same group.

    Parameters
    ----------
    input_file_path : pathlib.Path
        Path to the input CSV file.
    class_name : str
        FHWA vehicle class associated with the input file.

    Returns
    -------
    pandas.DataFrame
        DataFrame containing axle-group load, group type, and
           FHWA class.
    """
    if not input_file_path.exists():
        return pd.DataFrame()

    df = pd.read_csv(input_file_path, low_memory=False)
    if df.empty:
        return pd.DataFrame()
```

```
99
100     all_axles = []
101
102     for _, row in df.iterrows():
103         num_axles = int(row["AxleNumber"])
104         i = 1
105
106         while i <= num_axles:
107             axle_type_code =
                    int(row.get(f"MultipleAxleLoad_{i}", 1))
108             axle_type = map_axle_code_to_string(axle_type_code)
109             current_axle_load = row.get(f"AxleLoad_{i}", 0)
110
111             # Single axle (or uncategorized case)
112             if axle_type in ["Single", "Other"]:
113                 all_axles.append(
114                     {
115                         "AxleLoad": current_axle_load,
116                         "TypeString": axle_type,
117                         "FHWA_Class": class_name,
118                     }
119                 )
120                 i += 1
121
122             # Multiple-axle group (tandem, tridem, quad)
123             elif axle_type in ["Tandem", "Tridem", "Quad"]:
124                 group_load = current_axle_load
125                 j = i + 1
126
127                 while j <= num_axles:
128                     if int(row.get(f"MultipleAxleLoad_{j}", 0))
                            == axle_type_code:
129                         group_load += row.get(f"AxleLoad_{j}",
                                0)
130                         j += 1
131                     else:
132                         break
133
```

```
                all_axles.append(
                    {
                        "AxleLoad": group_load,
                        "TypeString": axle_type,
                        "FHWA_Class": class_name,
                    }
                )
                i = j

            else:
                i += 1

    return pd.DataFrame(all_axles)


def generate_axle_load_distribution(
    axle_dataframes: list[pd.DataFrame],
    month_label: str,
    output_path: Path,
) -> None:
    """
    Generate axle-load distribution files for each axle-group
       type.

    Parameters
    ----------
    axle_dataframes : list[pandas.DataFrame]
        List of DataFrames containing axle-group data for the
           considered month.
    month_label : str
        Label identifying the month being processed.
    output_path : pathlib.Path
        Output directory for the generated CSV files.
    """
    if axle_dataframes:
        df_all_axles = pd.concat(axle_dataframes,
           ignore_index=True)
    else:
```

```
169         df_all_axles = pd.DataFrame(
170             columns=["AxleLoad", "TypeString", "FHWA_Class"]
171         )
172 
173     for axle_type, params in LOAD_CLASSES_LB.items():
174         df_type = df_all_axles[df_all_axles["TypeString"] ==
                axle_type].copy()
175 
176         # Definition of bin centers and bin boundaries
177         centers = np.arange(
178             params["start_center"],
179             params["end_center"] + params["step"],
180             params["step"],
181         )
182         bins = np.concatenate(
183             [[centers[0] - params["half_step"]], centers +
                params["half_step"]]
184         )
185 
186         if not df_type.empty:
187             df_type["Load_Bin"] = pd.cut(
188                 df_type["AxleLoad"],
189                 bins=bins,
190                 right=False,
191                 labels=centers,
192             )
193 
194             df_pivot = (
195                 df_type.groupby(["FHWA_Class", "Load_Bin"],
                        observed=False)
196                 .size()
197                 .unstack(fill_value=0)
198             )
199             df_pivot = df_pivot.reindex(FHWA_CLASSES_ORDERED,
                    fill_value=0)
200 
201         else:
202             df_pivot = pd.DataFrame(
```

```
                0,
                index=FHWA_CLASSES_ORDERED,
                columns=centers,
            )

        # Column formatting
        df_pivot.columns = [f"{int(float(col))}" for col in
            df_pivot.columns]

        # Totals
        df_pivot.insert(0, "Total Axles", df_pivot.sum(axis=1))
        df_pivot.loc["Total"] = df_pivot.sum()

        # Final formatting and export
        df_output = df_pivot.reset_index()
        df_output.insert(0, "Month", month_label)
        df_output.rename(columns={"index": "Class"},
            inplace=True)

        output_file = output_path /
            f"{axle_type}_Axle_Load_Distribution.csv"
        df_output.to_csv(output_file, index=False)

        print(f"Saved: {output_file.name}")

# ============================================================
# SCRIPT EXECUTION
# ============================================================

if __name__ == "__main__":
    print("Starting generation of axle-load distributions [lb]")
    print("=" * 60)

    for month in FILE_SUFFIXES:
        current_folder = BASE_DIR / month

        if not current_folder.exists():
            print(f"[WARNING] Folder not found: {month}.
```

```
                Skipping.")
238             continue
239
240         print(f"Processing month: {month}")
241
242         monthly_axle_data = []
243
244         # Load data for each FHWA class
245         for class_name in FHWA_CLASSES_ORDERED:
246             input_file = current_folder / f"{class_name}.csv"
247
248             if input_file.exists():
249                 df_axles = extract_axle_data(input_file,
                        class_name)
250                 if not df_axles.empty:
251                     monthly_axle_data.append(df_axles)
252
253         # Generate the axle-load distribution files for the
                current month
254         generate_axle_load_distribution(
255             axle_dataframes=monthly_axle_data,
256             month_label=month,
257             output_path=current_folder,
258         )
259
260     print("=" * 60)
261     print("Axle-load distributions generated successfully.")
```

Code A.3: Python script for axle-load distribution generation

A.3 Development of the CNR-based axle load distributions

The starting point is the road type-based traffic spectra proposed in the CNR catalog, reported in fig. A.1.

CNR Vehicle class distribution HV_i [%] within each CNR class	CNR vehicle class															
Road type	1	2	3	4	5	6	7	8	9	10	11	12	13	14	15	16
1) Rural motorways	12.2	-	24.4	14.6	2.4	12.2	2.4	4.9	2.4	4.9	2.4	4.9	0.1	-	-	12.2
2) Urban motorways	18.2	18.2	16.5	-	-	-	-	-	-	-	-	-	1.6	18.2	27.3	-
3) Rural multilane highways	-	13.1	39.5	10.5	7.9	2.6	2.6	2.5	2.6	2.5	2.6	2.6	0.5	-	-	10.5
4) Two-lanes rural highways	-	-	58.8	29.4	-	5.9	-	2.8	-	-	-	-	0.2	-	-	2.9
5) Two-lanes tourist highways	24.5	-	40.8	16.3	-	4.2	-	2.0	-	-	-	-	0.05	-	-	12.2
6) Urban arterials	18.2	18.2	16.5	-	-	-	-	-	-	-	-	-	1.6	18.2	27.3	-
7) Urban collectors	80.0	-	-	-	-	-	-	-	-	-	-	-	-	20.0	-	-
8) Dedicated lanes	-	-	-	-	-	-	-	-	-	-	-	-	-	47.0	53.0	-

Figure A.1: Road type-based traffic spectra

For each road type, the percentages of the traffic spectra are aggregated into FHWA classes, as shown in fig. A.2. For the sake of clarity, the new aggregated Italian classes are identified by a 'letter-number' code in this stage.

CNR Vehicle class distribution HV [%] within each FHWA class	CNR to FHWA vehicle class					
Road type	A-5	B-6	C-8	D-9	E-11	F-4
1) Rural motorways	51.2	14.6	7.3	7.3	7.4	12.2
2) Urban motorways	52.9	-	-	-	1.6	45.5
3) Rural multilane highways	63.1	10.5	5.1	5.1	5.7	10.5
4) Two-lanes rural highways	88.2	5.9	2.8	-	0.2	2.9
5) Two-lanes tourist highways	81.6	4.15	2.0	-	0.1	12.2
6) Urban arterials	52.9	-	-	-	1.6	45.5
7) Urban collectors	80.0	-	-	-	-	20.0
8) Dedicated lanes	-	-	-	-	-	100.0

Figure A.2: Traffic spectra aggregation into FHWA classes

The traffic spectra are disaggregated again into the Italian classes. However, the percentages proposed in fig. A.3 are calculated by normalizing the traffic spectra coefficients from fig. A.1 over the FHWA class aggregated total from fig. A.2, rather than the road type total. Thus, the new spectra are obtained for each Italian class within each road type: Italian classes sum up to 100 % if aggregated into FHWA classes.

HV_i/HV within each CNR class [%]	CNR vehicle class															
Road type	1	2	3	4	5	6	7	8	9	10	11	12	13	14	15	16
1) Rural motorways	23.8	-	47.7	28.5	16.4	83.6	32.9	67.1	32.9	67.1	32.4	66.2	1.4	-	-	100.0
2) Urban motorways	34.4	34.4	31.2	-	-	-	-	-	-	-	-	-	100.0	40.0	60.0	-
3) Rural multilane highways	-	20.8	62.6	16.6	75.2	24.8	51.0	49.0	51.0	49.0	45.6	45.6	8.8	-	-	100.0
4) Two-lanes rural highways	-	-	66.7	33.3	-	100.0	-	100.0	-	-	-	-	100.0	-	-	100.0
5) Two-lanes tourist highways	30.0	-	50.0	20.0	-	100.0	-	100.0	-	-	-	-	100.0	-	-	100.0
6) Urban arterials	34.4	34.4	31.2	-	-	-	-	-	-	-	-	-	100.0	40.0	60.0	-
7) Urban collectors	100.0	-	-	-	-	-	-	-	-	-	-	-	-	100.0	-	-
8) Dedicated lanes	-	-	-	-	-	-	-	-	-	-	-	-	-	47.0	53.0	-

Figure A.3: Traffic spectra within FHWA class for each road type

At that point, the percentages obtained in fig. A.3 are disaggregated in the specific axle group type within each Italian Class. At this stage, the weight assigned to each axle group is the same regardless of the type. The outputs of this computation is presented in figs. A.4 to A.6.

AXLE GROUP-WEIGHTED SPECTRA (Axle % within each CNR class)	CNR vehicle class											
	1		2		3		4		5		6	
	1 1 2 x Single Axle		1 1 2 x Single Axle		1 1 2 x Single Axle		1 1 2 x Single Axle		1 2 2 1 x Single Axle 1 x Tandem Axle		1 2 2 1 x Single Axle 1 x Tandem Axle	
	Single Axle	Single Axle	Single Axle	Single Axle	Single Axle	Single Axle	Single Axle	Single Axle	Single Axle	Tandem Axle	Single Axle	Tandem Axle
Road type	10 kN	20 kN	15 kN	30 kN	40 kN	80 kN	50 kN	110 kN	40 kN	160 kN	60 kN	200 kN
1) Rural motorways	11.9	11.9	0.0	0.0	23.8	23.8	14.3	14.3	8.2	8.2	41.8	41.8
2) Urban motorways	17.2	17.2	17.2	17.2	15.6	15.6	0.0	0.0	0.0	0.0	0.0	0.0
3) Rural multilane highways	0.0	0.0	10.4	10.4	31.3	31.3	8.3	8.3	37.6	37.6	12.4	12.4
4) Two-lanes rural highways	0.0	0.0	0.0	0.0	33.3	33.3	16.7	16.7	0.0	0.0	50.0	50.0
5) Two-lanes tourist highways	15.0	15.0	0.0	0.0	25.0	25.0	10.0	10.0	0.0	0.0	50.0	50.0
6) Urban arterials	17.2	17.2	17.2	17.2	15.6	15.6	0.0	0.0	0.0	0.0	0.0	0.0
7) Urban collectors	50.0	50.0	0.0	0.0	0.0	0.0	0.0	0.0	0.0	0.0	0.0	0.0
8) Dedicated lanes	0.0	0.0	0.0	0.0	0.0	0.0	0.0	0.0	0.0	0.0	0.0	0.0

Figure A.4: Axle group-weighted traffic spectra (classes 1 to 4)

AXLE GROUP-WEIGHTED SPECTRA (Axle % within each CNR class)	CNR vehicle class													
	7				8				9			10		
	1 1 1 1 4 x Single Axle				1 1 1 1 4 x Single Axle				1 2 2 2 2 1 x Single Axle 2 x Tandem Axle			1 2 2 2 2 1 x Single Axle 2 x Tandem Axle		
	Single Axle	Single Axle	Single Axle	Single Axle	Single Axle	Single Axle	Single Axle	Single Axle	Single Axle	Tandem Axle	Tandem Axle	Single Axle	Tandem Axle	Tandem Axle
Road type	40 kN	90 kN	80 kN	80 kN	60 kN	100 kN	100 kN	100 kN	40 kN	160 kN	160 kN	60 kN	180 kN	200 kN
1) Rural motorways	8.2	8.2	8.2	8.2	16.8	16.8	16.8	16.8	11.0	11.0	11.0	22.4	22.4	22.4
2) Urban motorways	0.0	0.0	0.0	0.0	0.0	0.0	0.0	0.0	0.0	0.0	0.0	0.0	0.0	0.0
3) Rural multilane highways	12.7	12.7	12.7	12.7	12.3	12.3	12.3	12.3	17.0	17.0	17.0	16.3	16.3	16.3
4) Two-lanes rural highways	0.0	0.0	0.0	0.0	25.0	25.0	25.0	25.0	0.0	0.0	0.0	0.0	0.0	0.0
5) Two-lanes tourist highways	0.0	0.0	0.0	0.0	25.0	25.0	25.0	25.0	0.0	0.0	0.0	0.0	0.0	0.0
6) Urban arterials	0.0	0.0	0.0	0.0	0.0	0.0	0.0	0.0	0.0	0.0	0.0	0.0	0.0	0.0
7) Urban collectors	0.0	0.0	0.0	0.0	0.0	0.0	0.0	0.0	0.0	0.0	0.0	0.0	0.0	0.0
8) Dedicated lanes	0.0	0.0	0.0	0.0	0.0	0.0	0.0	0.0	0.0	0.0	0.0	0.0	0.0	0.0

Figure A.5: Axle group-weighted traffic spectra (classes 7 to 10)

AXLE GROUP-WEIGHTED SPECTRA (Axle % within each CNR class)	CNR vehicle class														
	11			12			13			14		15		16	
	1 1 3 3 3 2 x Single Axle 1 x Tridem Axle			1 1 3 3 3 1 x Single Axle 2 x Tandem Axle			1 1 3 3 3 1 x Single Axle 2 x Tandem Axle			1 1 2 x Single Axle		1 1 2 x Single Axle		1 1 2 x Single Axle	
	Single Axle	Single Axle	Tridem Axle	Single Axle	Single Axle	Tridem Axle	Single Axle	Single Axle	Tridem Axle	Single Axle	Single Axle	Single Axle	Single Axle	Single Axle	Single Axle
Road type	40 kN	100 kN	240 kN	60 kN	110 kN	270 kN	50 kN	120 kN	390 kN	40 kN	80 kN	60 kN	100 kN	50 kN	80 kN
1) Rural motorways	10.8	10.8	10.8	22.1	22.1	22.1	0.5	0.5	0.5	0.0	0.0	0.0	0.0	50.0	50.0
2) Urban motorways	0.0	0.0	0.0	0.0	0.0	0.0	33.3	33.3	33.3	20.0	20.0	30.0	30.0	0.0	0.0
3) Rural multilane highways	15.2	15.2	15.2	15.2	15.2	15.2	2.9	2.9	2.9	0.0	0.0	0.0	0.0	50.0	50.0
4) Two-lanes rural highways	0.0	0.0	0.0	0.0	0.0	0.0	33.3	33.3	33.3	0.0	0.0	0.0	0.0	50.0	50.0
5) Two-lanes tourist highways	0.0	0.0	0.0	0.0	0.0	0.0	33.3	33.3	33.3	0.0	0.0	0.0	0.0	50.0	50.0
6) Urban arterials	0.0	0.0	0.0	0.0	0.0	0.0	33.3	33.3	33.3	20.0	20.0	30.0	30.0	0.0	0.0
7) Urban collectors	0.0	0.0	0.0	0.0	0.0	0.0	0.0	0.0	0.0	50.0	50.0	0.0	0.0	0.0	0.0
8) Dedicated lanes	0.0	0.0	0.0	0.0	0.0	0.0	0.0	0.0	0.0	23.5	23.5	26.5	26.5	0.0	0.0

Figure A.6: Axle group-weighted traffic spectra (classes 11 to 16)

Finally, the factors thus obtained are further disaggregated by axle group type and the loading bins used in the MEPDG. As a result, three tables are obtained, one for each axle group. The axle load distributions in tables A.1 and A.2 have the same layout as those implemented in the MEPDG.

Single	Total	3000 lb	4000 lb	5000 lb	6000 lb	7000 lb	8000 lb	9000 lb	10000 lb	11000 lb	12000 lb	13000 lb	14000 lb	15000 lb	16000 lb	17000 lb	18000 lb	19000 lb	20000 lb	21000 lb	22000 lb	23000 lb	24000 lb	25000 lb	26000 lb	27000 lb	28000 lb	29000 lb	30000 lb	31000 lb	32000 lb	33000 lb	34000 lb	35000 lb	36000 lb	37000 lb	38000 lb	39000 lb	40000 lb	41000 lb
4	100.00	0.00	0.00	0.00	0.00	0.00	0.00	0.00	0.00	50.00	0.00	0.00	0.00	0.00	0.00	0.00	50.00	0.00	0.00	0.00	0.00	0.00	0.00	0.00	0.00	0.00	0.00	0.00	0.00	0.00	0.00	0.00	0.00	0.00	0.00	0.00	0.00	0.00	0.00	0.00
5	100.00	0.00	14.00	0.00	0.00	0.00	0.00	27.00	0.00	16.00	0.00	0.00	0.00	0.00	0.00	0.00	27.00	0.00	0.00	0.00	0.00	0.00	0.00	16.00	0.00	0.00	0.00	0.00	0.00	0.00	0.00	0.00	0.00	0.00	0.00	0.00	0.00	0.00	0.00	0.00
6	100.00	0.00	0.00	0.00	0.00	0.00	0.00	16.00	0.00	0.00	0.00	84.00	0.00	0.00	0.00	0.00	0.00	0.00	0.00	0.00	0.00	0.00	0.00	0.00	0.00	0.00	0.00	0.00	0.00	0.00	0.00	0.00	0.00	0.00	0.00	0.00	0.00	0.00	0.00	0.00
7	0.00	0.00	0.00	0.00	0.00	0.00	0.00	0.00	0.00	0.00	0.00	0.00	0.00	0.00	0.00	0.00	0.00	0.00	0.00	0.00	0.00	0.00	0.00	0.00	0.00	0.00	0.00	0.00	0.00	0.00	0.00	0.00	0.00	0.00	0.00	0.00	0.00	0.00	0.00	0.00
8	100.00	0.00	0.00	0.00	0.00	0.00	0.00	9.00	0.00	0.00	0.00	17.00	0.00	0.00	0.00	0.00	16.00	0.00	8.00	0.00	50.00	0.00	0.00	0.00	0.00	0.00	0.00	0.00	0.00	0.00	0.00	0.00	0.00	0.00	0.00	0.00	0.00	0.00	0.00	0.00
9	100.00	0.00	0.00	0.00	0.00	0.00	0.00	33.00	0.00	0.00	0.00	67.00	0.00	0.00	0.00	0.00	0.00	0.00	0.00	0.00	0.00	0.00	0.00	0.00	0.00	0.00	0.00	0.00	0.00	0.00	0.00	0.00	0.00	0.00	0.00	0.00	0.00	0.00	0.00	0.00
10	0.00	0.00	0.00	0.00	0.00	0.00	0.00	0.00	0.00	0.00	0.00	0.00	0.00	0.00	0.00	0.00	0.00	0.00	0.00	0.00	0.00	0.00	0.00	0.00	0.00	0.00	0.00	0.00	0.00	0.00	0.00	0.00	0.00	0.00	0.00	0.00	0.00	0.00	0.00	0.00
11	100.00	0.00	0.00	0.00	0.00	0.00	0.00	16.00	0.00	1.00	0.00	33.00	0.00	0.00	0.00	0.00	0.00	0.00	0.00	0.00	16.00	0.00	0.00	33.00	0.00	1.00	0.00	0.00	0.00	0.00	0.00	0.00	0.00	0.00	0.00	0.00	0.00	0.00	0.00	0.00
12	0.00	0.00	0.00	0.00	0.00	0.00	0.00	0.00	0.00	0.00	0.00	0.00	0.00	0.00	0.00	0.00	0.00	0.00	0.00	0.00	0.00	0.00	0.00	0.00	0.00	0.00	0.00	0.00	0.00	0.00	0.00	0.00	0.00	0.00	0.00	0.00	0.00	0.00	0.00	0.00
13	0.00	0.00	0.00	0.00	0.00	0.00	0.00	0.00	0.00	0.00	0.00	0.00	0.00	0.00	0.00	0.00	0.00	0.00	0.00	0.00	0.00	0.00	0.00	0.00	0.00	0.00	0.00	0.00	0.00	0.00	0.00	0.00	0.00	0.00	0.00	0.00	0.00	0.00	0.00	0.00

Tandem	Total	6000 lb	8000 lb	10000 lb	12000 lb	14000 lb	16000 lb	18000 lb	20000 lb	22000 lb	24000 lb	26000 lb	28000 lb	30000 lb	32000 lb	34000 lb	36000 lb	38000 lb	40000 lb	42000 lb	44000 lb	46000 lb	48000 lb	50000 lb	52000 lb	54000 lb	56000 lb	58000 lb	60000 lb	62000 lb	64000 lb	66000 lb	68000 lb	70000 lb	72000 lb	74000 lb	76000 lb	78000 lb	80000 lb	82000 lb
4	0.00	0.00	0.00	0.00	0.00	0.00	0.00	0.00	0.00	0.00	0.00	0.00	0.00	0.00	0.00	0.00	0.00	0.00	0.00	0.00	0.00	0.00	0.00	0.00	0.00	0.00	0.00	0.00	0.00	0.00	0.00	0.00	0.00	0.00	0.00	0.00	0.00	0.00	0.00	0.00
5	0.00	0.00	0.00	0.00	0.00	0.00	0.00	0.00	0.00	0.00	0.00	0.00	0.00	0.00	0.00	0.00	0.00	0.00	0.00	0.00	0.00	0.00	0.00	0.00	0.00	0.00	0.00	0.00	0.00	0.00	0.00	0.00	0.00	0.00	0.00	0.00	0.00	0.00	0.00	0.00
6	100.00	0.00	0.00	0.00	0.00	0.00	0.00	0.00	0.00	0.00	0.00	0.00	0.00	0.00	0.00	0.00	16.00	0.00	0.00	0.00	84.00	0.00	0.00	0.00	0.00	0.00	0.00	0.00	0.00	0.00	0.00	0.00	0.00	0.00	0.00	0.00	0.00	0.00	0.00	0.00
7	0.00	0.00	0.00	0.00	0.00	0.00	0.00	0.00	0.00	0.00	0.00	0.00	0.00	0.00	0.00	0.00	0.00	0.00	0.00	0.00	0.00	0.00	0.00	0.00	0.00	0.00	0.00	0.00	0.00	0.00	0.00	0.00	0.00	0.00	0.00	0.00	0.00	0.00	0.00	0.00
8	0.00	0.00	0.00	0.00	0.00	0.00	0.00	0.00	0.00	0.00	0.00	0.00	0.00	0.00	0.00	0.00	0.00	0.00	0.00	0.00	0.00	0.00	0.00	0.00	0.00	0.00	0.00	0.00	0.00	0.00	0.00	0.00	0.00	0.00	0.00	0.00	0.00	0.00	0.00	0.00
9	100.00	0.00	0.00	0.00	0.00	0.00	0.00	0.00	0.00	0.00	0.00	0.00	0.00	0.00	0.00	0.00	32.00	0.00	34.00	0.00	34.00	0.00	0.00	0.00	0.00	0.00	0.00	0.00	0.00	0.00	0.00	0.00	0.00	0.00	0.00	0.00	0.00	0.00	0.00	0.00
10	0.00	0.00	0.00	0.00	0.00	0.00	0.00	0.00	0.00	0.00	0.00	0.00	0.00	0.00	0.00	0.00	0.00	0.00	0.00	0.00	0.00	0.00	0.00	0.00	0.00	0.00	0.00	0.00	0.00	0.00	0.00	0.00	0.00	0.00	0.00	0.00	0.00	0.00	0.00	0.00
11	0.00	0.00	0.00	0.00	0.00	0.00	0.00	0.00	0.00	0.00	0.00	0.00	0.00	0.00	0.00	0.00	0.00	0.00	0.00	0.00	0.00	0.00	0.00	0.00	0.00	0.00	0.00	0.00	0.00	0.00	0.00	0.00	0.00	0.00	0.00	0.00	0.00	0.00	0.00	0.00
12	0.00	0.00	0.00	0.00	0.00	0.00	0.00	0.00	0.00	0.00	0.00	0.00	0.00	0.00	0.00	0.00	0.00	0.00	0.00	0.00	0.00	0.00	0.00	0.00	0.00	0.00	0.00	0.00	0.00	0.00	0.00	0.00	0.00	0.00	0.00	0.00	0.00	0.00	0.00	0.00
13	0.00	0.00	0.00	0.00	0.00	0.00	0.00	0.00	0.00	0.00	0.00	0.00	0.00	0.00	0.00	0.00	0.00	0.00	0.00	0.00	0.00	0.00	0.00	0.00	0.00	0.00	0.00	0.00	0.00	0.00	0.00	0.00	0.00	0.00	0.00	0.00	0.00	0.00	0.00	0.00

Tridem	Total	12000 lb	15000 lb	18000 lb	21000 lb	24000 lb	27000 lb	30000 lb	33000 lb	36000 lb	39000 lb	42000 lb	45000 lb	48000 lb	51000 lb	54000 lb	57000 lb	60000 lb	63000 lb	66000 lb	69000 lb	72000 lb	75000 lb	78000 lb	81000 lb	84000 lb	87000 lb	90000 lb	93000 lb	96000 lb	99000 lb	102000 lb
4	0.00	0.00	0.00	0.00	0.00	0.00	0.00	0.00	0.00	0.00	0.00	0.00	0.00	0.00	0.00	0.00	0.00	0.00	0.00	0.00	0.00	0.00	0.00	0.00	0.00	0.00	0.00	0.00	0.00	0.00	0.00	0.00
5	0.00	0.00	0.00	0.00	0.00	0.00	0.00	0.00	0.00	0.00	0.00	0.00	0.00	0.00	0.00	0.00	0.00	0.00	0.00	0.00	0.00	0.00	0.00	0.00	0.00	0.00	0.00	0.00	0.00	0.00	0.00	0.00
6	0.00	0.00	0.00	0.00	0.00	0.00	0.00	0.00	0.00	0.00	0.00	0.00	0.00	0.00	0.00	0.00	0.00	0.00	0.00	0.00	0.00	0.00	0.00	0.00	0.00	0.00	0.00	0.00	0.00	0.00	0.00	0.00
7	0.00	0.00	0.00	0.00	0.00	0.00	0.00	0.00	0.00	0.00	0.00	0.00	0.00	0.00	0.00	0.00	0.00	0.00	0.00	0.00	0.00	0.00	0.00	0.00	0.00	0.00	0.00	0.00	0.00	0.00	0.00	0.00
8	0.00	0.00	0.00	0.00	0.00	0.00	0.00	0.00	0.00	0.00	0.00	0.00	0.00	0.00	0.00	0.00	0.00	0.00	0.00	0.00	0.00	0.00	0.00	0.00	0.00	0.00	0.00	0.00	0.00	0.00	0.00	0.00
9	0.00	0.00	0.00	0.00	0.00	0.00	0.00	0.00	0.00	0.00	0.00	0.00	0.00	0.00	0.00	0.00	0.00	0.00	0.00	0.00	0.00	0.00	0.00	0.00	0.00	0.00	0.00	0.00	0.00	0.00	0.00	0.00
10	0.00	0.00	0.00	0.00	0.00	0.00	0.00	0.00	0.00	0.00	0.00	0.00	0.00	0.00	0.00	0.00	0.00	0.00	0.00	0.00	0.00	0.00	0.00	0.00	0.00	0.00	0.00	0.00	0.00	0.00	0.00	0.00
11	100.00	0.00	0.00	0.00	0.00	0.00	0.00	0.00	0.00	0.00	0.00	0.00	0.00	0.00	0.00	33.00	0.00	66.00	0.00	0.00	0.00	0.00	0.00	0.00	0.00	0.00	1.00	0.00	0.00	0.00	0.00	0.00
12	0.00	0.00	0.00	0.00	0.00	0.00	0.00	0.00	0.00	0.00	0.00	0.00	0.00	0.00	0.00	0.00	0.00	0.00	0.00	0.00	0.00	0.00	0.00	0.00	0.00	0.00	0.00	0.00	0.00	0.00	0.00	0.00
13	0.00	0.00	0.00	0.00	0.00	0.00	0.00	0.00	0.00	0.00	0.00	0.00	0.00	0.00	0.00	0.00	0.00	0.00	0.00	0.00	0.00	0.00	0.00	0.00	0.00	0.00	0.00	0.00	0.00	0.00	0.00	0.00

Table A.1: CNR-based axle load distributions for single, tandem, and tridem groups – Rural motorways

Single	Total	3000 lb	4000 lb	5000 lb	6000 lb	7000 lb	8000 lb	9000 lb	10000 lb	11000 lb	12000 lb	13000 lb	14000 lb	15000 lb	16000 lb	17000 lb	18000 lb	19000 lb	20000 lb	21000 lb	22000 lb	23000 lb	24000 lb	25000 lb	26000 lb	27000 lb	28000 lb	29000 lb	30000 lb	31000 lb	32000 lb	33000 lb	34000 lb	35000 lb	36000 lb	37000 lb	38000 lb	39000 lb	40000 lb	41000 lb
4	100.00	0.00	0.00	0.00	0.00	0.00	0.00	0.00	0.00	50.00	0.00	0.00	0.00	0.00	0.00	0.00	50.00	0.00	0.00	0.00	0.00	0.00	0.00	0.00	0.00	0.00	0.00	0.00	0.00	0.00	0.00	0.00	0.00	0.00	0.00	0.00	0.00	0.00	0.00	0.00
5	100.00	0.00	18.00	0.00	0.00	0.00	0.00	29.00	0.00	12.00	0.00	0.00	0.00	0.00	0.00	0.00	29.00	0.00	0.00	0.00	0.00	0.00	0.00	12.00	0.00	0.00	0.00	0.00	0.00	0.00	0.00	0.00	0.00	0.00	0.00	0.00	0.00	0.00	0.00	0.00
6	100.00	0.00	0.00	0.00	0.00	0.00	0.00	0.00	0.00	0.00	0.00	100.00	0.00	0.00	0.00	0.00	0.00	0.00	0.00	0.00	0.00	0.00	0.00	0.00	0.00	0.00	0.00	0.00	0.00	0.00	0.00	0.00	0.00	0.00	0.00	0.00	0.00	0.00	0.00	0.00
7	0.00	0.00	0.00	0.00	0.00	0.00	0.00	0.00	0.00	0.00	0.00	0.00	0.00	0.00	0.00	0.00	0.00	0.00	0.00	0.00	0.00	0.00	0.00	0.00	0.00	0.00	0.00	0.00	0.00	0.00	0.00	0.00	0.00	0.00	0.00	0.00	0.00	0.00	0.00	0.00
8	100.00	0.00	0.00	0.00	0.00	0.00	0.00	0.00	0.00	0.00	0.00	25.00	0.00	0.00	0.00	0.00	0.00	0.00	0.00	0.00	75.00	0.00	0.00	0.00	0.00	0.00	0.00	0.00	0.00	0.00	0.00	0.00	0.00	0.00	0.00	0.00	0.00	0.00	0.00	0.00
9	0.00	0.00	0.00	0.00	0.00	0.00	0.00	0.00	0.00	0.00	0.00	0.00	0.00	0.00	0.00	0.00	0.00	0.00	0.00	0.00	0.00	0.00	0.00	0.00	0.00	0.00	0.00	0.00	0.00	0.00	0.00	0.00	0.00	0.00	0.00	0.00	0.00	0.00	0.00	0.00
10	0.00	0.00	0.00	0.00	0.00	0.00	0.00	0.00	0.00	0.00	0.00	0.00	0.00	0.00	0.00	0.00	0.00	0.00	0.00	0.00	0.00	0.00	0.00	0.00	0.00	0.00	0.00	0.00	0.00	0.00	0.00	0.00	0.00	0.00	0.00	0.00	0.00	0.00	0.00	0.00
11	100.00	0.00	0.00	0.00	0.00	0.00	0.00	0.00	0.00	50.00	0.00	0.00	0.00	0.00	0.00	0.00	0.00	0.00	0.00	0.00	0.00	0.00	0.00	0.00	0.00	50.00	0.00	0.00	0.00	0.00	0.00	0.00	0.00	0.00	0.00	0.00	0.00	0.00	0.00	0.00
12	0.00	0.00	0.00	0.00	0.00	0.00	0.00	0.00	0.00	0.00	0.00	0.00	0.00	0.00	0.00	0.00	0.00	0.00	0.00	0.00	0.00	0.00	0.00	0.00	0.00	0.00	0.00	0.00	0.00	0.00	0.00	0.00	0.00	0.00	0.00	0.00	0.00	0.00	0.00	0.00
13	0.00	0.00	0.00	0.00	0.00	0.00	0.00	0.00	0.00	0.00	0.00	0.00	0.00	0.00	0.00	0.00	0.00	0.00	0.00	0.00	0.00	0.00	0.00	0.00	0.00	0.00	0.00	0.00	0.00	0.00	0.00	0.00	0.00	0.00	0.00	0.00	0.00	0.00	0.00	0.00

Tandem	Total	6000 lb	8000 lb	10000 lb	12000 lb	14000 lb	16000 lb	18000 lb	20000 lb	22000 lb	24000 lb	26000 lb	28000 lb	30000 lb	32000 lb	34000 lb	36000 lb	38000 lb	40000 lb	42000 lb	44000 lb	46000 lb	48000 lb	50000 lb	52000 lb	54000 lb	56000 lb	58000 lb	60000 lb	62000 lb	64000 lb	66000 lb	68000 lb	70000 lb	72000 lb	74000 lb	76000 lb	78000 lb	80000 lb	82000 lb
4	0.00	0.00	0.00	0.00	0.00	0.00	0.00	0.00	0.00	0.00	0.00	0.00	0.00	0.00	0.00	0.00	0.00	0.00	0.00	0.00	0.00	0.00	0.00	0.00	0.00	0.00	0.00	0.00	0.00	0.00	0.00	0.00	0.00	0.00	0.00	0.00	0.00	0.00	0.00	0.00
5	0.00	0.00	0.00	0.00	0.00	0.00	0.00	0.00	0.00	0.00	0.00	0.00	0.00	0.00	0.00	0.00	0.00	0.00	0.00	0.00	0.00	0.00	0.00	0.00	0.00	0.00	0.00	0.00	0.00	0.00	0.00	0.00	0.00	0.00	0.00	0.00	0.00	0.00	0.00	0.00
6	100.00	0.00	0.00	0.00	0.00	0.00	0.00	0.00	0.00	0.00	0.00	0.00	0.00	0.00	0.00	0.00	0.00	0.00	0.00	0.00	100.00	0.00	0.00	0.00	0.00	0.00	0.00	0.00	0.00	0.00	0.00	0.00	0.00	0.00	0.00	0.00	0.00	0.00	0.00	0.00
7	0.00	0.00	0.00	0.00	0.00	0.00	0.00	0.00	0.00	0.00	0.00	0.00	0.00	0.00	0.00	0.00	0.00	0.00	0.00	0.00	0.00	0.00	0.00	0.00	0.00	0.00	0.00	0.00	0.00	0.00	0.00	0.00	0.00	0.00	0.00	0.00	0.00	0.00	0.00	0.00
8	0.00	0.00	0.00	0.00	0.00	0.00	0.00	0.00	0.00	0.00	0.00	0.00	0.00	0.00	0.00	0.00	0.00	0.00	0.00	0.00	0.00	0.00	0.00	0.00	0.00	0.00	0.00	0.00	0.00	0.00	0.00	0.00	0.00	0.00	0.00	0.00	0.00	0.00	0.00	0.00
9	0.00	0.00	0.00	0.00	0.00	0.00	0.00	0.00	0.00	0.00	0.00	0.00	0.00	0.00	0.00	0.00	0.00	0.00	0.00	0.00	0.00	0.00	0.00	0.00	0.00	0.00	0.00	0.00	0.00	0.00	0.00	0.00	0.00	0.00	0.00	0.00	0.00	0.00	0.00	0.00
10	0.00	0.00	0.00	0.00	0.00	0.00	0.00	0.00	0.00	0.00	0.00	0.00	0.00	0.00	0.00	0.00	0.00	0.00	0.00	0.00	0.00	0.00	0.00	0.00	0.00	0.00	0.00	0.00	0.00	0.00	0.00	0.00	0.00	0.00	0.00	0.00	0.00	0.00	0.00	0.00
11	0.00	0.00	0.00	0.00	0.00	0.00	0.00	0.00	0.00	0.00	0.00	0.00	0.00	0.00	0.00	0.00	0.00	0.00	0.00	0.00	0.00	0.00	0.00	0.00	0.00	0.00	0.00	0.00	0.00	0.00	0.00	0.00	0.00	0.00	0.00	0.00	0.00	0.00	0.00	0.00
12	0.00	0.00	0.00	0.00	0.00	0.00	0.00	0.00	0.00	0.00	0.00	0.00	0.00	0.00	0.00	0.00	0.00	0.00	0.00	0.00	0.00	0.00	0.00	0.00	0.00	0.00	0.00	0.00	0.00	0.00	0.00	0.00	0.00	0.00	0.00	0.00	0.00	0.00	0.00	0.00
13	0.00	0.00	0.00	0.00	0.00	0.00	0.00	0.00	0.00	0.00	0.00	0.00	0.00	0.00	0.00	0.00	0.00	0.00	0.00	0.00	0.00	0.00	0.00	0.00	0.00	0.00	0.00	0.00	0.00	0.00	0.00	0.00	0.00	0.00	0.00	0.00	0.00	0.00	0.00	0.00

Tridem	Total	12000 lb	15000 lb	18000 lb	21000 lb	24000 lb	27000 lb	30000 lb	33000 lb	36000 lb	39000 lb	42000 lb	45000 lb	48000 lb	51000 lb	54000 lb	57000 lb	60000 lb	63000 lb	66000 lb	69000 lb	72000 lb	75000 lb	78000 lb	81000 lb	84000 lb	87000 lb	90000 lb	93000 lb	96000 lb	99000 lb	102000 lb
4	0.00	0.00	0.00	0.00	0.00	0.00	0.00	0.00	0.00	0.00	0.00	0.00	0.00	0.00	0.00	0.00	0.00	0.00	0.00	0.00	0.00	0.00	0.00	0.00	0.00	0.00	0.00	0.00	0.00	0.00	0.00	0.00
5	0.00	0.00	0.00	0.00	0.00	0.00	0.00	0.00	0.00	0.00	0.00	0.00	0.00	0.00	0.00	0.00	0.00	0.00	0.00	0.00	0.00	0.00	0.00	0.00	0.00	0.00	0.00	0.00	0.00	0.00	0.00	0.00
6	0.00	0.00	0.00	0.00	0.00	0.00	0.00	0.00	0.00	0.00	0.00	0.00	0.00	0.00	0.00	0.00	0.00	0.00	0.00	0.00	0.00	0.00	0.00	0.00	0.00	0.00	0.00	0.00	0.00	0.00	0.00	0.00
7	0.00	0.00	0.00	0.00	0.00	0.00	0.00	0.00	0.00	0.00	0.00	0.00	0.00	0.00	0.00	0.00	0.00	0.00	0.00	0.00	0.00	0.00	0.00	0.00	0.00	0.00	0.00	0.00	0.00	0.00	0.00	0.00
8	0.00	0.00	0.00	0.00	0.00	0.00	0.00	0.00	0.00	0.00	0.00	0.00	0.00	0.00	0.00	0.00	0.00	0.00	0.00	0.00	0.00	0.00	0.00	0.00	0.00	0.00	0.00	0.00	0.00	0.00	0.00	0.00
9	0.00	0.00	0.00	0.00	0.00	0.00	0.00	0.00	0.00	0.00	0.00	0.00	0.00	0.00	0.00	0.00	0.00	0.00	0.00	0.00	0.00	0.00	0.00	0.00	0.00	0.00	0.00	0.00	0.00	0.00	0.00	0.00
10	0.00	0.00	0.00	0.00	0.00	0.00	0.00	0.00	0.00	0.00	0.00	0.00	0.00	0.00	0.00	0.00	0.00	0.00	0.00	0.00	0.00	0.00	0.00	0.00	0.00	0.00	0.00	0.00	0.00	0.00	0.00	0.00
11	100.00	0.00	0.00	0.00	0.00	0.00	0.00	0.00	0.00	0.00	0.00	0.00	0.00	0.00	0.00	0.00	0.00	0.00	0.00	0.00	0.00	0.00	0.00	0.00	0.00	0.00	100.00	0.00	0.00	0.00	0.00	0.00
12	0.00	0.00	0.00	0.00	0.00	0.00	0.00	0.00	0.00	0.00	0.00	0.00	0.00	0.00	0.00	0.00	0.00	0.00	0.00	0.00	0.00	0.00	0.00	0.00	0.00	0.00	0.00	0.00	0.00	0.00	0.00	0.00
13	0.00	0.00	0.00	0.00	0.00	0.00	0.00	0.00	0.00	0.00	0.00	0.00	0.00	0.00	0.00	0.00	0.00	0.00	0.00	0.00	0.00	0.00	0.00	0.00	0.00	0.00	0.00	0.00	0.00	0.00	0.00	0.00

Table A.2: CNR-based axle load distributions for single, tandem, and tridem groups – Two-lane tourist highways

Appendix B

Axle load distributions for the case studies

B.1 Axle load distributions for the A3 motorway in Napoli

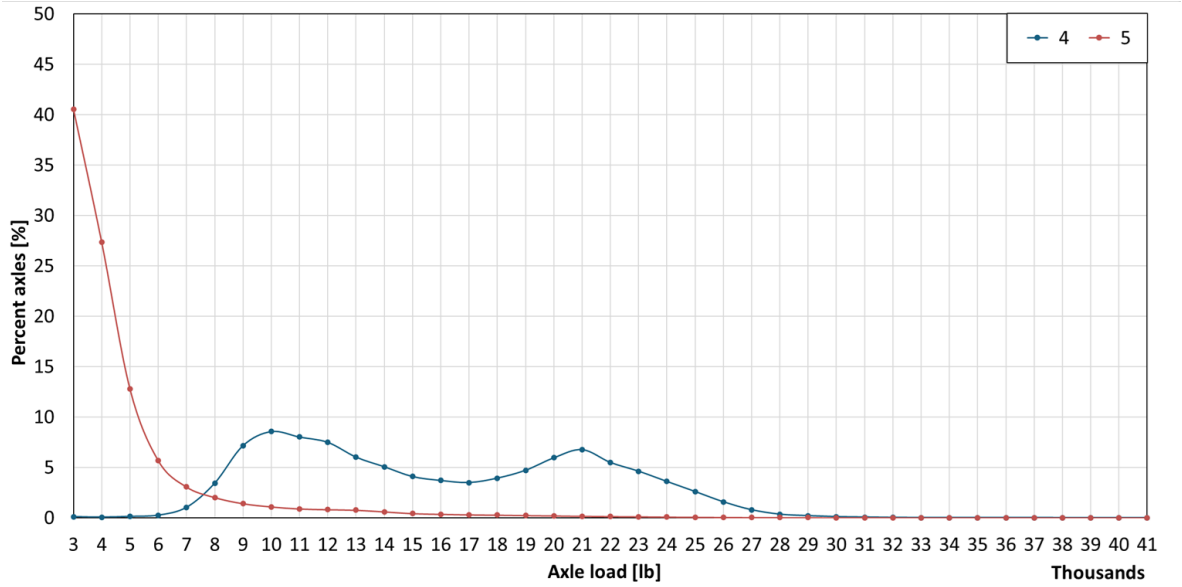

Figure B.1: Single axle load distributions of vehicle classes 4 and 5 – October

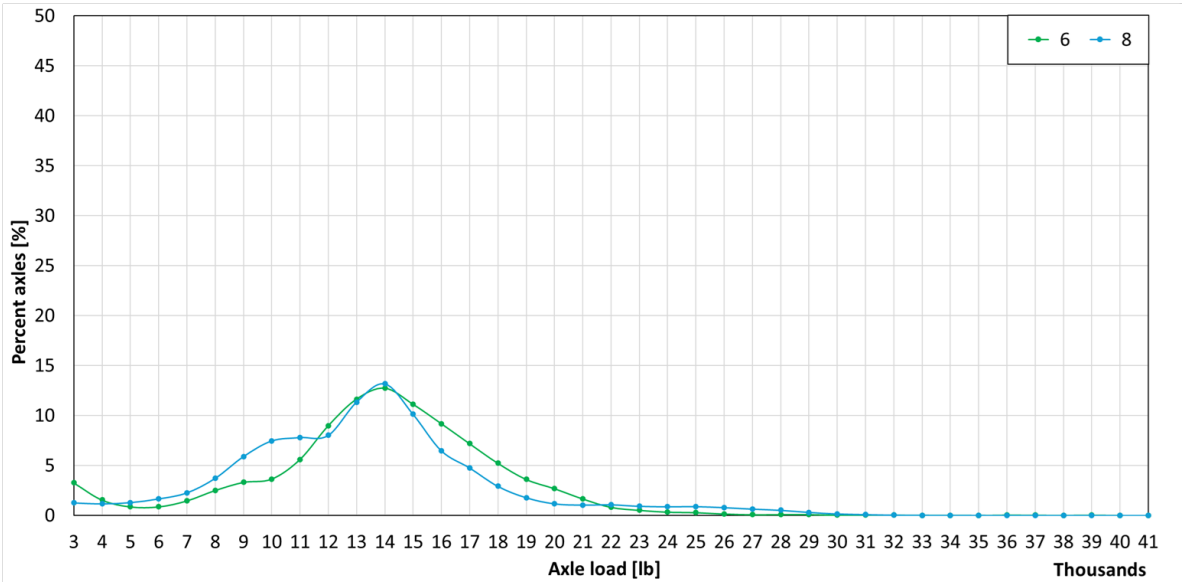

Figure B.2: Single axle load distributions of vehicle classes 6 and 8 – October

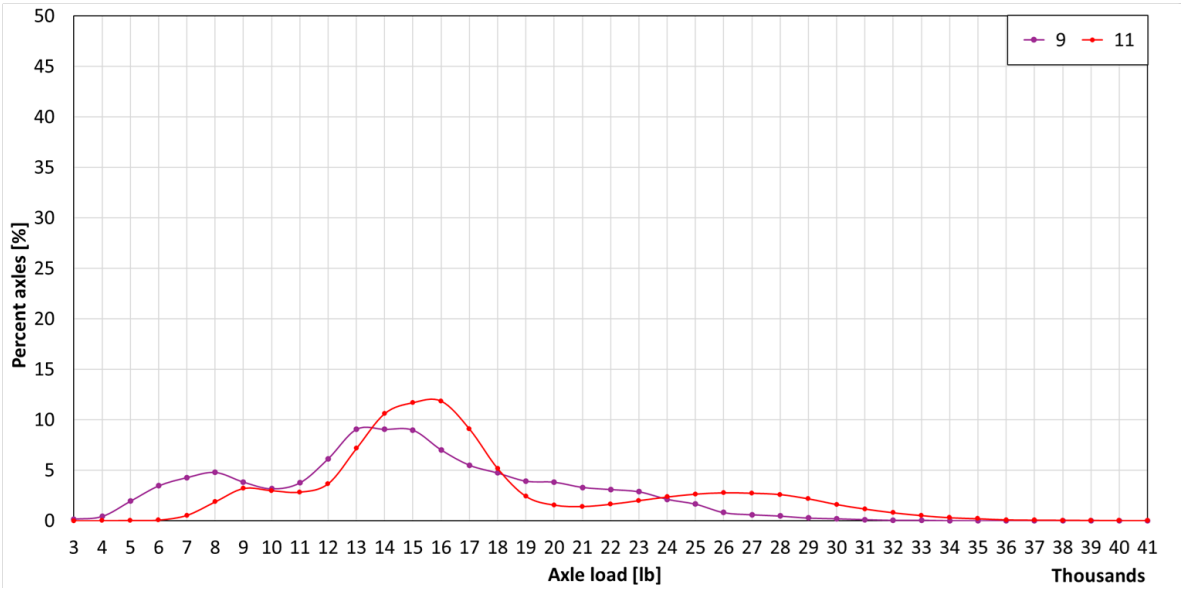

Figure B.3: Single axle load distributions of vehicle classes 9 and 11 – October

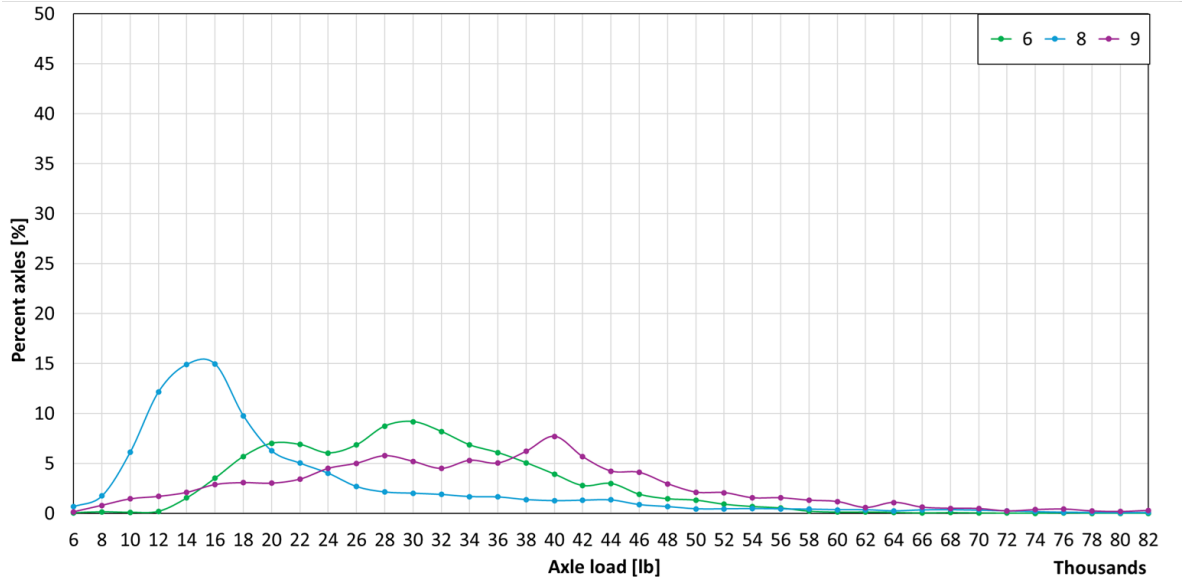

Figure B.4: Tandem axle load distributions – October

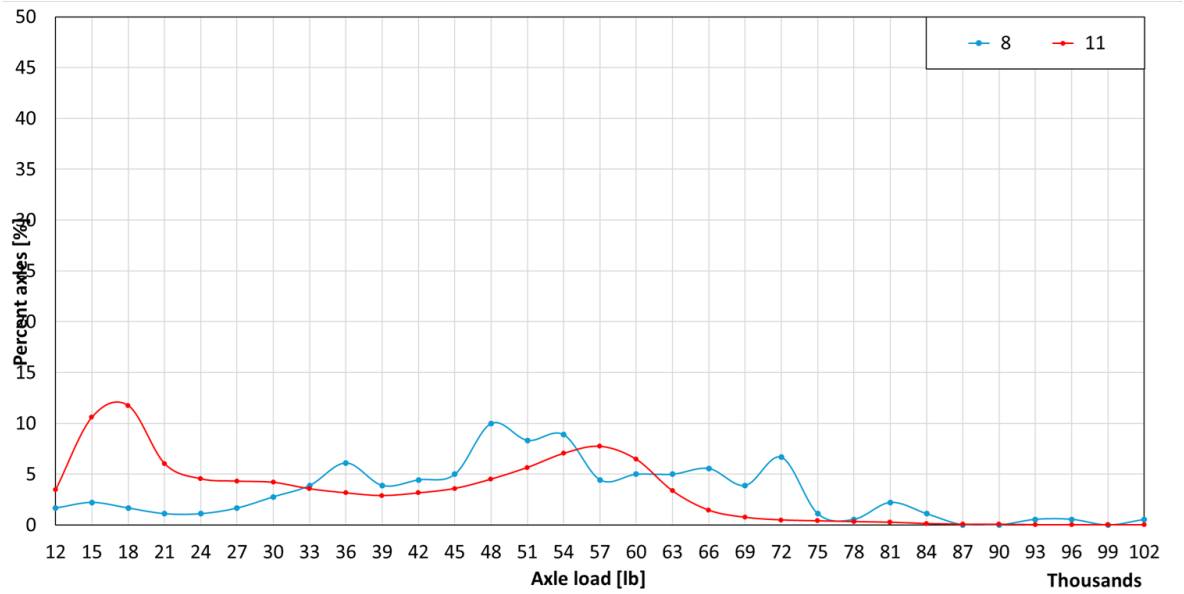

Figure B.5: Tridem axle load distributions – October

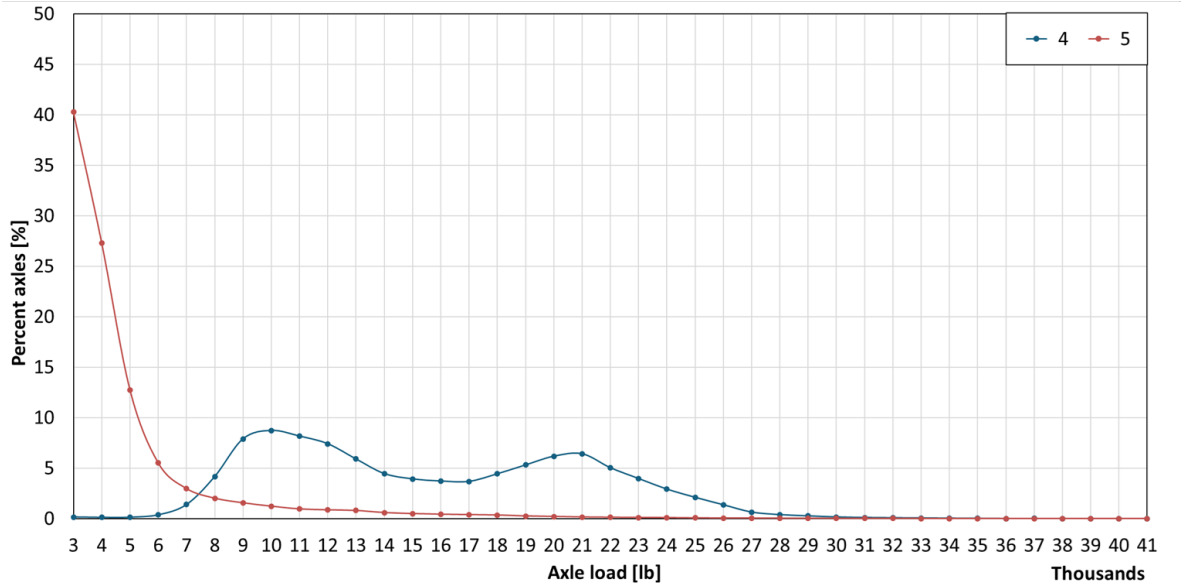

Figure B.6: Single axle load distributions of vehicle classes 4 and 5 – November

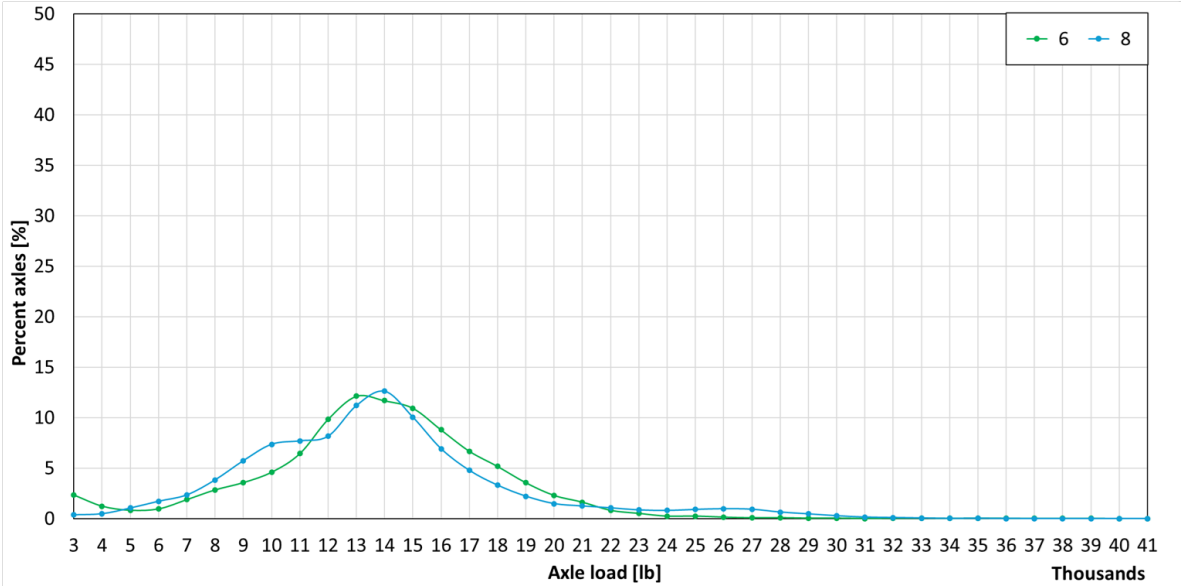

Figure B.7: Single axle load distributions of vehicle classes 6 and 8 – November

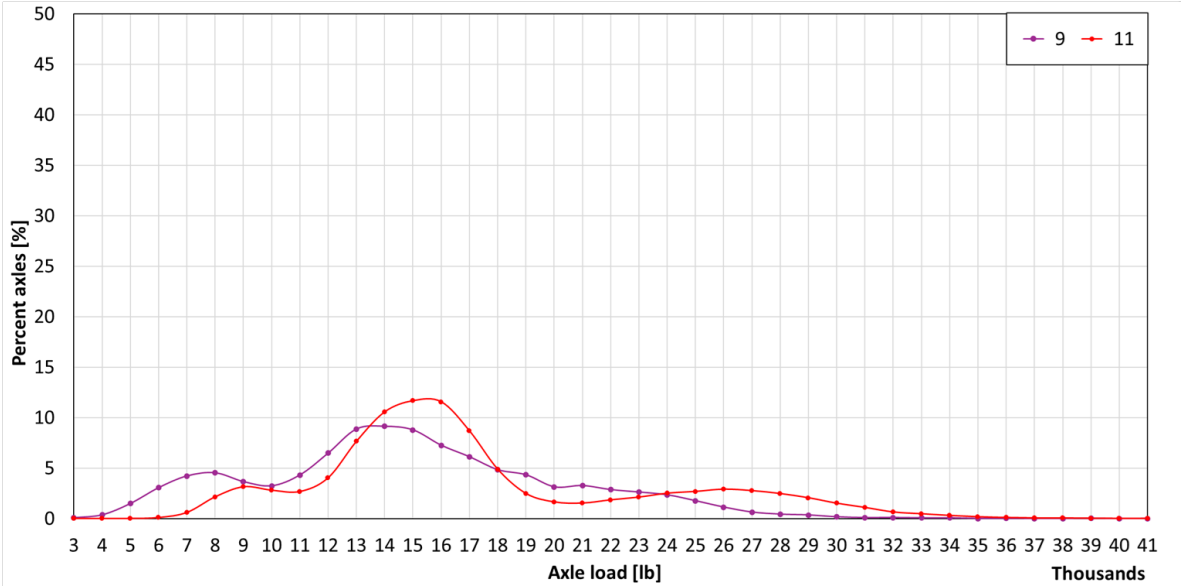

Figure B.8: Single axle load distributions of vehicle classes 9 and 11 – November

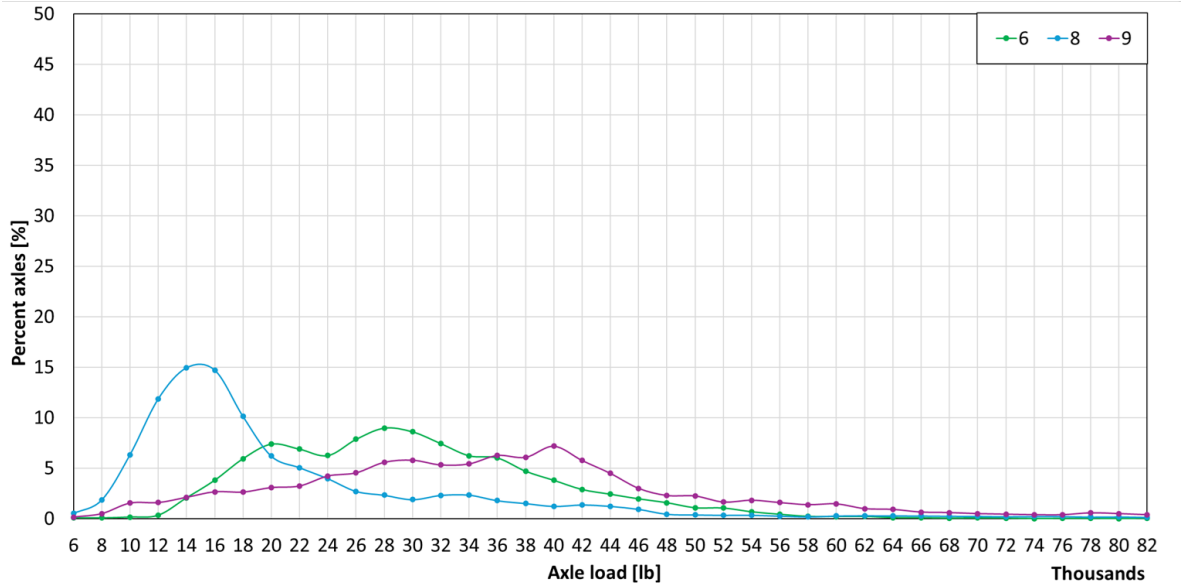

Figure B.9: Tandem axle load distributions – November

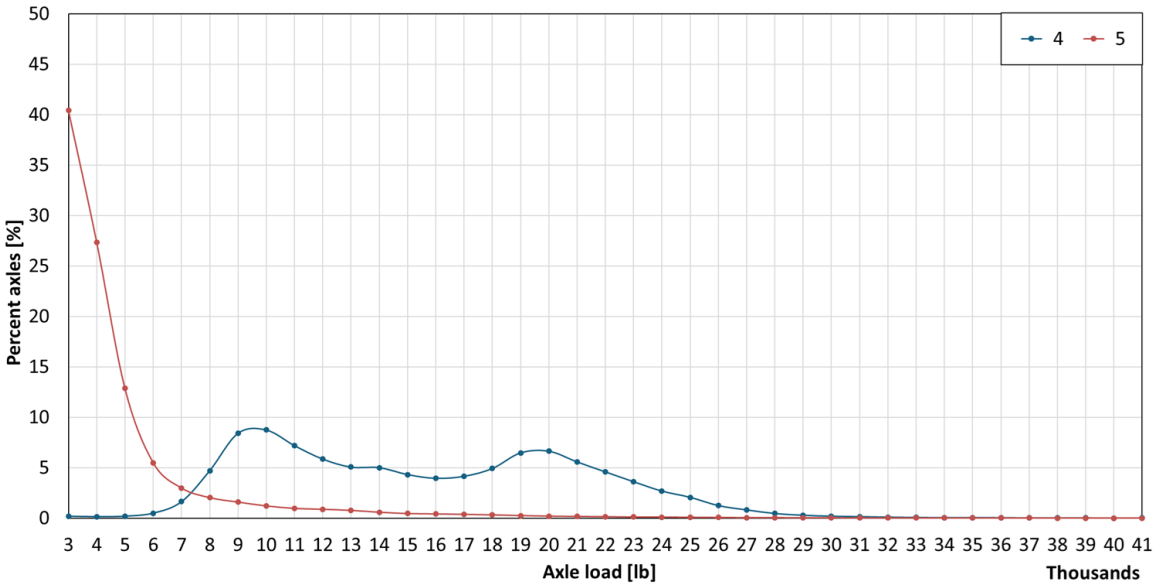

Figure B.10: Single axle load distributions of vehicle classes 4 and 5 – December

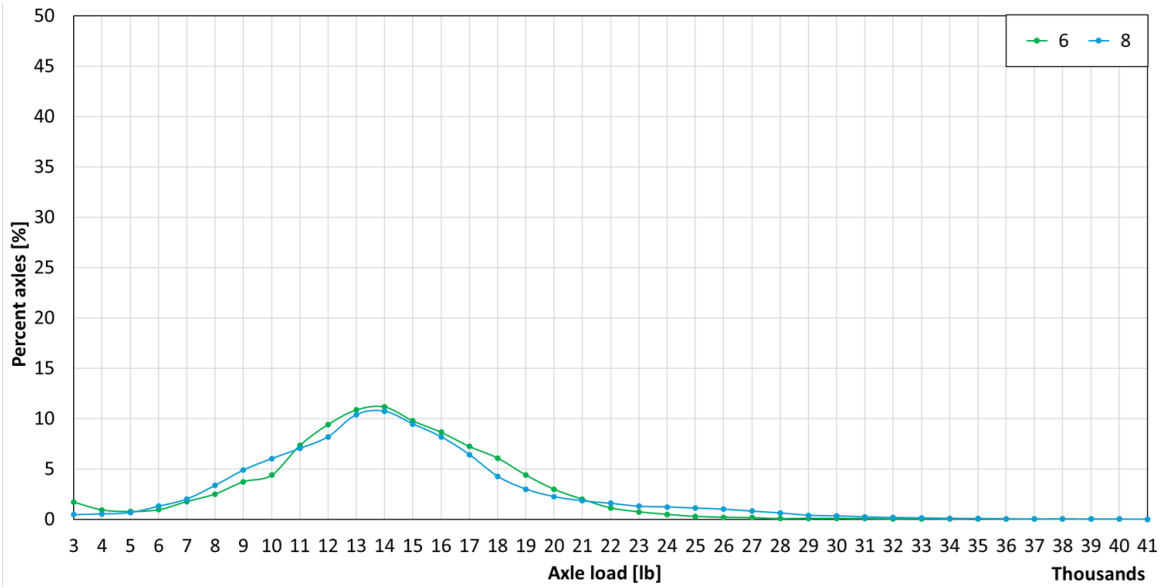

Figure B.11: Single axle load distributions of vehicle classes 6 and 8 – December

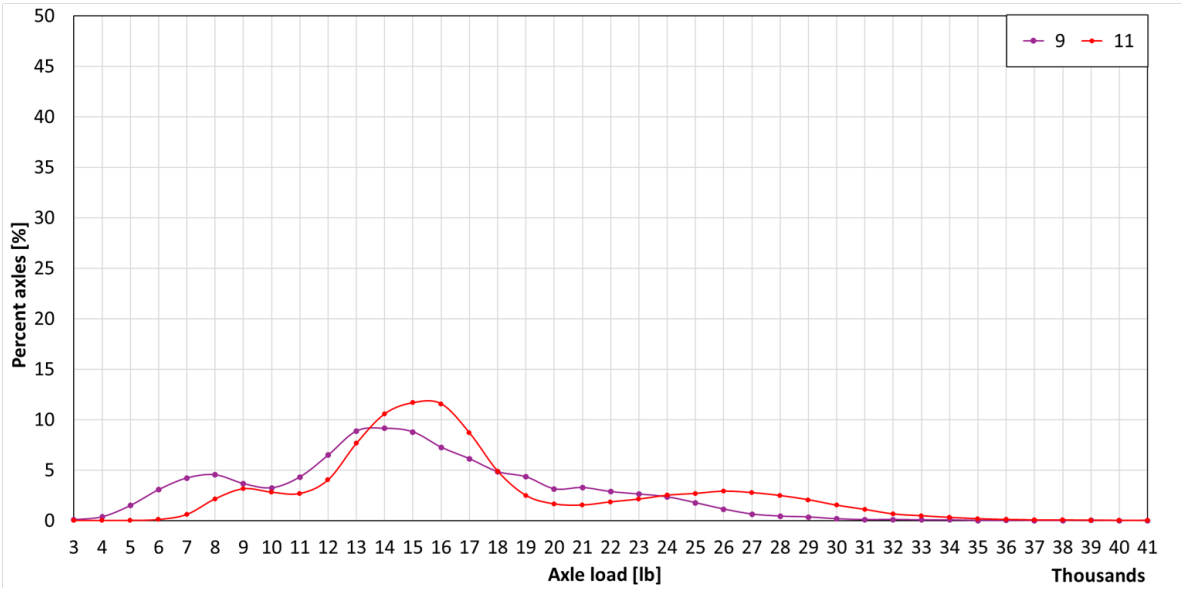

Figure B.12: Single axle load distributions of vehicle classes 9 and 11 – December

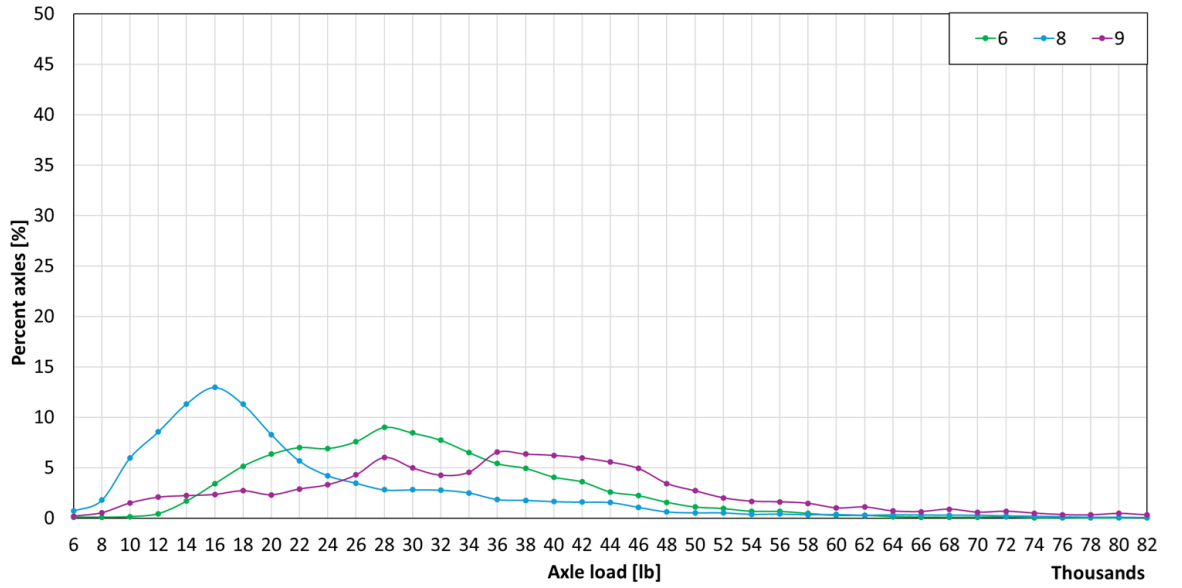

Figure B.13: Tandem axle load distributions – December

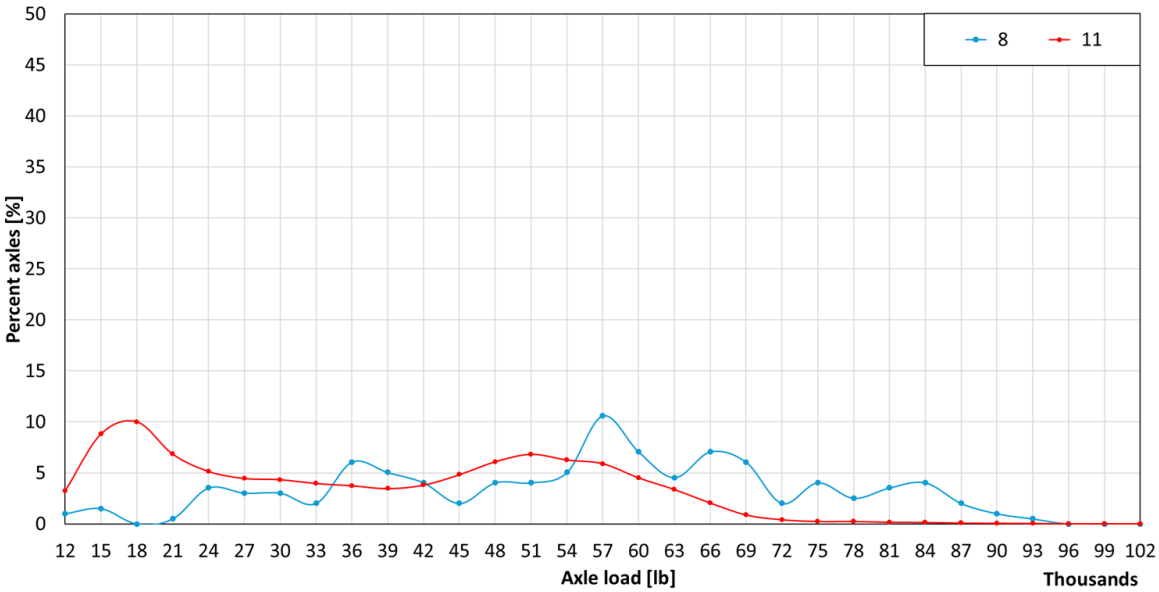

Figure B.14: Tridem axle load distributions – December

Month	Class	Total	3000 lb	4000 lb	5000 lb	6000 lb	7000 lb	8000 lb	9000 lb	10000 lb	11000 lb	12000 lb	13000 lb	14000 lb	15000 lb	16000 lb	17000 lb	18000 lb	19000 lb	20000 lb	21000 lb	22000 lb	23000 lb	24000 lb	25000 lb	26000 lb	27000 lb	28000 lb	29000 lb	30000 lb	31000 lb	32000 lb	33000 lb	34000 lb	35000 lb	36000 lb	37000 lb	38000 lb	39000 lb	40000 lb	41000 lb
2021_08	4	100	0.04	0.06	0.05	0.23	0.97	3.04	6.74	8.57	8.18	7.51	5.79	5.18	3.76	3.34	2.95	3.78	5.09	6.73	7.03	6.36	4.71	3.74	2.83	1.47	0.85	0.32	0.23	0.12	0.08	0.04	0.06	0.02	0.03	0.02	0.02	0.03	0.01	0.01	0.01
	5	100	45.97	24.57	11.88	6.06	3.11	1.83	1.12	0.81	0.66	0.62	0.56	0.45	0.33	0.28	0.25	0.23	0.21	0.19	0.17	0.14	0.12	0.09	0.07	0.06	0.05	0.04	0.03	0.02	0.02	0.01	0.01	0.01	0.01	0.01	0.01	0.00	0.00	0.00	0.00
	6	100	5.10	2.60	1.18	0.92	2.10	2.17	2.69	3.26	5.60	9.38	12.30	12.22	10.50	8.95	6.60	5.13	3.46	2.25	1.22	0.78	0.55	0.35	0.23	0.10	0.07	0.06	0.05	0.01	0.02	0.01	0.01	0.01	0.02	0.01	0.01	0.01	0.04	0.01	0.02
	7	0	0.00	0.00	0.00	0.00	0.00	0.00	0.00	0.00	0.00	0.00	0.00	0.00	0.00	0.00	0.00	0.00	0.00	0.00	0.00	0.00	0.00	0.00	0.00	0.00	0.00	0.00	0.00	0.00	0.00	0.00	0.00	0.00	0.00	0.00	0.00	0.00	0.00	0.00	0.00
	8	100	2.88	2.11	1.85	2.38	3.00	4.34	6.32	7.57	7.45	7.98	11.81	13.00	8.90	5.67	3.87	2.53	1.56	1.05	0.84	0.80	0.69	0.66	0.68	0.58	0.54	0.34	0.25	0.14	0.09	0.06	0.03	0.02	0.01	0.00	0.00	0.00	0.00	0.00	0.00
	9	100	0.21	0.56	1.60	3.44	4.73	5.31	5.01	3.43	3.86	6.21	7.67	7.32	6.89	6.16	5.51	4.32	3.63	3.00	3.84	4.05	3.61	2.94	2.07	1.84	1.08	0.68	0.48	0.21	0.14	0.08	0.05	0.03	0.03	0.00	0.00	0.01	0.00	0.00	0.00
	10	100	0.00	0.00	0.00	0.00	0.00	0.00	0.00	0.00	0.00	0.00	0.00	0.00	0.00	0.00	0.00	0.00	0.00	0.00	0.00	0.00	0.00	0.00	0.00	0.00	0.00	0.00	0.00	0.00	0.00	0.00	0.00	0.00	0.00	0.00	0.00	0.00	0.00	0.00	0.00
	11	100	0.00	0.00	0.04	0.19	0.83	2.20	3.11	3.39	3.33	4.25	8.19	10.53	11.02	11.10	8.40	4.56	2.23	1.41	1.28	1.43	1.88	2.07	2.51	2.89	2.73	2.62	2.27	1.82	1.29	0.93	0.60	0.36	0.23	0.14	0.07	0.05	0.02	0.02	0.01
	12	0	0.00	0.00	0.00	0.00	0.00	0.00	0.00	0.00	0.00	0.00	0.00	0.00	0.00	0.00	0.00	0.00	0.00	0.00	0.00	0.00	0.00	0.00	0.00	0.00	0.00	0.00	0.00	0.00	0.00	0.00	0.00	0.00	0.00	0.00	0.00	0.00	0.00	0.00	0.00
	13	0	0.00	0.00	0.00	0.00	0.00	0.00	0.00	0.00	0.00	0.00	0.00	0.00	0.00	0.00	0.00	0.00	0.00	0.00	0.00	0.00	0.00	0.00	0.00	0.00	0.00	0.00	0.00	0.00	0.00	0.00	0.00	0.00	0.00	0.00	0.00	0.00	0.00	0.00	0.00
2021_10	4	100	0.09	0.07	0.14	0.26	1.04	3.45	7.18	8.58	8.04	7.51	6.04	5.08	4.10	3.71	3.51	3.95	4.73	5.97	6.79	5.51	4.64	3.62	2.62	1.59	0.80	0.36	0.21	0.11	0.08	0.04	0.03	0.02	0.03	0.02	0.03	0.02	0.01	0.01	0.01
	5	100	40.54	27.34	12.81	5.70	3.08	2.03	1.43	1.11	0.91	0.83	0.78	0.62	0.44	0.37	0.32	0.28	0.25	0.21	0.17	0.15	0.12	0.10	0.08	0.06	0.05	0.04	0.03	0.03	0.02	0.02	0.01	0.01	0.01	0.01	0.01	0.01	0.01	0.00	0.01
	6	100	3.28	1.55	0.87	0.87	1.47	2.51	3.32	3.65	5.61	8.98	11.65	12.74	11.14	9.20	7.19	5.24	3.62	2.70	1.67	0.83	0.53	0.35	0.30	0.16	0.08	0.10	0.10	0.03	0.04	0.03	0.02	0.02	0.01	0.04	0.03	0.02	0.04	0.01	0.00
	7	0	0.00	0.00	0.00	0.00	0.00	0.00	0.00	0.00	0.00	0.00	0.00	0.00	0.00	0.00	0.00	0.00	0.00	0.00	0.00	0.00	0.00	0.00	0.00	0.00	0.00	0.00	0.00	0.00	0.00	0.00	0.00	0.00	0.00	0.00	0.00	0.00	0.00	0.00	0.00
	8	100	1.31	1.18	1.30	1.67	2.28	3.72	5.90	7.47	7.81	8.02	11.34	13.17	10.14	6.49	4.77	2.93	1.79	1.18	1.05	1.08	0.93	0.88	0.90	0.80	0.65	0.53	0.32	0.17	0.10	0.04	0.03	0.02	0.02	0.00	0.00	0.01	0.00	0.00	0.00
	9	100	0.18	0.44	1.95	3.47	4.28	4.80	3.84	3.17	3.77	6.15	9.06	9.06	8.98	7.01	5.51	4.74	3.93	3.83	3.31	3.10	2.88	2.14	1.66	0.82	0.61	0.48	0.28	0.21	0.13	0.06	0.07	0.02	0.02	0.01	0.01	0.02	0.00	0.00	0.00
	10	100	0.00	0.00	0.00	0.00	0.00	0.00	0.00	0.00	0.00	0.00	0.00	0.00	0.00	0.00	0.00	0.00	0.00	0.00	0.00	0.00	0.00	0.00	0.00	0.00	0.00	0.00	0.00	0.00	0.00	0.00	0.00	0.00	0.00	0.00	0.00	0.00	0.00	0.00	0.00
	11	100	0.00	0.01	0.01	0.07	0.54	1.88	3.20	2.99	2.84	3.68	7.16	10.63	11.71	11.86	9.09	5.16	2.42	1.55	1.42	1.64	2.00	2.36	2.65	2.77	2.73	2.60	2.18	1.61	1.16	0.79	0.51	0.30	0.20	0.09	0.07	0.05	0.04	0.02	0.01
	12	0	0.00	0.00	0.00	0.00	0.00	0.00	0.00	0.00	0.00	0.00	0.00	0.00	0.00	0.00	0.00	0.00	0.00	0.00	0.00	0.00	0.00	0.00	0.00	0.00	0.00	0.00	0.00	0.00	0.00	0.00	0.00	0.00	0.00	0.00	0.00	0.00	0.00	0.00	0.00
	13	0	0.00	0.00	0.00	0.00	0.00	0.00	0.00	0.00	0.00	0.00	0.00	0.00	0.00	0.00	0.00	0.00	0.00	0.00	0.00	0.00	0.00	0.00	0.00	0.00	0.00	0.00	0.00	0.00	0.00	0.00	0.00	0.00	0.00	0.00	0.00	0.00	0.00	0.00	0.00
2021_11	4	100	0.14	0.12	0.14	0.38	1.39	4.17	7.90	8.74	8.18	7.42	5.91	4.46	3.94	3.73	3.69	4.44	5.32	6.18	6.42	5.04	3.97	2.93	2.11	1.37	0.65	0.40	0.27	0.16	0.11	0.09	0.07	0.05	0.03	0.02	0.02	0.02	0.01	0.01	0.00
	5	100	40.28	27.31	12.76	5.52	2.98	2.02	1.57	1.23	0.96	0.87	0.81	0.60	0.50	0.44	0.39	0.36	0.26	0.21	0.16	0.13	0.11	0.10	0.07	0.06	0.06	0.04	0.04	0.03	0.02	0.02	0.02	0.01	0.01	0.01	0.01	0.01	0.01	0.00	0.01
	6	100	2.33	1.23	0.82	0.96	1.88	2.85	3.57	4.60	6.45	9.85	12.14	11.69	10.95	8.80	6.68	5.17	3.56	2.30	1.63	0.82	0.52	0.24	0.25	0.14	0.08	0.09	0.05	0.05	0.02	0.05	0.04	0.02	0.05	0.03	0.02	0.02	0.03	0.01	0.01
	7	0	0.00	0.00	0.00	0.00	0.00	0.00	0.00	0.00	0.00	0.00	0.00	0.00	0.00	0.00	0.00	0.00	0.00	0.00	0.00	0.00	0.00	0.00	0.00	0.00	0.00	0.00	0.00	0.00	0.00	0.00	0.00	0.00	0.00	0.00	0.00	0.00	0.00	0.00	0.00
	8	100	0.38	0.48	1.05	1.72	2.35	3.84	5.74	7.37	7.71	8.17	11.21	12.62	10.06	6.92	4.78	3.31	2.22	1.49	1.25	1.07	0.86	0.80	0.90	0.98	0.92	0.65	0.47	0.28	0.15	0.11	0.06	0.02	0.03	0.02	0.01	0.00	0.00	0.00	0.00
	9	100	0.07	0.37	1.49	3.06	4.22	4.53	3.66	3.25	4.32	6.49	8.88	9.14	8.79	7.26	6.12	4.84	4.34	3.14	3.27	2.87	2.63	2.35	1.77	1.14	0.64	0.44	0.36	0.17	0.09	0.10	0.07	0.07	0.01	0.02	0.00	0.00	0.02	0.00	0.01
	10	100	0.00	0.00	0.00	0.00	0.00	0.00	0.00	0.00	0.00	0.00	0.00	0.00	0.00	0.00	0.00	0.00	0.00	0.00	0.00	0.00	0.00	0.00	0.00	0.00	0.00	0.00	0.00	0.00	0.00	0.00	0.00	0.00	0.00	0.00	0.00	0.00	0.00	0.00	0.00
	11	100	0.01	0.01	0.01	0.12	0.60	2.15	3.14	2.80	2.67	4.04	7.65	10.57	11.67	11.56	8.68	4.88	2.48	1.64	1.53	1.85	2.12	2.50	2.68	2.90	2.77	2.47	2.05	1.51	1.09	0.64	0.47	0.30	0.17	0.10	0.06	0.05	0.03	0.02	0.01
	12	0	0.00	0.00	0.00	0.00	0.00	0.00	0.00	0.00	0.00	0.00	0.00	0.00	0.00	0.00	0.00	0.00	0.00	0.00	0.00	0.00	0.00	0.00	0.00	0.00	0.00	0.00	0.00	0.00	0.00	0.00	0.00	0.00	0.00	0.00	0.00	0.00	0.00	0.00	0.00
	13	0	0.00	0.00	0.00	0.00	0.00	0.00	0.00	0.00	0.00	0.00	0.00	0.00	0.00	0.00	0.00	0.00	0.00	0.00	0.00	0.00	0.00	0.00	0.00	0.00	0.00	0.00	0.00	0.00	0.00	0.00	0.00	0.00	0.00	0.00	0.00	0.00	0.00	0.00	0.00
2021_12	4	100	0.19	0.14	0.19	0.49	1.62	4.70	8.41	8.73	7.19	5.85	5.06	5.00	4.32	3.94	4.15	4.92	6.47	6.63	5.57	4.59	3.61	2.68	2.06	1.24	0.81	0.46	0.28	0.19	0.14	0.10	0.06	0.04	0.05	0.04	0.02	0.02	0.02	0.01	0.01
	5	100	40.44	27.34	12.85	5.49	2.98	2.03	1.59	1.21	0.96	0.87	0.76	0.58	0.45	0.41	0.37	0.32	0.25	0.19	0.16	0.14	0.11	0.10	0.08	0.06	0.05	0.04	0.04	0.03	0.02	0.02	0.02	0.01	0.01	0.01	0.01	0.00	0.00	0.00	0.00
	6	100	1.68	0.91	0.77	0.94	1.76	2.50	3.72	4.38	7.34	9.41	10.86	11.16	9.77	8.64	7.22	6.08	4.39	2.98	1.98	1.12	0.74	0.48	0.28	0.19	0.15	0.06	0.09	0.08	0.06	0.03	0.05	0.03	0.04	0.04	0.01	0.04	0.01	0.01	0.00
	7	0	0.00	0.00	0.00	0.00	0.00	0.00	0.00	0.00	0.00	0.00	0.00	0.00	0.00	0.00	0.00	0.00	0.00	0.00	0.00	0.00	0.00	0.00	0.00	0.00	0.00	0.00	0.00	0.00	0.00	0.00	0.00	0.00	0.00	0.00	0.00	0.00	0.00	0.00	0.00
	8	100	0.45	0.53	0.66	1.29	2.01	3.36	4.87	6.01	7.02	8.18	10.38	10.71	9.45	8.18	6.42	4.26	2.99	2.25	1.83	1.58	1.29	1.22	1.11	1.00	0.80	0.63	0.40	0.34	0.23	0.17	0.13	0.09	0.06	0.03	0.02	0.01	0.02	0.01	0.01
	9	100	0.26	0.25	0.92	2.42	3.24	3.76	3.44	4.15	4.54	5.64	6.63	8.27	7.99	7.43	5.98	5.77	5.35	4.27	4.34	3.16	2.63	2.43	2.23	1.65	1.17	0.72	0.53	0.26	0.23	0.09	0.09	0.05	0.01	0.04	0.01	0.01	0.00	0.01	0.03
	10	100	0.00	0.00	0.00	0.00	0.00	0.00	0.00	0.00	0.00	0.00	0.00	0.00	0.00	0.00	0.00	0.00	0.00	0.00	0.00	0.00	0.00	0.00	0.00	0.00	0.00	0.00	0.00	0.00	0.00	0.00	0.00	0.00	0.00	0.00	0.00	0.00	0.00	0.00	0.00
	11	100	0.00	0.01	0.01	0.08	0.55	1.68	2.59	2.67	3.19	5.13	8.07	9.36	9.62	8.93	7.48	5.92	4.65	3.26	2.37	2.08	2.06	2.28	2.40	2.55	2.57	2.27	1.97	1.70	1.38	1.10	0.75	0.50	0.33	0.19	0.13	0.08	0.04	0.03	0.02
	12	0	0.00	0.00	0.00	0.00	0.00	0.00	0.00	0.00	0.00	0.00	0.00	0.00	0.00	0.00	0.00	0.00	0.00	0.00	0.00	0.00	0.00	0.00	0.00	0.00	0.00	0.00	0.00	0.00	0.00	0.00	0.00	0.00	0.00	0.00	0.00	0.00	0.00	0.00	0.00
	13	0	0.00	0.00	0.00	0.00	0.00	0.00	0.00	0.00	0.00	0.00	0.00	0.00	0.00	0.00	0.00	0.00	0.00	0.00	0.00	0.00	0.00	0.00	0.00	0.00	0.00	0.00	0.00	0.00	0.00	0.00	0.00	0.00	0.00	0.00	0.00	0.00	0.00	0.00	0.00

Table B.1: Single axle load distribution factors for August, October, November, December

Month	Class	Total	6000 lb	8000 lb	10000 lb	12000 lb	14000 lb	16000 lb	18000 lb	20000 lb	22000 lb	24000 lb	26000 lb	28000 lb	30000 lb	32000 lb	34000 lb	36000 lb	38000 lb	40000 lb	42000 lb	44000 lb	46000 lb	48000 lb	50000 lb	52000 lb	54000 lb	56000 lb	58000 lb	60000 lb	62000 lb	64000 lb	66000 lb	68000 lb	70000 lb	72000 lb	74000 lb	76000 lb	78000 lb	80000 lb	82000 lb
2021_08	4	0	0.00	0.00	0.00	0.00	0.00	0.00	0.00	0.00	0.00	0.00	0.00	0.00	0.00	0.00	0.00	0.00	0.00	0.00	0.00	0.00	0.00	0.00	0.00	0.00	0.00	0.00	0.00	0.00	0.00	0.00	0.00	0.00	0.00	0.00	0.00	0.00	0.00	0.00	0.00
	5	0	0.00	0.00	0.00	0.00	0.00	0.00	0.00	0.00	0.00	0.00	0.00	0.00	0.00	0.00	0.00	0.00	0.00	0.00	0.00	0.00	0.00	0.00	0.00	0.00	0.00	0.00	0.00	0.00	0.00	0.00	0.00	0.00	0.00	0.00	0.00	0.00	0.00	0.00	0.00
	6	100	0.10	0.18	0.15	0.33	1.58	3.14	5.84	6.65	6.25	5.15	6.04	9.18	8.69	7.90	7.79	6.27	5.47	3.79	3.03	3.05	2.29	2.28	1.62	1.32	0.72	0.44	0.24	0.09	0.11	0.06	0.08	0.02	0.02	0.05	0.01	0.02	0.02	0.03	0.00
	7	0	0.00	0.00	0.00	0.00	0.00	0.00	0.00	0.00	0.00	0.00	0.00	0.00	0.00	0.00	0.00	0.00	0.00	0.00	0.00	0.00	0.00	0.00	0.00	0.00	0.00	0.00	0.00	0.00	0.00	0.00	0.00	0.00	0.00	0.00	0.00	0.00	0.00	0.00	0.00
	8	100	0.64	1.67	6.20	14.03	18.45	16.42	10.19	5.69	4.52	3.21	2.45	1.59	1.34	1.40	1.05	0.98	0.92	0.92	1.04	1.26	0.81	0.56	0.35	0.28	0.29	0.28	0.36	0.25	0.44	0.47	0.51	0.44	0.31	0.28	0.18	0.08	0.06	0.05	0.03
	9	100	0.15	0.84	3.22	2.66	2.34	4.00	3.66	5.34	4.56	3.66	3.75	4.53	3.66	3.41	4.69	4.72	6.44	8.31	6.69	5.12	3.09	2.50	2.03	1.47	1.50	0.97	1.12	0.87	0.66	0.56	0.62	0.44	0.37	0.41	0.34	0.31	0.31	0.34	0.34
	10	0	0.00	0.00	0.00	0.00	0.00	0.00	0.00	0.00	0.00	0.00	0.00	0.00	0.00	0.00	0.00	0.00	0.00	0.00	0.00	0.00	0.00	0.00	0.00	0.00	0.00	0.00	0.00	0.00	0.00	0.00	0.00	0.00	0.00	0.00	0.00	0.00	0.00	0.00	0.00
	11	0	0.00	0.00	0.00	0.00	0.00	0.00	0.00	0.00	0.00	0.00	0.00	0.00	0.00	0.00	0.00	0.00	0.00	0.00	0.00	0.00	0.00	0.00	0.00	0.00	0.00	0.00	0.00	0.00	0.00	0.00	0.00	0.00	0.00	0.00	0.00	0.00	0.00	0.00	0.00
	12	0	0.00	0.00	0.00	0.00	0.00	0.00	0.00	0.00	0.00	0.00	0.00	0.00	0.00	0.00	0.00	0.00	0.00	0.00	0.00	0.00	0.00	0.00	0.00	0.00	0.00	0.00	0.00	0.00	0.00	0.00	0.00	0.00	0.00	0.00	0.00	0.00	0.00	0.00	0.00
	13	0	0.00	0.00	0.00	0.00	0.00	0.00	0.00	0.00	0.00	0.00	0.00	0.00	0.00	0.00	0.00	0.00	0.00	0.00	0.00	0.00	0.00	0.00	0.00	0.00	0.00	0.00	0.00	0.00	0.00	0.00	0.00	0.00	0.00	0.00	0.00	0.00	0.00	0.00	0.00
2021_10	4	100	0.00	0.00	0.00	0.00	0.00	0.00	0.00	0.00	0.00	0.00	0.00	0.00	0.00	0.00	0.00	0.00	0.00	0.00	0.00	0.00	0.00	0.00	0.00	0.00	0.00	0.00	0.00	0.00	0.00	0.00	0.00	0.00	0.00	0.00	0.00	0.00	0.00	0.00	0.00
	5	0	0.00	0.00	0.00	0.00	0.00	0.00	0.00	0.00	0.00	0.00	0.00	0.00	0.00	0.00	0.00	0.00	0.00	0.00	0.00	0.00	0.00	0.00	0.00	0.00	0.00	0.00	0.00	0.00	0.00	0.00	0.00	0.00	0.00	0.00	0.00	0.00	0.00	0.00	0.00
	6	0	0.06	0.17	0.12	0.22	1.57	3.54	5.71	7.02	6.90	6.06	6.87	8.75	9.19	8.20	6.86	6.09	5.08	3.93	2.79	3.00	1.92	1.47	1.34	0.92	0.69	0.55	0.23	0.14	0.14	0.10	0.05	0.08	0.05	0.03	0.03	0.06	0.03	0.02	0.02
	7	100	0.00	0.00	0.00	0.00	0.00	0.00	0.00	0.00	0.00	0.00	0.00	0.00	0.00	0.00	0.00	0.00	0.00	0.00	0.00	0.00	0.00	0.00	0.00	0.00	0.00	0.00	0.00	0.00	0.00	0.00	0.00	0.00	0.00	0.00	0.00	0.00	0.00	0.00	0.00
	8	0	0.68	1.76	6.15	12.19	14.93	14.96	9.78	6.26	5.03	4.02	2.69	2.15	2.03	1.90	1.69	1.65	1.39	1.28	1.33	1.35	0.88	0.69	0.47	0.46	0.49	0.46	0.43	0.37	0.37	0.26	0.36	0.38	0.33	0.25	0.18	0.12	0.11	0.07	0.10
	9	100	0.17	0.81	1.46	1.70	2.11	2.89	3.08	3.03	3.43	4.51	5.02	5.78	5.21	4.51	5.32	5.05	6.24	7.73	5.67	4.24	4.11	2.97	2.13	2.08	1.57	1.57	1.32	1.19	0.59	1.11	0.62	0.51	0.49	0.24	0.38	0.43	0.24	0.19	0.30
	10	100	0.00	0.00	0.00	0.00	0.00	0.00	0.00	0.00	0.00	0.00	0.00	0.00	0.00	0.00	0.00	0.00	0.00	0.00	0.00	0.00	0.00	0.00	0.00	0.00	0.00	0.00	0.00	0.00	0.00	0.00	0.00	0.00	0.00	0.00	0.00	0.00	0.00	0.00	0.00
	11	0	0.00	0.00	0.00	0.00	0.00	0.00	0.00	0.00	0.00	0.00	0.00	0.00	0.00	0.00	0.00	0.00	0.00	0.00	0.00	0.00	0.00	0.00	0.00	0.00	0.00	0.00	0.00	0.00	0.00	0.00	0.00	0.00	0.00	0.00	0.00	0.00	0.00	0.00	0.00
	12	0	0.00	0.00	0.00	0.00	0.00	0.00	0.00	0.00	0.00	0.00	0.00	0.00	0.00	0.00	0.00	0.00	0.00	0.00	0.00	0.00	0.00	0.00	0.00	0.00	0.00	0.00	0.00	0.00	0.00	0.00	0.00	0.00	0.00	0.00	0.00	0.00	0.00	0.00	0.00
	13	0	0.00	0.00	0.00	0.00	0.00	0.00	0.00	0.00	0.00	0.00	0.00	0.00	0.00	0.00	0.00	0.00	0.00	0.00	0.00	0.00	0.00	0.00	0.00	0.00	0.00	0.00	0.00	0.00	0.00	0.00	0.00	0.00	0.00	0.00	0.00	0.00	0.00	0.00	0.00
2021_11	4	0	0.00	0.00	0.00	0.00	0.00	0.00	0.00	0.00	0.00	0.00	0.00	0.00	0.00	0.00	0.00	0.00	0.00	0.00	0.00	0.00	0.00	0.00	0.00	0.00	0.00	0.00	0.00	0.00	0.00	0.00	0.00	0.00	0.00	0.00	0.00	0.00	0.00	0.00	0.00
	5	100	0.00	0.00	0.00	0.00	0.00	0.00	0.00	0.00	0.00	0.00	0.00	0.00	0.00	0.00	0.00	0.00	0.00	0.00	0.00	0.00	0.00	0.00	0.00	0.00	0.00	0.00	0.00	0.00	0.00	0.00	0.00	0.00	0.00	0.00	0.00	0.00	0.00	0.00	0.00
	6	0	0.12	0.08	0.16	0.34	2.07	3.81	5.95	7.39	6.89	6.25	7.86	8.98	8.61	7.44	6.24	6.02	4.71	3.80	2.89	2.42	1.97	1.58	1.08	1.06	0.68	0.43	0.23	0.21	0.22	0.10	0.09	0.05	0.08	0.06	0.02	0.03	0.03	0.02	0.03
	7	0	0.00	0.00	0.00	0.00	0.00	0.00	0.00	0.00	0.00	0.00	0.00	0.00	0.00	0.00	0.00	0.00	0.00	0.00	0.00	0.00	0.00	0.00	0.00	0.00	0.00	0.00	0.00	0.00	0.00	0.00	0.00	0.00	0.00	0.00	0.00	0.00	0.00	0.00	0.00
	8	100	0.54	1.87	6.33	11.86	14.93	14.70	10.13	6.20	5.05	3.97	2.71	2.33	1.89	2.32	2.34	1.79	1.51	1.23	1.37	1.23	0.94	0.45	0.38	0.34	0.35	0.26	0.18	0.28	0.30	0.29	0.28	0.25	0.24	0.21	0.23	0.22	0.17	0.19	0.14
	9	0	0.19	0.50	1.54	1.59	2.11	2.66	2.64	3.08	3.24	4.23	4.54	5.59	5.79	5.32	5.43	6.26	6.08	7.18	5.77	4.49	3.00	2.30	2.24	1.64	1.83	1.59	1.38	1.46	0.99	0.91	0.65	0.60	0.50	0.44	0.39	0.39	0.57	0.50	0.39
	10	100	0.00	0.00	0.00	0.00	0.00	0.00	0.00	0.00	0.00	0.00	0.00	0.00	0.00	0.00	0.00	0.00	0.00	0.00	0.00	0.00	0.00	0.00	0.00	0.00	0.00	0.00	0.00	0.00	0.00	0.00	0.00	0.00	0.00	0.00	0.00	0.00	0.00	0.00	0.00
	11	100	0.00	0.00	0.00	0.00	0.00	0.00	0.00	0.00	0.00	0.00	0.00	0.00	0.00	0.00	0.00	0.00	0.00	0.00	0.00	0.00	0.00	0.00	0.00	0.00	0.00	0.00	0.00	0.00	0.00	0.00	0.00	0.00	0.00	0.00	0.00	0.00	0.00	0.00	0.00
	12	0	0.00	0.00	0.00	0.00	0.00	0.00	0.00	0.00	0.00	0.00	0.00	0.00	0.00	0.00	0.00	0.00	0.00	0.00	0.00	0.00	0.00	0.00	0.00	0.00	0.00	0.00	0.00	0.00	0.00	0.00	0.00	0.00	0.00	0.00	0.00	0.00	0.00	0.00	0.00
	13	0	0.00	0.00	0.00	0.00	0.00	0.00	0.00	0.00	0.00	0.00	0.00	0.00	0.00	0.00	0.00	0.00	0.00	0.00	0.00	0.00	0.00	0.00	0.00	0.00	0.00	0.00	0.00	0.00	0.00	0.00	0.00	0.00	0.00	0.00	0.00	0.00	0.00	0.00	0.00
2021_12	4	0	0.00	0.00	0.00	0.00	0.00	0.00	0.00	0.00	0.00	0.00	0.00	0.00	0.00	0.00	0.00	0.00	0.00	0.00	0.00	0.00	0.00	0.00	0.00	0.00	0.00	0.00	0.00	0.00	0.00	0.00	0.00	0.00	0.00	0.00	0.00	0.00	0.00	0.00	0.00
	5	0	0.00	0.00	0.00	0.00	0.00	0.00	0.00	0.00	0.00	0.00	0.00	0.00	0.00	0.00	0.00	0.00	0.00	0.00	0.00	0.00	0.00	0.00	0.00	0.00	0.00	0.00	0.00	0.00	0.00	0.00	0.00	0.00	0.00	0.00	0.00	0.00	0.00	0.00	0.00
	6	100	0.09	0.09	0.15	0.44	1.69	3.41	5.15	6.33	7.01	6.90	7.59	9.00	8.45	7.73	6.50	5.41	4.94	4.07	3.60	2.59	2.23	1.56	1.11	0.95	0.67	0.66	0.47	0.26	0.27	0.15	0.10	0.08	0.08	0.11	0.04	0.05	0.01	0.01	0.05
	7	0	0.00	0.00	0.00	0.00	0.00	0.00	0.00	0.00	0.00	0.00	0.00	0.00	0.00	0.00	0.00	0.00	0.00	0.00	0.00	0.00	0.00	0.00	0.00	0.00	0.00	0.00	0.00	0.00	0.00	0.00	0.00	0.00	0.00	0.00	0.00	0.00	0.00	0.00	0.00
	8	0	0.70	1.77	5.96	8.54	11.32	12.95	11.28	8.29	5.66	4.21	3.47	2.80	2.80	2.77	2.50	1.85	1.76	1.64	1.58	1.55	1.07	0.62	0.53	0.52	0.38	0.41	0.35	0.36	0.29	0.34	0.32	0.30	0.29	0.23	0.20	0.14	0.10	0.09	0.06
	9	100	0.19	0.52	1.49	2.07	2.22	2.34	2.70	2.31	2.89	3.31	4.28	6.01	4.98	4.25	4.56	6.53	6.35	6.23	5.98	5.56	4.92	3.43	2.70	2.00	1.67	1.61	1.46	1.00	1.09	0.70	0.64	0.88	0.58	0.67	0.49	0.33	0.30	0.46	0.30
	10	0	0.00	0.00	0.00	0.00	0.00	0.00	0.00	0.00	0.00	0.00	0.00	0.00	0.00	0.00	0.00	0.00	0.00	0.00	0.00	0.00	0.00	0.00	0.00	0.00	0.00	0.00	0.00	0.00	0.00	0.00	0.00	0.00	0.00	0.00	0.00	0.00	0.00	0.00	0.00
	11	100	0.00	0.00	0.00	0.00	0.00	0.00	0.00	0.00	0.00	0.00	0.00	0.00	0.00	0.00	0.00	0.00	0.00	0.00	0.00	0.00	0.00	0.00	0.00	0.00	0.00	0.00	0.00	0.00	0.00	0.00	0.00	0.00	0.00	0.00	0.00	0.00	0.00	0.00	0.00
	12	100	0.00	0.00	0.00	0.00	0.00	0.00	0.00	0.00	0.00	0.00	0.00	0.00	0.00	0.00	0.00	0.00	0.00	0.00	0.00	0.00	0.00	0.00	0.00	0.00	0.00	0.00	0.00	0.00	0.00	0.00	0.00	0.00	0.00	0.00	0.00	0.00	0.00	0.00	0.00
	13	0	0.00	0.00	0.00	0.00	0.00	0.00	0.00	0.00	0.00	0.00	0.00	0.00	0.00	0.00	0.00	0.00	0.00	0.00	0.00	0.00	0.00	0.00	0.00	0.00	0.00	0.00	0.00	0.00	0.00	0.00	0.00	0.00	0.00	0.00	0.00	0.00	0.00	0.00	0.00

Table B.2: Tandem axle load distribution factors for August, October, November, December

Month	Class	Total	12000 lb	15000 lb	18000 lb	21000 lb	24000 lb	27000 lb	30000 lb	33000 lb	36000 lb	39000 lb	42000 lb	45000 lb	48000 lb	51000 lb	54000 lb	57000 lb	60000 lb	63000 lb	66000 lb	69000 lb	72000 lb	75000 lb	78000 lb	81000 lb	84000 lb	87000 lb	90000 lb	93000 lb	96000 lb	99000 lb	102000 lb
2021_08	4	0	0.00	0.00	0.00	0.00	0.00	0.00	0.00	0.00	0.00	0.00	0.00	0.00	0.00	0.00	0.00	0.00	0.00	0.00	0.00	0.00	0.00	0.00	0.00	0.00	0.00	0.00	0.00	0.00	0.00	0.00	0.00
	5	0	0.00	0.00	0.00	0.00	0.00	0.00	0.00	0.00	0.00	0.00	0.00	0.00	0.00	0.00	0.00	0.00	0.00	0.00	0.00	0.00	0.00	0.00	0.00	0.00	0.00	0.00	0.00	0.00	0.00	0.00	0.00
	6	0	0.00	0.00	0.00	0.00	0.00	0.00	0.00	0.00	0.00	0.00	0.00	0.00	0.00	0.00	0.00	0.00	0.00	0.00	0.00	0.00	0.00	0.00	0.00	0.00	0.00	0.00	0.00	0.00	0.00	0.00	0.00
	7	0	0.00	0.00	0.00	0.00	0.00	0.00	0.00	0.00	0.00	0.00	0.00	0.00	0.00	0.00	0.00	0.00	0.00	0.00	0.00	0.00	0.00	0.00	0.00	0.00	0.00	0.00	0.00	0.00	0.00	0.00	0.00
	8	100	1.60	0.54	2.15	1.61	1.08	2.15	2.15	4.30	4.30	1.61	4.84	3.76	11.29	3.76	6.99	10.22	7.53	9.14	7.53	9.14	2.15	1.08	0.00	0.54	0.54	0.00	0.00	0.00	0.00	0.00	0.00
	9	0	0.00	0.00	0.00	0.00	0.00	0.00	0.00	0.00	0.00	0.00	0.00	0.00	0.00	0.00	0.00	0.00	0.00	0.00	0.00	0.00	0.00	0.00	0.00	0.00	0.00	0.00	0.00	0.00	0.00	0.00	0.00
	10	100	0.00	0.00	0.00	0.00	0.00	0.00	0.00	0.00	0.00	0.00	0.00	0.00	0.00	0.00	0.00	0.00	0.00	0.00	0.00	0.00	0.00	0.00	0.00	0.00	0.00	0.00	0.00	0.00	0.00	0.00	0.00
	11	100	4.24	11.82	12.92	6.52	4.30	3.64	3.45	2.78	2.50	2.49	2.78	3.19	4.22	5.92	7.53	8.58	6.52	3.49	1.19	0.53	0.35	0.30	0.24	0.13	0.13	0.08	0.07	0.05	0.02	0.01	0.01
	12	0	0.00	0.00	0.00	0.00	0.00	0.00	0.00	0.00	0.00	0.00	0.00	0.00	0.00	0.00	0.00	0.00	0.00	0.00	0.00	0.00	0.00	0.00	0.00	0.00	0.00	0.00	0.00	0.00	0.00	0.00	0.00
	13	0	0.00	0.00	0.00	0.00	0.00	0.00	0.00	0.00	0.00	0.00	0.00	0.00	0.00	0.00	0.00	0.00	0.00	0.00	0.00	0.00	0.00	0.00	0.00	0.00	0.00	0.00	0.00	0.00	0.00	0.00	0.00
2021_10	4	0	0.00	0.00	0.00	0.00	0.00	0.00	0.00	0.00	0.00	0.00	0.00	0.00	0.00	0.00	0.00	0.00	0.00	0.00	0.00	0.00	0.00	0.00	0.00	0.00	0.00	0.00	0.00	0.00	0.00	0.00	0.00
	5	0	0.00	0.00	0.00	0.00	0.00	0.00	0.00	0.00	0.00	0.00	0.00	0.00	0.00	0.00	0.00	0.00	0.00	0.00	0.00	0.00	0.00	0.00	0.00	0.00	0.00	0.00	0.00	0.00	0.00	0.00	0.00
	6	0	0.00	0.00	0.00	0.00	0.00	0.00	0.00	0.00	0.00	0.00	0.00	0.00	0.00	0.00	0.00	0.00	0.00	0.00	0.00	0.00	0.00	0.00	0.00	0.00	0.00	0.00	0.00	0.00	0.00	0.00	0.00
	7	0	0.00	0.00	0.00	0.00	0.00	0.00	0.00	0.00	0.00	0.00	0.00	0.00	0.00	0.00	0.00	0.00	0.00	0.00	0.00	0.00	0.00	0.00	0.00	0.00	0.00	0.00	0.00	0.00	0.00	0.00	0.00
	8	100	1.65	2.22	1.67	1.11	1.11	1.67	2.78	3.89	6.11	3.89	4.44	5.00	10.00	8.33	8.89	4.44	5.00	5.00	5.56	3.89	6.67	1.11	0.56	2.22	1.11	0.00	0.00	0.56	0.56	0.00	0.56
	9	0	0.00	0.00	0.00	0.00	0.00	0.00	0.00	0.00	0.00	0.00	0.00	0.00	0.00	0.00	0.00	0.00	0.00	0.00	0.00	0.00	0.00	0.00	0.00	0.00	0.00	0.00	0.00	0.00	0.00	0.00	0.00
	10	100	0.00	0.00	0.00	0.00	0.00	0.00	0.00	0.00	0.00	0.00	0.00	0.00	0.00	0.00	0.00	0.00	0.00	0.00	0.00	0.00	0.00	0.00	0.00	0.00	0.00	0.00	0.00	0.00	0.00	0.00	0.00
	11	100	3.47	10.61	11.75	6.04	4.54	4.31	4.19	3.56	3.15	2.89	3.15	3.59	4.51	5.66	7.05	7.74	6.46	3.35	1.45	0.75	0.49	0.40	0.32	0.26	0.13	0.07	0.06	0.02	0.01	0.01	0.01
	12	0	0.00	0.00	0.00	0.00	0.00	0.00	0.00	0.00	0.00	0.00	0.00	0.00	0.00	0.00	0.00	0.00	0.00	0.00	0.00	0.00	0.00	0.00	0.00	0.00	0.00	0.00	0.00	0.00	0.00	0.00	0.00
	13	0	0.00	0.00	0.00	0.00	0.00	0.00	0.00	0.00	0.00	0.00	0.00	0.00	0.00	0.00	0.00	0.00	0.00	0.00	0.00	0.00	0.00	0.00	0.00	0.00	0.00	0.00	0.00	0.00	0.00	0.00	0.00
2021_11	4	0	0.00	0.00	0.00	0.00	0.00	0.00	0.00	0.00	0.00	0.00	0.00	0.00	0.00	0.00	0.00	0.00	0.00	0.00	0.00	0.00	0.00	0.00	0.00	0.00	0.00	0.00	0.00	0.00	0.00	0.00	0.00
	5	0	0.00	0.00	0.00	0.00	0.00	0.00	0.00	0.00	0.00	0.00	0.00	0.00	0.00	0.00	0.00	0.00	0.00	0.00	0.00	0.00	0.00	0.00	0.00	0.00	0.00	0.00	0.00	0.00	0.00	0.00	0.00
	6	0	0.00	0.00	0.00	0.00	0.00	0.00	0.00	0.00	0.00	0.00	0.00	0.00	0.00	0.00	0.00	0.00	0.00	0.00	0.00	0.00	0.00	0.00	0.00	0.00	0.00	0.00	0.00	0.00	0.00	0.00	0.00
	7	0	0.00	0.00	0.00	0.00	0.00	0.00	0.00	0.00	0.00	0.00	0.00	0.00	0.00	0.00	0.00	0.00	0.00	0.00	0.00	0.00	0.00	0.00	0.00	0.00	0.00	0.00	0.00	0.00	0.00	0.00	0.00
	8	100	0.00	0.54	0.56	0.56	1.68	2.23	8.38	4.47	7.26	1.12	5.59	6.15	9.50	7.82	8.94	8.38	5.03	3.35	3.91	3.35	4.47	0.00	2.79	1.68	1.12	0.56	0.56	0.00	0.00	0.00	0.00
	9	0	0.00	0.00	0.00	0.00	0.00	0.00	0.00	0.00	0.00	0.00	0.00	0.00	0.00	0.00	0.00	0.00	0.00	0.00	0.00	0.00	0.00	0.00	0.00	0.00	0.00	0.00	0.00	0.00	0.00	0.00	0.00
	10	100	0.00	0.00	0.00	0.00	0.00	0.00	0.00	0.00	0.00	0.00	0.00	0.00	0.00	0.00	0.00	0.00	0.00	0.00	0.00	0.00	0.00	0.00	0.00	0.00	0.00	0.00	0.00	0.00	0.00	0.00	0.00
	11	100	3.60	10.76	10.56	5.63	4.68	4.69	4.50	3.79	3.14	3.07	3.47	4.18	5.15	6.43	7.04	7.18	5.82	2.98	1.25	0.57	0.36	0.35	0.30	0.18	0.14	0.10	0.03	0.01	0.02	0.01	0.01
	12	0	0.00	0.00	0.00	0.00	0.00	0.00	0.00	0.00	0.00	0.00	0.00	0.00	0.00	0.00	0.00	0.00	0.00	0.00	0.00	0.00	0.00	0.00	0.00	0.00	0.00	0.00	0.00	0.00	0.00	0.00	0.00
	13	0	0.00	0.00	0.00	0.00	0.00	0.00	0.00	0.00	0.00	0.00	0.00	0.00	0.00	0.00	0.00	0.00	0.00	0.00	0.00	0.00	0.00	0.00	0.00	0.00	0.00	0.00	0.00	0.00	0.00	0.00	0.00
2021_12	4	0	0.00	0.00	0.00	0.00	0.00	0.00	0.00	0.00	0.00	0.00	0.00	0.00	0.00	0.00	0.00	0.00	0.00	0.00	0.00	0.00	0.00	0.00	0.00	0.00	0.00	0.00	0.00	0.00	0.00	0.00	0.00
	5	0	0.00	0.00	0.00	0.00	0.00	0.00	0.00	0.00	0.00	0.00	0.00	0.00	0.00	0.00	0.00	0.00	0.00	0.00	0.00	0.00	0.00	0.00	0.00	0.00	0.00	0.00	0.00	0.00	0.00	0.00	0.00
	6	0	0.00	0.00	0.00	0.00	0.00	0.00	0.00	0.00	0.00	0.00	0.00	0.00	0.00	0.00	0.00	0.00	0.00	0.00	0.00	0.00	0.00	0.00	0.00	0.00	0.00	0.00	0.00	0.00	0.00	0.00	0.00
	7	0	0.00	0.00	0.00	0.00	0.00	0.00	0.00	0.00	0.00	0.00	0.00	0.00	0.00	0.00	0.00	0.00	0.00	0.00	0.00	0.00	0.00	0.00	0.00	0.00	0.00	0.00	0.00	0.00	0.00	0.00	0.00
	8	100	0.98	1.52	0.00	0.51	3.54	3.03	3.03	2.02	6.06	5.05	4.04	2.02	4.04	4.04	5.05	10.61	7.07	4.55	7.07	6.06	2.02	4.04	2.53	3.54	4.04	2.02	1.01	0.51	0.00	0.00	0.00
	9	0	0.00	0.00	0.00	0.00	0.00	0.00	0.00	0.00	0.00	0.00	0.00	0.00	0.00	0.00	0.00	0.00	0.00	0.00	0.00	0.00	0.00	0.00	0.00	0.00	0.00	0.00	0.00	0.00	0.00	0.00	0.00
	10	100	0.00	0.00	0.00	0.00	0.00	0.00	0.00	0.00	0.00	0.00	0.00	0.00	0.00	0.00	0.00	0.00	0.00	0.00	0.00	0.00	0.00	0.00	0.00	0.00	0.00	0.00	0.00	0.00	0.00	0.00	0.00
	11	100	3.23	8.83	10.02	6.84	5.15	4.46	4.34	3.97	3.74	3.46	3.80	4.83	6.10	6.83	6.27	5.91	4.52	3.37	2.05	0.88	0.41	0.24	0.23	0.16	0.14	0.08	0.06	0.04	0.02	0.01	0.01
	12	0	0.00	0.00	0.00	0.00	0.00	0.00	0.00	0.00	0.00	0.00	0.00	0.00	0.00	0.00	0.00	0.00	0.00	0.00	0.00	0.00	0.00	0.00	0.00	0.00	0.00	0.00	0.00	0.00	0.00	0.00	0.00
	13	0	0.00	0.00	0.00	0.00	0.00	0.00	0.00	0.00	0.00	0.00	0.00	0.00	0.00	0.00	0.00	0.00	0.00	0.00	0.00	0.00	0.00	0.00	0.00	0.00	0.00	0.00	0.00	0.00	0.00	0.00	0.00

Table B.3: Tridem axle load distribution factors for August, October, November, December

B.2 Axle load distributions for the SS45bis highway in Trento

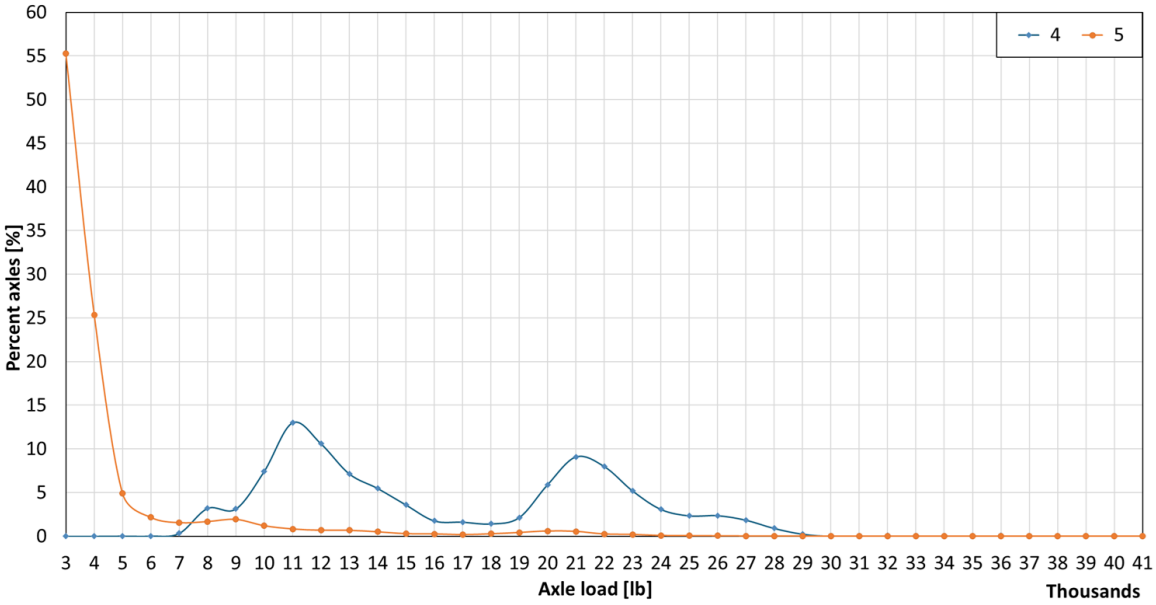

Figure B.15: Single axle load distributions of vehicle classes 4 and 5 – November

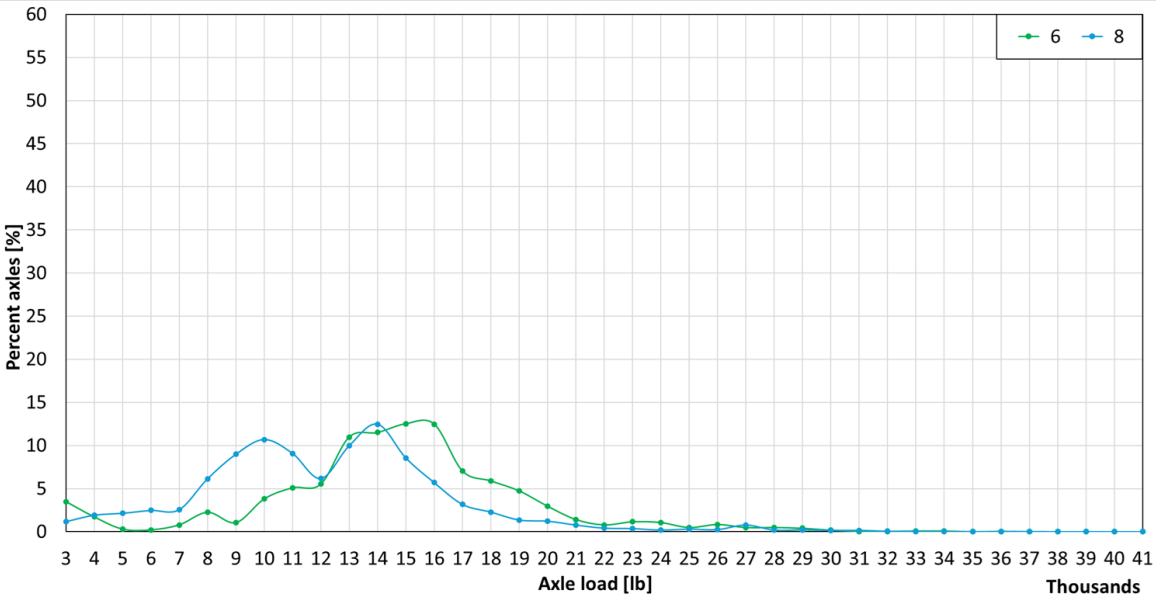

Figure B.16: Single axle load distributions of vehicle classes 6 and 8 – November

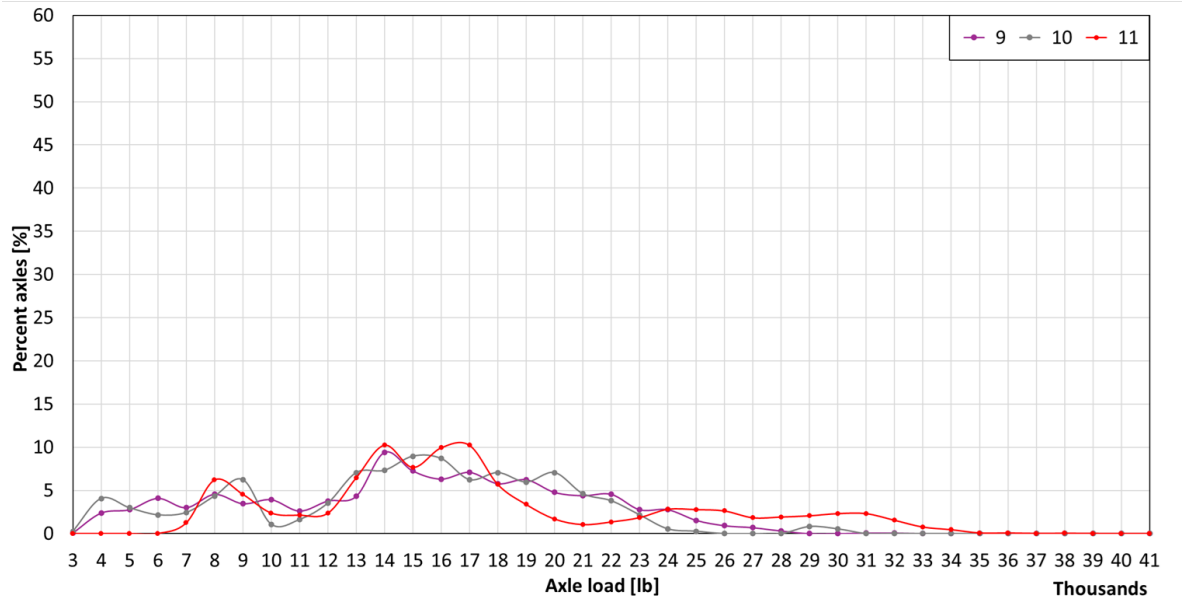

Figure B.17: Single axle load distributions of vehicle classes 9, 10, and 11 – November

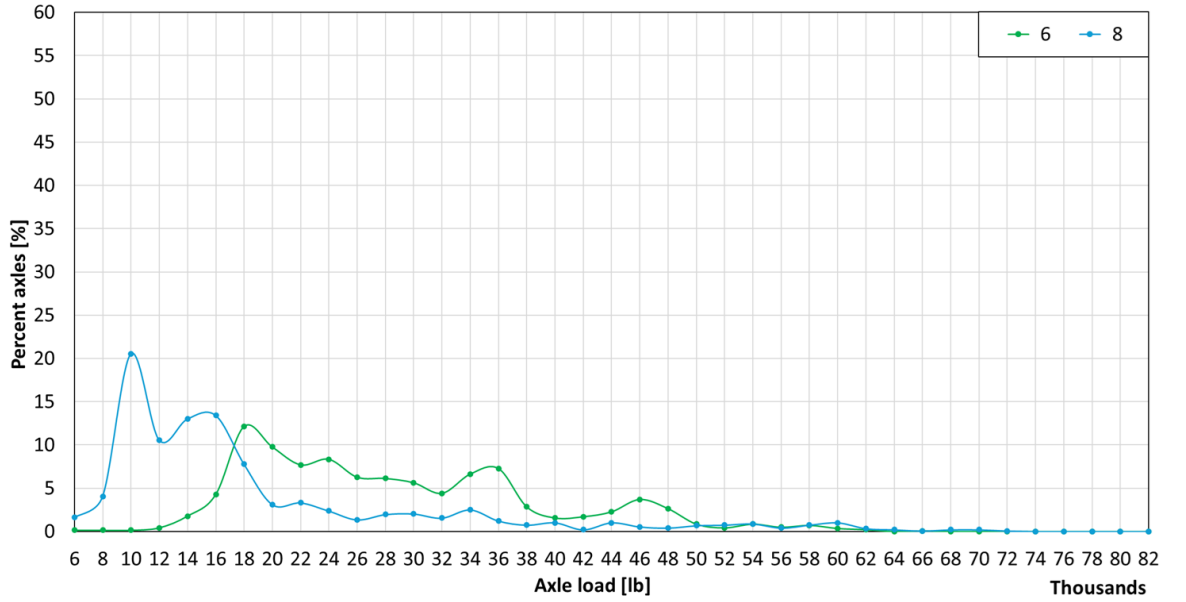

Figure B.18: Tandem axle load distributions of vehicle classes 6 and 8 – November

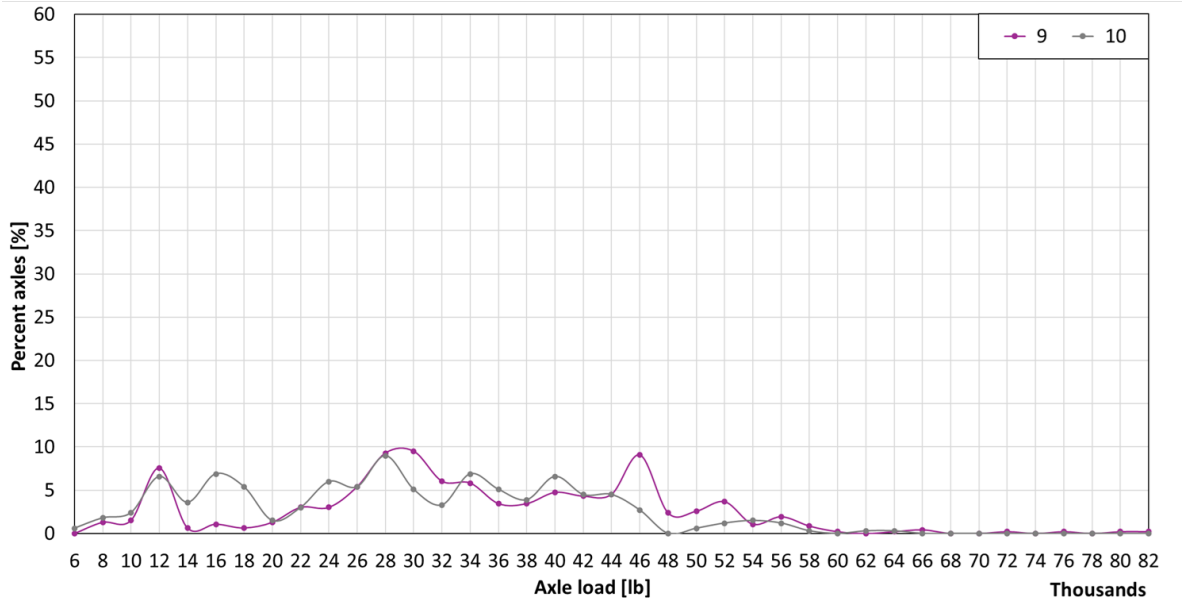

Figure B.19: Tandem axle load distributions of vehicle classes 9 and 10 – November

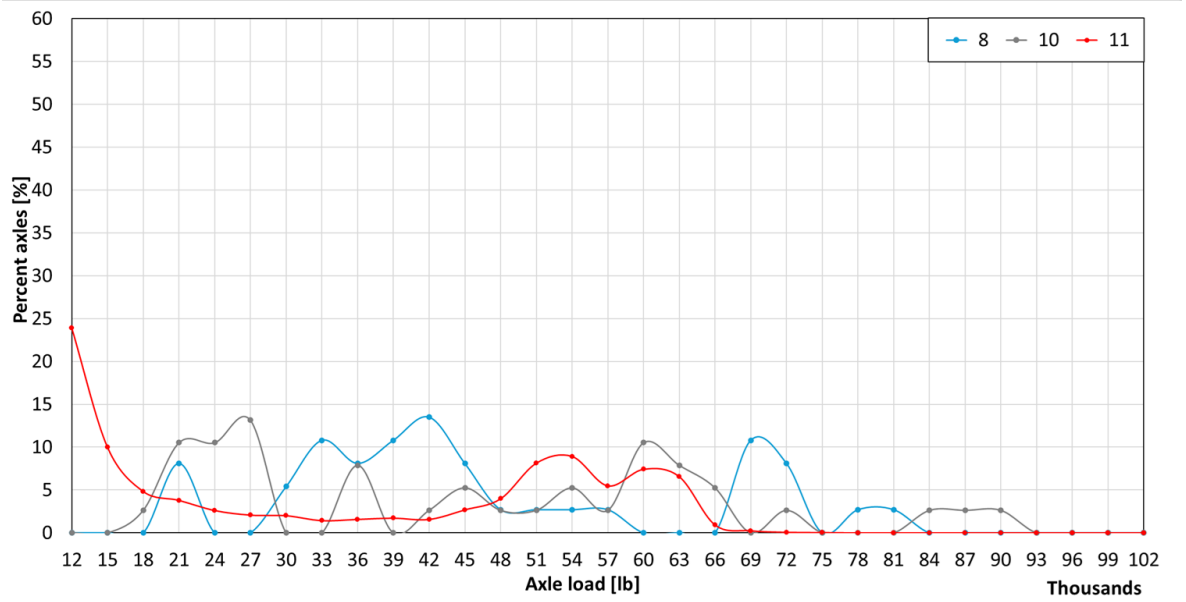

Figure B.20: Tridem axle load distributions – November

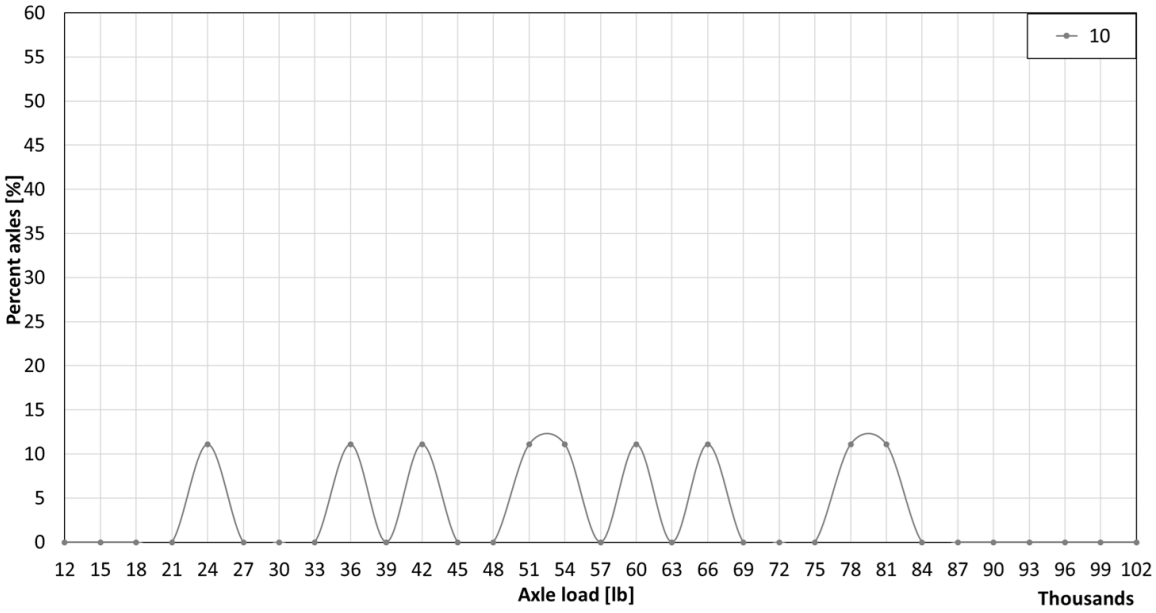

Figure B.21: Quad axle load distribution – November

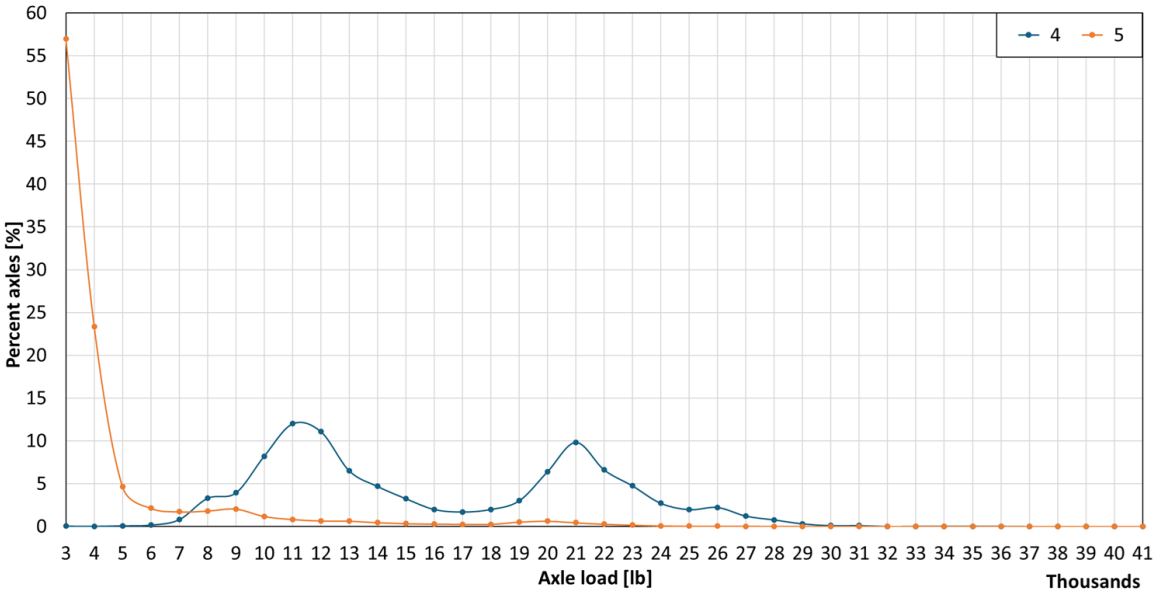

Figure B.22: Single axle load distributions of vehicle classes 4 and 5 – December

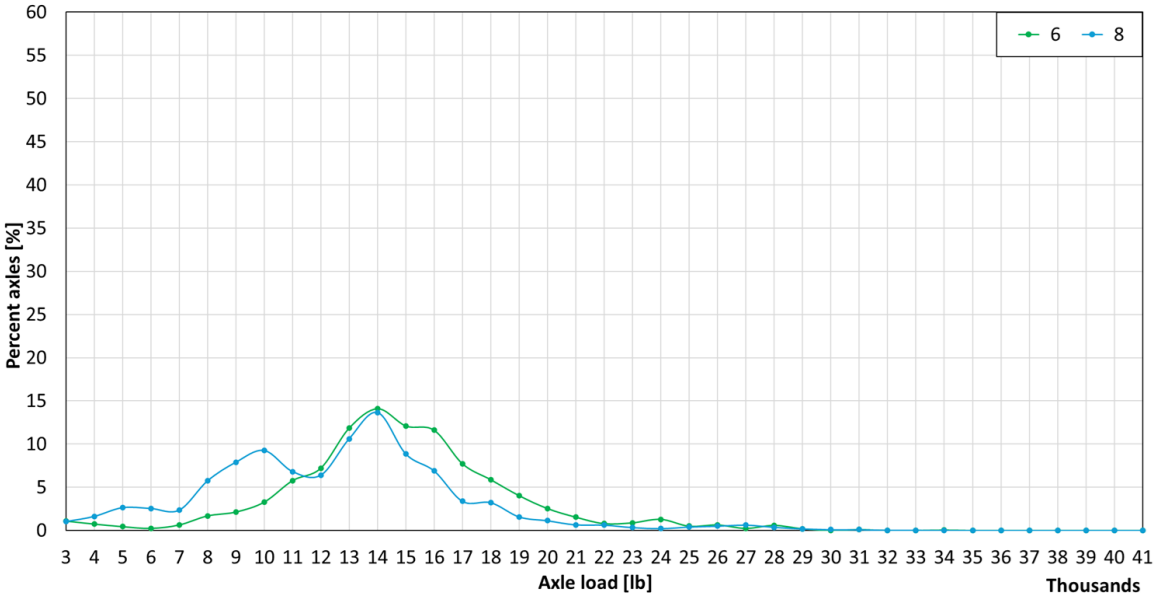

Figure B.23: Single axle load distributions of vehicle classes 6 and 8 – December

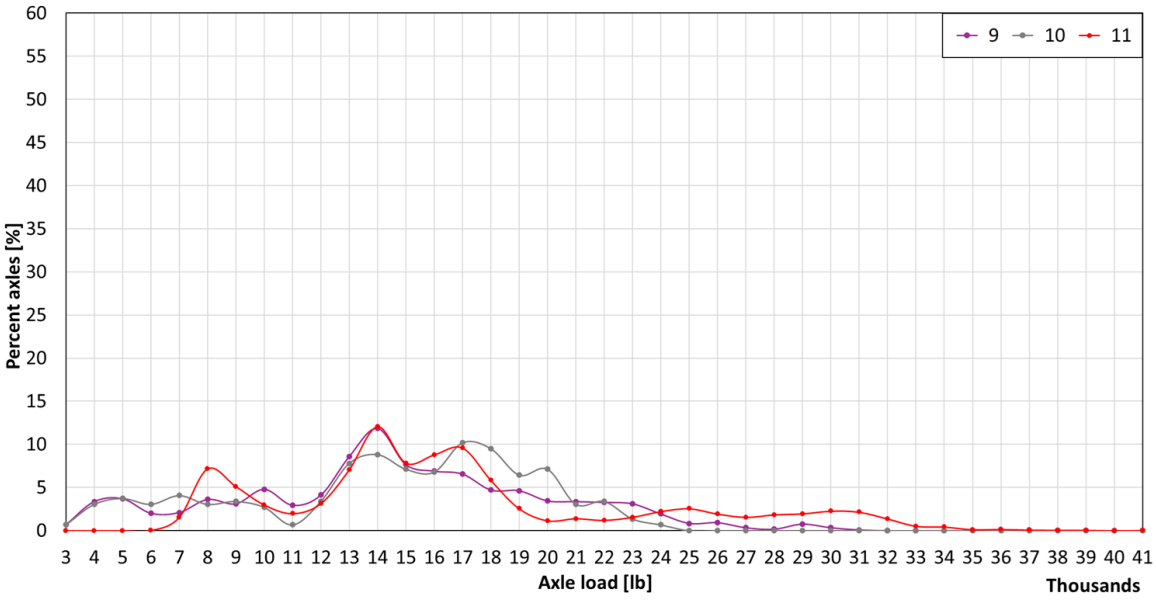

Figure B.24: Single axle load distributions of vehicle classes 9, 10, and 11 – December

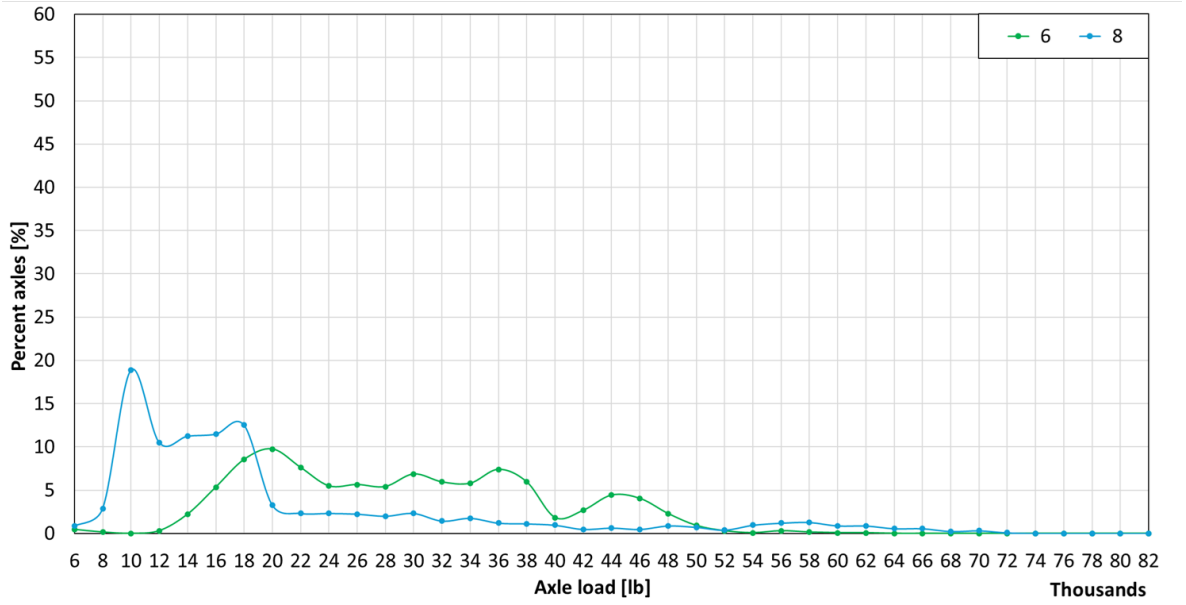

Figure B.25: Tandem axle load distributions of vehicle classes 6 and 8 – December

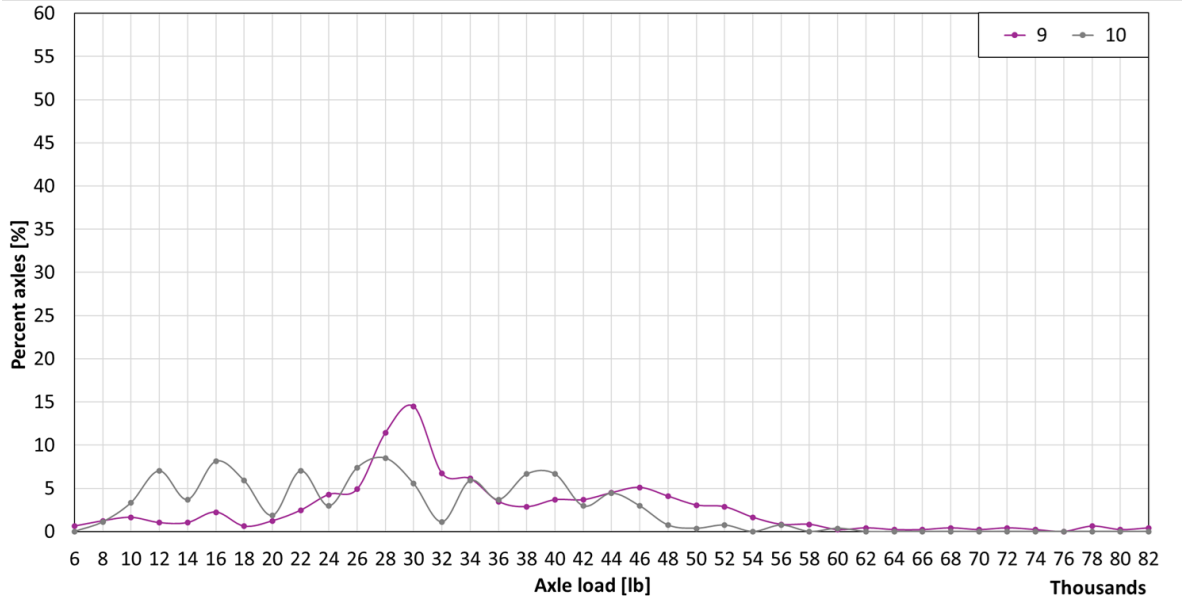

Figure B.26: Tandem axle load distributions of vehicle classes 9 and 10 – December

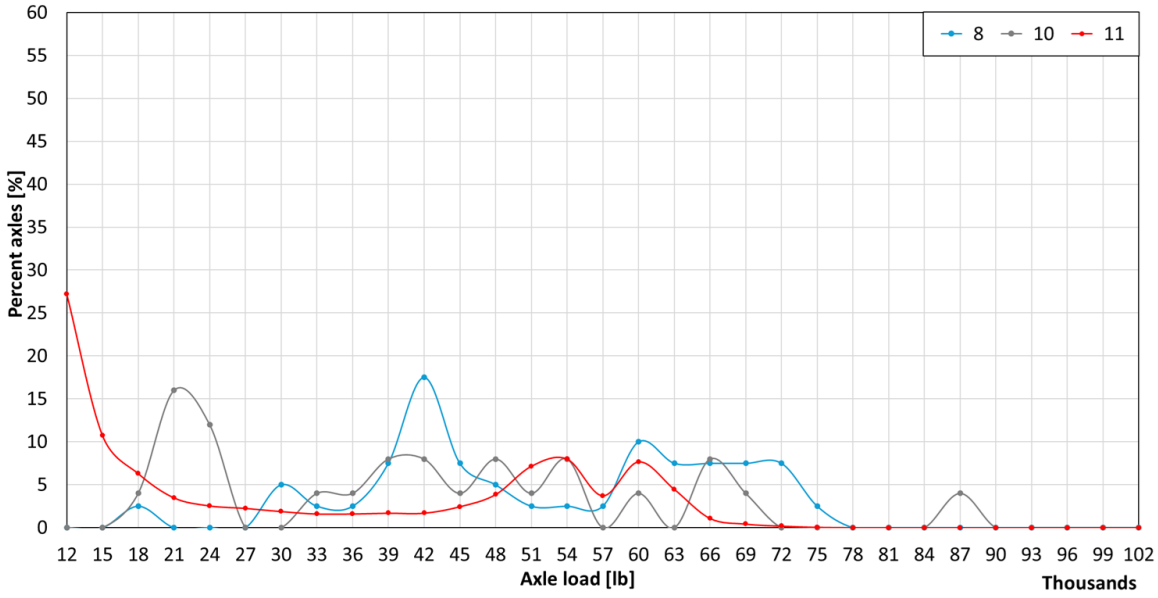

Figure B.27: Tridem axle load distributions – December

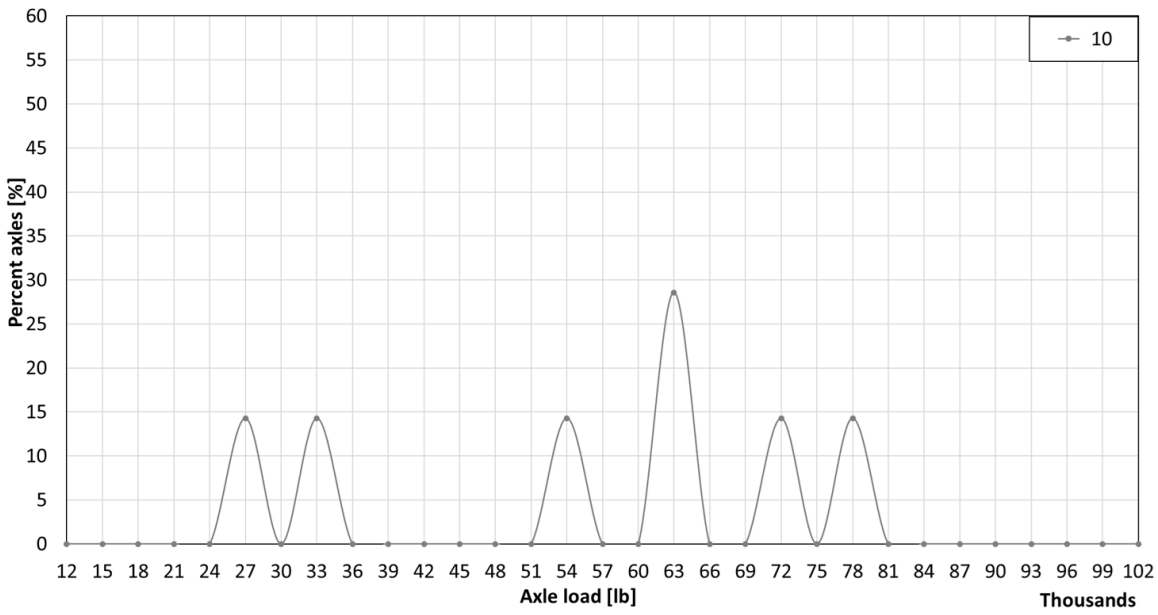

Figure B.28: Quad axle load distribution – December

Month	Class	Total	3000 lb	4000 lb	5000 lb	6000 lb	7000 lb	8000 lb	9000 lb	10000 lb	11000 lb	12000 lb	13000 lb	14000 lb	15000 lb	16000 lb	17000 lb	18000 lb	19000 lb	20000 lb	21000 lb	22000 lb	23000 lb	24000 lb	25000 lb	26000 lb	27000 lb	28000 lb	29000 lb	30000 lb	31000 lb	32000 lb	33000 lb	34000 lb	35000 lb	36000 lb	37000 lb	38000 lb	39000 lb	40000 lb	41000 lb
2025_10	4	100	0.00	0.00	0.05	0.05	0.22	2.76	3.51	6.12	10.69	11.92	8.43	5.61	3.60	2.34	2.12	1.28	1.61	4.55	9.07	8.88	4.94	3.47	2.39	2.08	2.07	1.57	0.37	0.13	0.04	0.02	0.05	0.02	0.04	0.00	0.00	0.00	0.00	0.00	0.00
	5	100	54.16	27.73	5.77	2.10	1.32	1.29	1.76	1.02	0.68	0.54	0.54	0.46	0.28	0.20	0.16	0.18	0.36	0.57	0.34	0.19	0.14	0.08	0.05	0.03	0.02	0.01	0.01	0.01	0.00	0.00	0.00	0.00	0.00	0.00	0.00	0.00	0.00	0.00	0.00
	6	100	6.61	3.98	1.27	0.65	0.69	1.70	1.27	2.35	4.51	5.62	8.98	12.05	11.40	11.10	7.84	7.02	4.18	2.48	1.11	0.91	0.59	1.11	0.82	0.49	0.42	0.33	0.36	0.10	0.00	0.03	0.00	0.03	0.00	0.00	0.00	0.00	0.00	0.00	0.00
	7	0	0.00	0.00	0.00	0.00	0.00	0.00	0.00	0.00	0.00	0.00	0.00	0.00	0.00	0.00	0.00	0.00	0.00	0.00	0.00	0.00	0.00	0.00	0.00	0.00	0.00	0.00	0.00	0.00	0.00	0.00	0.00	0.00	0.00	0.00	0.00	0.00	0.00	0.00	0.00
	8	100	0.89	1.33	1.69	2.69	1.64	4.27	12.22	13.46	12.10	7.31	6.38	10.74	7.88	5.50	3.62	2.60	1.36	0.83	0.71	0.45	0.36	0.26	0.29	0.24	0.21	0.29	0.21	0.10	0.12	0.19	0.02	0.02	0.02	0.00	0.00	0.00	0.00	0.00	0.00
	9	100	0.04	2.05	3.57	3.24	3.11	3.83	3.30	3.70	3.44	2.25	4.76	10.38	7.80	6.28	7.47	7.60	5.16	4.03	3.44	5.16	4.10	1.72	1.52	0.86	0.40	0.33	0.13	0.26	0.07	0.00	0.00	0.00	0.00	0.00	0.00	0.00	0.00	0.00	0.00
	10	100	0.60	3.08	3.64	2.24	4.20	4.76	4.76	1.96	1.68	3.36	3.64	5.88	9.52	6.44	10.08	10.08	3.64	7.56	4.20	3.64	2.24	0.84	0.28	0.56	0.00	0.28	0.56	0.00	0.00	0.00	0.00	0.00	0.00	0.00	0.00	0.28	0.00	0.00	0.00
	11	100	0.00	0.00	0.09	0.14	1.15	6.36	5.28	2.88	2.02	2.41	4.92	11.04	7.91	8.64	10.12	7.30	2.81	1.12	1.06	1.18	1.69	2.30	2.71	2.94	2.45	2.30	1.49	1.77	2.50	2.07	0.83	0.33	0.07	0.07	0.03	0.01	0.01	0.00	0.00
	12	0	0.00	0.00	0.00	0.00	0.00	0.00	0.00	0.00	0.00	0.00	0.00	0.00	0.00	0.00	0.00	0.00	0.00	0.00	0.00	0.00	0.00	0.00	0.00	0.00	0.00	0.00	0.00	0.00	0.00	0.00	0.00	0.00	0.00	0.00	0.00	0.00	0.00	0.00	0.00
	13	0	0.00	0.00	0.00	0.00	0.00	0.00	0.00	0.00	0.00	0.00	0.00	0.00	0.00	0.00	0.00	0.00	0.00	0.00	0.00	0.00	0.00	0.00	0.00	0.00	0.00	0.00	0.00	0.00	0.00	0.00	0.00	0.00	0.00	0.00	0.00	0.00	0.00	0.00	0.00
2025_11	4	100	0.00	0.00	0.03	0.02	0.33	3.19	3.12	7.42	12.99	10.60	7.15	5.49	3.60	1.77	1.62	1.42	2.14	5.90	9.08	7.99	5.20	3.08	2.34	2.36	1.85	0.90	0.25	0.00	0.02	0.04	0.00	0.02	0.00	0.04	0.02	0.00	0.00	0.02	0.00
	5	100	55.28	25.38	4.89	2.16	1.55	1.67	1.92	1.20	0.82	0.68	0.67	0.50	0.29	0.26	0.18	0.27	0.42	0.60	0.55	0.25	0.20	0.08	0.06	0.04	0.03	0.03	0.01	0.00	0.01	0.00	0.00	0.00	0.00	0.00	0.00	0.00	0.00	0.00	0.00
	6	100	3.49	1.73	0.31	0.22	0.80	2.26	1.06	3.81	5.09	5.53	10.97	11.50	12.52	12.48	7.04	5.88	4.73	2.96	1.42	0.80	1.15	1.06	0.49	0.84	0.49	0.49	0.40	0.18	0.04	0.04	0.09	0.09	0.00	0.04	0.00	0.00	0.00	0.00	0.00
	7	0	0.00	0.00	0.00	0.00	0.00	0.00	0.00	0.00	0.00	0.00	0.00	0.00	0.00	0.00	0.00	0.00	0.00	0.00	0.00	0.00	0.00	0.00	0.00	0.00	0.00	0.00	0.00	0.00	0.00	0.00	0.00	0.00	0.00	0.00	0.00	0.00	0.00	0.00	0.00
	8	100	1.14	1.92	2.14	2.47	2.56	6.14	8.97	10.70	9.09	6.17	9.97	12.48	8.56	5.70	3.17	2.28	1.36	1.22	0.78	0.42	0.36	0.19	0.31	0.25	0.78	0.19	0.22	0.17	0.17	0.06	0.03	0.00	0.00	0.00	0.03	0.00	0.00	0.00	0.00
	9	100	0.05	2.39	2.78	4.09	3.01	4.55	3.47	3.93	2.62	3.78	4.32	9.41	7.25	6.32	7.09	5.78	6.25	4.78	4.39	4.55	2.78	2.78	1.54	0.93	0.69	0.31	0.00	0.00	0.08	0.08	0.00	0.00	0.00	0.00	0.00	0.00	0.00	0.00	0.00
	10	100	0.25	4.08	2.99	2.17	2.45	4.35	6.25	1.09	1.63	3.53	7.07	7.34	8.97	8.70	6.25	7.07	5.98	7.07	4.62	3.80	2.17	0.54	0.27	0.00	0.00	0.00	0.82	0.54	0.00	0.00	0.00	0.00	0.00	0.00	0.00	0.00	0.00	0.00	0.00
	11	100	0.00	0.00	0.00	0.00	1.24	6.22	4.55	2.38	2.13	2.36	6.47	10.25	7.67	9.94	10.23	5.68	3.37	1.68	1.04	1.34	1.85	2.81	2.78	2.62	1.83	1.92	2.06	2.31	2.31	1.54	0.75	0.45	0.07	0.07	0.02	0.04	0.02	0.00	0.00
	12	0	0.00	0.00	0.00	0.00	0.00	0.00	0.00	0.00	0.00	0.00	0.00	0.00	0.00	0.00	0.00	0.00	0.00	0.00	0.00	0.00	0.00	0.00	0.00	0.00	0.00	0.00	0.00	0.00	0.00	0.00	0.00	0.00	0.00	0.00	0.00	0.00	0.00	0.00	0.00
	13	0	0.00	0.00	0.00	0.00	0.00	0.00	0.00	0.00	0.00	0.00	0.00	0.00	0.00	0.00	0.00	0.00	0.00	0.00	0.00	0.00	0.00	0.00	0.00	0.00	0.00	0.00	0.00	0.00	0.00	0.00	0.00	0.00	0.00	0.00	0.00	0.00	0.00	0.00	0.00
2025_12	4	100	0.03	0.02	0.08	0.17	0.80	3.30	3.93	8.22	12.01	11.10	6.52	4.69	3.26	2.00	1.70	2.00	3.01	6.41	9.84	6.62	4.75	2.71	1.98	2.23	1.22	0.78	0.32	0.11	0.11	0.00	0.02	0.02	0.02	0.02	0.00	0.00	0.00	0.00	0.00
	5	100	56.99	23.37	4.65	2.14	1.72	1.82	2.05	1.18	0.83	0.66	0.64	0.46	0.34	0.29	0.27	0.27	0.53	0.63	0.45	0.27	0.17	0.08	0.04	0.04	0.03	0.03	0.02	0.01	0.01	0.01	0.00	0.00	0.00	0.00	0.00	0.00	0.00	0.00	0.00
	6	100	1.09	0.75	0.45	0.25	0.65	1.69	2.14	3.29	5.78	7.22	11.85	14.09	12.10	11.60	7.72	5.88	4.03	2.54	1.54	0.80	0.90	1.29	0.50	0.65	0.25	0.60	0.20	0.00	0.10	0.00	0.00	0.05	0.00	0.00	0.00	0.00	0.00	0.00	0.00
	7	0	0.00	0.00	0.00	0.00	0.00	0.00	0.00	0.00	0.00	0.00	0.00	0.00	0.00	0.00	0.00	0.00	0.00	0.00	0.00	0.00	0.00	0.00	0.00	0.00	0.00	0.00	0.00	0.00	0.00	0.00	0.00	0.00	0.00	0.00	0.00	0.00	0.00	0.00	0.00
	8	100	1.07	1.64	2.65	2.56	2.37	5.75	7.90	9.26	6.83	6.42	10.62	13.65	8.85	6.89	3.38	3.22	1.58	1.14	0.66	0.63	0.35	0.22	0.41	0.51	0.63	0.38	0.19	0.09	0.09	0.03	0.03	0.00	0.00	0.00	0.00	0.00	0.00	0.00	0.00
	9	100	0.67	3.37	3.70	2.02	2.10	3.62	3.11	4.80	2.95	4.12	8.59	11.87	7.66	6.90	6.57	4.71	4.63	3.45	3.37	3.28	3.11	1.94	0.84	0.93	0.34	0.17	0.76	0.34	0.08	0.00	0.00	0.00	0.00	0.00	0.00	0.00	0.00	0.00	0.00
	10	100	0.67	3.05	3.73	3.05	4.07	3.05	3.39	2.71	0.68	3.39	7.80	8.81	7.12	6.78	10.17	9.49	6.44	7.12	3.05	3.39	1.36	0.68	0.00	0.00	0.00	0.00	0.00	0.00	0.00	0.00	0.00	0.00	0.00	0.00	0.00	0.00	0.00	0.00	0.00
	11	100	0.00	0.00	0.00	0.03	1.53	7.15	5.13	2.99	1.98	3.13	7.03	12.04	7.83	8.77	9.57	5.83	2.54	1.15	1.39	1.20	1.55	2.21	2.54	1.93	1.55	1.83	1.95	2.26	2.14	1.36	0.52	0.42	0.12	0.14	0.07	0.05	0.05	0.00	0.02
	12	0	0.00	0.00	0.00	0.00	0.00	0.00	0.00	0.00	0.00	0.00	0.00	0.00	0.00	0.00	0.00	0.00	0.00	0.00	0.00	0.00	0.00	0.00	0.00	0.00	0.00	0.00	0.00	0.00	0.00	0.00	0.00	0.00	0.00	0.00	0.00	0.00	0.00	0.00	0.00
	13	0	0.00	0.00	0.00	0.00	0.00	0.00	0.00	0.00	0.00	0.00	0.00	0.00	0.00	0.00	0.00	0.00	0.00	0.00	0.00	0.00	0.00	0.00	0.00	0.00	0.00	0.00	0.00	0.00	0.00	0.00	0.00	0.00	0.00	0.00	0.00	0.00	0.00	0.00	0.00

Table B.4: Single axle load distribution factors for October, November, December

Month	Class	Total	6000 lb	8000 lb	10000 lb	12000 lb	14000 lb	16000 lb	18000 lb	20000 lb	22000 lb	24000 lb	26000 lb	28000 lb	30000 lb	32000 lb	34000 lb	36000 lb	38000 lb	40000 lb	42000 lb	44000 lb	46000 lb	48000 lb	50000 lb	52000 lb	54000 lb	56000 lb	58000 lb	60000 lb	62000 lb	64000 lb	66000 lb	68000 lb	70000 lb	72000 lb	74000 lb	76000 lb	78000 lb	80000 lb	82000 lb
2025_10	4	0	0.00	0.00	0.00	0.00	0.00	0.00	0.00	0.00	0.00	0.00	0.00	0.00	0.00	0.00	0.00	0.00	0.00	0.00	0.00	0.00	0.00	0.00	0.00	0.00	0.00	0.00	0.00	0.00	0.00	0.00	0.00	0.00	0.00	0.00	0.00	0.00	0.00	0.00	0.00
	5	0	0.00	0.00	0.00	0.00	0.00	0.00	0.00	0.00	0.00	0.00	0.00	0.00	0.00	0.00	0.00	0.00	0.00	0.00	0.00	0.00	0.00	0.00	0.00	0.00	0.00	0.00	0.00	0.00	0.00	0.00	0.00	0.00	0.00	0.00	0.00	0.00	0.00	0.00	0.00
	6	100	0.48	0.65	0.05	0.27	1.94	4.64	8.80	8.96	8.31	6.91	7.18	6.15	6.15	6.48	6.04	5.99	3.35	2.16	1.35	3.02	3.13	2.86	0.92	0.49	0.43	0.81	1.13	0.70	0.54	0.11	0.00	0.00	0.00	0.00	0.00	0.00	0.00	0.00	0.00
	7	0	0.00	0.00	0.00	0.00	0.00	0.00	0.00	0.00	0.00	0.00	0.00	0.00	0.00	0.00	0.00	0.00	0.00	0.00	0.00	0.00	0.00	0.00	0.00	0.00	0.00	0.00	0.00	0.00	0.00	0.00	0.00	0.00	0.00	0.00	0.00	0.00	0.00	0.00	0.00
	8	100	1.36	2.68	13.82	9.43	17.66	17.90	10.39	4.08	1.96	1.56	1.60	2.00	1.44	2.00	1.32	1.08	0.72	0.56	0.36	0.36	0.52	0.40	0.56	0.52	1.32	1.04	1.00	0.96	0.44	0.36	0.36	0.12	0.08	0.04	0.00	0.00	0.00	0.00	0.00
	9	100	0.00	1.54	4.85	1.73	0.52	1.21	0.69	0.87	2.60	3.29	3.47	6.24	14.21	6.76	4.33	2.95	5.37	4.51	4.51	5.72	7.80	5.55	2.77	1.39	1.91	0.69	0.69	0.69	0.00	0.35	0.35	0.52	0.17	0.35	0.00	0.35	0.35	0.35	0.35
	10	100	0.00	1.87	4.75	7.59	2.85	5.38	5.06	1.27	2.53	4.43	5.70	11.71	5.70	2.85	5.70	5.38	4.43	6.65	4.75	1.90	4.11	0.32	0.63	0.95	0.95	0.32	0.32	0.63	0.63	0.00	0.32	0.00	0.32	0.00	0.00	0.00	0.00	0.00	0.00
	11	0	0.00	0.00	0.00	0.00	0.00	0.00	0.00	0.00	0.00	0.00	0.00	0.00	0.00	0.00	0.00	0.00	0.00	0.00	0.00	0.00	0.00	0.00	0.00	0.00	0.00	0.00	0.00	0.00	0.00	0.00	0.00	0.00	0.00	0.00	0.00	0.00	0.00	0.00	0.00
	12	0	0.00	0.00	0.00	0.00	0.00	0.00	0.00	0.00	0.00	0.00	0.00	0.00	0.00	0.00	0.00	0.00	0.00	0.00	0.00	0.00	0.00	0.00	0.00	0.00	0.00	0.00	0.00	0.00	0.00	0.00	0.00	0.00	0.00	0.00	0.00	0.00	0.00	0.00	0.00
	13	0	0.00	0.00	0.00	0.00	0.00	0.00	0.00	0.00	0.00	0.00	0.00	0.00	0.00	0.00	0.00	0.00	0.00	0.00	0.00	0.00	0.00	0.00	0.00	0.00	0.00	0.00	0.00	0.00	0.00	0.00	0.00	0.00	0.00	0.00	0.00	0.00	0.00	0.00	0.00
2025_11	4	0	0.00	0.00	0.00	0.00	0.00	0.00	0.00	0.00	0.00	0.00	0.00	0.00	0.00	0.00	0.00	0.00	0.00	0.00	0.00	0.00	0.00	0.00	0.00	0.00	0.00	0.00	0.00	0.00	0.00	0.00	0.00	0.00	0.00	0.00	0.00	0.00	0.00	0.00	0.00
	5	0	0.00	0.00	0.00	0.00	0.00	0.00	0.00	0.00	0.00	0.00	0.00	0.00	0.00	0.00	0.00	0.00	0.00	0.00	0.00	0.00	0.00	0.00	0.00	0.00	0.00	0.00	0.00	0.00	0.00	0.00	0.00	0.00	0.00	0.00	0.00	0.00	0.00	0.00	0.00
	6	100	0.15	0.14	0.14	0.43	1.78	4.28	12.13	9.77	7.70	8.35	6.28	6.13	5.63	4.42	6.63	7.28	2.85	1.57	1.71	2.28	3.71	2.64	0.86	0.43	0.86	0.50	0.71	0.36	0.21	0.00	0.07	0.00	0.00	0.00	0.00	0.00	0.00	0.00	0.00
	7	0	0.00	0.00	0.00	0.00	0.00	0.00	0.00	0.00	0.00	0.00	0.00	0.00	0.00	0.00	0.00	0.00	0.00	0.00	0.00	0.00	0.00	0.00	0.00	0.00	0.00	0.00	0.00	0.00	0.00	0.00	0.00	0.00	0.00	0.00	0.00	0.00	0.00	0.00	0.00
	8	100	1.60	4.07	20.54	10.58	13.02	13.42	7.80	3.12	3.32	2.37	1.36	1.97	2.03	1.56	2.51	1.22	0.75	1.02	0.20	1.02	0.54	0.41	0.68	0.75	0.88	0.41	0.75	1.02	0.34	0.20	0.07	0.20	0.20	0.07	0.00	0.00	0.00	0.00	0.00
	9	100	0.00	1.27	1.51	7.56	0.65	1.08	0.65	1.30	3.02	3.02	5.40	9.29	9.50	6.05	5.83	3.46	3.46	4.75	4.32	4.54	9.07	2.38	2.59	3.67	1.08	1.94	0.86	0.22	0.00	0.22	0.43	0.00	0.00	0.22	0.00	0.22	0.00	0.22	0.22
	10	100	0.58	1.80	2.40	6.59	3.59	6.89	5.39	1.50	2.99	5.99	5.39	8.98	5.09	3.29	6.89	5.09	3.89	6.59	4.49	4.49	2.69	0.00	0.60	1.20	1.50	1.20	0.30	0.00	0.30	0.30	0.00	0.00	0.00	0.00	0.00	0.00	0.00	0.00	0.00
	11	0	0.00	0.00	0.00	0.00	0.00	0.00	0.00	0.00	0.00	0.00	0.00	0.00	0.00	0.00	0.00	0.00	0.00	0.00	0.00	0.00	0.00	0.00	0.00	0.00	0.00	0.00	0.00	0.00	0.00	0.00	0.00	0.00	0.00	0.00	0.00	0.00	0.00	0.00	0.00
	12	0	0.00	0.00	0.00	0.00	0.00	0.00	0.00	0.00	0.00	0.00	0.00	0.00	0.00	0.00	0.00	0.00	0.00	0.00	0.00	0.00	0.00	0.00	0.00	0.00	0.00	0.00	0.00	0.00	0.00	0.00	0.00	0.00	0.00	0.00	0.00	0.00	0.00	0.00	0.00
	13	0	0.00	0.00	0.00	0.00	0.00	0.00	0.00	0.00	0.00	0.00	0.00	0.00	0.00	0.00	0.00	0.00	0.00	0.00	0.00	0.00	0.00	0.00	0.00	0.00	0.00	0.00	0.00	0.00	0.00	0.00	0.00	0.00	0.00	0.00	0.00	0.00	0.00	0.00	0.00
2025_12	4	0	0.00	0.00	0.00	0.00	0.00	0.00	0.00	0.00	0.00	0.00	0.00	0.00	0.00	0.00	0.00	0.00	0.00	0.00	0.00	0.00	0.00	0.00	0.00	0.00	0.00	0.00	0.00	0.00	0.00	0.00	0.00	0.00	0.00	0.00	0.00	0.00	0.00	0.00	0.00
	5	0	0.00	0.00	0.00	0.00	0.00	0.00	0.00	0.00	0.00	0.00	0.00	0.00	0.00	0.00	0.00	0.00	0.00	0.00	0.00	0.00	0.00	0.00	0.00	0.00	0.00	0.00	0.00	0.00	0.00	0.00	0.00	0.00	0.00	0.00	0.00	0.00	0.00	0.00	0.00
	6	100	0.45	0.15	0.00	0.30	2.21	5.34	8.54	9.76	7.62	5.49	5.64	5.41	6.86	5.95	5.79	7.39	5.95	1.83	2.67	4.42	4.04	2.29	0.91	0.30	0.08	0.30	0.15	0.08	0.08	0.00	0.00	0.00	0.00	0.00	0.00	0.00	0.00	0.00	0.00
	7	0	0.00	0.00	0.00	0.00	0.00	0.00	0.00	0.00	0.00	0.00	0.00	0.00	0.00	0.00	0.00	0.00	0.00	0.00	0.00	0.00	0.00	0.00	0.00	0.00	0.00	0.00	0.00	0.00	0.00	0.00	0.00	0.00	0.00	0.00	0.00	0.00	0.00	0.00	0.00
	8	100	0.91	2.89	18.86	10.51	11.24	11.48	12.52	3.29	2.33	2.33	2.25	2.01	2.33	1.44	1.77	1.20	1.12	0.96	0.48	0.64	0.48	0.88	0.72	0.40	0.96	1.20	1.28	0.88	0.88	0.56	0.56	0.24	0.32	0.08	0.00	0.00	0.00	0.00	0.00
	9	100	0.65	1.22	1.63	1.02	1.02	2.24	0.61	1.22	2.45	4.29	4.90	11.43	14.49	6.73	6.12	3.47	2.86	3.67	3.67	4.49	5.10	4.08	3.06	2.86	1.63	0.82	0.82	0.20	0.41	0.20	0.20	0.41	0.20	0.41	0.20	0.00	0.61	0.20	0.41
	10	100	0.00	1.11	3.33	7.04	3.70	8.15	5.93	1.85	7.04	2.96	7.41	8.52	5.56	1.11	5.93	3.70	6.67	6.67	2.96	4.44	2.96	0.74	0.37	0.74	0.00	0.74	0.00	0.37	0.00	0.00	0.00	0.00	0.00	0.00	0.00	0.00	0.00	0.00	0.00
	11	0	0.00	0.00	0.00	0.00	0.00	0.00	0.00	0.00	0.00	0.00	0.00	0.00	0.00	0.00	0.00	0.00	0.00	0.00	0.00	0.00	0.00	0.00	0.00	0.00	0.00	0.00	0.00	0.00	0.00	0.00	0.00	0.00	0.00	0.00	0.00	0.00	0.00	0.00	0.00
	12	0	0.00	0.00	0.00	0.00	0.00	0.00	0.00	0.00	0.00	0.00	0.00	0.00	0.00	0.00	0.00	0.00	0.00	0.00	0.00	0.00	0.00	0.00	0.00	0.00	0.00	0.00	0.00	0.00	0.00	0.00	0.00	0.00	0.00	0.00	0.00	0.00	0.00	0.00	0.00
	13	0	0.00	0.00	0.00	0.00	0.00	0.00	0.00	0.00	0.00	0.00	0.00	0.00	0.00	0.00	0.00	0.00	0.00	0.00	0.00	0.00	0.00	0.00	0.00	0.00	0.00	0.00	0.00	0.00	0.00	0.00	0.00	0.00	0.00	0.00	0.00	0.00	0.00	0.00	0.00

Table B.5: Tandem axle load distribution factors for October, November, December

Month	Class	Total	12000 lb	15000 lb	18000 lb	21000 lb	24000 lb	27000 lb	30000 lb	33000 lb	36000 lb	39000 lb	42000 lb	45000 lb	48000 lb	51000 lb	54000 lb	57000 lb	60000 lb	63000 lb	66000 lb	69000 lb	72000 lb	75000 lb	78000 lb	81000 lb	84000 lb	87000 lb	90000 lb	93000 lb	96000 lb	99000 lb	102000 lb
2025_10	4	0	0.00	0.00	0.00	0.00	0.00	0.00	0.00	0.00	0.00	0.00	0.00	0.00	0.00	0.00	0.00	0.00	0.00	0.00	0.00	0.00	0.00	0.00	0.00	0.00	0.00	0.00	0.00	0.00	0.00	0.00	0.00
	5	0	0.00	0.00	0.00	0.00	0.00	0.00	0.00	0.00	0.00	0.00	0.00	0.00	0.00	0.00	0.00	0.00	0.00	0.00	0.00	0.00	0.00	0.00	0.00	0.00	0.00	0.00	0.00	0.00	0.00	0.00	0.00
	6	0	0.00	0.00	0.00	0.00	0.00	0.00	0.00	0.00	0.00	0.00	0.00	0.00	0.00	0.00	0.00	0.00	0.00	0.00	0.00	0.00	0.00	0.00	0.00	0.00	0.00	0.00	0.00	0.00	0.00	0.00	0.00
	7	0	0.00	0.00	0.00	0.00	0.00	0.00	0.00	0.00	0.00	0.00	0.00	0.00	0.00	0.00	0.00	0.00	0.00	0.00	0.00	0.00	0.00	0.00	0.00	0.00	0.00	0.00	0.00	0.00	0.00	0.00	0.00
	8	100	0.00	0.00	0.00	6.81	2.27	4.55	4.55	2.27	9.09	9.09	13.64	13.64	2.27	4.55	0.00	2.27	2.27	2.27	6.82	9.09	4.55	0.00	0.00	0.00	0.00	0.00	0.00	0.00	0.00	0.00	0.00
	9	0	0.00	0.00	0.00	0.00	0.00	0.00	0.00	0.00	0.00	0.00	0.00	0.00	0.00	0.00	0.00	0.00	0.00	0.00	0.00	0.00	0.00	0.00	0.00	0.00	0.00	0.00	0.00	0.00	0.00	0.00	0.00
	10	100	0.00	0.00	0.00	0.00	8.68	17.39	4.35	4.35	4.35	0.00	0.00	8.70	0.00	0.00	13.04	8.70	13.04	8.70	4.35	0.00	0.00	0.00	0.00	0.00	0.00	4.35	0.00	0.00	0.00	0.00	0.00
	11	100	23.56	10.99	4.99	4.25	3.13	1.95	1.61	1.44	1.64	0.92	2.12	1.66	3.90	6.77	8.70	5.65	4.97	9.39	1.92	0.29	0.09	0.03	0.03	0.00	0.00	0.00	0.00	0.00	0.00	0.00	0.00
	12	0	0.00	0.00	0.00	0.00	0.00	0.00	0.00	0.00	0.00	0.00	0.00	0.00	0.00	0.00	0.00	0.00	0.00	0.00	0.00	0.00	0.00	0.00	0.00	0.00	0.00	0.00	0.00	0.00	0.00	0.00	0.00
	13	0	0.00	0.00	0.00	0.00	0.00	0.00	0.00	0.00	0.00	0.00	0.00	0.00	0.00	0.00	0.00	0.00	0.00	0.00	0.00	0.00	0.00	0.00	0.00	0.00	0.00	0.00	0.00	0.00	0.00	0.00	0.00
2025_11	4	0	0.00	0.00	0.00	0.00	0.00	0.00	0.00	0.00	0.00	0.00	0.00	0.00	0.00	0.00	0.00	0.00	0.00	0.00	0.00	0.00	0.00	0.00	0.00	0.00	0.00	0.00	0.00	0.00	0.00	0.00	0.00
	5	0	0.00	0.00	0.00	0.00	0.00	0.00	0.00	0.00	0.00	0.00	0.00	0.00	0.00	0.00	0.00	0.00	0.00	0.00	0.00	0.00	0.00	0.00	0.00	0.00	0.00	0.00	0.00	0.00	0.00	0.00	0.00
	6	0	0.00	0.00	0.00	0.00	0.00	0.00	0.00	0.00	0.00	0.00	0.00	0.00	0.00	0.00	0.00	0.00	0.00	0.00	0.00	0.00	0.00	0.00	0.00	0.00	0.00	0.00	0.00	0.00	0.00	0.00	0.00
	7	0	0.00	0.00	0.00	0.00	0.00	0.00	0.00	0.00	0.00	0.00	0.00	0.00	0.00	0.00	0.00	0.00	0.00	0.00	0.00	0.00	0.00	0.00	0.00	0.00	0.00	0.00	0.00	0.00	0.00	0.00	0.00
	8	100	0.00	0.00	0.00	8.12	0.00	0.00	5.41	10.81	8.11	10.81	13.51	8.11	2.70	2.70	2.70	2.70	0.00	0.00	0.00	10.81	8.11	0.00	2.70	2.70	0.00	0.00	0.00	0.00	0.00	0.00	0.00
	9	0	0.00	0.00	0.00	0.00	0.00	0.00	0.00	0.00	0.00	0.00	0.00	0.00	0.00	0.00	0.00	0.00	0.00	0.00	0.00	0.00	0.00	0.00	0.00	0.00	0.00	0.00	0.00	0.00	0.00	0.00	0.00
	10	100	0.00	0.00	2.65	10.53	10.53	13.16	0.00	0.00	7.89	0.00	2.63	5.26	2.63	2.63	5.26	2.63	10.53	7.89	5.26	0.00	2.63	0.00	0.00	0.00	2.63	2.63	2.63	0.00	0.00	0.00	0.00
	11	100	23.87	10.00	4.84	3.80	2.62	2.08	2.01	1.43	1.58	1.72	1.58	2.69	3.98	8.13	8.92	5.48	7.42	6.56	0.93	0.25	0.07	0.04	0.00	0.00	0.00	0.00	0.00	0.00	0.00	0.00	0.00
	12	0	0.00	0.00	0.00	0.00	0.00	0.00	0.00	0.00	0.00	0.00	0.00	0.00	0.00	0.00	0.00	0.00	0.00	0.00	0.00	0.00	0.00	0.00	0.00	0.00	0.00	0.00	0.00	0.00	0.00	0.00	0.00
	13	0	0.00	0.00	0.00	0.00	0.00	0.00	0.00	0.00	0.00	0.00	0.00	0.00	0.00	0.00	0.00	0.00	0.00	0.00	0.00	0.00	0.00	0.00	0.00	0.00	0.00	0.00	0.00	0.00	0.00	0.00	0.00
2025_12	4	0	0.00	0.00	0.00	0.00	0.00	0.00	0.00	0.00	0.00	0.00	0.00	0.00	0.00	0.00	0.00	0.00	0.00	0.00	0.00	0.00	0.00	0.00	0.00	0.00	0.00	0.00	0.00	0.00	0.00	0.00	0.00
	5	0	0.00	0.00	0.00	0.00	0.00	0.00	0.00	0.00	0.00	0.00	0.00	0.00	0.00	0.00	0.00	0.00	0.00	0.00	0.00	0.00	0.00	0.00	0.00	0.00	0.00	0.00	0.00	0.00	0.00	0.00	0.00
	6	0	0.00	0.00	0.00	0.00	0.00	0.00	0.00	0.00	0.00	0.00	0.00	0.00	0.00	0.00	0.00	0.00	0.00	0.00	0.00	0.00	0.00	0.00	0.00	0.00	0.00	0.00	0.00	0.00	0.00	0.00	0.00
	7	0	0.00	0.00	0.00	0.00	0.00	0.00	0.00	0.00	0.00	0.00	0.00	0.00	0.00	0.00	0.00	0.00	0.00	0.00	0.00	0.00	0.00	0.00	0.00	0.00	0.00	0.00	0.00	0.00	0.00	0.00	0.00
	8	100	0.00	0.00	2.50	0.00	0.00	0.00	5.00	2.50	2.50	7.50	17.50	7.50	5.00	2.50	2.50	2.50	10.00	7.50	7.50	7.50	7.50	2.50	0.00	0.00	0.00	0.00	0.00	0.00	0.00	0.00	0.00
	9	0	0.00	0.00	0.00	0.00	0.00	0.00	0.00	0.00	0.00	0.00	0.00	0.00	0.00	0.00	0.00	0.00	0.00	0.00	0.00	0.00	0.00	0.00	0.00	0.00	0.00	0.00	0.00	0.00	0.00	0.00	0.00
	10	100	0.00	0.00	4.00	16.00	12.00	0.00	0.00	4.00	4.00	8.00	8.00	4.00	8.00	4.00	8.00	0.00	4.00	0.00	8.00	4.00	0.00	0.00	0.00	0.00	0.00	4.00	0.00	0.00	0.00	0.00	0.00
	11	100	27.18	10.72	6.30	3.48	2.54	2.26	1.88	1.60	1.60	1.69	1.69	2.45	3.86	7.15	8.00	3.72	7.67	4.47	1.08	0.42	0.19	0.05	0.00	0.00	0.00	0.00	0.00	0.00	0.00	0.00	0.00
	12	0	0.00	0.00	0.00	0.00	0.00	0.00	0.00	0.00	0.00	0.00	0.00	0.00	0.00	0.00	0.00	0.00	0.00	0.00	0.00	0.00	0.00	0.00	0.00	0.00	0.00	0.00	0.00	0.00	0.00	0.00	0.00
	13	0	0.00	0.00	0.00	0.00	0.00	0.00	0.00	0.00	0.00	0.00	0.00	0.00	0.00	0.00	0.00	0.00	0.00	0.00	0.00	0.00	0.00	0.00	0.00	0.00	0.00	0.00	0.00	0.00	0.00	0.00	0.00

Table B.6: Tridem axle load distribution factors for October, November, December

Month	Class	Total	12000 lb	15000 lb	18000 lb	21000 lb	24000 lb	27000 lb	30000 lb	33000 lb	36000 lb	39000 lb	42000 lb	45000 lb	48000 lb	51000 lb	54000 lb	57000 lb	60000 lb	63000 lb	66000 lb	69000 lb	72000 lb	75000 lb	78000 lb	81000 lb	84000 lb	87000 lb	90000 lb	93000 lb	96000 lb	99000 lb	102000 lb
2025_10	4	0	0.00	0.00	0.00	0.00	0.00	0.00	0.00	0.00	0.00	0.00	0.00	0.00	0.00	0.00	0.00	0.00	0.00	0.00	0.00	0.00	0.00	0.00	0.00	0.00	0.00	0.00	0.00	0.00	0.00	0.00	0.00
	5	0	0.00	0.00	0.00	0.00	0.00	0.00	0.00	0.00	0.00	0.00	0.00	0.00	0.00	0.00	0.00	0.00	0.00	0.00	0.00	0.00	0.00	0.00	0.00	0.00	0.00	0.00	0.00	0.00	0.00	0.00	0.00
	6	0	0.00	0.00	0.00	0.00	0.00	0.00	0.00	0.00	0.00	0.00	0.00	0.00	0.00	0.00	0.00	0.00	0.00	0.00	0.00	0.00	0.00	0.00	0.00	0.00	0.00	0.00	0.00	0.00	0.00	0.00	0.00
	7	0	0.00	0.00	0.00	0.00	0.00	0.00	0.00	0.00	0.00	0.00	0.00	0.00	0.00	0.00	0.00	0.00	0.00	0.00	0.00	0.00	0.00	0.00	0.00	0.00	0.00	0.00	0.00	0.00	0.00	0.00	0.00
	8	0	0.00	0.00	0.00	0.00	0.00	0.00	0.00	0.00	0.00	0.00	0.00	0.00	0.00	0.00	0.00	0.00	0.00	0.00	0.00	0.00	0.00	0.00	0.00	0.00	0.00	0.00	0.00	0.00	0.00	0.00	0.00
	9	0	0.00	0.00	0.00	0.00	0.00	0.00	0.00	0.00	0.00	0.00	0.00	0.00	0.00	0.00	0.00	0.00	0.00	0.00	0.00	0.00	0.00	0.00	0.00	0.00	0.00	0.00	0.00	0.00	0.00	0.00	0.00
	10	100	0.00	0.00	0.00	11.12	0.00	22.22	11.11	11.11	0.00	0.00	11.11	0.00	11.11	0.00	0.00	0.00	0.00	11.11	0.00	11.11	0.00	0.00	0.00	0.00	0.00	0.00	0.00	0.00	0.00	0.00	0.00
	11	0	0.00	0.00	0.00	0.00	0.00	0.00	0.00	0.00	0.00	0.00	0.00	0.00	0.00	0.00	0.00	0.00	0.00	0.00	0.00	0.00	0.00	0.00	0.00	0.00	0.00	0.00	0.00	0.00	0.00	0.00	0.00
	12	0	0.00	0.00	0.00	0.00	0.00	0.00	0.00	0.00	0.00	0.00	0.00	0.00	0.00	0.00	0.00	0.00	0.00	0.00	0.00	0.00	0.00	0.00	0.00	0.00	0.00	0.00	0.00	0.00	0.00	0.00	0.00
	13	0	0.00	0.00	0.00	0.00	0.00	0.00	0.00	0.00	0.00	0.00	0.00	0.00	0.00	0.00	0.00	0.00	0.00	0.00	0.00	0.00	0.00	0.00	0.00	0.00	0.00	0.00	0.00	0.00	0.00	0.00	0.00
2025_11	4	0	0.00	0.00	0.00	0.00	0.00	0.00	0.00	0.00	0.00	0.00	0.00	0.00	0.00	0.00	0.00	0.00	0.00	0.00	0.00	0.00	0.00	0.00	0.00	0.00	0.00	0.00	0.00	0.00	0.00	0.00	0.00
	5	0	0.00	0.00	0.00	0.00	0.00	0.00	0.00	0.00	0.00	0.00	0.00	0.00	0.00	0.00	0.00	0.00	0.00	0.00	0.00	0.00	0.00	0.00	0.00	0.00	0.00	0.00	0.00	0.00	0.00	0.00	0.00
	6	0	0.00	0.00	0.00	0.00	0.00	0.00	0.00	0.00	0.00	0.00	0.00	0.00	0.00	0.00	0.00	0.00	0.00	0.00	0.00	0.00	0.00	0.00	0.00	0.00	0.00	0.00	0.00	0.00	0.00	0.00	0.00
	7	0	0.00	0.00	0.00	0.00	0.00	0.00	0.00	0.00	0.00	0.00	0.00	0.00	0.00	0.00	0.00	0.00	0.00	0.00	0.00	0.00	0.00	0.00	0.00	0.00	0.00	0.00	0.00	0.00	0.00	0.00	0.00
	8	0	0.00	0.00	0.00	0.00	0.00	0.00	0.00	0.00	0.00	0.00	0.00	0.00	0.00	0.00	0.00	0.00	0.00	0.00	0.00	0.00	0.00	0.00	0.00	0.00	0.00	0.00	0.00	0.00	0.00	0.00	0.00
	9	0	0.00	0.00	0.00	0.00	0.00	0.00	0.00	0.00	0.00	0.00	0.00	0.00	0.00	0.00	0.00	0.00	0.00	0.00	0.00	0.00	0.00	0.00	0.00	0.00	0.00	0.00	0.00	0.00	0.00	0.00	0.00
	10	100	0.00	0.00	0.00	0.00	11.12	0.00	0.00	0.00	11.11	0.00	11.11	0.00	0.00	11.11	11.11	0.00	11.11	0.00	11.11	0.00	0.00	0.00	11.11	11.11	0.00	0.00	0.00	0.00	0.00	0.00	0.00
	11	0	0.00	0.00	0.00	0.00	0.00	0.00	0.00	0.00	0.00	0.00	0.00	0.00	0.00	0.00	0.00	0.00	0.00	0.00	0.00	0.00	0.00	0.00	0.00	0.00	0.00	0.00	0.00	0.00	0.00	0.00	0.00
	12	0	0.00	0.00	0.00	0.00	0.00	0.00	0.00	0.00	0.00	0.00	0.00	0.00	0.00	0.00	0.00	0.00	0.00	0.00	0.00	0.00	0.00	0.00	0.00	0.00	0.00	0.00	0.00	0.00	0.00	0.00	0.00
	13	0	0.00	0.00	0.00	0.00	0.00	0.00	0.00	0.00	0.00	0.00	0.00	0.00	0.00	0.00	0.00	0.00	0.00	0.00	0.00	0.00	0.00	0.00	0.00	0.00	0.00	0.00	0.00	0.00	0.00	0.00	0.00
2025_12	4	0	0.00	0.00	0.00	0.00	0.00	0.00	0.00	0.00	0.00	0.00	0.00	0.00	0.00	0.00	0.00	0.00	0.00	0.00	0.00	0.00	0.00	0.00	0.00	0.00	0.00	0.00	0.00	0.00	0.00	0.00	0.00
	5	0	0.00	0.00	0.00	0.00	0.00	0.00	0.00	0.00	0.00	0.00	0.00	0.00	0.00	0.00	0.00	0.00	0.00	0.00	0.00	0.00	0.00	0.00	0.00	0.00	0.00	0.00	0.00	0.00	0.00	0.00	0.00
	6	0	0.00	0.00	0.00	0.00	0.00	0.00	0.00	0.00	0.00	0.00	0.00	0.00	0.00	0.00	0.00	0.00	0.00	0.00	0.00	0.00	0.00	0.00	0.00	0.00	0.00	0.00	0.00	0.00	0.00	0.00	0.00
	7	0	0.00	0.00	0.00	0.00	0.00	0.00	0.00	0.00	0.00	0.00	0.00	0.00	0.00	0.00	0.00	0.00	0.00	0.00	0.00	0.00	0.00	0.00	0.00	0.00	0.00	0.00	0.00	0.00	0.00	0.00	0.00
	8	0	0.00	0.00	0.00	0.00	0.00	0.00	0.00	0.00	0.00	0.00	0.00	0.00	0.00	0.00	0.00	0.00	0.00	0.00	0.00	0.00	0.00	0.00	0.00	0.00	0.00	0.00	0.00	0.00	0.00	0.00	0.00
	9	0	0.00	0.00	0.00	0.00	0.00	0.00	0.00	0.00	0.00	0.00	0.00	0.00	0.00	0.00	0.00	0.00	0.00	0.00	0.00	0.00	0.00	0.00	0.00	0.00	0.00	0.00	0.00	0.00	0.00	0.00	0.00
	10	100	0.00	0.00	0.00	0.00	0.00	14.27	0.00	14.29	0.00	0.00	0.00	0.00	0.00	0.00	14.29	0.00	0.00	28.57	0.00	0.00	14.29	0.00	14.29	0.00	0.00	0.00	0.00	0.00	0.00	0.00	0.00
	11	0	0.00	0.00	0.00	0.00	0.00	0.00	0.00	0.00	0.00	0.00	0.00	0.00	0.00	0.00	0.00	0.00	0.00	0.00	0.00	0.00	0.00	0.00	0.00	0.00	0.00	0.00	0.00	0.00	0.00	0.00	0.00
	12	0	0.00	0.00	0.00	0.00	0.00	0.00	0.00	0.00	0.00	0.00	0.00	0.00	0.00	0.00	0.00	0.00	0.00	0.00	0.00	0.00	0.00	0.00	0.00	0.00	0.00	0.00	0.00	0.00	0.00	0.00	0.00
	13	0	0.00	0.00	0.00	0.00	0.00	0.00	0.00	0.00	0.00	0.00	0.00	0.00	0.00	0.00	0.00	0.00	0.00	0.00	0.00	0.00	0.00	0.00	0.00	0.00	0.00	0.00	0.00	0.00	0.00	0.00	0.00

Table B.7: Quad axle load distribution factors for October, November, December

Appendix C

User guide to AASHTOWare Pavement ME Design

The PavMe software is structured around the three categories of input described by the MEPDG, which are organized into separate modules: climate, traffic, and materials. They will be assessed individually in this section.

Once all input data and calibration factors are correctly entered, the analysis can be run.

This guide is developed with reference to the Software version 2.6.2.2.

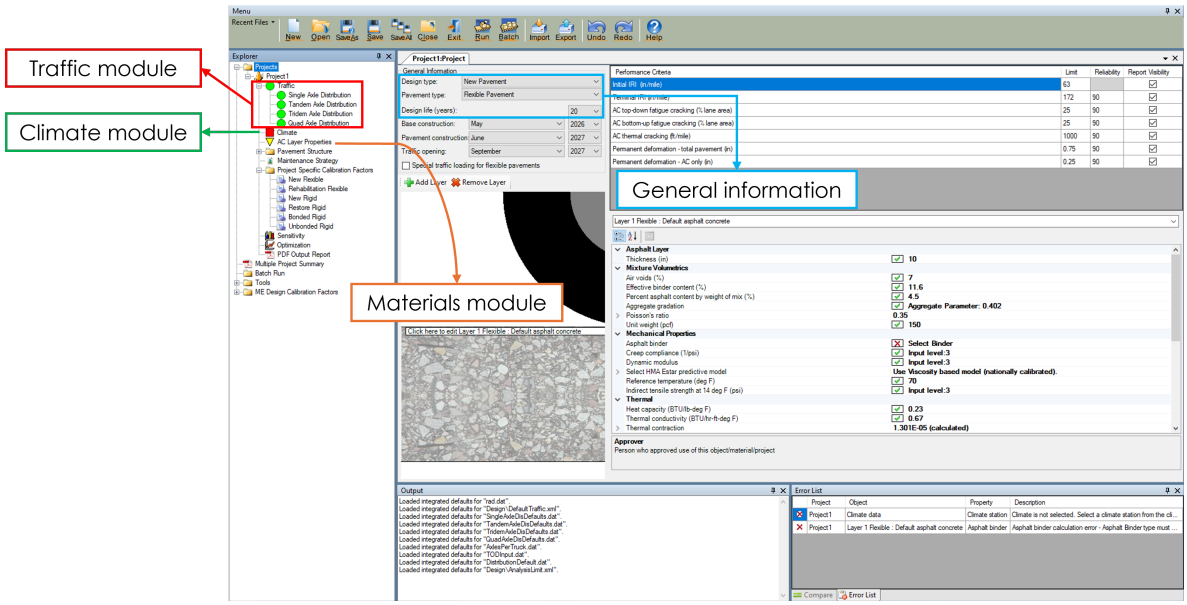

Figure C.1: PavMe main interface

C.1 Climate module

The Mechanistic Empirical Pavement Design Guide integrates the weather station-driven EICM model (Enhanced Integrated Climatic Model). The module includes a network of virtual weather stations whose data are derived from the reanalysis datasets produced by the MERRA-2 program. The aforementioned virtual weather stations will be referred to as "real" weather stations for clarity.

No input data needs to be entered manually. The user may select up to 6 real weather stations near the location of interest. The data from the real stations are interpolated to provide a virtual weather station with accurate modeled information for the pavement location.

The weather stations are actually empty by default. The climatic data dataset has to be downloaded from the LTPP InfoPave portal in the Hourly Climate Data (.hcd) format and uploaded to the corresponding weather station in the Software. When this occurs, the station is activated, and its data can be used by the EICM model. The .hcd file may be downloaded in both the International System and Imperial units. However, the software works with Imperial units, so it is recommended that they be downloaded accordingly. The climate file contains the climate data in the format as follows:

- YYYYMMDDHH
- Temperature, [°F]
- Wind Speed, [mi/h]
- Sunshine, [%]
- Precipitation, [in]
- Relative Humidity, [%]

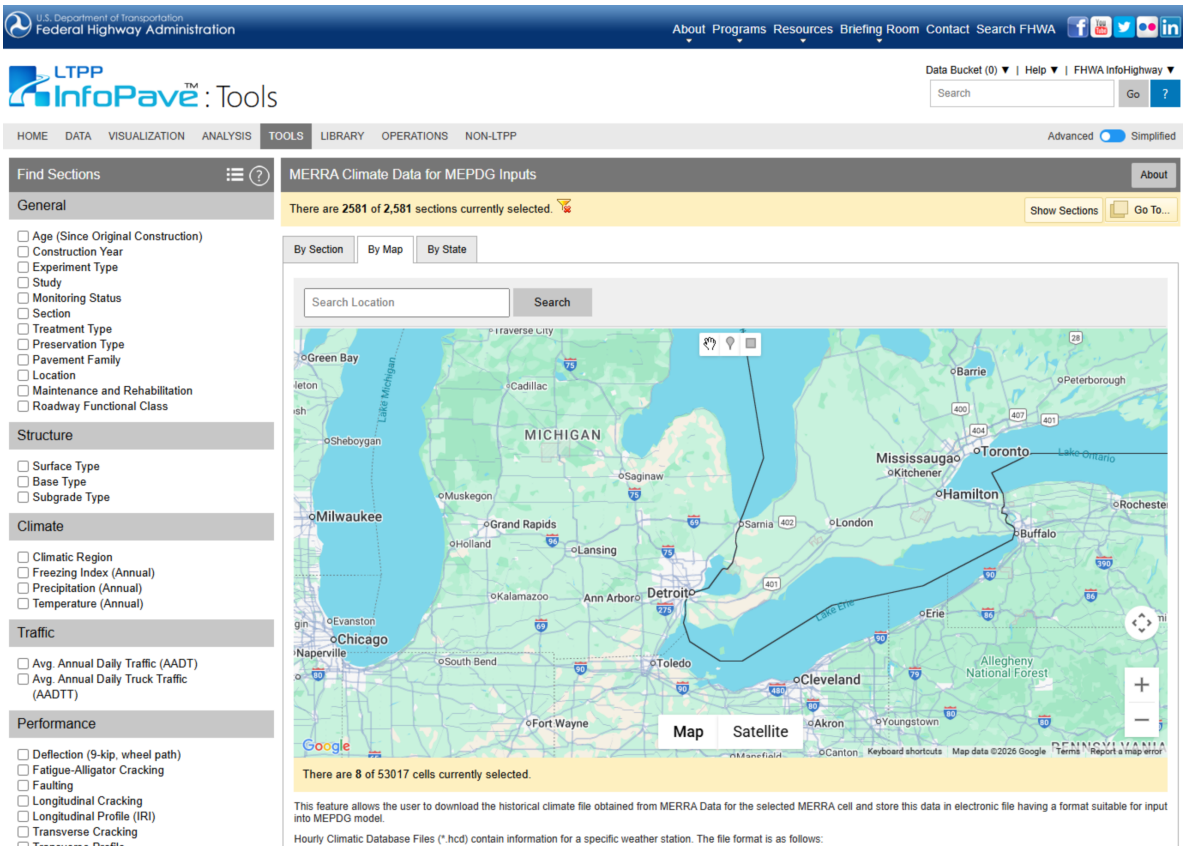

Figure C.2: The LTPP InfoPave section for the download of the climate datasets

The following screenshot shows some of the real weather stations belonging to the MERRA-2 network: the blue markers correspond to the "active" weather stations, whereas the red markers indicate the empty ones.

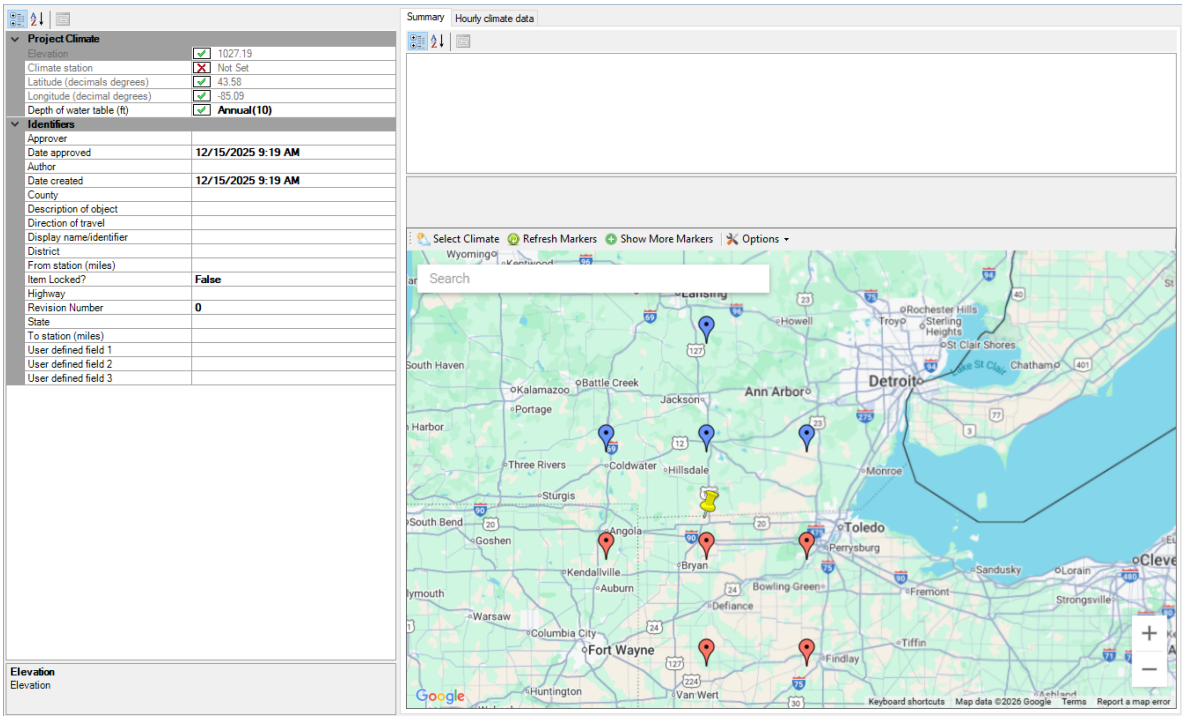

Figure C.3: The climate module in the PavME Software

C.2 Materials module

After selecting the design and pavement type in the "General Information" box, the trial section can be defined by adding the necessary layers and editing their material properties. Each layer features its own window for entering material-specific input data. By way of example, fig. C.4 illustrates the interface for the subgrade input data.

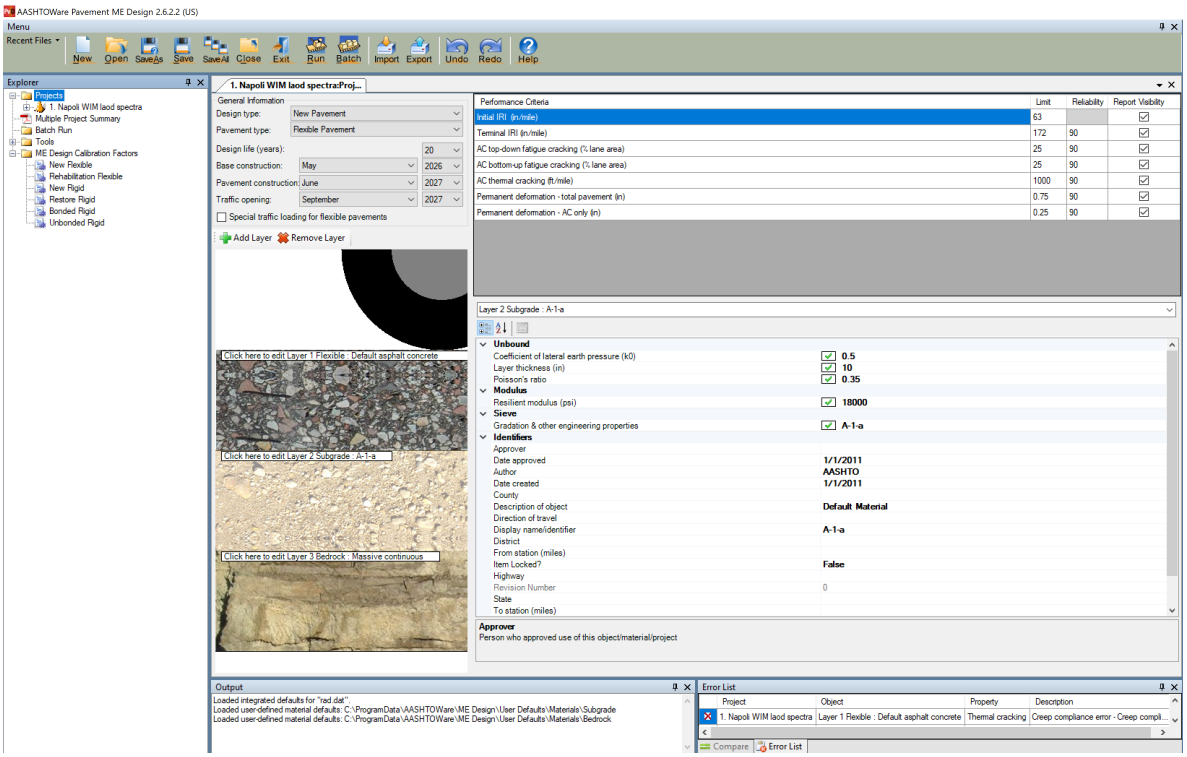

Figure C.4: The materials module in the PavME Software

Some clarification is needed on the resilient modulus input data. Although the NCHRP 1-37A Project was originally intended to implement the dependence of resilient modulus on the stress state and material moisture content, neither is included in the current version of the Software; only Input Level 2 or 3 is supported. The resilient modulus temperature-susceptibility can be considered either by entering monthly representative values of the parameter or by entering a single representative value and using the EICM to adjust it for seasonal climate effects, as illustrated in fig. C.5. The designer may choose not to account for the resilient modulus temperature-susceptibility by entering an annual representative value.

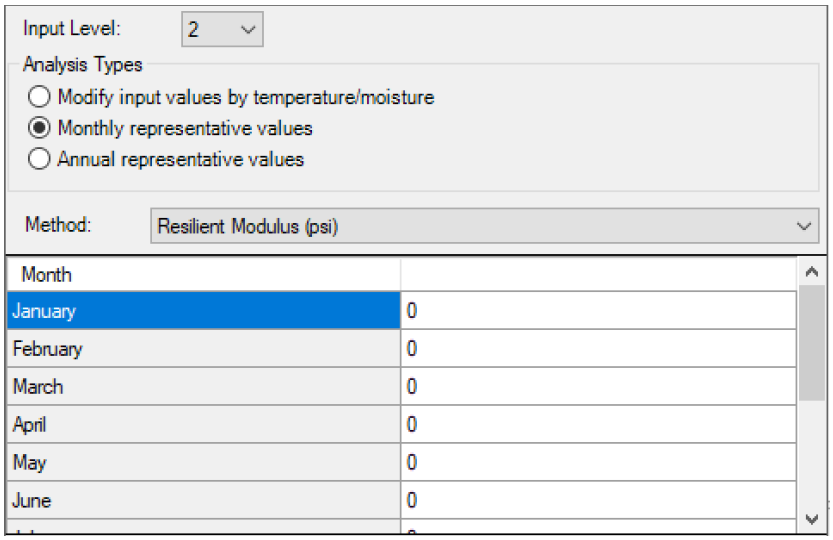

Figure C.5: Resilient modulus input interface in PavME

The interface for the calibration factors is shown in fig. C.6. This section enables modification of both the coefficients of the damage and transfer functions. The factors can be applied to multiple projects at once by clicking the "Update Open Projects" button. Alternatively, each file can be customized individually.

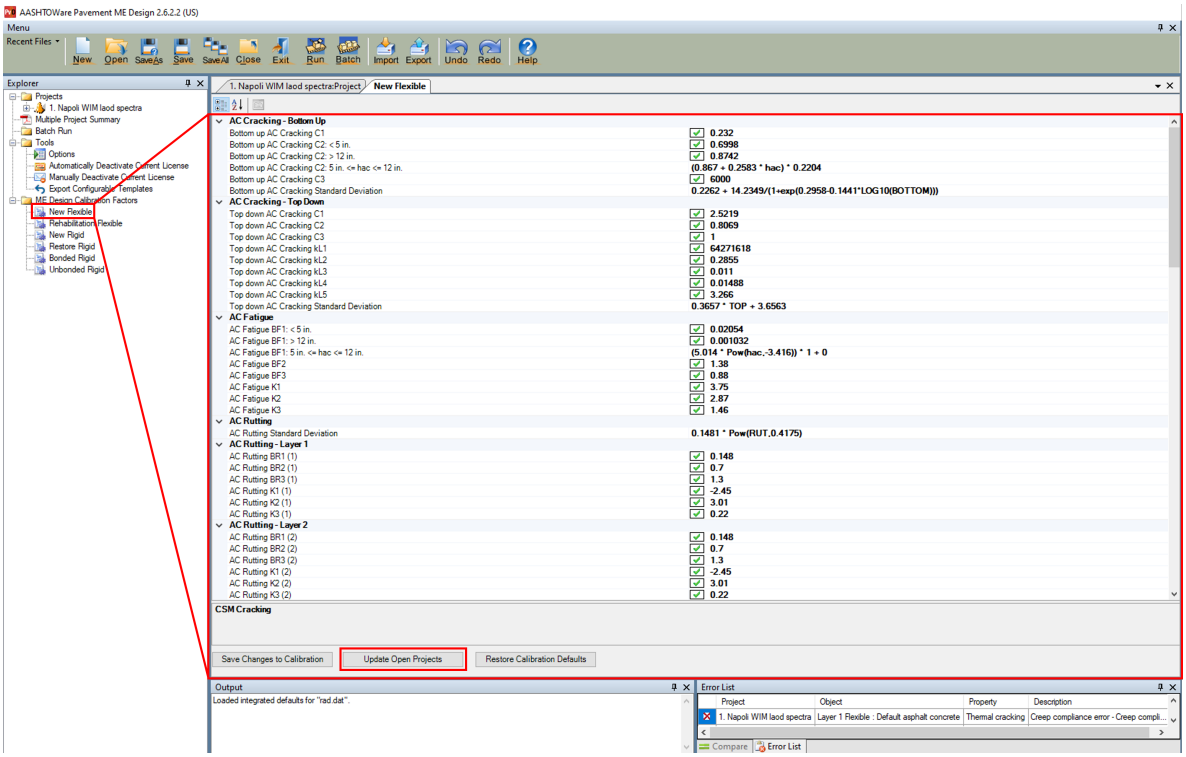

Figure C.6: PavMe interface for the transfer and damage functions calibration

C.3 Traffic module

Traffic information has to be processed and arranged using the same layout as PavME. By doing so, they can be copied and pasted easily into the traffic section of the Software.

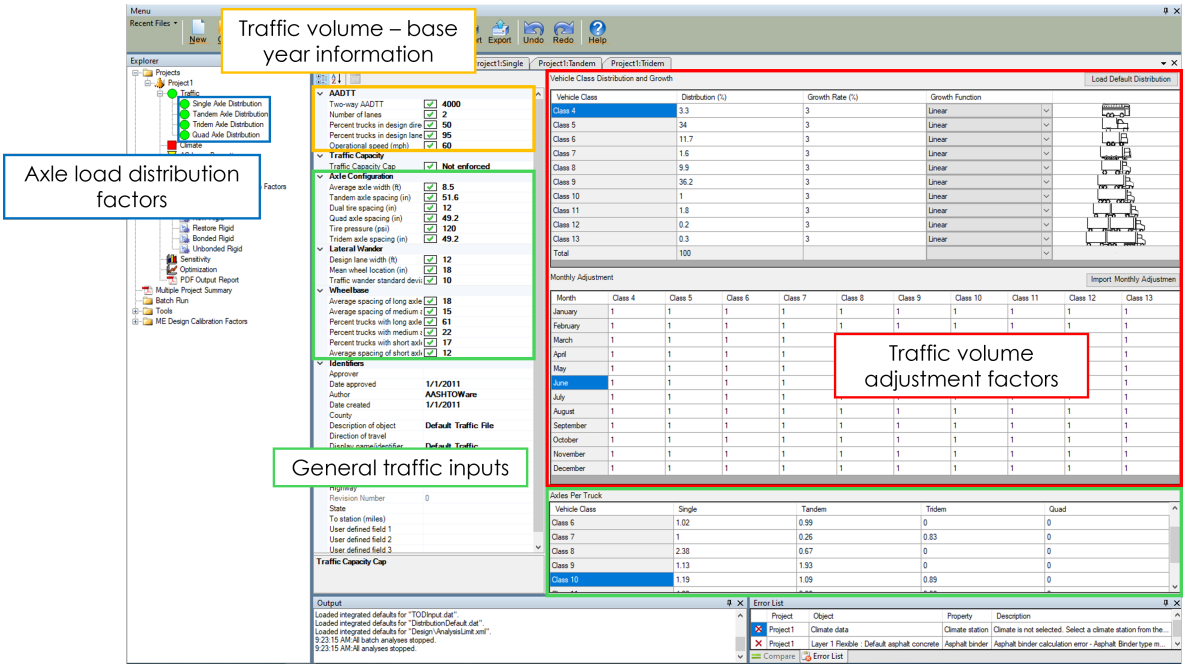

Figure C.7: The traffic module in the PavME Software

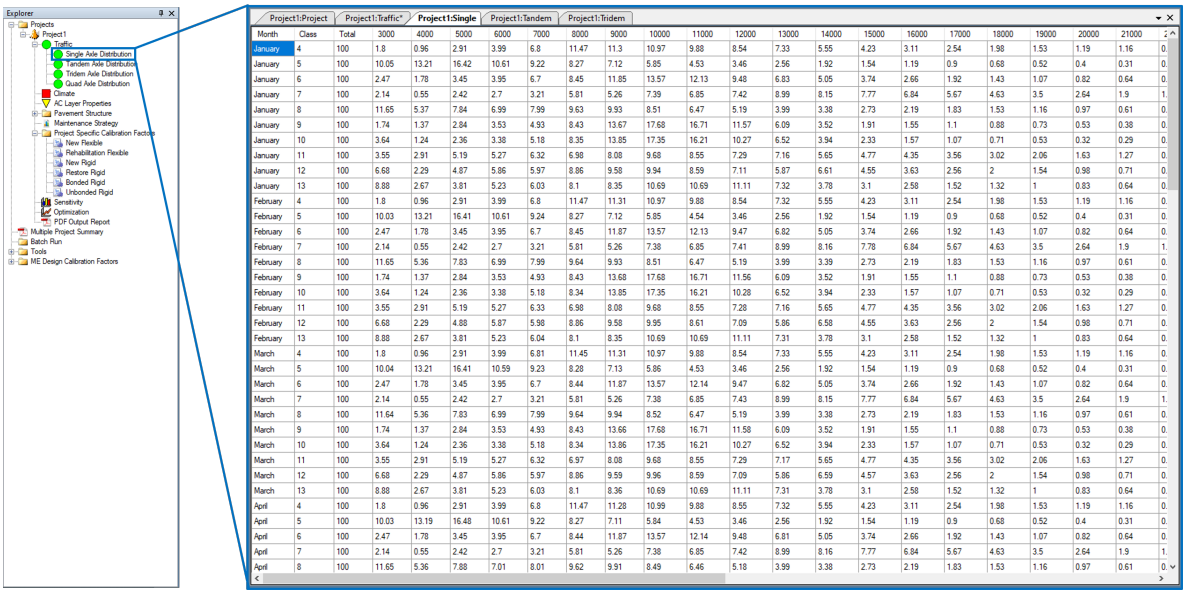

Figure C.8: The traffic module in the PavME Software: single axle load distribution factors